

pH-Cleavable and Hyperbranched Polyether Architectures: From Novel Synthesis Strategies to Applications in Nanotechnology and Biomedicine

Dissertation zur Erlangung des Grades
„Doktor rerum naturalium“ (Dr. rer. nat.)
der Fachbereiche

08 – Physik, Mathematik und Informatik

09 – Chemie, Pharmazie und Geowissenschaften

10 – Biologie und der Unimedizin

der Johannes Gutenberg-Universität

Matthias Worm

Mainz, 2016

Reviewer 1:

Reviewer 2:

Date of Oral Examination: 19.12.2016

I hereby declare that I wrote the dissertation submitted without any unauthorized external assistance and used only sources acknowledged in the work. All textual passages which are appropriated verbatim or paraphrased from published and unpublished texts as well as all information obtained from oral sources are duly indicated and listed in accordance with bibliographical rules. In carrying out this research, I complied with the rules of standard scientific practice as formulated in the statutes of Johannes Gutenberg-University Mainz to insure standard scientific practice.

Für Meine Eltern

„Die Neugier steht immer an erster Stelle eines Problems, das gelöst werden will.“

Galileo Galilei

Danksagung

In den vergangenen drei Jahren haben mich viele Menschen tatkräftig unterstützt und auf verschiedene Weisen zum Gelingen dieser Arbeit beigetragen. Ich möchte mich herzlich bei all diesen Menschen bedanken.



Table of Contents

Danksagung	1
Motivation and Objectives	7
Abstract	11
Zusammenfassung.....	15
Graphical Abstract.....	19
1 Introduction.....	21
1.1 Functional Poly(ethylene glycol)s and their Application.....	23
1.2 Liposomes in Biomedicine – An Introduction	35
1.3 Block Copolymers of Poly(ethylene glycol) and Poly(propylene oxide).....	48
1.4 Cleavable Polyethers	61
2 pH-Cleavable Polyether-based Surfactants.....	71
2.1 Acid-labile Amphiphilic PEO- <i>b</i> -PPO- <i>b</i> -PEO Copolymers: Degradable Poloxamer Analogs	73
Supporting Information.....	87
3 pH-Cleavable Poly(ethylene glycol)s	101
3.1 Cleavable Polyethylene Glycol (PEG): 3,4-Epoxy-1-butene (EPB) as a Comonomer to Establish Degradability at Physiologically Relevant pH.....	103
Supporting Information.....	120
4 pH-Sensitive PEG-Lipids for Liposomal Applications.....	133
4.1 Ketal- and Acetal-functional Dialkyl-PEG Lipids for pH-Sheddable Liposomes.....	135
Supporting Information	171
5 Hyperbranched Polyglycerol-based Lipids in Liposomes.....	179
5.1 Hyperbranched Polyglycerol- and PEG-Lipids – Synthesis and Characterization.....	181
5.2 Size Control of <i>hb</i> PG-modified Liposomes <i>via</i> Dual Centrifugation.....	195
5.3 <i>In Vivo</i> Biodistribution Studies of ¹⁸ F-Radiolabeled Lipids and Liposomes by Positron Emission Tomography Imaging	200
Supporting Information.....	209
Outlook.....	212
Appendix.....	219
A.1 Biodegradable Hyperbranched Polyether-lipids with In-chain pH-sensitive Linkages	221
A.2 Orthogonal Click Conjugation to the Liposomal Surface Reveals the Stability of the Lipid Anchorage as Crucial for Targeting	234
A.3 List of Publications	240

Motivation and Objectives

The unique properties of aliphatic polyethers have always attracted strong attention and have given rise to numerous applications in industries and academia. In particular, poly(ethylene glycol) PEG exhibits fascinating properties. Aside from its chemically inert and flexible structure, which is typical for aliphatic polyethers, PEG is highly water-soluble, non-toxic, and almost non-immunogenic. Therefore, PEG has been universally employed as a hydrophilic polymeric component in various fields of research, including food technology and cosmetics industries in addition to more specialized applications in biomedicine and nanotechnology. For example, amphiphilic, surface-active polymers (surfactants) containing PEG as nonionic, hydrophilic building blocks are utilized as detergents and lubricants in industrial processes, and are employed as emulsifying agents for the preparation of nanoparticles *via* emulsion polymerization techniques. Most prominently, PEG is frequently used to improve the pharmacokinetic properties of therapeutic drugs or nanoscale drug carrier systems. Covalent attachment of PEG to bioactive molecules or to the surface of nanoparticles, known as PEGylation, enhances or conveys water solubility, avoids recognition by cells of the immune system and reduces the rate of renal filtration, resulting in prolonged blood circulation times and a reduction of undesired effects. In particular, PEGylated lipids have attracted considerable attention in liposomal research and have proven advantageous for the design of sterically stabilized liposomes (“stealth liposomes”).

Although PEG promotes various favorable properties as outlined for the above-mentioned systems, the non-degradability of polyethers constitutes a drawback to many of these applications. For instance, the use of PEG for biomedical purposes is restricted to an upper molecular weight limit of around $30.000 \text{ g mol}^{-1}$ to avoid accumulation in the tissue that can lead to storage diseases and potentially liver cancer. In nanomedicine, the presence of a PEG “stealth” layer on the surface of liposomes results in enhanced stability profiles, albeit at the expense of hampered cellular uptake and restrained drug release from the carriers. If nanoparticles are prepared by emulsion

polymerization processes, they usually suffer from large amounts of surfactant that may compromise the particle properties and can raise environmental concerns. Here, the non-degradability of polyether-based surfactants such as PEO-*b*-PPO-*b*-PEO copolymers (poloxamers) prevents controlled fragmentation of the surfactant after MEPs that would enable an efficient removal of the additive from the nanoparticles.

To address these drawbacks, the incorporation of pH-cleavable moieties into the PEG backbone or into PEG-based lipids and surfactants is considered as highly promising to allow for a triggered degradation to smaller fragments upon changes in pH. Depending on the application, scission of polymers could be induced by exploiting idiosyncrasies of certain physiological media e.g. the lowered pH values in tumor microenvironments and in cellular compartments to facilitate PEG fragmentation or the detachment of PEG from stealth liposomes, enabling rapid degradation. Alternatively, scission could also be initiated by an external control of the pH in case of cleavable PEG-derived surfactants used for nanoparticle preparation. In this context, the major objective of this thesis is the design of general pathways to novel pH-cleavable PEGs and PEG-based amphiphilic polymer structures.

Aside from a lack of degradability, PEG solely contains two hydroxyl groups available for chemical modification that can limit its utility, if the attachment of multiple functional molecules is necessary, for example to permit active targeting and carrier trafficking of liposomes. In this case, hyperbranched polyglycerol (*hbPG*) can serve as a multifunctional PEG substitute, and a spin-off project of this thesis focusses on evaluating the properties of *hbPG*-lipids in comparison to PEG-based lipids.

The specific objectives of this thesis are summarized in the following:

i) *pH-Cleavable Surfactants for Mini Emulsion Polymerizations (MEPs)*: The synthesis of pH-cleavable polyether-based amphiphiles as surfactants for miniemulsion polymerizations (MEPs) is the focus of the first part of this thesis. The separation of surfactants from nanoparticles represents

a major challenge with MEPs as discussed above. To this end, poloxamer analogous structures (PEO-*b*-PPO-*b*-PEO copolymers) with in-chain pH-hydrolyzable acetal units are synthesized and used in a collaboration with the group of Dr. Frederik Wurm (Max Planck Institute for Polymer Research) to stabilize nanoparticles during MEP, allowing for an efficient removal of the surfactant fragments after particle formation via acid-triggered surfactant cleavage.

ii) *Overcoming the Non-Degradability of PEG – pH-cleavable P(EPB-co-EG) copolymers:* The non-degradability of PEG limits its utility to an upper molecular weight threshold in biomedical applications. To extend the scope of PEG beyond these restrictions, in this part of the thesis, copolymerization of 3,4-epoxy-1-butene (EPB) with ethylene oxide is explored to incorporate multiple pH-hydrolyzable vinyl ether moieties into the backbone of PEG to allow its degradation. These potential PEG substitutes should combine a well-defined structure with controlled hydrolysis kinetics at physiologically relevant pH and the possibility to conjugate other functional molecules e.g. therapeutic drugs.

iii) *pH-cleavable PEG-Lipids:* Acid-sensitive polyether-based lipids appear ideally suited to exploit the lowered pH in the microenvironment of tumors or in cellular compartments for triggered release strategies from liposomes. Upon shedding of the PEG stealth layer at the site of action, cellular uptake and release of cargo are promoted. The major objectives for this part of the thesis are to establish a synthesis for well-defined, pH-cleavable PEG-lipids with tunable hydrolysis kinetics that allow either burst PEG shedding or slow controlled hydrolysis under mild acidic conditions (pH 5 - 6). Shedding properties of lipids in liposomal formulations are investigated in a collaboration with the group of Prof. Mark Helm (Institute of Pharmacy and Biochemistry, Johannes Gutenberg-University Mainz). The lipids should be functionalizable at the chain end to permit carrier/lipid trafficking, and in addition, should be stably entrenched in the bilayer membrane. Finding cleavable moieties that can be introduced in a few synthetic steps and withstand anionic polymerization conditions, but at the same time enable the desired burst release profiles is one particular challenge in this part.

iv) Multifunctional Polyether-Based Lipids in Liposomes: Besides stimuli-responsiveness of liposomes, the perspective to attach multiple functional molecules onto polyether-based lipids to achieve a multivalence effect in active targeting is highly desired for liposomal carriers. By synthesizing multifunctional *hbPG*- and monofunctional PEG-based lipids of similar molecular weights, the influence of the polymer architecture on the properties of liposomes prepared *via* dual centrifugation should be studied in a collaboration with the group of Prof. Mark Helm (Institute of Pharmacy and Biochemistry, Johannes Gutenberg-University Mainz). Furthermore, positron emission tomography (PET) imaging should serve to evaluate biodistribution of ^{18}F -labeled lipid components and liposomes *in vivo* in a collaboration with the group of Prof. Frank Rösch (Institute of Nuclear Chemistry, Johannes Gutenberg-University of Mainz).

In the appendix, several chapters summarize coauthored contributions to other research areas in the field of polyether chemistry that result from projects with other collaboration partners and colleagues from the group of Prof. Frey. These contributions specifically tackle the membrane stability of cholesterol- and dialkyl-derived polyether-lipids in liposomes, as well as the development of pH-degradable hyperbranched polyglycerol-based lipids.

Abstract

The use of polyethylene glycol (PEG) is diverse, ranging from food technology and cosmetics to applications in nanotechnology and pharmaceutical industries. However, despite the various favorable properties of PEG, its non-degradability and the low number of functional groups can be a drawback to many applications. The aim of this thesis is to establish cleavability of PEG and PEG-derived lipids and surfactants by exploring novel synthetic pathways to incorporate pH-hydrolyzable moieties into the polyether structures. A strong emphasis is put on elucidating the hydrolysis kinetics of the novel materials to evaluate their potential for future applications. Furthermore, hyperbranched polyglycerol (*hbPG*) architectures are investigated that contain a large number of hydroxyl functionalities, which render *hbPGs* interesting PEG substitutes if multifunctionality of the polyether is a requirement.

Chapter 1.1 serves as an introduction to the chemistry of PEG and presents an overview on various routes to incorporate functional moieties into the backbone or at the chain ends of PEG. A particular focus is directed at the anionic ring-opening polymerization (AROP) of epoxide monomers, which constitutes the fundamental polymerization technique employed in this thesis. **Chapter 1.2** represents an introduction into liposome research, which highlights the development of sterically stabilized liposomes (“stealth liposomes”), active cell targeting and stimuli-responsive drug release strategies. Especially, the usefulness of pH-cleavable PEG-lipids in liposomal formulations is illustrated. In **Chapter 1.3** block copolymers composed of poly(propylene oxide) (PPO) and PEG (denoted as PEO) are introduced, focusing on the broad range of applications for PEO-*b*-PPO-*b*-PEO copolymers (poloxamers) as surfactants and reflecting recent trends in this area. An overview on cleavable PEG architectures is given in **Chapter 1.4** summarizing current achievements in addressing the non-degradability of PEG. Problems arising from PEG’s biopersistence are discussed that, for instance, set an upper molecular weight limit of PEG for the use in biomedical applications.

Chapters 1.3 and 1.4 are sections of a comprehensive review article that was published in *Chemical Reviews*.

In **Chapter 2**, the design of pH-cleavable poloxamer analogs (PEO-*b*-PPO-*b*-PEO copolymers) is presented that contain acid-sensitive acetal linkages at the block junctions. In a proof-of-concept experiment, the novel amphiphilic polymers were used as surfactants for the miniemulsion polymerization of styrene in a collaboration with the group of Dr. Frederik Wurm (Max Planck Institute for Polymer Research) to prepare well-defined polystyrene nanoparticles. pH-triggered precipitation of these nanoparticles from stable miniemulsions allowed efficient removal of surfactant fragments to obtain additive-free nanoparticles. Separation of surfactants is a major challenge with MEPS, however, is desirable due to environmental concerns and potential surfactant-mediated changes of particle properties.

To address the non-degradability of PEG, in **Chapter 3** the anionic ring-opening copolymerization of ethylene oxide and 3,4-epoxy-1-butene (EPB) was explored to introduce multiple pH-sensitive vinyl ether moieties in the PEG backbone after catalytic isomerization of the allylic double bonds. Well-defined, acid-cleavable copolymers of tailorable molecular weight with low contents of EPB (4 mol%) were synthesized in an efficient two-step procedure. Analysis of degradation products via SEC indicated moderate molecular weight distribution ($\mathcal{D} = 1.6 - 1.8$). Hydrolysis profiles of pH-cleavable P(EPB-*co*-EG) copolymers were monitored by ^1H NMR spectroscopy in a physiologically relevant pH range of 4.4 to 5.4, revealing promising cleavage kinetics with respect to biomedical application, e.g. for cleavable, long-circulating polymer-drug conjugates.

The synthesis of pH-sensitive PEG-lipids with in-chain cleavable ketal and acetal units for the application in pH-responsive “stealth” liposomes is reported in **Chapter 4**. To this end, a novel synthesis strategy towards asymmetric ketals in polymers was developed providing access to PEG-lipids of tunable molecular weights and with a defined hydroxyl end group facilitating post-modification reactions. *In situ* ^1H NMR kinetic studies on the hydrolysis rates of the pure lipids

suggested significantly faster cleavage of ketals compared to acetals. The behavior of the lipids in liposomal formulations was further analyzed *via* time-resolved fluorescence spectroscopy and gel electrophoresis assays in a collaboration with the group of Prof. Mark Helm (Institute of Pharmacy and Biochemistry, Johannes Gutenberg-University Mainz), to monitor pH-dependent detachment of PEG from the liposomal surface. Highly promising PEG shedding properties in mildly acidic media (pH 5.5 to 6.5) were found for the ketal-functional PEG-lipids that suggest great potential for pH-triggered drug release strategies from liposomes e.g. in tumor therapy.

In liposomal research, *hbPGs* are promising alternatives to PEG as they can convey a multivalence effect in active cell targeting. In order to study the effect of the polyether architecture on liposomal properties, in **Chapter 5** dialkyl-functional *hbPG*- and PEG-lipids were synthesized with molecular weights of 3 to 7 kg mol⁻¹. A novel *linPG*-lipid precursor offered access to the *hbPG*-lipids using slow monomer addition of the latent AB₂-type monomer glycidol. Liposomes containing linear or hyperbranched lipids were prepared by dual centrifugation in a collaboration with the group of Prof. Mark Helm (Institute of Pharmacy and Biochemistry, Johannes Gutenberg-University Mainz). Tuning of the diameter of liposomes in a range below 100 nm could be achieved, which has been proposed as an optimum for antitumor therapy. First *in vivo* biodistribution studies of ¹⁸F-radiolabeled lipids by positron emission tomography (PET) imaging were performed in collaboration with the group of Prof. Frank Rösch (Institute of Nuclear Chemistry, Johannes Gutenberg-University Mainz) that suggest efficient renal clearance of the PEG-/*hbPG*-lipids. In addition, blood circulation of radiolabeled, polyether-modified liposomes for more than 1 h was observed, providing evidence for *hbPG*-mediated “stealth” properties of liposomes *in vivo*.

Zusammenfassung

Polyethylenglykol (PEG) ist ein hydrophiler, aliphatischer Polyether mit einem breiten Anwendungsspektrum in Nahrungsmitteln und Kosmetikartikeln. PEG findet zudem vielfachen Einsatz in der pharmazeutischen Industrie sowie der Nanotechnologie. Trotz der mannigfachen, wertvollen Eigenschaften von PEG stellen in vielen Anwendungen sowohl das chemisch robuste PEG-Rückgrat als auch die geringe Anzahl funktioneller Gruppen erhebliche Nachteile dar. Im Rahmen dieser Arbeit wurden verschiedene Synthesestrategien entwickelt, die eine gezielte, pH-gesteuerte Spaltbarkeit von PEG, PEG-basierten Lipiden und Tensiden ermöglichen. Große Aufmerksamkeit galt dabei der Untersuchung der Hydrolysekinetiken der neuartigen Materialien, um deren Potential im Hinblick auf zukünftige Anwendungsgebiete zu evaluieren. In einem weiteren Projektabschnitt wurden hyperverzweigte Polyglycerin-Strukturen synthetisiert, die wegen ihrer Vielzahl an funktionellen Hydroxylgruppen als vielversprechende Alternativen zu PEG diskutiert werden.

Kapitel 1.1 gibt eine kurze Einführung zur Chemie von PEG, in deren Verlauf unterschiedliche synthetische Ansätze zum Einbau funktioneller Gruppen in das Polyetherrückgrat bzw. an den Kettenenden vorgestellt werden. Ein besonderes Augenmerk liegt hierbei auf der anionischen Ring-Öffnungspolymerisation (AROP), welche die grundlegende Polymerisationstechnik dieser Arbeit darstellt.

Kapitel 1.2 bietet eine Übersicht zu Liposomen als Wirkstofftransportsysteme und präsentiert aktuelle Entwicklungen in den Bereichen sterisch stabilisierte Liposomen („Stealth Liposomen“), aktives Targeting und stimuli-gesteuerte Wirkstofffreisetzung. Insbesondere die Vorteile von pH-spaltbaren PEG-Lipiden in liposomalen Formulierungen werden in diesem Kapitel diskutiert.

Blockcopolymer-Strukturen auf Basis von Polypropylenoxid (PPO) und PEG (bzw. PEO), mit einem Schwerpunkt auf PEO-*b*-PPO-*b*-PEO Copolymeren (Poloxameren), werden in **Kapitel 1.3** vorgestellt

sowie deren breites Anwendungsspektrum als Tenside. Zudem werden aktuelle Trends im Bereich nicht-ionischer, PEO-/PPO-basierter Tenside erörtert.

Die Nachteile der Nicht-Abbaubarkeit von PEG im Hinblick auf Molekulargewichtsbeschränkungen für den Einsatz in der Biomedizin stehen im Fokus der Betrachtung in **Kapitel 1.4**, wobei vor allem aktuelle Entwicklungen auf dem Gebiet der spaltbaren PEGs zusammengefasst werden. **Kapitel 1.3** und **1.4** sind Auszüge aus einem umfassenden Übersichtsartikel, der in der englischsprachigen Zeitschrift *Chemical Reviews* publiziert wurde.

Kapitel 2 beschäftigt sich mit der Herstellung von Acetal-funktionellen, amphiphilen PEO-*b*-PPO-*b*-PEO Copolymeren und deren Einsatz als pH-spaltbare Tenside (Surfactants) in Miniemulsionspolymerisationen (MEPs). Die säurespaltbaren Poloxamer-Analoga wurden in einem *Proof-of-Concept* Experiment zur Herstellung von Polystyrol-Nanopartikeln mittels MEP in Kooperation mit der Arbeitsgruppe von Dr. Frederik Wurm (Max-Planck-Institut für Polymerforschung) verwendet. Durch eine pH-gesteuerte Spaltung der Polyether-Tenside konnte eine Präzipitation der Nanopartikel induziert werden, die eine effiziente Abtrennung der Additive ermöglicht, wodurch Tensid-freie Nanopartikel erhalten wurden. Diese sind zum einen aus umwelttechnischen Gesichtspunkten von Bedeutung, zum anderen können enthaltene Tenside eine Beeinträchtigung der Partikeleigenschaften bewirken. Die Abtrennung von nicht-spaltbaren Tensiden nach erfolgreicher MEP ist häufig mit großem Aufwand verbunden.

Die Synthese pH-spaltbarer PEGs mit einer einstellbaren Anzahl an säurelabilen Vinylether-Gruppen im Polyetherrückgrat und einer definierten Hydroxyl-Endgruppe wird in **Kapitel 3** behandelt. Durch die anionische ring-öffnende Copolymerisation von 3,4-Epoxy-1-butene (EPB) und Ethylenoxid mit anschließender katalytischer Isomerisierung der Allylether-Gruppen konnten engverteilte, pH-spaltbare P(EPB-*co*-EG) Copolymere mit niedrigen Anteilen an EPB (4 mol%) in einer zweistufigen Synthese hergestellt werden. Durch gelpermeationschromatographische Untersuchungen wurden moderate Molekulargewichtsverteilungen ($\bar{M}_w = 1.6 - 1.8$) der Spaltprodukte ermittelt. Die

Untersuchung der Hydrolysekinetik der Copolymere durch *in situ* ^1H NMR Spektroskopie in einem physiologisch-relevanten pH-Bereich (4.4 – 5.4) zeigte vielversprechende Abbaukinetiken im Hinblick auf biomedizinische Anwendungen, z.B. für spaltbare, langzirkulierende Polymer-Wirkstoff-Konjugate.

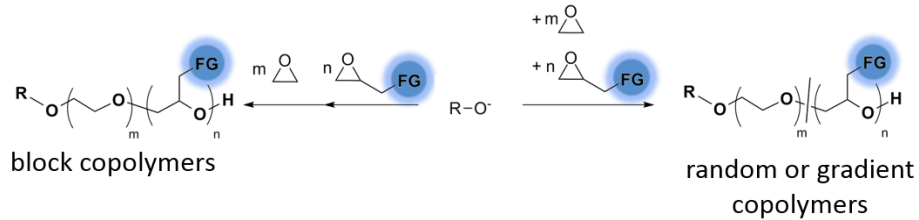
Kapitel 4 beschreibt die Synthese von pH-spaltbaren PEG-Lipiden mit säurelabilen Acetal- und Ketal-Gruppen und deren Einsatz in pH-responsiven „Stealth“-Liposomen. Eine neue Synthesestrategie zur Einführung asymmetrischer Ketale in Polymere wurde entwickelt, um PEG-Lipide mit einstellbaren Molekulargewichten und einer definierten Hydroxyl-Endgruppe zu generieren, wodurch weitere polymeranaloge Umsetzungen möglich sind. Mit Hilfe von *in situ* ^1H NMR Spektroskopie konnte eine signifikant höhere Hydrolysegeschwindigkeit der Ketal-PEG-Lipide im Vergleich zu den Acetal-Derivaten nachgewiesen werden. Die Abspaltungskinetik der PEG-Ketten von der Liposomen-Membran konnte durch speziell entwickelte zeitabhängige, fluoreszenzspektroskopische und gelelektrophoretische Experimente analysiert werden, die in Kooperation mit der Arbeitsgruppe von Prof. Mark Helm (Institut für Pharmazie und Biochemie, Johannes Gutenberg-Universität Mainz) stattfanden. Die mit Ketal-PEG-Lipiden modifizierten Liposomen zeigten schnelle Abspaltungskinetiken der PEG-Korona im schwach sauren Milieu (pH = 5.5 – 6.5), was die neuartigen Lipide zu einer vielversprechenden Strukturklasse für Liposomen-basierte, pH-gesteuerte Wirkstofffreisetzungstrategien insbesondere für die Tumorthherapie macht.

Kapitel 5 stellt einen Vergleich zwischen monofunktionellen, linearen PEG-Lipiden und multifunktionellen, hypervverzweigten Polyglycerin (*hbPG*)-Lipiden hinsichtlich deren Eigenschaften in liposomalen Formulierungen vor. *HbPG*-Lipide mit Molekulargewichten von 3 bis 7 kg mol⁻¹ wurden unter Verwendung eines neuartigen, Dialkyl-basierten *linPG*-Lipids als Makroinitiator für die hypervverzweigende, anionische Ringöffnungspolymerisation von Glycidol durch langsame Monomerzugabe hergestellt. Zudem konnten Dialkyl-PEG-Lipide mit vergleichbaren Molekulargewichten durch AROP von Ethylenoxid synthetisiert werden. In Kooperation mit der

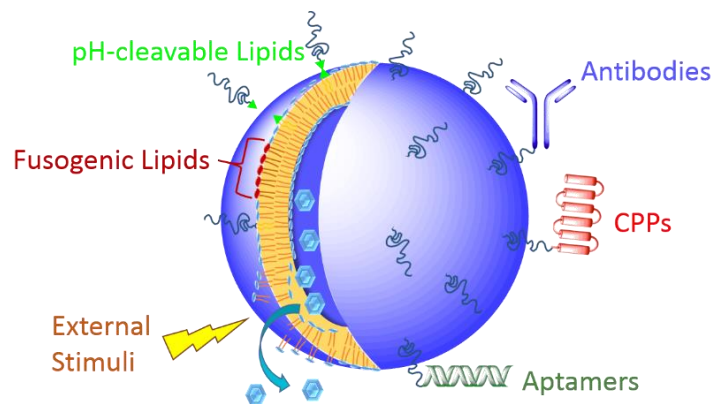
Arbeitsgruppe von Prof. Mark Helm (Institut für Pharmazie und Biochemie, Johannes Gutenberg-Universität Mainz) wurden die *hbPG*-/PEG-Lipide mittels dualer Zentrifugation in Liposomen formuliert, wobei eine Kontrolle der Liposomendurchmesser unterhalb von 100 nm erzielt werden konnte. Dies wurde als optimale Größe für nanoskopische Trägersysteme in der Antitumorthherapie beschrieben. In Zusammenarbeit mit der Arbeitsgruppe von Prof. Frank Rösch (Institut für Kernchemie, Johannes Gutenberg-Universität Mainz) konnten erste *in vivo* Biodistributionsstudien mit ¹⁸F-markierten Lipiden unter Verwendung von Positronen-Emissions-Tomographie (PET) die erwünschte, schnelle renale Ausscheidung der reinen linearen/hyperverzweigten Lipide bestätigen. Für radiomarkierte, Polyether-modifizierte Liposomen wurden Blutzirkulationszeiten von mehr als 1h beobachtet, wodurch erstmals „Stealth“-Eigenschaften *hbPG*-modifizierter Liposomen *in vivo* nachgewiesen werden konnten.

Graphical Abstract

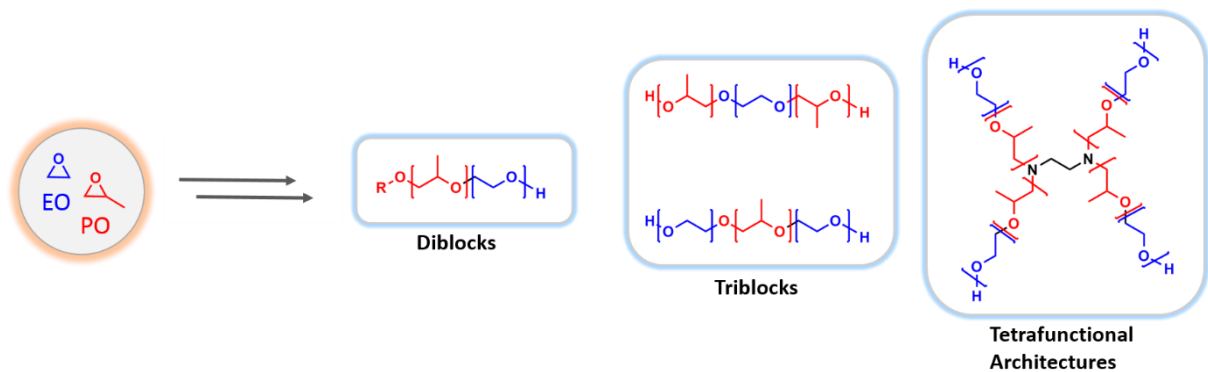
1.1 Functional Poly(ethylene glycol)s and their Application



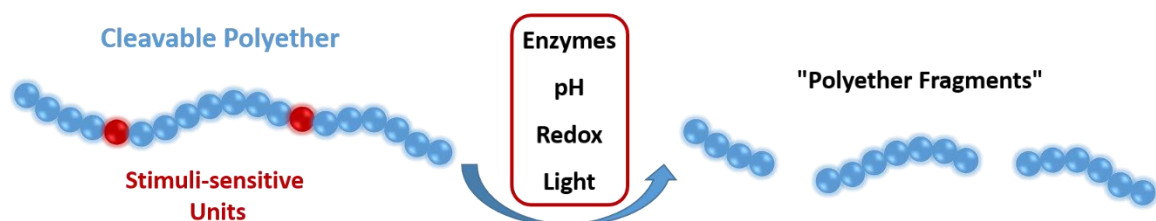
1.2 Liposomes in Biomedicine – An Introduction



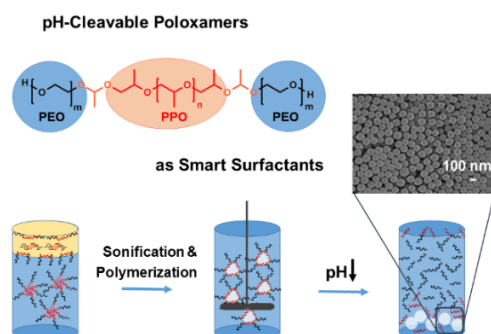
1.3 Block Copolymers of Poly(ethylene glycol) and Poly(propylene oxide)



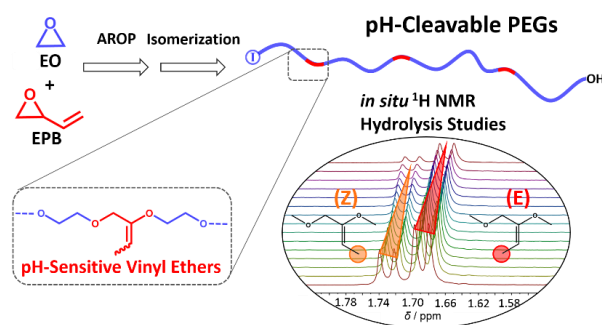
1.4 Cleavable Polyethers



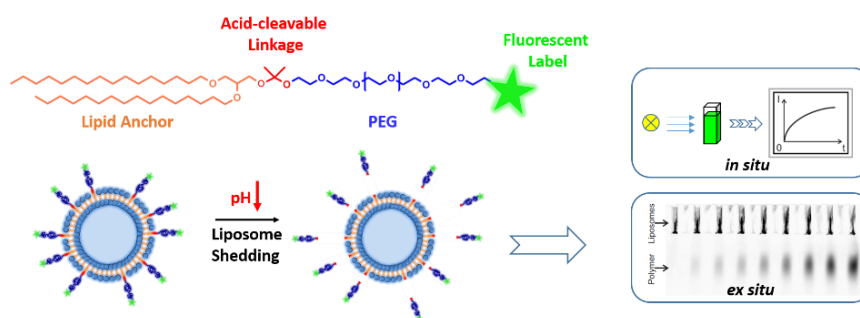
2.1 Acid-labile Amphiphilic PEO-*b*-PPO-*b*-PEO Copolymers: Degradable Poloxamer Analogs



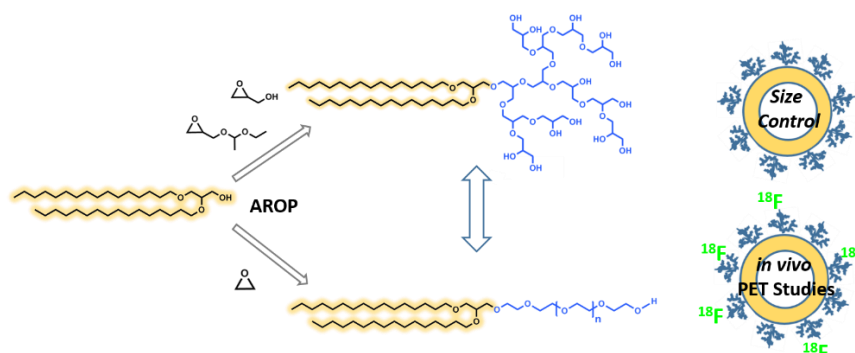
3.1 Cleavable Polyethylene Glycol (PEG): 3,4-Epoxy-1-butene (EPB) as a Comonomer to Establish Degradability at Physiologically Relevant pH



4.1 Ketal- and Acetal-functional Dialkyl-PEG Lipids for pH-Sheddable Liposomes



5.1 Hyperbranched Polyglycerol- and PEG-Lipids in Liposomes: Synthesis, Characterization, and *in vivo* Studies



1 Introduction

1.1 Functional Poly(ethylene glycol)s and their Application

This section provides a brief introduction into polyether chemistry and the utility of polyethers in a broad range of applications.

1.1.1 Aliphatic Polyethers

Polyethers represent a large and versatile class of polymers with unique properties that find widespread application in industries and academia, and are contained in various commodity products.^[1,2] Especially aliphatic polyethers encompass valuable properties due to their high chain flexibility affording low glass transition temperatures and the hydrophilic C–O–C ether linkages along the polymer backbone. These features crucially discriminate them from vinyl- or olefin-based polymers. Although aromatic polyethers offer desirable characteristics as well in terms of stability towards oxidation,^[3] they are beyond the scope of this introduction and will not be further discussed.

Aliphatic polyethers can be readily synthesized using ring-opening polymerization (ROP) of three- to five-membered cyclic ethers. While polymerization of oxetanes (four-membered rings) and oxolanes (five-membered rings) requires cationic polymerization techniques,^[4] epoxides or oxiranes (three-membered rings) can be polymerized not only via cationic, but also via anionic and coordination polymerization.^[5–7] Of these cyclic ethers, epoxides are by far the most versatile and widely used monomers as they are available on large scale, easily accessible by oxidation of olefins,^[8] and, as mentioned above, can be polymerized by different techniques.

The simplest epoxide is ethylene oxide (EO) with a low boiling point of $T_b = 10.5\text{ }^\circ\text{C}$ and a world annual production of twenty-five million tons obtained by oxidation of ethylene with oxygen in the presence of a silver catalyst.^[9,10] EO was first polymerized by Charles Adolphe Wurtz in 1863 with alkali metal hydroxides or zinc chloride,^[11] creating the foundation for later developments in EO polymerization that led to a commercialization of EO-derived polymers in the 1930s. Depending on the field of application and the molecular weight, different names have been associated with

polymers of EO. High molecular weight polymers exceeding $30\,000\text{ g mol}^{-1}$ are often referred to as poly(ethylene oxide) (PEO) or poly(oxy ethylene) (POE), especially in industrial applications, whereas lower MW polymers are usually called poly(ethylene glycol) (PEG). In a pharmaceutical and biomedical context, the term PEG is almost exclusively used. The utility of PEG is diverse, ranging from food additives, skin care products, and detergents to more specialized applications in pharmaceutical formulations.^[2]

1.1.2 Anionic Ring-Opening Polymerization

Anionic ring-opening polymerization (AROP) is regarded as the 'classical' route to polymerize ethylene oxide utilizing nucleophiles to initiate the polymerization. It is noteworthy that aside from AROP, a variety of different techniques, such as activated monomer approaches, metal-free strategies and double metal cyanide (DMC) catalysis have been developed for ethylene oxide polymerization. These techniques have been comprehensively reviewed recently,^[9] and will not be further discussed. In case of AROP, mostly, alkali metal alkoxides of sodium, potassium and cesium are used as initiators, however amides and aryls have likewise been employed.^[6] Merely partial deprotonation of the alcohol compound is required due to rapid proton exchange reactions that occur orders of magnitude faster than initiation and propagation (See Figure 1). Polar, aprotic solvents such as tetrahydrofuran (THF), dimethyl sulfoxide (DMSO) and dioxane are typically used for the AROP.^[12] By choice of the alcohol used as initiator, functional moieties can be incorporated at the α -terminus of PEG, as will be shown in the following paragraph. In addition, the reactive alkoxide chain end can be converted with suitable electrophiles to yield α,ω -functional PEGs in a one-pot reaction. It is noteworthy that AROP needs to be conducted in the absence of moisture as water can initiate the polymerization leading to the formation hydroxyl-initiated PEGs and causing deviations of the molecular weights from the targeted values. Examples of functional groups that have been attached to PEG by conversion of the reactive end group include mesylates,^[13] methacrylates,^[14,15] vinyl benzyl ethers,^[16] hemisuccinates,^[17] and propargyl ethers (See Figure 1).^[18]

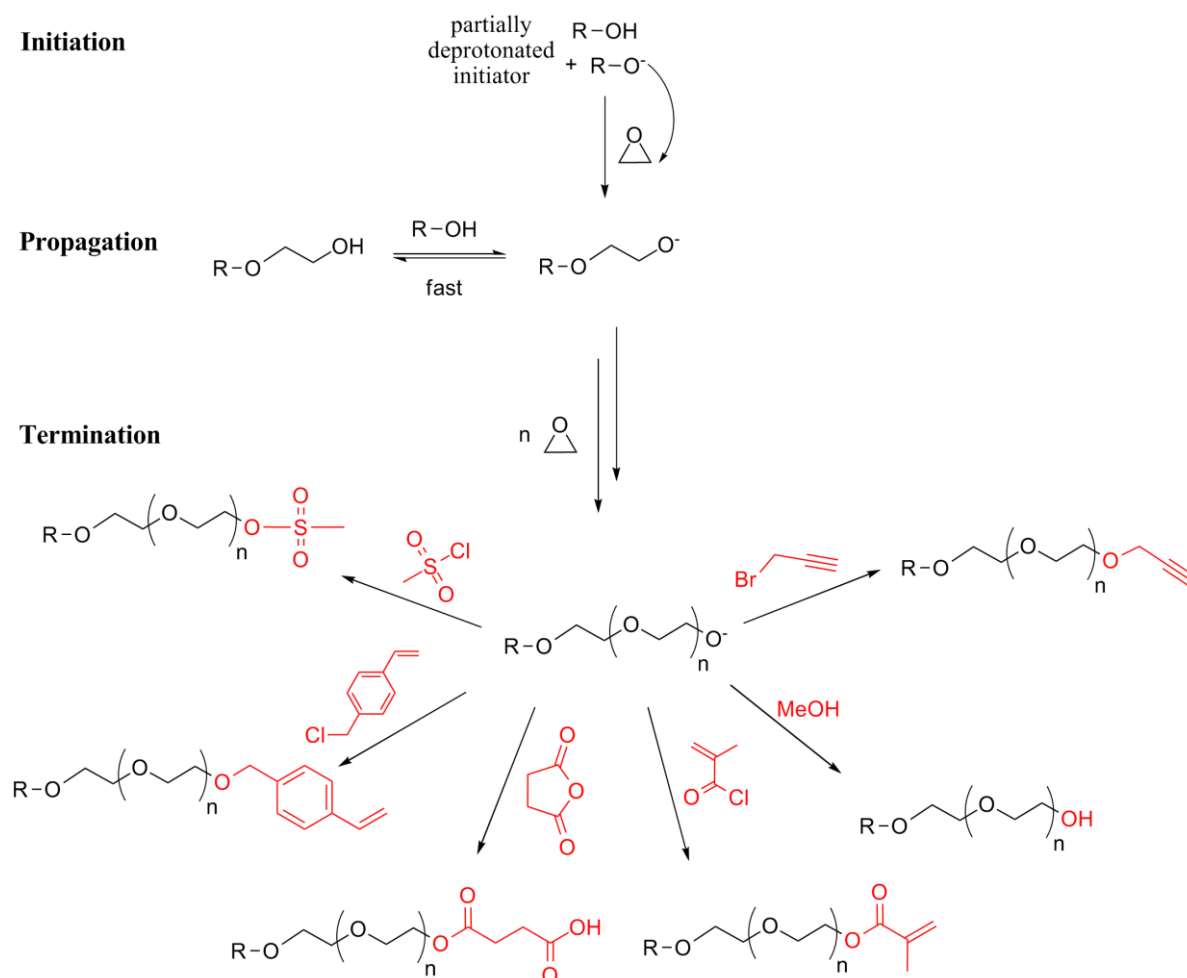


Figure 1: Anionic ring-opening polymerization (AROP) of ethylene oxide including initiation, propagation and termination steps. Termination of the alkoxide end groups with suitable electrophiles provides access to functional PEGs.^[13–18]

Although this compilation of functionalities only displays few examples of possible end groups, a great variety of chemical modifications can be derived from them. For instance, mesylates can be conveniently converted to halides, azides and thiols via nucleophilic substitution reactions,^[13,18] whereas alkynes and succinates are frequently used to conjugate other functional molecules, such as polymeric substrates,^[19,20] peptides and proteins.^[21,22] In contrast, methacrylates and vinyl benzyl ethers can be polymerized via radical or UV-initiated polymerization to access PEG-based hydro- or nanogels. The broad spectrum of end-functionalized PEGs has been excellently reviewed by Riffle and coworkers.^[23]

As for all ionic polymerizations, the choice of solvent as well as the counter ion have crucial impact on polymerization kinetics, as they dictate the reactivity of the chain end (See Figure 2). For instance, in solvents of low to medium polarity, aggregation of alkali metal alkoxides usually leads to a very slow rate of propagation and complex reaction kinetics.^[12] However, in polar solvents such as THF and in the presence of weak Lewis acids as counter ions, i.e. K^+ and Cs^+ , propagation predominantly proceeds via the free alkoxide (dissociated ion pair).^[24] Cryptands (crown ethers) can further serve to increase reactivity of the alkoxide species by complexation of the alkali metal ions.^[25]

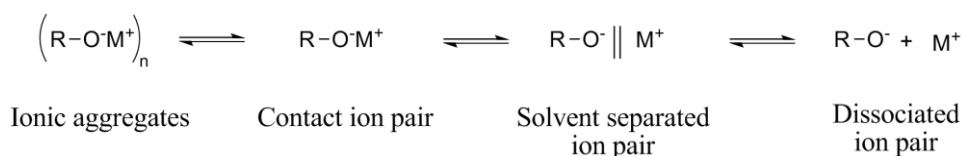


Figure 2: Equilibrium between the different states of metal alkoxides in solution.

Due to the living character of the polymerization, this technique permits the generation of PEGs with Poisson-distributions of molecular weight^[26] and dispersities $\mathcal{D} = M_w/M_n$ below 1.1.^[12] By using functional initiators for the AROP, various end groups, e.g. amines,^[27,28] alkynes,^[29] alkenes,^[30–32] aldehydes,^[33,34] hydroxyl groups,^[18] and catechols^[35,36] can be introduced at the α -terminus of PEG (See Figure 3). In most cases, suitable protective groups need to be installed to ensure integrity of the functional moiety during the polymerization. These protective groups exhibit stability towards strong bases and can typically be cleaved by hydrogenation^[27,28] or acidic hydrolysis.^[18,33–36] If lipophilic alcohols such as cholesterol or 1,2-dialkyl glycols are employed as initiators, amphiphilic block structures can be generated that have been proven particularly advantageous for surface modifications of liposomes.^[37,38] This topic will be highlighted in the following chapter.

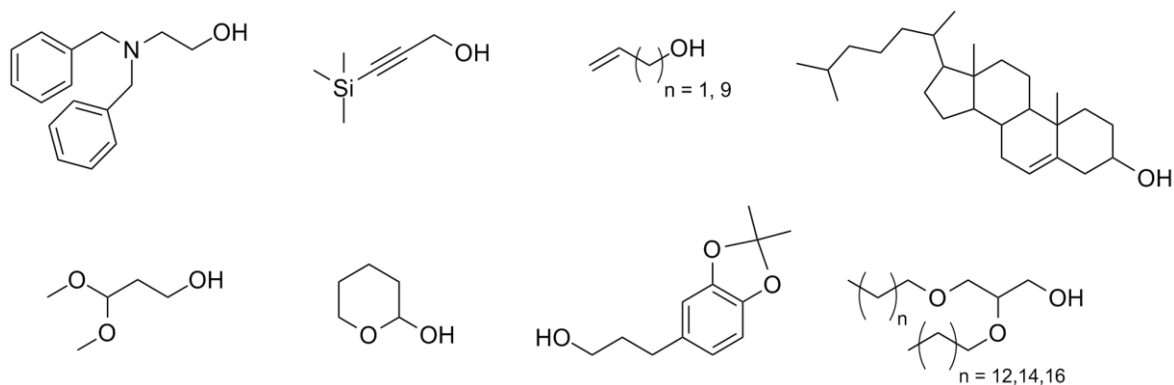


Figure 3: Examples of functional initiators suitable for AROP including protected amines,^[27,28] alkynes,^[29] aldehydes,^[33,34] hydroxyl groups,^[18] and catechols,^[35,36] as well as alkenes,^[30–32] 1,2-dialkyl glycerols and cholesterol.^[37,38]

1.1.3 Multifunctional PEG

Aside from derivatizing PEG at the chain ends, copolymerization of ethylene oxide with other epoxide monomers provides a versatile approach to introduce functional groups distributed along the PEG backbone. The respective epoxide monomers can either be sequentially added to the initiator, resulting in block copolymer formation or may be added simultaneously to yield random or gradient copolymers (See Figure 4). Whether random or gradient structures are formed, strongly depends on the copolymerization parameters for a specific pair of monomers and has recently been investigated with increasing effort.^[39–41]

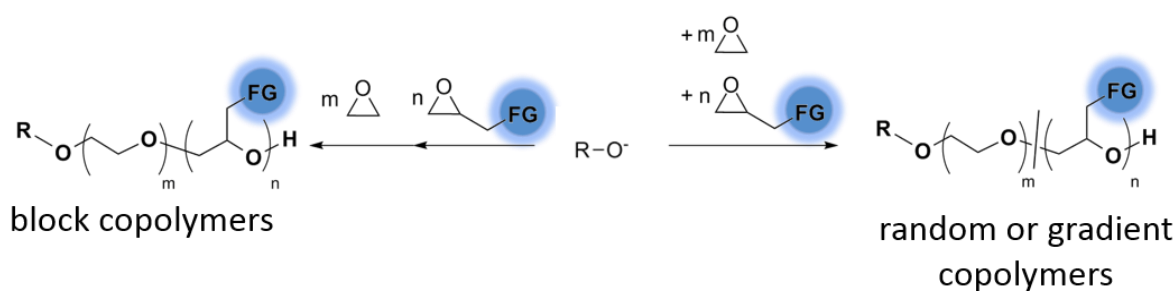


Figure 4: Copolymerization of ethylene oxide and epoxide monomers containing functional groups (FG) resulting in block copolymers in case of sequential monomer addition, whereas random or gradient copolymers are obtained if both monomers are added at once.

Figure 5 compiles various functional epoxides used for the copolymerization of EO via AROP that offer access to multifunctional PEGs (*mf*PEG) with a diverse spectrum of properties. In particular,

pH-, redox- and thermo-responsive PEGs have been the main focus of interest within the last decades. pH-responsive moieties in PEG include protective units e.g. acetals and ketals (**A**) that liberate hydroxyl groups upon acidic hydrolysis,^[27,42,43] as well as *N*-alkyl amines (**C**) that are protonated at lower pH values resulting in a solubility switch from hydrophobic to highly water-soluble.^[44,45] Furthermore, *N*-allyl- and *N*-benzyl protected epoxides (**B**) provide a facile option to introduce primary amines into *mf*PEG that, aside from their pH-responsiveness, facilitate multiple conjugation of functional substrates via conventional amine chemistry.^[46,47]

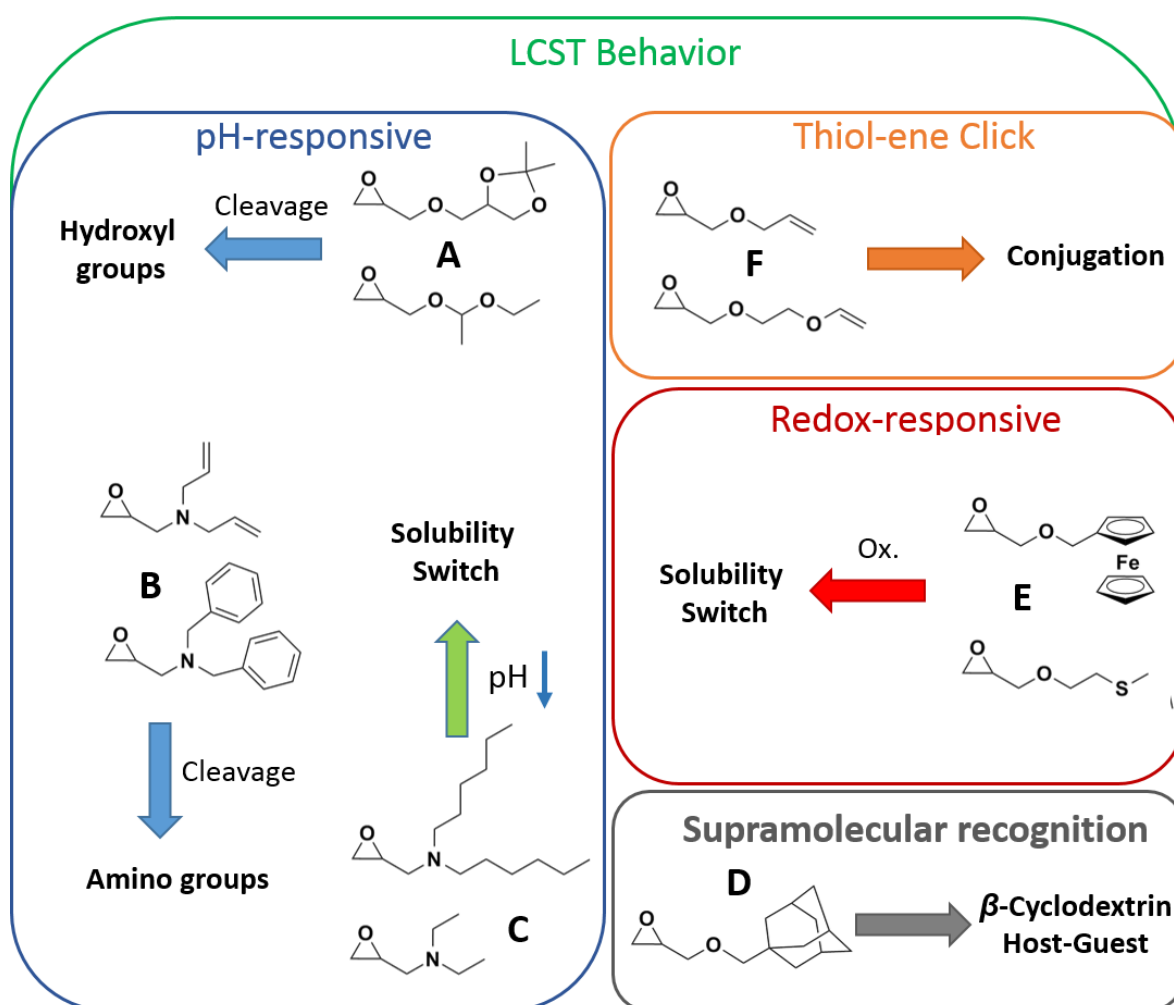


Figure 5: Compilation of functional epoxide monomers that have been copolymerized with ethylene oxide to generate multifunctional PEGs. Depending on the functional group of the epoxide, pH- (blue), redox- (red) and thermo-responsive (green) properties can be introduced or influenced. Functional moieties such as hydroxyl groups **A**, amino groups **B**, vinyl/allyl ethers **F**, and adamantyl residues **D** can further allow for conjugation strategies or supramolecular recognition.

By incorporating functional moieties susceptible to oxidation, such as ferrocene^[48,49] or methyl thioethers (**E**),^[40] solubility switches can be induced in the presence of oxidizing agents. Methyl thioethers represent interesting functional moieties as their oxidation to water-soluble sulfoxides or sulfones can occur in oxidative inflammatory tissue,^[50] rendering the respective *mf*PEGs promising for redox-triggered drug delivery strategies. Olefinic double bonds represent another versatile class of functional groups that have been introduced into PEG via copolymerization of allyl and vinyl ether containing epoxides (**F**).^[51–53] These moieties allow post-polymerization modification by thiol-ene click chemistry,^[53–55] which is also suited for bioconjugation, e.g. by conversion of the cysteine residues in proteins or peptides.^[52] Supramolecular recognition via host-guest complexes has attracted considerable attention lately. For instance, the high binding affinity of adamantanes towards the cavity of β -cyclodextrin has motivated the synthesis of PEG-derived architectures bearing adamantane moieties (**D**).^[56] Notably, PEG constitutes a prominent example of a thermo-responsive polymer exhibiting so called LCST (lower critical solution temperature) behavior. Thermo-responsiveness, in this case, refers to the property of PEG to undergo dehydration and cleavage of hydrogen bonds upon heating, which result in a loss of solubility in water at elevated temperatures (cloud point, $T_c \leq 100$ °C). By introducing functional groups into PEG, interactions of water molecules with the polyether backbone are compromised, leading to altered temperature-dependent solubility and a change in the LCST. The majority of the abovementioned multifunctional PEGs have therefore been investigated in terms of their thermo-responsiveness.^[45,57] As one major incentive, LCST behavior of *mf*PEGs around body temperature (37 °C) might facilitate applications as drug delivery systems for temperature-controlled drug release strategies.

A variety of highly desirable properties has rendered PEG the gold standard polymer for biomedical applications. Due to its excellent biocompatibility, very low immunogenicity, and high water-solubility,^[58] PEG has been covalently attached to bioactive molecules, known as 'PEGylation',^[59,60] in order to improve their pharmacokinetic properties.^[61–63] In particular, PEGylation of a drug reduces antigenic activity and prevents enzymatic degradation and phagocytosis, thereby affording

enhanced blood circulation times,^[64,65] while preserving bioactivity of the pharmaceutical.^[66] Until now, 13 PEGylated proteins and one PEG-aptamer have been approved by the American Food and Drug Administration (FDA) and are available for the treatment of various diseases.^[67] This shielding effect of PEG ('stealth effect') has long been attributed to the dense hydrate shell of solvated PEG chains forming a steric barrier that prevents unspecific protein adsorption.^[68] However, recent findings in this area suggest that PEGylation causes a change in the composition of adsorbed proteins, so called opsonins, that is responsible for the 'stealth effect'.^[69]

In this chapter, an introduction to the chemistry of poly(ethylene glycol)s has been presented with an emphasis on synthetic strategies to incorporate various functional moieties into the backbone or at the polymer chain ends and a brief overview of the broad range of application has been provided. In the next section, a closer look will be taken at the use of PEG in liposomal formulations.

References

- [1] Hargreaves, A. E.; Hargreaves, T. *Royal Society of Chemistry*, London, **2003**, Vol. 32.
- [2] Dingels, C.; Schömer, M.; Frey, H. *CIUZ*, **2011**, *45*, 338–349.
- [3] Jayakannan, M.; Ramakrishnan, S. *Macromol. Rapid Commun.*, **2001**, *22*, 1463–1473.
- [4] Penczek, S.; Kubisa, P.; Matyjaszewski, K. *Adv. Polym. Sci.*, **1985**, *68*, 1–298.
- [5] Penczek, S. *J. Polym. Sci. A Polym. Chem.*, **2000**, *38*, 1919–1933.
- [6] Penczek, S.; Cypryk, M.; Duda, A.; Kubisa, P.; Słomkowski, S. *Prog. Polym. Sci.*, **2007**, *32*, 247–282.
- [7] Dimitrov, I.; Tsvetanov, C. B.; *Polymer Science: A Comprehensive Reference*; Vol. 4, 551-569; Penczek, S.; Grubbs, R. H., Eds.; Matyjaszewski, K.; Möller, M. Series Eds.; Elsevier: Amsterdam, 2012.
- [8] Fingerhut, A.; Serdyuk, O. V.; Tsogoeva, S. B. *Green Chem.*, **2015**, *17*, 2042–2058.
- [9] Herzberger, J.; Niederer, K.; Pohlitz, H.; Seiwert, J.; Worm, M.; Wurm, F. R.; Frey, H. *Chem. Rev.*, **2015**, *116*, 2170–2243.
- [10] Ribeiro, L. G.; Taqueda, M. E. S. *Chem. Eng. Technol.*, **2015**, *38*, 2235–2242.
- [11] Wurtz, C. A. *Ann. Chim. Phys.*, **1863**, *69*, 317–354.
- [12] Deffieux, Alain; Carlotti, Stéphane; Barrère, A. *Polymer Science: A Comprehensive Reference*, Vol. 4, 117-140; Penczek, S.; Grubbs, R. H., Eds.; Matyjaszewski, K.; Möller, M. Series Eds.; Elsevier: Amsterdam, 2012.
- [13] Akiyama, Y.; Otsuka, H.; Nagasaki, Y.; Kato, M.; Kataoka, K. *Bioconjugate Chem.*, **2000**, *11*, 947–950.
- [14] Yagci, Y.; Ito, K. *Macromol. Symp.*, **2005**, *226*, 87–96.
- [15] Ishizu, K.; Furukawa, T. *Polymer*, **2001**, *42*, 7233–7236.
- [16] Hayashi, H.; Iijima, M.; Kataoka, K.; Nagasaki, Y. *Macromolecules*, **2004**, *37*, 5389–5396.
- [17] Ishii, T.; Yamada, M.; Hirase, T.; Nagasaki, Y. *Polym. J.*, **2005**, *37*, 221–228.
- [18] Hiki, S.; Kataoka, K. *Bioconjugate Chem.*, **2010**, *21*, 248–254.

- [19] Jing, R.; Wang, G.; Zhang, Y.; Huang, J. *Macromolecules*, **2011**, *44*, 805–810.
- [20] Opsteen, J. A.; van Hest, J. C. M. *Chem. Commun.*, **2005**, *1*, 57-59.
- [21] Deiters, A.; Cropp, T. Ashton; Summerer, D.; Mukherji, M.; Schultz, P. G. *Bioorg. Med. Chem. Lett.*, **2004**, *14*, 5743–5745.
- [22] Atassi, M. Z.; Manshouri, T. *J. Protein Chem.*, **1991**, *10*, 623–627.
- [23] Thompson, M. S.; Vadala, T. P.; Vadala, M. L.; Lin, Y.; Riffle, J. S. *Polymer*, **2008**, *49*, 345–373.
- [24] Deffieux, A.; Boileau, S. *Polymer*, **1977**, *18*, 1047–1050.
- [25] Stolarzewicz, A.; Neugebauer, D.; Grobelny, J. *Macromol. Rapid Commun.*, **1996**, *17*, 787–793.
- [26] Flory, P. J. *J. Am. Chem. Soc.*, **1940**, *62*, 1561–1565.
- [27] Mangold, C.; Wurm, F.; Obermeier, B.; Frey, H. *Macromol. Rapid Commun.*, **2010**, *31*, 258–264.
- [28] Wurm, F.; Klos, J.; Räder, H. J.; Frey, H. *J. Am. Chem. Soc.*, **2009**, *131*, 7954–7955.
- [29] Xie, Y. M.; Duan, S. F.; Laird Forrest, M. *Drug Discov. Ther.*, **2010**, *4*, 240–245.
- [30] Cammas, S.; Nagasaki, Y.; Kataoka, K. *Bioconjugate Chem.*, **1995**, *6*, 226–230.
- [31] Yue, J.; Li, X.; Mo, G.; Wang, R.; Huang, Y.; Jing, X. *Macromolecules*, **2010**, *43*, 9645–9654.
- [32] Pozza, Gladys M. -E.; Barthel, M. J.; Crotty, S.; Vitz, J.; Schacher, F. H.; Lutz, P. J.; Schubert, U. S. *Eur. Polym. J.*, **2014**, *57*, 221–236.
- [33] Otsuka, H.; Nagasaki, Y.; Kataoka, K. *Langmuir*, **2004**, *20*, 11285–11287.
- [34] Studer, P.; Limal, D.; Breton, P.; Riess, G. *Bioconjugate Chem.*, **2005**, *16*, 223–229.
- [35] Wilms, V. S.; Bauer, H.; Tonhauser, C.; Schilman, A. M.; Muller, M. C.; Tremel, W.; Frey, H. *Biomacromolecules*, **2013**, *14*, 193–199.
- [36] Thomas, A.; Bauer, H.; Schilman, A.-M.; Fischer, K.; Tremel, W.; Frey, H. *Macromolecules*, **2014**, *47*, 4557–4566.
- [37] Hofmann, A. M.; Wurm, F.; Hühn, E.; Nawroth, T.; Langguth, P.; Frey, H. *Biomacromolecules*, **2010**, *11*, 568–574.

- [38] Hofmann, A. M.; Wurm, F.; Frey, H. *Macromolecules*, **2011**, *44*, 4648–4657.
- [39] Lee, B. F.; Wolffs, M.; Delaney, K. T.; Sprafke, J. K.; Leibfarth, F. A.; Hawker, C. J.; Lynd, N. A. *Macromolecules*, **2012**, *45*, 3722–3731.
- [40] Herzberger, J.; Fischer, K.; Leibig, D.; Bros, M.; Thiermann, R.; Frey, H. *J. Am. Chem. Soc.*, **2016**, *138*, 9212–9223.
- [41] Niederer, K.; Schüll, C.; Leibig, D.; Johann, T.; Frey, H. *Macromolecules*, **2016**, *49*, 1655–1665.
- [42] Thomas, A.; Niederer, K.; Wurm, F.; Frey, H. *Polym. Chem.*, **2014**, *5*, 899–909.
- [43] Southan, A.; Hoch, E.; Schonhaar, V.; Borchers, K.; Schuh, C.; Muller, M.; Bach, M.; Tovar, Gunter E. M. *Polym. Chem.*, **2014**, *5*, 5350–5359.
- [44] Reuss, V. S.; Werre, M.; Frey, H. *Macromol. Rapid Commun.*, **2012**, *33*, 1556–1561.
- [45] Herzberger, J.; Kurzbach, D.; Werre, M.; Fischer, K.; Hinderberger, D.; Frey, H. *Macromolecules*, **2014**, *47*, 7679–7690.
- [46] Reuss, V. S.; Obermeier, B.; Dingels, C.; Frey, H. *Macromolecules*, **2012**, *45*, 4581–4589.
- [47] Obermeier, B.; Wurm, F.; Frey, H. *Macromolecules*, **2010**, *43*, 2244–2251.
- [48] Tonhauser, C.; Alkan, A.; Schömer, M.; Dingels, C.; Ritz, S.; Mailänder, V.; Frey, H.; Wurm, F. R. *Macromolecules*, **2013**, *46*, 647–655.
- [49] Alkan, A.; Natalello, A.; Wagner, M.; Frey, H.; Wurm, F. R. *Macromolecules*, **2014**, *47*, 2242–2249.
- [50] Napoli, A.; Valentini, M.; Tirelli, N.; Muller, M.; Hubbell, J. A. *Nat. Mater.*, **2004**, *3*, 183–189.
- [51] Lee, B. F.; Kade, M. J.; Chute, J. A.; Gupta, N.; Campos, L. M.; Fredrickson, G. H.; Kramer, E. J.; Lynd, N. A.; Hawker, C. J. *J. Polym. Sci. A Polym. Chem.*, **2011**, *49*, 4498–4504.
- [52] Obermeier, B.; Frey, H. *Bioconjugate Chem.*, **2011**, *22*, 436–444.
- [53] Mangold, C.; Dingels, C.; Obermeier, B.; Frey, H.; Wurm, F. *Macromolecules*, **2011**, *44*, 6326–6334.

- [54] Sokolovskaya, E.; Yoon, J.; Misra, A. C.; Bräse, S.; Lahann, J. *Macromol. Rapid Commun.*, **2013**, *34*, 1554–1559.
- [55] Koyama, Y.; Umehara, M.; Mizuno, A.; Itaba, M.; Yasukouchi, T.; Natsume, K.; Suginaka, A. *Bioconjugate Chem.*, **1996**, *7*, 298–301.
- [56] Moers, C.; Wrazidlo, R.; Natalello, A.; Netz, I.; Mondeshki, M.; Frey, H. *Macromol. Rapid Commun.*, **2014**, *35*, 1075–1080.
- [57] Mangold, C.; Obermeier, B.; Wurm, F.; Frey, H. *Macromol. Rapid Commun.*, **2011**, *32*, 1930–1934.
- [58] Fruijtier-Pölloth, C. *Toxicology*, **2005**, *214*, 1–38.
- [59] Abuchowski, A.; McCoy, J. R.; Palczuk, N. C.; van Es, T.; Davis, F. F. *J. Biol. Chem.*, **1977**, *252*, 3582–3586.
- [60] Abuchowski, A.; van Es, T.; Palczuk, N. C.; Davis, F. F. *J. Biol. Chem.*, **1977**, *252*, 3578–3581.
- [61] Roberts, M. J.; Bentley, M. D.; Harris, J. M., **2012**, *64*, 116–127.
- [62] Ryan, S. M.; Mantovani, G.; Wang, X.; Haddleton, D. M.; Brayden, D. J. *Expert Opin. Drug Deliv.*, **2008**, *5*, 371–383.
- [63] Caliceti, P.; Veronese, F. M. *Adv. Drug Delivery Rev.*, **2003**, *55*, 1261–1277.
- [64] Khandare, J.; Minko, T. *Prog. Polym. Sci.*, **2006**, *31*, 359–397.
- [65] Harris, J. Milton; Chess, R. B. *Nat Rev Drug Discov*, **2003**, *2*, 214–221.
- [66] Bailon, P.; Won, C.-Y. *Expert Opin. Drug Deliv.*, **2009**, *6*, 1–16.
- [67] Alconcel, Steevens N. S.; Baas, A. S.; Maynard, H. D. *Polym. Chem.*, **2011**, *2*, 1442–1448.
- [68] Pasut, G.; Veronese, F. M. *J. Control. Release*, **2012**, *161*, 461–472.
- [69] Schöttler, S.; Becker, G.; Winzen, S.; Steinbach, T.; Mohr, K.; Landfester, K.; Mailänder, V.; Wurm, F. R. *Nat. Nano*, **2016**, *11*, 372–377.

1.2 Liposomes in Biomedicine – An Introduction

1.2.1 Liposomes – Characteristics and Properties

Since their discovery by Bangham in the 1960s,^[1] liposomes have experienced an evolution from interesting biophysical objects to pharmaceutical drug carriers of choice in numerous clinical applications.^[2] Liposomes are composed of natural phospholipids assembled in spherical bilayer structures that consist of an aqueous core and a lipophilic bilayer membrane. In addition to their excellent biocompatibility, these amphiphilic core-shell structures permit encapsulation of hydrophilic and hydrophobic cargo molecules rendering liposomes versatile carrier systems in food technology,^[3,4] cosmetics,^[5,6] and biomedical applications.^[2,7] Figure 1 shows an overview of the different types of liposomes that are known.

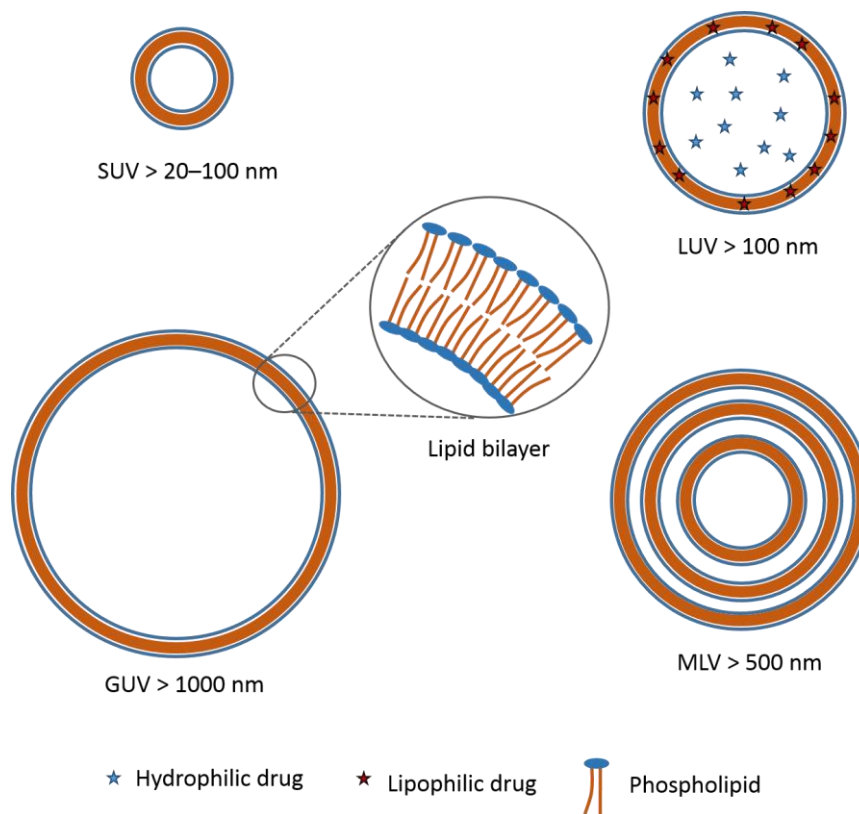


Figure 6: Bilayer vesicles composed of phospholipids with different size and lamellarity classified as small unilamellar vesicles (SUVs), large unilamellar vesicles (LUVs), giant unilamellar vesicles (GUVs) and multilamellar vesicles (MLVs). Hydrophilic drugs can be entrapped in the core, whereas lipophilic drugs are incorporated into the bilayer membrane.

Among bilayer vesicles, four different types of liposomes can be classified depending of their size and lamellarity, as shown in Figure 6. In case of liposomes comprised of a single bilayer, small (SUVs), large (LUVs) and giant lamellar vesicles (GUVs) are usually distinguished. It is important to note that the size of a liposome crucially affects its fate *in vivo*, as larger liposomes are generally taken up more rapidly by the reticulo-endothelial system (RES) compared to their smaller counterparts.^[8] If the number of bilayers increases, as in multilamellar vesicles (MLVs), differences in drug entrapment capacities, drug release profiles, liposome-cell interactions and internalization are observed.^[9]

Aside from size and lamellarity, the composition of lipids predominately dictates the properties of liposomes. In particular, the phase transition temperature T_M of the phospholipid constitutes an important parameter affecting stability. Below T_M , lipids exist in a gel state that undergoes a transition into a fluid phase upon heating ($T > T_M$) that is accompanied by a drop in stability and increased leakiness of the liposome.^[7] In general, phospholipids containing unsaturated alkyl chains such as 1,2-dioleoyl-*sn*-glycero-3-phosphocholine (DOPC) or 1,2-dioleoyl-*sn*-glycero-3-phosphoethanolamine (DOPE) exhibit lower values of T_M , opposed to saturated lipids e.g., 1,2-distearoyl-*sn*-glycero-3-phosphoethanolamine (DSPE). In order to further increase stability of the bilayer, cholesterol can be added to the formulations.^[10] On the other hand, the chemical nature of the polar head group, also contributes to the stability of liposome, since electrostatic repulsion between cationic or anionic head groups leads to decreased stability profiles and promotes aggregation of liposomes. Despite these stability-related issues, cationic lipids are frequently employed to encapsulate nucleic acids such as DNA or RNA (lipoplex formation) for gene therapy and to initiate cell internalization due to interactions of cationic liposomes with negatively charged cell membranes.^[11]

To date, several liposomal drug formulations have been approved for the treatment of various diseases, including fungal infections,^[12] hepatitis A,^[13] influenza,^[14] and various cancer types.^[15–17] Many of these systems are based on surface-modified liposomes ('stealth liposomes') that will be

discussed in detail in the next section. Moreover, numerous potential candidates are currently tested in clinical trials.^[7]

Various methods are available for the preparation of liposomes including conventional techniques such as thin film hydration,^[18] membrane extrusion,^[19] and reverse phase evaporation,^[20] as well as novel methods e.g. micro hydrodynamic focusing,^[21] supercritical reverse phase evaporation,^[22] and dual centrifugation.^[23,24] Depending on the choice of technique, properties of the liposomes differ with respect to size, polydispersity, lamellarity and encapsulation efficiency (EE). Conventional methods are generally well-suited for straightforward, small-scale preparations, however, they usually lack the possibility for scale-up and control of EEs, and often result in broad size distributions.^[7] In contrast, some of the novel methods are performed in continuous flow that allow scale-up and precise control of liposomal properties.^[21]

1.2.2 Sterically Stabilized Liposomes

Despite their mimicry of cells and their excellent biocompatibility, conventional liposomes are subjected to interactions with plasma proteins when applied *in vivo* that result in uptake by macrophages predominantly in the liver and the spleen affecting short blood circulation times.^[25] A prominent strategy to avoid uptake by the RES is based on the use of polyethylene glycol (PEG), introduced in Chapter 1.1, to modify the surface of liposomes. In liposomal research, PEGylated lipids have been inserted into lipid bilayers with the PEG chains projecting into the surrounding aqueous medium to form sterically stabilized liposomes (SSLs), also known as ‘stealth liposomes’ (See Figure 7). Compared to conventional liposomes, stealth liposomes exhibit prolonged serum half-lives and improved safety profiles.^[26,27] The stealth effect has been shown to be more efficient for higher molecular weights of PEG and increased molar content of the PEG-lipids in the lipid composition due to a transition of PEG chains from a so-called ‘mushroom’ to a ‘brush conformation’ that strongly influences protein binding at the liposomal surface.^[28]

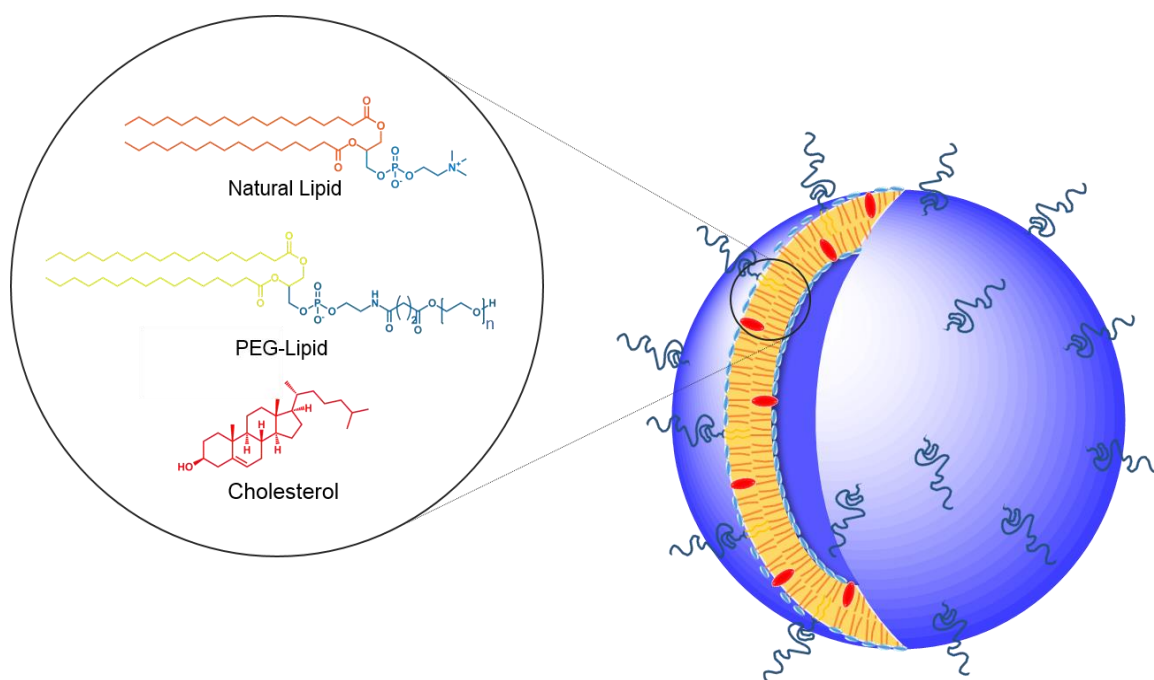


Figure 7: Schematic representation of a typical stealth liposome composed of the natural phospholipid 1,2-distearoyl-sn-glycero-3-phosphoethanolamine DSPE, PEGylated DSPE and cholesterol.

Especially in anti-cancer therapy, stealth liposomes have proven particular advantageous.^[2] It is a generally accepted view, that liposomes and other nanoparticles passively accumulate in the tumor tissue due to enlarged gaps between the endothelial cells and the leaky vasculature in the tumor microenvironment compared to healthy tissue.^[29,30] In addition, lymphatic drainage is usually down-regulated in tumor tissue effecting a retention of the drug carriers.^[31] This phenomenon was termed “enhanced permeability and retention” (EPR) effect,^[31,32] and is generally held responsible for the enhanced accumulation of long-circulating liposomes at the tumor site.^[33] To what extent a certain tumor is susceptible towards passive targeting, strongly depends on the state of the tumor and the specific cell line.^[29] Several studies suggest that a diameter of 100 nm can be considered as an optimum for liposomes in terms of drug efficiencies.^[34]

However, it has been observed that even in case of EPR-mediated concentration of liposomes in the tumor tissue, cellular uptake, endosomal escape and drug release from the bilayer vesicles is hampered in the presence of a PEG stealth layer.^[35] Moreover, with complex tumor microenvironments, homogenous distribution of drug-loaded liposomes throughout the entire

tumor is not always possible, which can result in insufficient local drug administration and multidrug resistance of tumors.^[36,37]

It is important to note that, in spite of the above-mentioned challenges, PEG-modified liposomes are routinely employed in a variety of clinical applications and many of the currently investigated nanocarrier systems utilize the concept of PEGylation.

1.2.3 Stimuli-Triggered Drug Release and Active Cell Targeting

One interesting strategy to circumvent the hampering effect of a PEG stealth layer on cellular uptake is based on introducing stimuli-responsive behavior to liposomes. By exploiting certain physiological characteristics of the targeted tissue or cellular compartments, stimuli-triggered detachment of PEG from liposomes can promote cell internalization and drug release. Especially the lowered pH value (≤ 6.0) in the microenvironment of various tumors,^[38] has motivated the development of pH-sensitive liposomes (PSLs) that are stable at physiological pH, but are subjected to PEG shedding once they reach the tumor site. A variety of pH-hydrolyzable moieties have been incorporated at the block junctions of PEG-lipids to implement pH-triggered release strategies, for instance hydrazone linkages,^[39–41] orthoesters,^[42–44] acetals,^[45] and vinyl ethers.^[46,47]

Accelerated blood clearance (ABC) represents one major disadvantage of PEGylated nanoparticles that arises upon repeated administration of a formulation affecting an increased uptake by the liver.^[48–50] PSLs have recently been demonstrated to circumvent the ABC phenomena,^[39,50] justifying the use of pH-cleavable lipids and providing further motivation for future research in this field.

Moreover, the use of ‘fusogenic’ lipids,^[51] or peptides, also known as pH low insertion peptides (pHLIPs),^[52,53] have recently attracted considerable attention. These structures are stable at neutral pH and undergo conformational changes in acidic media that trigger insertion into membranes and lead to fusion of the liposomes with cell membranes.^[54] For instance, drug release from endosomal cellular compartments into the cytoplasm (endosomal escape) can be induced by using fusogenic

lipids to promote the delivery and transfection of oligo- or polynucleotides like siRNA or plasmid DNA.^[55]

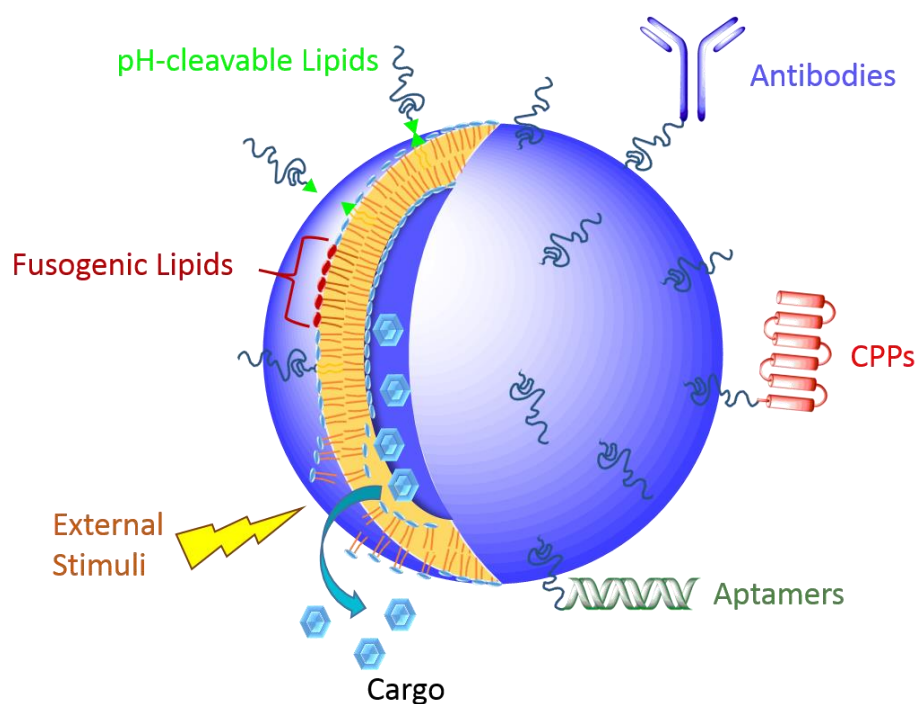


Figure 8: Schematic representation of a modified stealth liposome illustrating strategies to allow active targeting by attaching antibodies, aptamers or cell-penetrating peptides (CPPs) onto the surface, and to accomplish stimuli-triggered drug (cargo) release by using fusogenic lipids, pH-cleavable lipids or external stimuli (magnetic fields, ultrasound, heat).

Aside from physiologically determined release strategies, external stimuli have also been examined as triggers for drug release from liposomes. Prominent examples include thermosensitive liposomes that show increased drug permeability of the lipid bilayer upon locally applied mild hypothermia,^[56] and ecogenic liposomes that release encapsulated air by mechanical stimulation *via* ultrasound causing disruption of the membrane.^[57] In addition, magnetically sensitive liposomes have been designed by incorporating magnetic nanoparticles into liposomes permitting triggered drug release in the presence of an external magnetic field.^[58]

To further improve the efficacy of long-circulating liposomal drug carriers, targeting ligands can be attached to the liposomes that show high binding affinities towards specific receptors on cell membranes. These receptors should be exclusively expressed or at least, overexpressed on the

targeted cells to avoid non-specific binding and undesired toxic effects.^[7] This concept is known as active targeting and various targeting units including antibodies,^[59–62] folates,^[63,64] and aptamers^[65] have been successfully utilized to enhance the efficiency of drug-loaded liposomes. Another class of active targeting molecules are cell penetrating peptides (CPPs) that lack the selectivity of the above-mentioned systems, however, are capable of inducing cell internalization of liposomes and cargo release when exposed on the vesicles' surfaces.^[66,67] In case of PEGylated liposomes, active targeting is more effective, if the targeting ligand is linked to the distal end of the PEG chains opposed to direct conjugation to the surface of liposomes.^[68]

As a disadvantage for the further development of targeting concepts, PEG-lipids solely exhibit a single terminal hydroxyl group that is available for functionalization, limiting chemical modifications and prohibiting the attachment of multiple functional moieties e.g. fluorescent dyes, radio tracers and target units to the same lipid. To this end, lipids containing hyperbranched polyglycerol (*hbPG*) as multifunctional PEG substitutes have been developed recently,^[69] and were successfully functionalized with fluorescent labels and radioactive nuclides to monitor the fate of the liposomes *in vitro* and *in vivo*.^[70,71] Significant advancements in dynamic light scattering (DLS) methodology developed by Schmidt and Coworkers enabled investigation of the behavior of polyether-modified liposomes in human serum. The reported findings suggest favorable properties of *hbPG*-functional lipids compared to PEG-lipids in terms of liposome aggregation in serum.^[72] However, so far, studies on the biodistribution of liposomes containing *hbPG*-lipids *via* positron emission tomography (PET) imaging in mice, revealed low carrier stability *in vivo* and rapid renal excretion of lipid components,^[71] raising demand for further research activities in this field to establish enhanced stability profiles of these liposomal carriers.

An innovative approach combining many of the aforementioned concepts has recently been reported by Apte *et al.*^[73] who employed hydrazone-linked PEG₂₀₀₀-lipids bearing monoclonal antibodies (mAb) at the distal chain ends combined with non-cleavable PEG₁₀₀₀-lipids functionalized with CPPs. While the long-chain ($M_n = 2000 \text{ g mol}^{-1}$), pH-cleavable PEG-lipids prevent uptake by the

RES during blood circulation and allow debonding of the PEG chains inside the tumor tissue, the presence of antibodies provides active targeting. Upon detachment of PEG, CPPs are exposed at the liposomal surface to induce additional cell uptake. Significant reduction of tumor size was observed compared to unmodified stealth liposomes.

Although, tremendous progress has been achieved in the design of liposomal carriers as illustrated in this chapter, current systems do not fulfill all requirements for a highly efficient and selective treatment. Novel pathways in the design of lipids seem necessary (I) to assure high carrier stability during circulation, (II) to warrant selective uptake by the targeted cells and (III) to induce controlled drug release from the liposomes at the intracellular site of action.

References

- [1] Bangham, A. D.; Standish, M. M.; Watkins, J. C. *J. Mol. Biol.*, **1965**, *13*, 238–252.
- [2] Torchilin, V. P. *Nat Rev Drug Discov*, **2005**, *4*, 145–160.
- [3] Reza Mozafari, M.; Johnson, C.; Hatziantoniou, S.; Demetzos, C. *J. Liposome Res.*, **2008**, *18*, 309–327.
- [4] Taylor, T. Matthew; Weiss, J.; Davidson, P. Michael; Bruce, B. D. *Critical Reviews in Food Science and Nutrition*, **2005**, *45*, 587–605.
- [5] Mu, L.; Sprando, R. L. *Pharm. Res.*, **2010**, *27*, 1746–1749.
- [6] Betz, G.; Aeppli, A.; Menshutina, N.; Leuenberger, H. *Int. J. Pharm.*, **2005**, *296*, 44–54.
- [7] Pattni, B. S.; Chupin, V. V.; Torchilin, V. P. *Chem. Rev.*, **2015**, *115*, 10938–10966.
- [8] Allen, T. M.; Everest, J. M. *J. Pharmacol. Exp. Ther.*, **1983**, *226*, 539.
- [9] Fröhlich, M.; Brecht, V.; Peschka-Süss, R. *Chem. Phys. Lipids*, **2001**, *109*, 103–112.
- [10] Vemuri, S.; Rhodes, C. T. *Pharm. Acta Helv.*, **1995**, *70*, 95–111.
- [11] Miller, C. R.; Bondurant, B.; McLean, S. D.; McGovern, K. A.; O'Brien, D. F. *Biochemistry*, **1998**, *37*, 12875–12883.
- [12] Meunier, F.; Prentice, H. G.; Ringdén, O. *J. Antimicrob. Chemother.*, **1991**, *28*, 83–91.
- [13] Usonis, V.; Bakasénas, V.; Valentelis, R.; Katiliene, G.; Vidzeniene, D.; Herzog, C. *Vaccine*, **2003**, *21*, 4588–4592.
- [14] Mischler, R.; Metcalfe, I. C. *Vaccine*, **2002**, *20*, Supplement 5, B17–B23.
- [15] Park, J. W. *Breast Cancer Res.*, **2002**, *4*, 95–99.
- [16] Fassas, A.; Anagnostopoulos, A. *Leuk. Lymphoma*, **2005**, *46*, 795–802.
- [17] Andreopoulou, E.; Gaiotti, D.; Kim, E.; Downey, A.; Mirchandani, D.; Hamilton, A.; Jacobs, A.; Curtin, J.; Muggia, F. *Ann. Oncol.*, **2007**, *18*, 716–721.
- [18] Reeves, J. P.; Dowben, R. M. *J. Cell. Physiol.*, **1969**, *73*, 49–60.
- [19] Popa, R.; Vrânceanu, M.; Nikolaus, S.; Nirschl, H.; Lenewit, G. *Langmuir*, **2008**, *24*, 13030–13036.

- [20] Szoka, F.; Papahadjopoulos, D. *PNAS*, **1978**, *75*, 4194–4198.
- [21] Jahn, A.; Vreeland, W. N.; Gaitan, M.; Locascio, L. E. *J. Am. Chem. Soc.*, **2004**, *126*, 2674–2675.
- [22] Otake, K.; Imura, T.; Sakai, H.; Abe, M. *Langmuir*, **2001**, *17*, 3898–3901.
- [23] Massing, U.; Cicko, S.; Ziroli, V. *J. Control. Release*, **2008**, *125*, 16–24.
- [24] Meier, S.; Pütz, G.; Massing, U.; Hagemeyer, C. E.; Elverfeldt, D. von; Meißner, M.; Ardipradja, K.; Barnert, S.; Peter, K.; Bode, C.; Schubert, R.; von zur Muhlen, C. *Biomaterials*, **2015**, *53*, 137–148.
- [25] Awasthi, V. D.; Garcia, D.; Goins, B. A.; Phillips, W. T. *Int. J. Pharm.*, **2003**, *253*, 121–132.
- [26] Woodle, M. C. *Chem. Phys. Lipids*, **1993**, *64*, 249–262.
- [27] Pasut, G.; Paolino, D.; Celia, C.; Mero, A.; Joseph, A. S.; Wolfram, J.; Cosco, D.; Schiavon, O.; Shen, H.; Fresta, M. *J. Control. Release*, **2015**, *199*, 106–113.
- [28] Lee, H.; Larson, R. G. *Biomacromolecules*, **2016**, *17*, 1757–1765.
- [29] Yuan, F.; Dellian, M.; Fukumura, D.; Leunig, M.; Berk, D. A.; Torchilin, V. P.; Jain, R. K. *Cancer Res.*, **1995**, *55*, 3752.
- [30] Hobbs, S. K.; Monsky, W. L.; Yuan, F.; Roberts, W. Gregory; Griffith, L.; Torchilin, V. P.; Jain, R. K. *PNAS*, **1998**, *95*, 4607–4612.
- [31] Fang, J.; Nakamura, H.; Maeda, H. *Adv. Drug Delivery Rev.*, **2011**, *63*, 136–151.
- [32] Matsumura, Y.; Maeda, H. *Cancer Res.*, **1986**, *46*, 6387.
- [33] Torchilin, V. *Adv. Drug Delivery Rev.*, **2011**, *63*, 131–135.
- [34] Nagayasu, A.; Uchiyama, K.; Kiwada, H. *Adv. Drug Delivery Rev.*, **1999**, *40*, 75–87.
- [35] Hong, R.-L.; Huang, C.-J.; Tseng, Y.-L.; Pang, V. F.; Chen, S.-T.; Liu, J.-J.; Chang, F.-H. *Clin. Cancer Res.*, **1999**, *5*, 3645.
- [36] Bae, Y. H. *J. Control. Release*, **2009**, *133*, 2–3.
- [37] Patel, N. R.; Pattni, B. S.; Abouzeid, A. H.; Torchilin, V. P. *Adv. Drug Delivery Rev.*, **2013**, *65*, 1748–1762.

- [38] Gerweck, L. E.; Vijayappa, S.; Kozin, S. *AACT*, **2006**, *5*, 1275–1279.
- [39] Chen, D.; Liu, W.; Shen, Y.; Mu, H.; Zhang, Y.; Liang, R.; Wang, A.; Sun, K.; Fu, F. *J. Nanomed.*, **2011**, *6*, 2053–2061.
- [40] Daquan Chen; Xiaoqun Jiang; Yanyu Huang; Can Zhang; Qineng Ping *J. Bioact. Compat. Polym.*, **2010**, *25*, 527–542.
- [41] Zhang, L.; Wang, Y.; Yang, Y.; Liu, Y.; Ruan, S.; Zhang, Q.; Tai, X.; Chen, J.; Xia, T.; Qiu, Y.; Gao, H.; He, Q. *ACS Appl. Mater. Interfaces*, **2015**, *7*, 9691–9701.
- [42] Guo, X.; Szoka, F. C. J., *Bioconjugate Chem.*, **2001**, *12*, 291–300.
- [43] Li, W.; Huang, Z.; MacKay, J. A.; Grube, S.; Szoka, F. C. *J. Gene Med.*, **2005**, *7*, 67–79.
- [44] Masson, C.; Garinot, M.; Mignet, N.; Wetzter, B.; Mailhe, P.; Scherman, D.; Bessodes, M. *J. Control. Release*, **2004**, *99*, 423–434.
- [45] Wong, J. B.; Grosse, S.; Tabor, A. B.; Hart, S. L.; Hailes, H. C. *Mol. Biosyst.*, **2008**, *4*, 532–541.
- [46] Shin, J.; Shum, P.; Thompson, D. H. *J. Control. Release*, **2003**, *91*, 187–200.
- [47] Shin, J.; Shum, P.; Grey, J.; Fujiwara, S.-i.; Malhotra, G. S.; González-Bonet, A.; Hyun, S.-H.; Moase, E.; Allen, T. M.; Thompson, D. H. *Mol. Pharmaceutics*, **2012**, *9*, 3266–3276.
- [48] Dams, Els T. M.; Laverman, P.; Oyen, Wim J. G.; Storm, G.; Scherphof, G. L.; van der Meer, Jos W. M.; Corstens, Frans H. M.; Boerman, O. C. *J. Pharm. Exp. Ther.*, **2000**, *292*, 1071–1079.
- [49] Laverman, P.; Carstens, M. G.; Boerman, O. C.; Th. M. Dams, Els; Oyen, Wim J. G.; van Rooijen, N.; Corstens, Frans H. M.; Storm, G. *J. Pharm. Exp. Ther.*, **2001**, *298*, 607–612.
- [50] Abu Lila, Amr S.; Kiwada, H.; Ishida, T. *J. Control. Release*, **2013**, *172*, 38–47.
- [51] Deshpande, P. P.; Biswas, S.; Torchilin, V. P. *Nanomedicine (London, England)*, **2013**, *8*, 1509–1528.
- [52] Yao, L.; Daniels, J.; Wijesinghe, D.; Andreev, O. A.; Reshetnyak, Y. K. *J. Control. Release*, **2013**, *167*, 228–237.

- [53] Sosunov, E. A.; Anyukhovskiy, E. P.; Sosunov, A. A.; Moshnikova, A.; Wijesinghe, D.; Engelman, D. M.; Reshetnyak, Y. K.; Andreev, O. A. *PNAS*, **2012**, *110*, 82–86.
- [54] Andreev, O. A.; Engelman, D. M.; Reshetnyak, Y. K. *Front. Physiol.*, **2014**, *5*, 1–7.
- [55] Farhood, H.; Serbina, N.; Huang, L. *BBA-Biomembranes*, **1995**, *1235*, 289–295.
- [56] Landon, C. D.; Park, J.-Y.; Needham, D.; Dewhurst, M. W. *Open Nanomed. J.*, **2011**, *3*, 38–64.
- [57] Paul, S.; Nahire, R.; Mallik, S.; Sarkar, K. *Comput. Mech.*, **2014**, *53*, 413–435.
- [58] Reimhult, E. *ECB*, **2015**, *32*, 665–672.
- [59] Blume, G.; Cevc, G.; Crommelin, M. D. J. A.; Bakker-Woudenberg, I. A. J. M.; Kluft, C.; Storm, G. *BBA-Biomembranes*, **1993**, *1149*, 180–184.
- [60] Lopes de Menezes, Daniel E.; Kirchmeier, M. J.; Gagne, J.-F.; Pilarski, L. M.; Allen, T. M. *J. Liposome Res.*, **1999**, *9*, 199–228.
- [61] Sapra, P.; Allen, T. M. *Prog. Lipid Res.*, **2003**, *42*, 439–462.
- [62] Sofou, S.; Sgouros, G. *Expert Opin. Drug Deliv.*, **2008**, *5*, 189–204.
- [63] Yamada, A.; Taniguchi, Y.; Kawano, K.; Honda, T.; Hattori, Y.; Maitani, Y. *Clin. Cancer Res.*, **2008**, *14*, 8161.
- [64] Gabizon, A.; Tzemach, D.; Gorin, J.; Mak, L.; Amitay, Y.; Shmeeda, H.; Zalipsky, S. *Cancer Chemother. Pharmacol.*, **2010**, *66*, 43–52.
- [65] Baek, S. E.; Lee, K. H.; Park, Y. S.; Oh, D.-K.; Oh, S.; Kim, K.-S.; Kim, D.-E. *J. Control. Release*, **2014**, *196*, 234–242.
- [66] Gupta, B.; Levchenko, T. S.; Torchilin, V. P. *Oncology Research Featuring Preclinical and Clinical Cancer Therapeutics*, **2006**, *16*, 351–359.
- [67] Pappalardo, J. S.; Quattrocchi, V.; Langellotti, C.; Di Giacomo, S.; Gnazzo, V.; Olivera, V.; Calamante, G.; Zamorano, P. I.; Levchenko, T. S.; Torchilin, V. P. *J. Control. Release*, **2009**, *134*, 41–46.

- [68] Kirpotin, D.; Park, J. W.; Hong, K.; Zalipsky, S.; Li, W.-L.; Carter, P.; Benz, C. C.; Papahadjopoulos, D. *Biochemistry*, **1997**, *36*, 66–75.
- [69] Hofmann, A. M.; Wurm, F.; Hühn, E.; Nawroth, T.; Langguth, P.; Frey, H. *Biomacromolecules*, **2010**, *11*, 568–574.
- [70] Fritz, T.; Hirsch, M.; Richter, F. C.; Müller, S. S.; Hofmann, A. M.; Rusitzka, Kristiane A. K.; Markl, J.; Massing, U.; Frey, H.; Helm, M. *Biomacromolecules*, **2014**, *15*, 2440–2448.
- [71] Reibel, A. T.; Müller, S. S.; Pektor, S.; Bausbacher, N.; Miederer, M.; Frey, H.; Rösch, F. *Biomacromolecules*, **2015**, *16*, 842–851.
- [72] Mohr, K.; Müller, S. S.; Müller, L. K.; Rusitzka, K.; Gietzen, S.; Frey, H.; Schmidt, M. *Langmuir*, **2014**, *30*, 14954–14962.
- [73] Apte, A.; Koren, E.; Koshkaryev, A.; Torchilin, V. P. *Cancer Biol. Ther.*, **2013**, *15*, 69–80.

1.3 Block Copolymers of Poly(ethylene glycol) and Poly(propylene oxide)

Jana Herzberger,^{1,2} Kerstin Niederer,¹ Hannah Pohlitz,^{3,1,2} Jan Seiwert,¹ Matthias Worm,¹ Frederik R. Wurm,⁴ Holger Frey*^{1,2}

¹Institute of Organic Chemistry, Johannes Gutenberg-University Mainz, Duesbergweg 10-14, D-55128 Mainz, Germany.

²Graduate School Materials Science in Mainz, Staudingerweg 9, D-55128 Mainz, Germany.

³Department of Dermatology, University Medical Center, Langenbeckstraße 1, D-55131 Mainz, Germany.

⁴Max Planck Institute for Polymer Research, Ackermannweg 10, D-55128 Mainz, Germany.

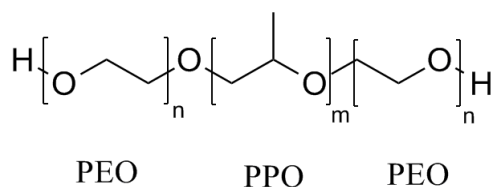
Published in Chemical Reviews, **2015**, 116 (4), pp. 2170-2243.

Reprinted with permission from J. Herzberger, K. Niederer, H. Pohlitz, J. Seiwert, M. Worm, F. R. Wurm, H. Frey, *Chemical Reviews*, **2015**, 116 (4), 2170-2243. Copyright (2015) American Chemical Society.

Note: Chapters 1.3 and 1.4 have been published in *Chemical Reviews*, **2015**, 116 (4), pp. 2170-2243 as Chapters 4 and 6.2 and represent M.W.'s contributions to the review article.

1.3.1 Poloxamers and Poloxamines

Block copolymers composed of PPO and PEO are an important class of biocompatible polymers in both industry as well as academia. Namely, ABA-triblock copolymers with the structure PEO-*b*-PPO-*b*-PEO are known as poloxamers (see Scheme 1) or Pluronics (trade mark BASF) are among the most relevant non-ionic surfactants (= surface active agents) and have been extensively investigated over the last decades.^[1,2] Due to the high water-solubility of PEO in a wide temperature range (0° - 100°C) and the low solubility of PPO in water at temperatures exceeding T_c (> 15°C; cloud point), these block copolymers exhibit amphiphilic character accompanied by surface-active properties.^[3]



Scheme 1: Structure of poloxamers composed of two PEO blocks and a central PPO block.

Consequently, PEO-*b*-PPO-*b*-PEO copolymers are widely utilized as lubricants, detergents, defoamers and emulsifying agents in industrial and agricultural processes, as well as in cosmetic products, paints and food additives.^[2] Pluronics are prepared via sequential anionic ring-opening polymerization of PO and EO using potassium and sodium hydroxide as the activator.^[4] First, the central PPO segment is synthesized as a precursor, and subsequently chain extended by the polymerization of EO. In order to obtain highly purified block copolymers and to reduce the content of admixtures, such as PPO homopolymers and low molecular weight block copolymers, chromatographic fractionation is often employed after the polymerization.^[5]

Due to the vast variety of Pluronics with different molecular composition, a categorization system has been established to allow for an easy evaluation of structure and properties of a given copolymer. For the non-proprietary name poloxamer, the abbreviated expression starts with the capital letter 'P' followed by one or two digits corresponding to the approximate molecular weight of the PPO block, when multiplied by a factor of 100. The last digit multiplied by 10 refers to the weight percentage of PEO within the block copolymer. For example, 'Poloxamer P407' conforms to a copolymer with a PPO block of about 4000 g/mol and 70 % weight content of PEO (see Table 1).

In case of trade names like Pluronic (BASF), Lutrol (BASF) or Synperonic (Croda) prefix letters 'L', 'P' and 'F' classify the physical appearance of the pure copolymer as liquid (L), paste (P) and flakes (F). The first one or two digits multiplied by 300 represent the approximate molecular weight of PPO whereas the last digit multiplied by 10 indicates the total weight percentage of PEO within the polymer. For the previous example of a PEO-*b*-PPO-*b*-PEO copolymer ($M_n = 4000 \text{ g/mol}$, 70 % PEO),

this leads to the term F127. Accordingly, the nomenclature for Pluronics can be converted to the generic term for poloxamers by multiplying the first one or two digits by a factor of 3.^[6]

In particular, self-aggregation of PEO-b-PPO-b-PEO copolymers into micellar structures plays a decisive role regarding a majority of applications especially in nanoscience and nanomedicine.^[6,7]

Poloxamer micelles composed of PPO-cores and PEO-coronas allow encapsulation of a wide range of hydrophobic compounds. This behavior motivates their use as drug and gene delivery systems,^[5] as well as in nanotechnological applications, for example as surfactants in emulsion polymerization techniques.^[8]

Table 1: Table of Pluronics compositions and properties.

Pluronic	poloxamer	Mn ^a	N _{EO} ^b	N _{PO} ^c	cmc ^d	HLB ^e	cloud point ^f
L35	101	1900	21.6	16.4	5.3*10 ⁻³	19	73
L43	123	1850	12.6	22.3	2.2*10 ⁻³	12	42
L44	124	2200	20.0	22.8	3.6*10 ⁻³	16	65
L61	181	2000	4.5	31.0	1.1*10 ⁻⁴	3	24
L64	184	2900	26.4	30.0	4.8*10 ⁻⁴	15	58
P84	234	4200	38.3	43.4	7.1*10 ⁻⁵	14	74
P85	235	4600	52.3	39.7	6.5*10 ⁻⁵	16	85
L88	238	11400	207.8	39.3	2.5*10 ⁻⁴	28	>100
P103	333	4950	33.8	59.7	6.1*10 ⁻⁶	9	86
F108	335	14600	265.4	50.3	2.2*10 ⁻⁵	27	>100
P123	403	5750	39.2	69.4	4.4*10 ⁻⁶	8	90
F127	407	12600	200.4	65.2	2.8*10 ⁻⁶	22	>100

^a Average molecular weights in g/mol; ^{b/c} Average number of EO/PO units per polymer taken from ref ^[14]; ^d critical micelle concentration in mol/l as determined by pyrene probe measurements and taken from ref ^[14]; ^e Hydrophilic-lipophilic-balance values were taken from ref ^[14]; ^f Cloud points in °C taken from ref ^[15].

These self-assembled aggregates vary in size and shape from spherical to rod-like to lamellar structures.^[9] In this case, the molecular weights of the PEO/PPO segments crucially dictate the properties of the block copolymers such as water-solubility, critical micelle concentration (CMC), critical micelle temperature (CMT), structure of micelles and aggregation numbers.^[10-13] Namely, CMC values are of fundamental significance to evaluate emulsifying properties of poloxamers.

In general, CMC values tend to decrease with increasing hydrophobic PPO chain length due to an increase of the net hydrophobicity favoring the formation of micelles. On the contrary, CMCs increase with growing chain length of the PEO blocks, which has been ascribed to a reduced core hydrophobicity that leads to a destabilization of micelles.^[11] Systematic studies on aggregation behavior of Pluronics in aqueous solution have been reported in numerous articles.^[10,11]

The remarkable self-assembly and emulsifying properties of Pluronics in conjunction with their excellent biocompatibility has proven particularly advantageous for biomedical and pharmaceutical applications and the development of drug delivery systems.^[1,5] Namely, Pluronic formulations have been shown to exhibit great potential in anti-cancer research, especially regarding the treatment of multi-drug resistant (MDR) tumor cell types. Studies in this field report an enhancement in cytotoxic activity of the chemotherapeutic drug doxorubicin towards MDR tumor cell lines by 2 or 3 orders of magnitude.^[14,16,17] Besides operating as drug carriers to improve pharmacokinetic performance, Pluronics appeal as biological response modifiers capable of sensitizing multidrug resistant (MDR) cancer cells and increasing drug transport across cellular barriers. Currently, micelles of Pluronic L61 and F127 loaded with doxorubicin are investigated for the treatment of cancer cells resistant to doxorubicin in clinical trials.^[18] Credit has to be granted to Kabanov *et al.* as the pioneers within this research area. Highly promising findings regarding Pluronic-based micelles loaded with paclitaxel as anticancer agent have further been reported by Tsvetanov *et al.* A comparison of these micellar drug formulations with Taxol revealed improved pharmacokinetic properties and enhanced blood circulation times.^[19] Recent developments regarding the effect of

Pluronics on MDR tumor cells and their promising perspective in this particular field have been comprehensively reviewed lately.^[16]

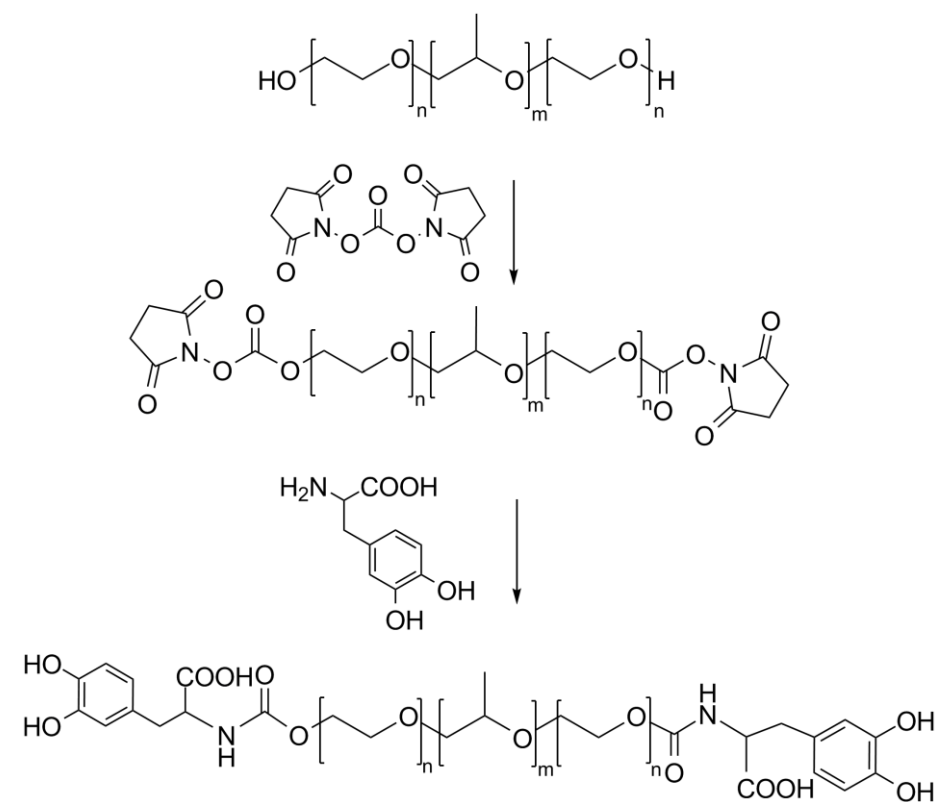
As well, drug carrier systems based on Pluronic block copolymer technology represent promising candidates to penetrate the blood brain barrier in order to transport therapeutics to the brain.^[20]

Another specialized application of Pluronic-based formulations has emerged within the field of gene therapy. When injected into skeletal muscle, plasmid DNA induces gene expression which can be exploited for vaccination strategies or the generation of therapeutic proteins. In several studies, Pluronics have been employed to increase the efficiency of gene transfer technologies.^[5]

However, a major challenge for drug-loaded micelles as nanocarrier systems arises from the thermodynamic instability of micelles upon dilution, which is also valid for Pluronic-based micellar formulations. In particular, very hydrophilic block copolymers with high cmc/cmt values suffer from low micelle stability and are crucially subjected to disassembly of micelles. To overcome this drawback, several strategies have been proposed to increase stability of Pluronic micelles. For example, polymerization of monomers (e.g.: N-isopropylacrylamides, N,N-diethylacrylamide) forming thermo-responsive hydrogels (LCST behavior) inside the micellar core can afford micelles with improved stability profiles and good drug loading capacities. However, the stability gained from this approach was found to be impermanent and depletes within a time frame of days or weeks.^[2] Other strategies focused on the cross-linking of the micellar shell to lower the CMC by converting the hydroxyl groups into aldehydes and introducing imine linkages via the addition of diamines.^[21] Another noteworthy approach reported by Petrov et. al to effectively stabilize Pluronic-based micelles implied the formation of an interpenetrating network via light-initiated crosslinking of a tetrafunctional acrylate monomer.^[22] Nevertheless, stabilization of Pluronic micelles without affecting drug release profiles and drug loading capacities remains a fundamental challenge for all these modifications.

Moreover, Pluronics are utilized for surface-coating of drug-loaded, hydrophobic nanoparticles in order to prolong blood circulation times of the drug carriers. Depending on the size of particles and properties of the coated surface, a certain selectivity in the site of deposition within the body is observed. By controlling the balance between adsorption and desorption of specific blood components referred to as opsonization and dysopsonization, site specific deposition can be influenced using Pluronics as surface-coatings. Effective enhancement of serum life times have been achieved for polymeric particles in a size range from 70 to 200 nm.^[7]

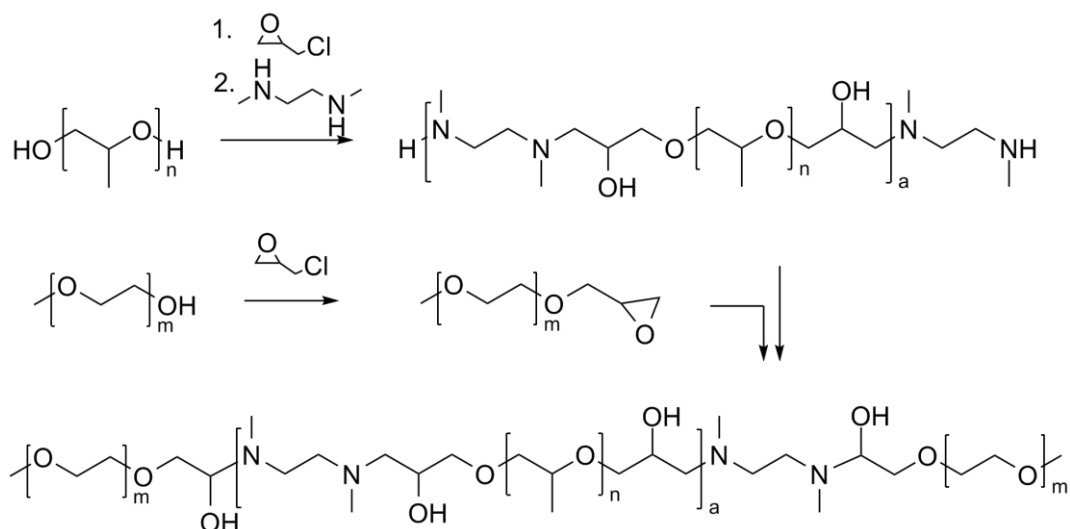
Another remarkable property of PEO-*b*-PPO-*b*-PEO copolymers in aqueous solution results from their ability to undergo thermo-reversible gelation at concentrations above the CMC. In particular, gelation of poloxamer 407 (Pluronic F127) has proved beneficial for biomedical purposes as concentrated solutions appear as viscous liquids at room temperature forming a semi-solid transparent gel at body temperature (37 °C).^[23] This behavior has motivated use of poloxamer gels for prolonged drug release strategies^[23] and for tissue engineering.^[1,24–26] Although, poloxamers are generally regarded as non-toxic, higher doses (up to 137,5 mg/kg in rabbits) of Poloxamer 407 have been reported to affect serum concentrations of triglycerides and cholesterol.^[23] Due to the comparatively weak mechanical strength and rapid erosion of poloxamer gels, for instance, covalent cleavable linkages such as carbonates have been introduced to improve mechanical properties, simultaneously ensuring renal excretion of the degradation fragments.^[23] Moreover, pH-responsive poloxamer-based gels have been formed from graft copolymers of poly acrylic acid (PAA) and poloxamers (poloxamer-*g*-PAA).



Scheme 2: Synthesis of catechol-functional poloxamers according to Messersmith *et al.*^[28]

This reduces the amount of material needed to form stable gels at body temperature and represent a promising tool for pH-triggered release strategies.^[27] Messersmith and coworkers reported the attachment of DOPA (3,4-dihydroxyphenyl-L-alanine) moieties at both termini of Pluronics to attach catechol groups facilitating bioadhesive hydrogels (see Scheme 2).^[28] There are several other reports on chemically modified PEO-*b*-PPO-*b*-PEO copolymers and the corresponding hydrogels, these are, however, beyond the scope of this review.

Another interesting approach mimicking the structure of poloxamers has been demonstrated by Park *et al.* by incorporating multiple hydroxyl groups into the backbone to enable the covalent attachment of pharmaceutical drugs.^[29] These structures were accessed by, first, generating a PPO precursor polymer via a step-growth polymerization of *N,N'*-dimethylethylenediamine and diepoxy-functional PPO subsequently end-capping with epoxy-functional mPEG. (see Scheme 3)



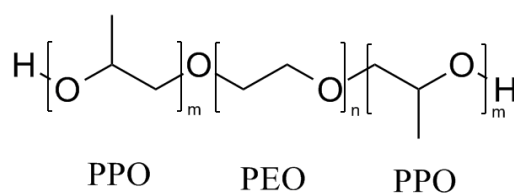
Scheme 3: Synthesis of poloxamer mimicking block structures according to Park *et al.*^[29]

A promising approach to access novel types of poloxamer analogs bearing multiple hydroxyl functionalities was developed by Tsvetanov and coworkers.^[30–32] Using PPO as a macroinitiator for the AROP of the acetal-protected glycerol derivative EEGE, linPG-*b*-PPO-*b*-linPG triblock copolymer were obtained after subsequent hydrolysis of the acetal moieties. In several study, physico-chemical properties of materials were investigated.^[9,33]

Given the immense spectra of applications of poloxamers or poloxamer-based formulations and the strong emphasis on post-modification strategies to improve their performance, to the best of our knowledge, no synthetic routes have been explored to develop novel block copolymer architectures compared to the commercially available standards, e.g., by using multifunctional PEG or PPO blocks to incorporate specific functional groups already during the synthesis.

Besides poloxamers, related triblock copolymers with an inverted substructure composed of a central PEO block flanked by two PPO segments are known as reverse poloxamers (Pluronic R) and are likewise commercially available. Although these structures exhibit interesting properties and are diversely used, for example, as wetting and defoaming agents in industrial processes,^[34] these systems have been less investigated compared to the materials mentioned above.^[35] However, more recently, increasing attention was drawn to studies of phase behavior and aggregation of

reverse poloxamers in aqueous solution.^[36–38] In contrast to poloxamers, reverse poloxamers (see Scheme 4) show a reduced ability to form regular micelles in aqueous medium ascribed to a loss of entropy attributed to the looping of the PEO middle block in micellar structures.^[35] Instead, PPO-*b*-PEO-*b*-PPO triblock copolymers have been reported to either form random network structures or micellar associations, depending on the concentration, with the two terminal blocks located in different PPO domains.^[39]



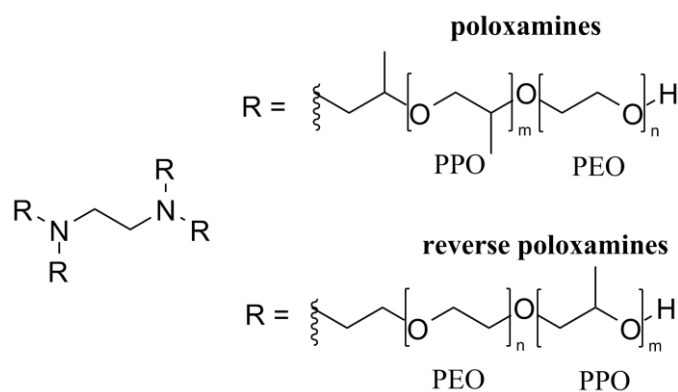
Scheme 4: Structure of reverse poloxamers composed of two PPO and a central PEO block.

In addition, micellization and gelation of poloxamer/reverse poloxamer mixtures have been investigated suggesting a critical composition ratio above which the appearance of bridged poloxamer micelles strongly hinders the gelation process.^[40,41]

The spectrum of applications for reverse poloxamers, however, appears to be limited in comparison to “normal” poloxamers. This is probably attributed to their unfavorable self-assembly. However lately, a new perspective for the application of reverse poloxamers has been proposed within the field of gene therapy. Herein, PPO-*b*-PEO-*b*-PPO copolymers were evaluated in terms of their ability to increase muscle transfection compared to naked DNA. It was found that reverse Pluronics promote muscle gene transfer in mice as effectively as regular Pluronics, which might encourage further research activities.^[42] However, in order to compete with the steadily growing significance of regular poloxamers, applications benefitting from the use of reverse poloxamers opposed to regular poloxamers need to be developed.

1.3.2 Poloxamines

Another group of amphiphilic block copolymers based on PEO and PPO are poloxamines with a distinct tetrabranched block structure bearing a central ethylene diamine bridge. Four symmetric blocks, composed of PEO and PPO, are attached to the amine units and can either contain the PEO block as the outer segment (poloxamines, tradename Tetronics) or as the inner segment (reverse poloxamines, tradename TetronicsR) (see Scheme 5). Poloxamines and reverse poloxamines are synthesized using ethylene diamine as an initiator for the sequential anionic polymerization of PO and EO, resulting in X-shaped polymer architectures.



Scheme 5: Structures of poloxamines (Tetronics) and reverse poloxamines (TetronicsR)

The presence of the tertiary amine groups adds a dual responsive behavior to these polymeric amphiphiles. Poloxamines exhibit thermo- and pH-responsiveness, which distinguishes their properties from poloxamers. Moreover, the additional amine functionalities enable further modification reactions, such as quarternization to promote cell adhesion for tissue engineering purposes.^[43]

Compared to poloxamers, studies on the phase behavior of poloxamines have been neglected for a long time. However, within the last decade, favorable physicochemical properties of poloxamines regarding drug delivery strategies and tissue engineering have been elucidated^[44] and have motivated increasing research efforts in this area.^[45] In analogy to their linear counterparts, poloxamines show self-assembly into micellar aggregates in aqueous medium. In contrast,

however, aggregation behavior of poloxamines is strongly pH-dependent. The pK_a values of the amine groups of 3.8-4.0 and 8.0, respectively, do not vary substantially with different PEO/PPO block lengths.^[46] A decrease in pH leads to a reduced tendency to aggregate and a more narrow temperature range, in which aggregation occurs. This behavior can be attributed to the coulombic repulsion between the positively charged polymers. At physiological conditions (pH = 7.4), poloxamines are present as single protonated species.^[2] A noteworthy approach deploying the pH-dependent aggregation of poloxamines to stabilize DNA complexes was proposed by Pitard et. al. Therein, negatively charged DNA-poloxamine supramolecular assemblies were introduced as potential gene delivery systems for the therapy of skeletal or heart muscle-related diseases.^[47]

In accordance with poloxamers, surface-coating of hydrophobic nanoparticles using poloxamines has become increasingly attractive in order to prolong the particles' blood circulation times and render them as potential drug delivery systems for medical and pharmaceutical purposes.^[48] The efficiency of the coatings to prevent recognition of the hydrophobic nanoparticles by macrophages strongly depends on the molecular weight and composition of the PEO-PPO copolymers. With increasing hydrophilicity and molecular weight, this shielding effect is reported to become more effective. In particular, surface-coating strategies of nanoparticles based on biodegradable polymers such as polylactides or polyglycolides have attracted increasing attention lately.^[7] A major challenge in this field, however, remains the establishment of a correlation between the structure of particles and their specific interaction with blood components in order to allow for the design of targetable nanocarriers.

Mathet *et al.* investigated the effect of poloxamines with different molecular architectures on the inhibition of efflux transporters in multidrug-resistant (MDR) tumor cell lines. They proposed poloxamine T304 as both a promising drug carrier system and efflux transport inhibitor for the treatment of MDR tumors.^[49] Aside from that, these studies report cytotoxic behavior for the majority of poloxamines investigated, raising the demand for further studies to evaluate their biocompatibility regarding future applications in a pharmaceutical context.

Although reverse poloxamines are commercially available PEO-PPO copolymers and exhibit potential usefulness for some specialized applications,^[50] to date their physicochemical properties have only been scarcely investigated^[39,45] and will not be discussed within this review.

1.3.3 PEO-PPO Diblock Copolymers

Diblock copolymers composed of PEO and PPO represent another class of non-ionic amphiphiles based on polyethers. Although diblock structures might be regarded as the most obvious block copolymer structure, these surfactants turn out to be rarely investigated in terms of bulk properties^[51] and phase behavior in aqueous solution^[52,53] compared to their triblock relatives (PEO-*b*-PPO-*b*-PEO). In contrast to the aforementioned bi- and multi-functional block structures, PEO-PPO diblock copolymers are mono-functional macromolecular alcohols. This characteristic results from the use of mono-functional low-molecular weight alcohols as initiators for the sequential anionic ring-opening polymerization of EO and PO in their synthesis.

Notably, PEO-PPO diblock copolymers have been introduced as valuable structural templates for the preparation of two-dimensional mesoporous silica films,^[54] and have been shown to act as size-specific solubilizing agents for carbon nanotubes, offering perspectives for improved fractionation strategies.^[55]

Lately, increasing attention is dedicated to the behavior of PEO-PPO diblock copolymers at the air-water interface and properties of their polymeric monolayers. These studies, however, exclusively aimed at a fundamental understanding of interfacial dynamics.^[56,57]

A promising perspective for diblock copolymers based on PEO and PPO has been demonstrated by Firestone *et al.* for the stabilization of lipid bilayer vesicles (e.g. liposomes) for drug delivery purposes as an inexpensive alternative to PEG-lipid conjugates. In this case the hydrophobic PPO segments function as anchor units within the lipid bilayer, whereas the PEO chain projects into the aqueous surrounding, leading to an enhanced robustness of the vesicular structure. Interestingly,

PEO-*b*-PPO copolymers exhibit superior performance compared to poloxamers in terms of their ability to sterically stabilize lipid-based nanocarriers.^[58]

Although these diblock copolymers are commercially available as their triblock analogs, so far a significantly smaller range of applications has been proposed and less effort has been put into elucidating their physicochemical properties. Moreover, to the best of our knowledge and in contrast to the other members of the PEO/PPO-based amphiphiles, no end-functionalized derivatives have been reported, which might be due to their monofunctional nature limiting chemical modification.

The immense versatility and broad spectrum of applications of PEO/PPO block copolymers in various research areas have been illustrated in this chapter, focusing on trends and developments within the last 15 years. This class of polyethers undoubtedly represents one of the most widely used amphiphilic materials with paramount significance to industries and academia. Especially their low cost and commercial availability in a wide range of molecular weights and compositions as well as different architectures (diblock, triblock, tetrabranched) combined with interesting physical and chemical properties warrants the development of further applications. Most of the research carried out in this area to date has been dedicated to PEO-*b*-PPO-*b*-PEO copolymers (poloxamers) while the other members have been neglected for a long time, though lately increasing interest has been pronounced for the properties of the less explored candidates^[7,44,49] In a pharmaceutical context, PEO/PPO copolymers exhibit particular usefulness concerning drug- and gene delivery strategies,^[16] which will encourage future research activities in this field. However, aside from numerous reports on chemical modification^[28,43] of the commercially available standards, so far, no emphasis has been put on exploring novel polymeric architectures based on PEO and PPO block-type structures by, for example, using other multifunctional initiators for the polymerization.

1.4 Cleavable Polyethers

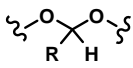
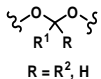
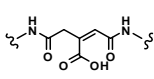
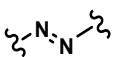
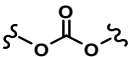
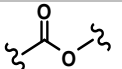
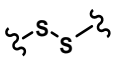
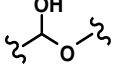
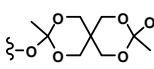
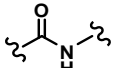
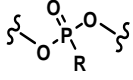
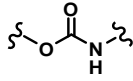
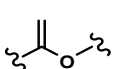
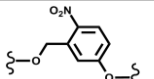
1.4.1 Polyethers bearing cleavable moieties

Ethers are characterized by their high stability towards chemical or physical treatment. Low molecular weight ethers are typical solvents in organic chemistry. Also polyethers are very stable and flexible polymers. Under oxidative stress, however, PEG may be degraded by reactive oxygen species (ROS) due to β -scission, as observed in long-term *in vivo* experiments.^[59] Degradation of PEG under application of voltage and air,^[60] UV light,^[61] ultrasonication,^[62] and temperature^[61] is described in literature. The degradation rate depends on whether the experiment is conducted in bulk or in aqueous solution and on pH values.^[63]

If a higher oxidation stability is required for certain applications, aromatic polyethers can be applied.^[64] Aromatic polyethers are known to exhibit higher stability against oxidation compared to PEG, albeit at the expense of low solubility in water and a lack of biocompatibility.

If PEG-derivatives are expected to degrade, which may be beneficial for biomedical applications such as reversible PEGylation, the incorporation of cleavable moieties into the polymer backbone is necessary. PEG is regarded as the gold standard for polymer-drug conjugation in order to prevent proteolytic degradation of pharmaceutical agents, as it is non-toxic, chemically inert, water-soluble and has a low immunogenicity.^[65] However, PEG is not biodegradable restricting its use to a maximum molecular weight of 40 kDa, as higher molecular weight PEGs can accumulate in human tissue and may lead to storage diseases.^[66] This molecular weight threshold represents the renal excretion limit of human kidneys exhibiting a natural boundary for the utility of PEG. However, the use of high molecular weight PEG is particularly favorable, as blood circulation times of PEGylated drugs prolong with increasing molecular weights of PEG^[67] making the design of in-chain cleavable PEG derivatives especially desirable.

Table 2: Compilation of cleavable groups, synthesis strategies and respective cleaving stimuli reported for PEGs and derivatives. Adapted with permission from Dingels, C.; Frey, H. In *Hierarchical Macromolecular Structures: 60 Years after the Staudinger Nobel Prize II*; Percec, V., Ed.; Springer International Publishing: **2013**; Vol. 262, p 167. Copyright 2013 Springer.¹⁷

Cleavable Unit	Structure	Synthetic Approach	Degradation ^[a]	Ref.
Acetals		PEG coupling	pH < 7.4	[70-73]
Acetals/ ketals		Cleavable AROP initiator	pH < 7.4	[74,75]
Aconitic acid diamides		PEG coupling	pH < 7.4	[76]
Azo groups		PEG coupling	enzymatic	[77,78]
Carbonates		PEG coupling	basic hydrolysis	[79,80]
Carboxylates		PEG coupling	hydrolytic, enzymatic	[81,82]
Disulfides		PEG coupling	reductive	[83,84]
Hemi-acetals		PEG oxidation	acidic or basic	[85]
Ortho-esters		PEG coupling	pH < 7.4	[86]
Peptides		PEG coupling	enzymatic	[87,88]
Phospho-esters		PEG coupling	acidic or basic	[89,90]
Urethane		PEG coupling	(hydrolytic)	[91,92]
Vinyl ethers		Elimination functionalized PEG, PEG coupling	pH < 7.4 or light/ ¹ O ₂	[93]
o-Nitro benzyl ethers		PEG coupling	light	[69]

^[a] Conditions may vary for the same cleavable unit due to different adjacent moieties.

A variety of different stimuli, such as a potential pH-sensitivity, redox-response and enzymatic cleavage, have been employed to trigger the in-chain scission of the PEG backbone or the detachment of PEGs from the drug conjugate within a targeted tissue or cellular compartment.^[68]

More recently, light as stimulus has likewise been exploited to induce a cleavage of PEG-derived structures.^[69] Table 2 compiles different cleavable moieties which have been used as linkers of PEG conjugates or have been incorporated into the polyether backbone as in-chain junctions. Additionally, their synthesis strategies and the respective cleaving stimuli are attributed.

A review article has recently been published focusing on strategies to incorporate cleavable moieties into PEG chains and PEG conjugates.^[94]

It is noteworthy that PEG-based lipids bearing cleavable moieties have become increasingly attractive for the design of surface-modified liposomes (stealth liposomes) as drug delivery systems.^{[95]682} The presence of stimuli-cleavable linkers in the lipid structures triggers shedding of liposomes within a particular cellular compartment or tissue to improve the efficacy of a liposomal formulation. Numerous reports on acid-labile PEG lipids based on cholesterol with cleavable junctions, such as aconitic acid, hydrazones or vinyl ethers, have been established.^[96]

Alternative polymers which combine the properties of PEG, such as high water-solubility, low protein adsorption with degradability may be polypeptides, polypeptoides (i.e. polysarcosin), HES, poly-*N*-(2-hydroxypropyl) methacrylamide (PHPMA), polyglutamic acid (PGA), polyacetal (“fleximer”), poly(oxazoline)s, poly(phosphoester)s, and polysialic acid.^[97–104]

References

- [1] Fusco, S.; Borzacchiello, A.; Netti, P. A. *J. Bioact. Compat. Polym.*, **2006**, *21*, 149–164.
- [2] Chiappetta, D. A.; Sosnik, A. *Eur. J. Pharm. Biopharm.*, **2007**, *66*, 303–317.
- [3] Mortensen, K.; Pedersen, J. S. *Macromolecules*, **1993**, *26*, 805–812.
- [4] Schmolka, I. *J. Am. Oil Chem. Soc.*, **1977**, *54*, 110–116.
- [5] Kabanov, A. V.; Batrakova, E. V.; Alakhov, V. Y. *J. Control. Release*, **2002**, *82*, 189–212.
- [6] Torcello-Gómez, A.; Wulff-Pérez, M.; Gálvez-Ruiz, M. J.; Martín-Rodríguez, A.; Cabrerizo-Vílchez, M.; Maldonado-Valderrama, J. *Adv. Colloid Interface Sci.*, **2014**, *206*, 414–427.
- [7] Stolnik, S.; Illum, L.; Davis, S. S. *Adv. Drug Delivery Rev.*, **2012**, *64*, Supplement, 290–301.
- [8] Durand, A.; Marie, E. *Adv. Colloid Interface Sci.*, **2009**, *150*, 90–105.
- [9] Nagarajan, R. *Colloids Surf., B*, **1999**, *16*, 55–72.
- [10] Alexandridis, P.; Holzwarth, J. F.; Hatton, T. A. *Macromolecules*, **1994**, *27*, 2414–2425.
- [11] Alexandridis, P.; Alan Hatton, T. *Colloids Surf., A*, **1995**, *96*, 1–46.
- [12] Kozlov, M. Y.; Melik-Nubarov, N. S.; Batrakova, E. V.; Kabanov, A. V. *Macromolecules*, **2000**, *33*, 3305–3313.
- [13] Hecht, E.; Hoffmann, H. *Langmuir*, **1994**, *10*, 86–91.
- [14] Batrakova, E.; Lee, S.; Li, S.; Venne, A.; Alakhov, V.; Kabanov, A. *Pharm. Res.*, **1999**, *16*, 1373–1379.
- [15] Alexandridis, P. *Curr. Opin. Colloid Interface Sci.*, **1997**, *2*, 478–489.
- [16] Alakhova, D. Y.; Kabanov, A. V. *Mol. Pharmaceutics*, **2014**, *11*, 2566–2578.
- [17] Alakhov, V. Y.; Moskaleva, E. Y.; Batrakova, E. V.; Kabanov, A. V. *Bioconjugate Chem.*, **1996**, *7*, 209–216.
- [18] Pitto-Barry, A.; Barry, Nicolas P. E. *Polym. Chem.*, **2014**, *5*, 3291–3297.
- [19] Yoncheva, K.; Calleja, P.; Agüeros, M.; Petrov, P.; Miladinova, I.; Tsvetanov, C.; Irache, J. M. *Int. J. Pharm.*, **2012**, *436*, 258–264.
- [20] Kabanov, A. V.; Batrakova, E. V.; Miller, D. W. *Adv. Drug Delivery Rev.*, **2003**, *55*, 151–164.

- [21] Yang, T.-F.; Chen, C.-N.; Chen, M.-C.; Lai, C.-H.; Liang, H.-F.; Sung, H.-W. *Biomaterials*, **2007**, *28*, 725–734.
- [22] Petrov, P.; Bozukov, M.; Tsvetanov, C. B. *J. Mater. Chem.*, **2005**, *15*, 1481–1486.
- [23] Ruel-Gariépy, E.; Leroux, J.-C. *Eur. J. Pharm. Biopharm.*, **2004**, *58*, 409–426.
- [24] Gutowska, A.; Jeong, B.; Jasionowski, M. *Anat. Rec.*, **2001**, *263*, 342–349.
- [25] Frisman, I.; Seliktar, D.; Bianco-Peled, H. *Biomaterials*, **2011**, *32*, 7839–7846.
- [26] Frisman, I.; Seliktar, D.; Bianco-Peled, H. *Acta Biomater.*, **2012**, *8*, 51–60.
- [27] Bromberg, L. *Expert Opin. Drug Deliv.*, **2005**, *2*, 1003–1013.
- [28] Huang, K.; Lee, B. P.; Ingram, D. R.; Messersmith, P. B. *Biomacromolecules*, **2002**, *3*, 397–406.
- [29] Lee, Y.; Park, S. Y.; Mok, H.; Park, T. G. *Bioconjugate Chem.*, **2008**, *19*, 525–531.
- [30] Halacheva, S.; Rangelov, S.; Tsvetanov, C. *Macromolecules*, **2006**, *39*, 6845–6852.
- [31] Halacheva, S.; Rangelov, S.; Tsvetanov, C.; Garamus, V. M. *Macromolecules*, **2010**, *43*, 772–781.
- [32] Halacheva, S.; Rangelov, S.; Tsvetanov, C. *Macromolecules*, **2008**, *41*, 7699–7705.
- [33] Li, Z.; Chau, Y. *Bioconjugate Chem.*, **2009**, *20*, 780–789.
- [34] D'Errico, G.; Paduano, L.; Khan, A. *J. Colloid Interface Sci.*, **2004**, *279*, 379–390.
- [35] Zhou, Z.; Chu, B. *Macromolecules*, **1994**, *27*, 2025–2033.
- [36] Naskar, B.; Ghosh, S.; Moulik, S. P. *Langmuir*, **2012**, *28*, 7134–7146.
- [37] Huff, A.; Patton, K.; Odhner, H.; Jacobs, D. T.; Clover, B. C.; Greer, S. C. *Langmuir*, **2011**, *27*, 1707–1712.
- [38] Jiang, R.; Jin, Q.; Li, B.; Ding, D.; Shi, A.-C. *Macromolecules*, **2006**, *39*, 5891–5896.
- [39] Larrañeta, E.; Isasi, J. R. *Langmuir*, **2012**, *28*, 12457–12462.
- [40] Wang, Q.; Li, L.; Jiang, S. *Langmuir*, **2005**, *21*, 9068–9075.
- [41] Xie, Y.; Tang, J.; Lu, Z.; Sun, Z.; An, L. *J. Polym. Sci. B Polym. Phys.*, **2012**, *52*, 1183–1197.

- [42] Guiraud, S.; Alimi-Guez, D.; van Wittenberghe, L.; Scherman, D.; Kichler, A. *Macromol. Biosci.*, **2011**, *11*, 590–594.
- [43] Sosnik, A.; Sefton, M. V. *Biomacromolecules*, **2006**, *7*, 331–338.
- [44] Cho, E.; Lee, J. S.; Webb, K. *Acta Biomater.*, **2012**, *8*, 2223–2232.
- [45] Gonzalez-Lopez, J.; Sandez-Macho, I.; Concheiro, A.; Alvarez-Lorenzo, C. *J. Phys. Chem. C*, **2010**, *114*, 1181–1189.
- [46] Dong, J.; Chowdhry, B. Z.; Leharne, S. A. *Colloids Surf., A*, **2003**, *212*, 9–17.
- [47] Pitard, B.; Bello-Roufaï, M.; Lambert, O.; Richard, P.; Desigaux, L.; Fernandes, S.; Lanctin, C.; Pollard, H.; Zeghal, M.; Rescan, P.-Y.; Escande, D. *Nucleic Acids Res.*, **2004**, *32*, e159.
- [48] Moghimi, S. M.; Hunter, A. C. *Trends Biotechnol.*, **2000**, *18*, 412–420.
- [49] Cuestas, M. L.; Sosnik, A.; Mathet, V. L. *Mol. Pharmaceutics*, **2011**, *8*, 1152–1164.
- [50] Gonzalez-Lopez, J.; Alvarez-Lorenzo, C.; Taboada, P.; Sosnik, A.; Sandez-Macho, I.; Concheiro, A. *Langmuir*, **2008**, *24*, 10688–10697.
- [51] Fairclough, J. Patrick A.; Yu, G.-E.; Mai, S.-M.; Crothers, M.; Mortensen, K.; Ryan, A. J.; Booth, Colin *Phys. Chem. Chem. Phys.*, **2000**, *2*, 1503–1507.
- [52] Mansur, Claudia R. E.; Oliveira, Clara M. F.; González, G.; Lucas, E. F. *J. Appl. Polym. Sci.*, **1997**, *66*, 1767–1772.
- [53] Mansur, Claudia R. E.; Benzi, M. R.; Lucas, E. F. *J. Appl. Polym. Sci.*, **2001**, *82*, 1668–1676.
- [54] Takahashi, M.; Kubo, W.; Miyata, H. *Chem. Lett.*, **2013**, *42*, 909–911.
- [55] Nagarajan, R.; Bradley, R. A.; Nair, B. R. *J. Chem. Phys.*, **2009**, *131*, 104906.
- [56] Steinschulte, A. A.; Xu, W.; Draber, F.; Hebbeker, P.; Jung, A.; Bogdanovski, D.; Schneider, S.; Tsukruk, V. V.; Plamper, F. A. *Soft Matter*, **2015**, *11*, 3559–3565.
- [57] Deschênes, L.; Saint-Germain, F.; Lyklema, J. *J. Colloid Interface Sci.*, **2015**, *449*, 494–505.
- [58] Firestone, M. A.; Seifert, S. *Biomacromolecules*, **2005**, *6*, 2678–2687.
- [59] Ulbricht, J.; Jordan, R.; Luxenhofer, R. *Biomaterials*, **2014**, *35*, 4848–4861.

- [60] Harding, J. R.; Amanchukwu, C. V.; Hammond, P. T.; Shao-Horn, Y. *J. Phys. Chem. C*, **2015**, *119*, 6947–6955.
- [61] de Sainte Claire, Pascal *Macromolecules*, **2009**, *42*, 3469–3482.
- [62] Kawasaki, H.; Takeda, Y.; Arakawa, R. *Anal. Chem.*, **2007**, *79*, 4182–4187.
- [63] Hassouna, F.; Morlat-Thérias, S.; Mailhot, G.; Gardette, J. L. *Polym. Degrad. Stab.*, **2007**, *92*, 2042–2050.
- [64] Jayakannan, M.; Ramakrishnan, S. *Macromol. Rapid Commun.*, **2001**, *22*, 1463–1473.
- [65] Alconcel, Steevens N. S.; Baas, A. S.; Maynard, H. D. *Polym. Chem.*, **2011**, *2*, 1442–1448.
- [66] Pasut, G.; Veronese, F. M. *Prog. Polym. Sci.*, **2007**, *32*, 933–961.
- [67] Yamaoka, T.; Tabata, Y.; Ikada, Y. *J. Pharm. Sci.*, **1994**, *83*, 601–606.
- [68] Pelegri-O’Day, E. M.; Lin, E.-W.; Maynard, H. D. *J. Am. Chem. Soc.*, **2014**, *136*, 14323–14332.
- [69] Yamahira, S.; Yamaguchi, S.; Kawahara, M.; Nagamune, T. *Macromol. Biosci.*, **2014**, *14*, 1670–1676.
- [70] Knorr, V.; Allmendinger, L.; Walker, G. F.; Paintner, F. F.; Wagner, E. *Bioconjugate Chem.*, **2007**, *18*, 1218–1225.
- [71] Cui, W.; Qi, M.; Li, X.; Huang, S.; Zhou, S.; Weng, J. *Int. J. Pharm.*, **2008**, *361*, 47–55.
- [72] Pohlit, H.; Bellinghausen, I.; Schömer, M.; Heydenreich, B.; Saloga, J.; Frey, H. *Biomacromolecules*, **2015**, *16*, 3103–3111.
- [73] Schroder, R.; Pohlit, H.; Schuler, T.; Panthofer, M.; Unger, R. E.; Frey, H.; Tremel, W. *J. Mater. Chem. B*, **2015**, *3*, 7079–7089.
- [74] Feng, X.; Chaikof, E. L.; Absalon, C.; Drummond, C.; Taton, D.; Gnanou, Y. *Macromol. Rapid Commun.*, **2011**, *32*, 1722–1728.
- [75] Dingels, C.; Müller, S. S.; Steinbach, T.; Tonhauser, C.; Frey, H. *Biomacromolecules*, **2013**, 448–459.

- [76] DuBois Clochard, M.-C.; Rankin, S.; Brocchini, S. *Macromol. Rapid Commun.*, **2000**, *21*, 853–859.
- [77] Lai, J.; Wang, L.-Q.; Tu, K.; Zhao, C.; Sun, W. *Macromol. Rapid Commun.*, **2005**, *26*, 1572–1577.
- [78] Lai, J.; Tu, K.; Wang, H.; Chen, Z.; Wang, L.-Q. *J. Appl. Polym. Sci.*, **2008**, *108*, 3305–3312.
- [79] Tziampazis, E.; Kohn, J.; Moghe, P. V. *Biomaterials*, **2000**, *21*, 511–520.
- [80] Sharma, R. I.; Kohn, J.; Moghe, P. V. *J. Biomed. Mater. Res. A*, **2004**, *69A*, 114–123.
- [81] Hawker, C. J.; Chu, F.; Pomery, P. J.; Hill, David J. T. *Macromolecules*, **1996**, *29*, 3831–3838.
- [82] d'Acunz, F.; Kohn, J. *Macromolecules*, **2002**, *35*, 9360–9365.
- [83] Lee, Y.; Koo, H.; Jin, G.-w.; Mo, H.; Cho, M. Y.; Park, J.-Y.; Choi, J. S.; Park, J. S. *Biomacromolecules*, **2005**, *6*, 24–26.
- [84] Lee, J.; Joo, M. K.; Kim, J.; Park, J. S.; Yoon, M.-Y.; Jeong, B. J. *Biomater. Sci. Polym. Ed.*, **2009**, *20*, 957–965.
- [85] Reid, B.; Tzeng, S.; Warren, A.; Kozielski, K.; Elisseeff, J. *Macromolecules*, **2010**, *43*, 9588–9590.
- [86] Qi, M.; Li, X.; Yang, Y.; Zhou, S. *Eur. J. Pharm. Biopharm.*, **2008**, *70*, 445–452.
- [87] Ulbrich, K.; Strohalm, J.; Kopeček, J. *Makromol. Chem.*, **1986**, *187*, 1131–1144.
- [88] Pechar, M.; Ulbrich, K.; Šubr, V.; Seymour, L. W.; Schacht, E. H. *Bioconjugate Chem.*, **2000**, *11*, 131–139.
- [89] Gitsov, I.; Johnson, F. E. *J. Polym. Sci. Pol. Chem.*, **2008**, *46*, 4130–4139.
- [90] Wang, D.-a.; Williams, C. G.; Li, Q.; Sharma, B.; Elisseeff, J. H. *Biomaterials*, **2003**, *24*, 3969–3980.
- [91] Fu, H.; Gao, H.; Wu, G.; Wang, Y.; Fan, Y.; Ma, J. *Soft Matter*, **2011**, *7*, 3546–3552.
- [92] Liu, X.-M.; Quan, L.-d.; Tian, J.; Laquer, F. C.; Ciborowski, P.; Wang, D. *Biomacromolecules*, **2010**, *11*, 2621–2628.

- [93] Lundberg, P.; Lee, B. F.; van den Berg, S. A.; Pressly, E. D.; Lee, A.; Hawker, C. J.; Lynd, N. A. *ACS Macro Lett.*, **2012**, *1*, 1240–1243.
- [94] Dingels, C.; Frey, H. *Adv. Polym. Sci.*, **2013**, *262*, 167-190.
- [95] Pattni, B. S.; Chupin, V. V.; Torchilin, V. P. *Chem. Rev.*, **2015**,
- [96] He, Z.-Y.; Chu, B.-Y.; Wei, X.-W.; Li, J.; Edwards Iii, Carl K.; Song, X.-R.; He, G.; Xie, Y.-M.; Wei, Y.-Q.; Qian, Z.-Y. *Int. J. Pharm.*, **2014**, *469*, 168–178.
- [97] Barz, M.; Luxenhofer, R.; Zentel, R.; Vicent, M. J. *Polym. Chem.*, **2011**, *2*, 1900–1918.
- [98] Duncan, R.; Vicent, M. J. *Adv. Drug Delivery Rev.*, **2013**, *65*, 60–70.
- [99] Duncan, R. *Nat. Rev. Cancer*, **2006**, *6*, 688–701.
- [100] Hardwicke, J.; Moseley, R.; Stephens, P.; Harding, K.; Duncan, R.; Thomas, D. W. *Mol. Pharmaceutics*, **2010**, *7*, 699–707.
- [101] Tao, L.; Liu, J.; Xu, J.; Davis, T. P. *Org. Biomol. Chem.*, **2009**, *7*, 3481–3485.
- [102] Besheer, A.; Hertel, T. C.; Kressler, J.; Mäder, K.; Pietzsch, M. *J. Pharm. Sci.*, **2009**, *98*, 4420–4428.
- [103] Mero, A.; Pasut, G.; Via, L. D.; Fijten, Martin W. M.; Schubert, U. S.; Hoogenboom, R.; Veronese, F. M. *J. Control. Release*, **2008**, *125*, 87–95.
- [104] Steinbach, T.; Wurm, F. R. *Angew. Chem. Int. Ed.*, **2015**, *54*, 6098–6108.

2 pH-Cleavable Polyether-based Surfactants

2.1 Acid-labile Amphiphilic PEO-*b*-PPO-*b*-PEO Copolymers: Degradable Poloxamer Analogs

Matthias Worm,^{a,b} Biao Kang,^c Carsten Dingels,^a Frederik R. Wurm,^{b,c} and Holger Frey^{a*}

^aInstitute of Organic Chemistry, Johannes Gutenberg-University, Duesbergweg 10-14, 55128 Mainz, Germany.

^bMax Planck Graduate Center (MPGC), Staudinger Weg 9, 55128 Mainz, Germany.

^cMax Planck Institute for Polymer Research, Ackermannweg 10, 55128 Mainz, Germany.

Published in Macromolecular Rapid Communication, 2016, 37, 775-780.

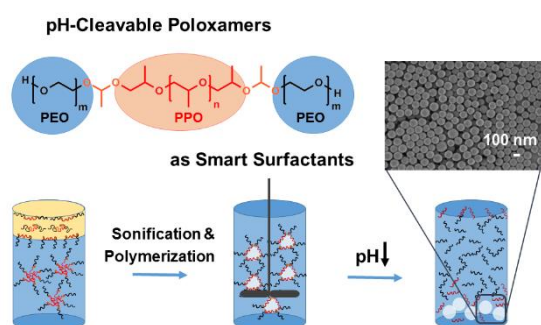
Reprinted with permission from M. Worm, B. Kang, C. Dingels, F. R. Wurm, H. Frey, *Macromolecular Rapid Communication, 2016, 37, 775-780*. Copyright 2011 WILEY-VCH Verlag GmbH & Co. KGaA, Weinheim. With permission from Wiley and Sons.

Abstract

Poly ((ethylene oxide)-*b*-(propylene oxide)-*b*-(ethylene oxide)) triblock copolymers commonly known as poloxamers or Pluronics[®] constitute an important class of non-ionic, biocompatible surfactants. We report a method to incorporate two acid-labile acetal moieties in the backbone of poloxamers to generate acid-cleavable nonionic surfactants. Poly(propylene oxide) was functionalized by means of an acetate-protected vinyl ether to introduce acetal units. Three cleavable PEO-PPO-PEO triblock copolymers ($M_{n,\text{total}} = 6600, 8000, 9150 \text{ g}\cdot\text{mol}^{-1}$; $M_{n,\text{PEO}} = 2200, 3600, 4750 \text{ g}\cdot\text{mol}^{-1}$) were synthesized using anionic ring-opening polymerization. The amphiphilic copolymers exhibited narrow molecular weight distributions ($\mathcal{D} = 1.06 - 1.08$). Surface tension measurements revealed surface-active behavior in aqueous solution comparable to established non-cleavable poloxamers. Complete hydrolysis of the labile junctions after acidic treatment was verified by size exclusion chromatography (SEC). The block copolymers were employed as surfactants in a miniemulsion polymerization to generate PS nanoparticles with mean diameters of approximately 200 nm and narrow size distribution, as determined by dynamic light scattering and

scanning electron microscopy (SEM). Acid-triggered precipitation facilitates removal of surfactant fragments from the nanoparticles, which simplifies purification and enables nanoparticle precipitation “on demand”.

Table of Contents Graphics

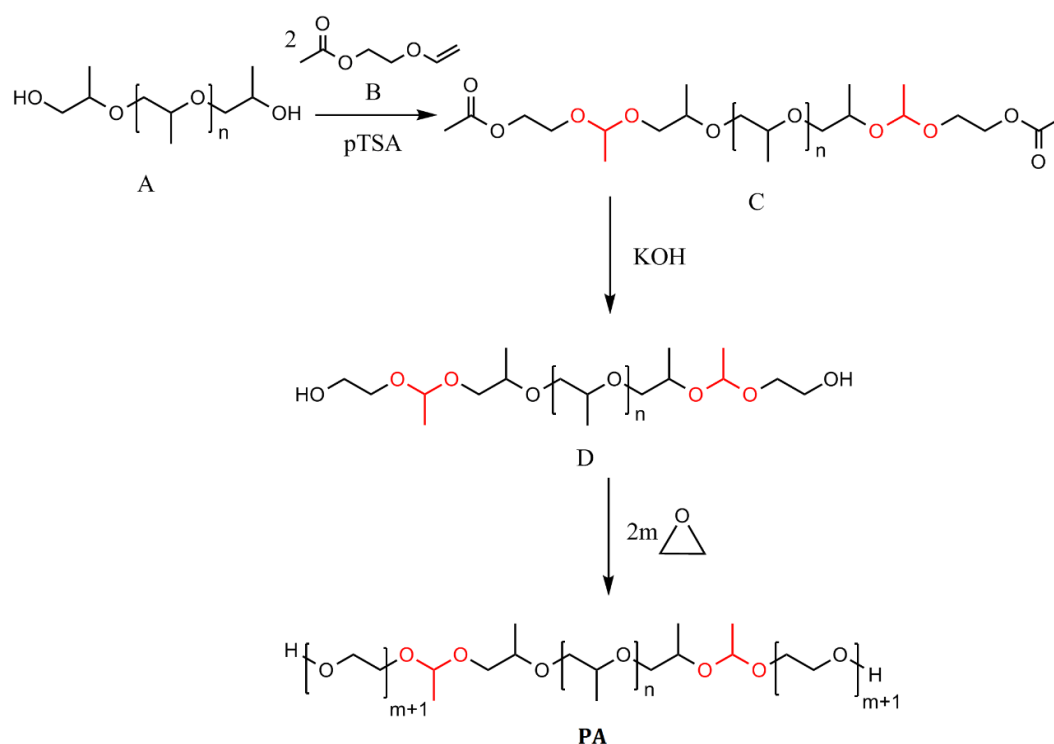


Block copolymers composed of a central hydrophobic poly(propylene oxide) (PPO) block flanked by two hydrophilic poly(ethylene oxide) (PEO) segments are commonly known as “poloxamers” and have been extensively utilized as non-ionic surfactants for sixty years. These biocompatible PEO-*b*-PPO-*b*-PEO copolymers are commercially available as Pluronics® in a broad range of molecular weights and compositions for a widespread area of applications, such as emulsifiers, dispersing agents, and lubricants in addition to more specialized applications in biomedicine, pharmaceutical sciences, and nanoscience.^[1–5] The inherently amphiphilic nature of poloxamers causes aggregation in aqueous solution, leading to the formation of micelles, i.e., spherical, polymeric assemblies comprised of a PPO-dominated core and a PEO-dominated corona.^[6] Aggregation of Pluronics® in solution has been investigated extensively, and numerous reports have focused on the determination of the critical micelle concentration (cmc).^[7] The aggregation as well as the emulsification properties of Pluronics® have given rise to their application as surfactants in miniemulsion polymerization (MEP) processes.^[8] This polymerization technique enables the one-step encapsulation of hydrophobic compounds in nanoparticles.^[9] Polymer particles of tailormade

compositions and structures have been obtained via this method using, Pluronics® as surfactants, including nanocapsules based on poly(vinyl acetate), polyurethanes, and polystyrene.^[10,11]

In recent years the integration of cleavable units into biocompatible polyethers has found increasing attention, in several cases relying on acetals and hemiacetals.^[12] These scissile units serve as molecular breaking points to assure the degradation of the polymeric structures to smaller fragments. Tomlinson *et.al.* first demonstrated the synthesis of polyacetals via polyaddition-type reactions of a divinylether/diol monomer system and proved the degradability via acidic hydrolysis.^[13] Notably, the synthesis of cleavable surface-active agents has been reported in some works, based on a variety of cleaving stimuli, such as pH, light, oxidative conditions, and temperature can be exploited to induce scission of surfactants.^[14–19] Environmental concerns, especially the toxicity of commercial detergents for aquatic organisms even at low concentrations have led to intense efforts to design scissile surfactants.^[20] Furthermore, application of surfactants containing labile units can prevent undesired foaming and further emulsification after usage of the surfactant. Especially, surfactants susceptible to acidic hydrolysis are becoming attractive because the degradation can be initiated by convenient lowering of the pH. Namely, non-ionic and ionic surfactants containing cyclic acetals and ketals as pH-sensitive linkers based on 1,3-dioxolane alkyl and 1,3-dioxane alkyl structures have been employed for pH-sensitive microemulsion formulations.^[20] The advantage of these surfactants with respect to their use in organic synthesis has been elegantly demonstrated by Bieniecki *et. al.* via the simplified recovery of the reaction product from a two phase system after acid-initiated decomposition of the surfactant.^[21] However, the emulsification properties of this class of surfactants were found to be inferior to conventional, non-cleavable surfactants due to the presence of in-chain cyclic, sterically demanding moieties.^[22] Acid-cleavable surfactants reported to date do not fulfil all requirements, such as excellent emulsification properties and well-defined structures. We introduce a novel class of cleavable, biocompatible amphiphiles based on PEO-*b*-PPO-*b*-PEO copolymers with narrow molecular weight distributions bearing two acyclic acetal units. Complete hydrolysis of the surfactants' acetal

moieties upon acidic treatment is verified by size exclusion chromatography (SEC). This new class of surfactants is derived from the well-known structure of poloxamers. Successful application of these novel amphiphiles as surfactants in the free radical miniemulsion polymerization of styrene is demonstrated. The presence of acetal moieties facilitates the acid-triggered precipitation of PS nanoparticles from the dispersion, allowing a straightforward particle purification or potential film formation “on demand”.



Scheme 6: Preparation of the cleavable PEO-*b*-PPO-*b*-PEO copolymers.

The incorporation of acetal moieties into the backbone of polyethers, such as PEG, has been developed by our group in previous works, wherein an acetate protected vinyl ether was implemented to functionalize polymeric alcohols.^[23,24] Here a bifunctional, hydroxyl-terminated poly(propylene oxide) **A** was used (Scheme 6), which contains a secondary and a primary terminal hydroxyl group. Two acetal junctions were introduced via an acid-catalyzed conversion of **A** with 2-acetoxyethoxy vinyl ether **B**. The precursor compound **B** was synthesized according to methods described in literature.^[25] Subsequently, saponification of the acetate protective groups led to the formation of the telechelic **D** that served as a macroinitiator for the anionic ring-opening

polymerization (AROP) of ethylene oxide to access the acid-labile PEO-*b*-PPO-*b*-PEO copolymers **PA**. Synthetic details are given in the Supp. Information. At first, modification of commercially available poly(propylene oxide) **A** with 2-acetoxyethoxy vinyl ether **B** was conducted using *p*-toluenesulfonic acid as a catalyst. Quenching of the reaction with triethylamine after 15 min was essential, as shorter reaction times led to incomplete functionalization. The successful formation of the acetyl-protected PPO derivative **C** was confirmed via ¹H NMR spectroscopy, SEC analysis, and MALDI ToF mass spectrometry (See SI, Figure S-1, S-2 and S-4). Complete conversion of the PPO hydroxyl groups was indicated by ¹H NMR spectroscopy. Integration of the acetal proton signals of both PPO termini at 4.9 and 4.8 ppm, respectively, exhibited normalized values of 1.0, concluding that functionalization of both hydroxyl groups of PPO occurred to the same extent (Figure S-1). Further verification of the quantitative functionalization of PPO was obtained via SEC hydrolysis experiments described in the following.

Complete saponification of the terminal acetate moieties in the second step of the synthesis was confirmed by FTIR spectroscopy. The disappearance of the carbonyl stretches at 1740 cm⁻¹ and the appearance of the expected broad stretch vibration of the liberated terminal hydroxyl groups at 3400 cm⁻¹ indicate complete removal of the terminal acetate units (Figure S-5). In addition, ¹H NMR spectroscopy revealed the loss of the acetate proton signals at 2.0 ppm, while the protons corresponding to the acetal groups remained unchanged. MALDI ToF MS confirmed the presence of the PPO derivative **D** unambiguously (Figure S-3 and S-6).

In the final step of the synthesis, AROP of ethylene oxide was carried out in THF solution, using the telechelic PPO **D** as a macroinitiator. The resulting acid-labile PEO-*b*-PPO-*b*-PEO block copolymers (henceforth referred to as **poloxamer analogs, PAs**) were isolated by precipitation in diethyl ether. Figure 1A shows the corresponding SEC traces of three polymer samples (**PA-1**, **PA-2**, **PA-3**) in comparison to the PPO precursor **A**. All samples exhibit narrow, monomodal molecular weight distributions ($\mathcal{D} = 1.06 - 1.08$) with significant shifts to higher molecular weights compared to the non-functionalized PPO. ¹H NMR spectroscopy confirmed the integrity of the acetal junctions at 4.8

ppm within the block copolymers and the presence of the PEO backbone protons at 3.6 ppm. PEO proton signals partly overlap with the polyether backbone of PPO between 3.8 and 3.2 ppm. In order to determine molecular weights of the block copolymers, integration of the backbone signals in ^1H NMR spectroscopy was conducted. The molecular weight of the PPO block was calculated from the PPO precursor **D** based on integration of the methyl backbone protons at 1.2 - 1.0 ppm in comparison to the normalized acetal proton signals at 4.9 and 4.8 ppm. (Figure S-3) The fact that the methyl protons of the PPO backbone were significantly shifted upfield in relation to the PEO, PPO methine and PPO methylene protons could be utilized to determine the molecular weights of the PEO blocks (Figure 1C). The values obtained for the acid-labile PEO-*b*-PPO-*b*-PEO copolymers as well as for the PEO and PPO blocks are summarized in Table 1. The generic terms (Pxy) according to the established nomenclature for poloxamers are employed. Therein, the first two digits multiplied by 100 correspond to the approximate molecular weight of the PPO block whereas the last digit multiplied by a factor of 10 represents the weight percentage of PEO. The synthesized PEO-*b*-PPO-*b*-PEO **PA-1**, **PA-2**, **PA-3** are categorized as P403, P404 and P405 according to this category system.

Table 3: Characteristics of acid-cleavable PEO-*b*-PPO-*b*-PEO copolymers **PA-1**, **PA-2** and **PA-3**.

Sample	$M_{n,\text{NMR}}$ (PA)	$M_{n,\text{NMR}}$ (PPO)	$M_{n,\text{NMR}}$ (PEO)	$M_{n,\text{SEC}}$ (PEO)	$n/[(\text{EO})_{2n}(\text{PO})_{63}]$	\mathcal{D}_{PA}	cmc / g L	HLB	Pxy
	g/mol								
PA-1	5700	3700	2000	2000	23	1.06	0.05	7.0	P403
PA-2	6900	3700	3200	3100	36	1.06	0.12	9.3	P404
PA-3	7900	3700	4200	4600	48	1.08	0.03	10.6	P405

$M_{n,\text{NMR}}(\text{PA})$ = molecular weights of PAs from NMR; $M_{n,\text{NMR}}(\text{PPO})$ = molecular weights of PPO block calculated from NMR using PPO precursor **D**; $M_{n,\text{NMR}}(\text{PEO})$ = molecular weights of PEO fraction calculated from NMR; $M_{n,\text{SEC}}(\text{PEO})$ = molecular weights of PEO fraction determined from SEC data after acidic hydrolysis using PEG standards; $n/[(\text{EO})_{2n}(\text{PO})_{63}]$ = degree of polymerization of PEO fraction; $\mathcal{D}_{\text{PA,SEC}} = M_w/M_n$ (dispersity); **cmc** = critical micelle concentrations determined by ring tensiometry measurements; **HLB** = hydrophilic-lipophilic balance; **Pxy** = generic term according to nomenclature of poloxamers.

Susceptibility to acidic hydrolysis of the synthesized PEO-*b*-PPO-*b*-PEO copolymers was studied by SEC analysis. Aliquots of the polymer samples were treated with diluted TFA and subsequently analyzed by SEC. Figure 1B illustrates the results obtained for sample **PA-1** before and after hydrolysis in comparison to the PPO precursor.

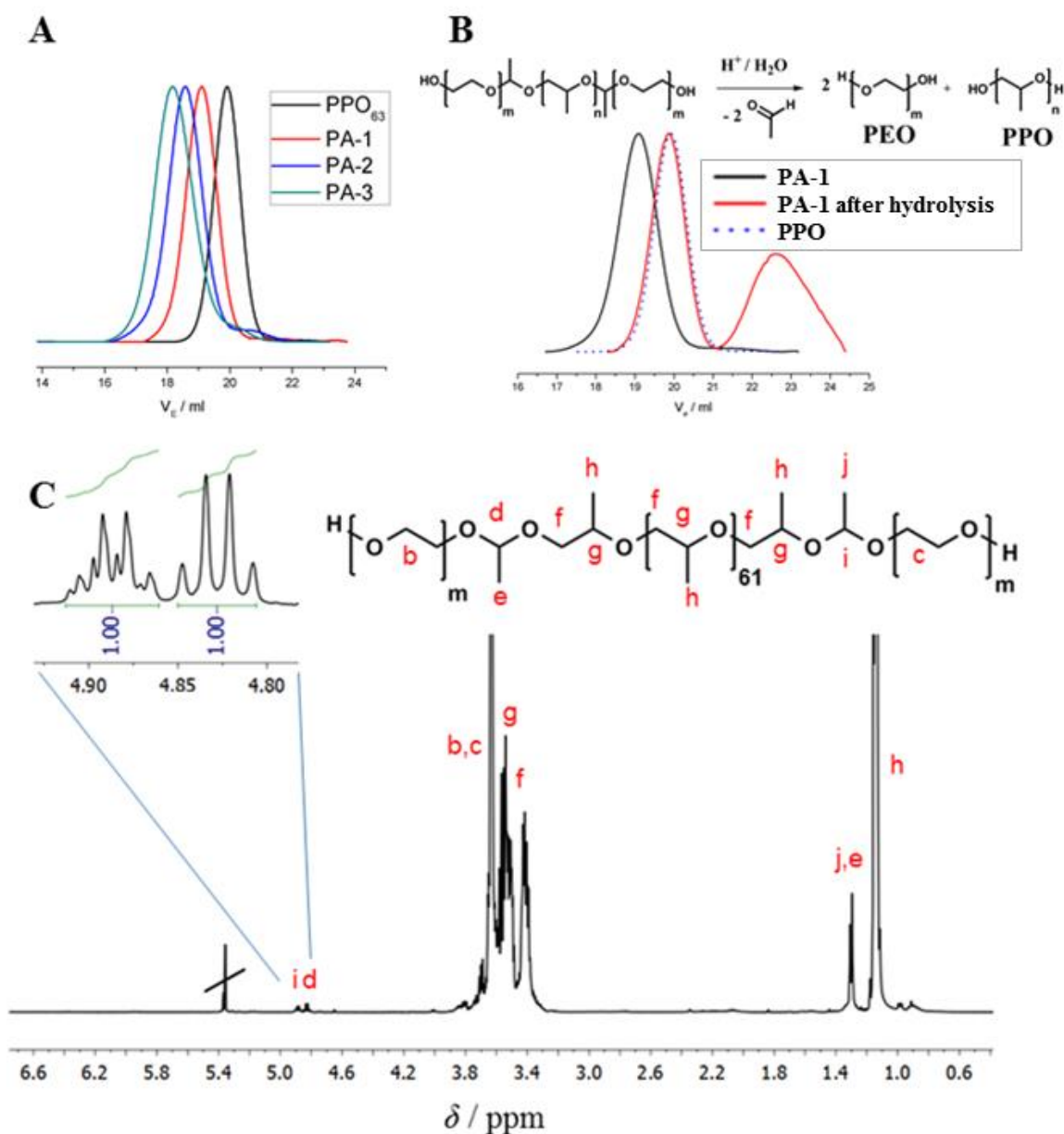


Figure 9: A: SEC traces of poloxamer analogs **PA-1,2,3** (red, blue, green) in comparison with the PPO precursor (black) using DMF as eluent. B: Top: Hydrolysis reaction. Bottom: SEC traces of **PA-1** before (black) and after (red) acidic hydrolysis in comparison with PPO precursor (dashed). C: ^1H NMR spectra of PA in CD_2Cl_2 at 400 MHz (298 K). The region between 4.9 - 4.6 ppm showing the acetal signals was magnified.

The SEC trace of the sample after acidic treatment revealed a bimodal size distribution, confirming the reaction given in the scheme below (Figure 1B). The good overlap of the high molecular weight fraction with the SEC trace of the PPO precursor verified that this size distribution corresponds to the non-functionalized PPO released during hydrolysis. Furthermore, the appearance of a second distribution at higher elution volume was attributed to the PEO fragments. In addition, the monomodal molecular weight distribution ($\mathcal{D} = 1.06$) accounted for the symmetry of the two PEO blocks introduced via AROP of ethylene oxide, resulting in poloxamer analogous structures. Moreover, the disappearance of the PEO-*b*-PPO-*b*-PEO block copolymer signal in the SEC trace confirms cleavability of the polymers and provides evidence that only scissile PEO-*b*-PPO-*b*-PEO structures are contained in the samples. This experiment retrospectively verifies quantitative functionalization of the PPO precursor **A** in the first reaction step. Equivalent results were obtained for the acidic hydrolysis of all polymer samples. (Figure S-13 and S-14)

Molecular weights of the PEO blocks were estimated from the SEC traces after hydrolysis using PEG standards. The values obtained were summarized in Table 1 and agree well with the results from NMR analysis. The novel acid-labile PEO-*b*-PPO-*b*-PEO copolymers were characterized by surface tension measurements revealing critical micelle concentrations (cmc) in the range of 0.03 to 0.12 g·L⁻¹ (Table 1). Critical micelle concentrations of Pluronics® have been discussed controversially in the literature and reported values differ by as much as three orders of magnitude. Mostly, fluorescent probe studies and surface tension measurements were reported, however Kabanov *et.al.* demonstrated that the values obtained from both techniques are in good agreement.^[26] Due to the lack of systematic surface tension data on cmc values of Pluronics®, results of fluorescent probe measurements were taken as a reference. A set of reported cmc data obtained via pyrene probe analysis for Pluronics® covering the molecular weight range of **PA** polymers in the region of 6000 to 12000 g·mol⁻¹ and M_n (PEO) ranging from 2400 to 8800 g·mol⁻¹ was found suitable for comparison.^[7] The respective cmc values range from 0.02 – 0.40 g·L⁻¹, matching well with the results obtained in the current study for the acid-labile PEO-*b*-PPO-*b*-PEO copolymers.

The application of the cleavable polymers as surfactants in miniemulsion polymerizations (MEPs) was studied in a proof-of-principle synthesis of polystyrene nanoparticles. As a reference experiment, the MEP of styrene was conducted using *Lutensol*[®] AT 25, a common non-ionic surfactant based on a polyalkylene glycol ether, to evaluate the properties of the novel cleavable amphiphiles. The polymerization was carried out in a direct (oil-in-water) miniemulsion. Styrene and the initiator (AIBN) were dispersed together with the osmotic pressure agent hexadecane in water containing the surfactants (8 wt%) (SI). Stable miniemulsions were only obtained in the case of polymer sample **PA-3**, due to the higher hydrophilicity of this surfactant compared to the other block copolymers. This observation is also in agreement with the HLB values of the surfactants. **PA-1** (HLB = 7.0) and **PA-2** (HLB = 9.3) exhibit values close to 8, whereas, in case of **PA-3** (HLB = 10.6), a HLB exceeding 10 suggests effective stabilization of oil-in-water emulsions.

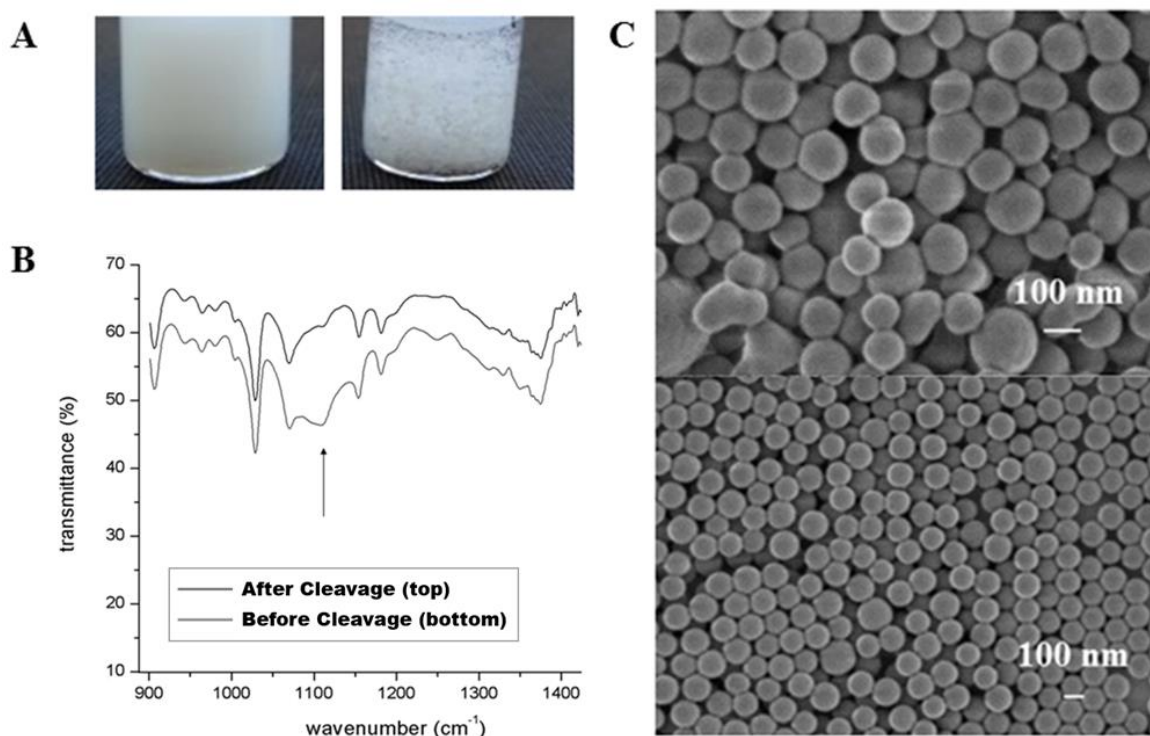


Figure 10: **A:** PS particle emulsions stabilized by Lutensol[®] (left) and PA-3 (right) after acidification. **B:** FTIR spectra of PS particles before (bottom) and after (top) acidification. **C:** SEM images of PS nanoparticles prepared via MEP using Lutensol[®] (top) and PA-3 (bottom) as surfactants.

After the MEP, the resulting PS nanoparticle dispersions were acidified by addition of hydrochloric acid, resulting in the immediate destabilization of the emulsion and precipitation of the particles. In contrast, *Lutensol*[®] miniemulsions remained stable under the same conditions. (Figure 2A) Destabilization of the emulsion is due to the cleavage of the acetal moieties and the scission of the surfactant triggered by acidic treatment (pH = 1.5). This property is highly desired, as the surfactant enables a simplified purification protocol of nanoparticles.

The successful cleavage of the surfactant and separation of the polyether fragments from polystyrene particles was proven by FTIR spectroscopy. The disappearance of the ether stretch vibration at 1095 cm⁻¹ after acidic treatment indicates the absence of polyether fragments in the particles and highlighted the advantage of this class of pH-cleavable surfactants as the purity of particles was improved significantly. The size of the PS nanoparticles was determined by dynamic light scattering (*Lutensol*[®]: 170 nm +/- 17 nm; **PA-3**: 210 nm +/- 17 nm) proving a narrow size distribution in both cases. SEM images of the PS nanoparticles further underline the homogeneous nature of generated nanoparticles (Figure 2).

In conclusion, novel acid-labile PEO-*b*-PPO-*b*-PEO copolymers were synthesized and effectively used as surfactants which are 'cleavable on demand' in miniemulsion polymerizations. Three different copolymers with similar PPO blocks and varying PEO segments ($M_n = 6600, 8000, 9150 \text{ g}\cdot\text{mol}^{-1}$; $M_{n,\text{PEO}} = 2200, 3600, 4750 \text{ g}\cdot\text{mol}^{-1}$) were prepared, exhibiting narrow molecular weight distributions with $\mathcal{D} < 1.1$. Susceptibility to acid hydrolysis of the cleavable moieties was verified by SEC analysis. The cmc of the block copolymers in aqueous solutions was investigated by surface tension measurements revealing values in the range of 0.03 - 0.12 g·L⁻¹ that are in good agreement with reported cmc values for Pluronics[®] of comparable molecular composition. The cleavable PEO-*b*-PPO-*b*-PEO copolymers were employed as surfactants in the miniemulsion polymerization of styrene. Only the block copolymer with the highest PEO content and an HLB value exceeding 10, i.e. sample **PA-3** enabled formation of stable emulsions yielding PS nanoparticles with average diameters of 200 nm, as confirmed by SEM and DLS. Acid-triggered precipitation simplified particle

purification and allowed for efficient separation of surfactant fragments, resulting in surfactant-free nanoparticles, as confirmed by IR spectroscopy. The simplified purification process highlights the fundamental advantage of this new class of surfactants. The degradable poloxamer analogs offer great potential for the fabrication of surfactant-free nanoparticles and -capsules as well as the development of pH-responsive colloidal formulations and pH-triggered film formation.

Associated Content

SI Supporting Information

Materials, experimental procedures, NMR spectra, MALDI-ToF MS and SEC characterization, DLS data.

Author Information

Corresponding Author

*Mailing address: Institute of Organic Chemistry, Johannes Gutenberg-University, Duesbergweg 10-14, D-55128 Mainz, Germany. Phone: +49 (0)6131-39 24078, fax: +49 (0)6131-39 26106, e-mail: hfrey@uni-mainz.de

Acknowledgments

M.W. is grateful to the Max Planck Graduate Center (MPGC) for a fellowship and financial support. F.R.W. thanks the Max Planck Graduate Center (MPGC). The authors thank Prof. Katharina Landfester for support and helpful discussions.

Notes

The authors declare no competing financial interest.

Keywords

Ploxamers, non-ionic surfactant, polyethers, acid-cleavable amphiphilic block copolymers, PEG, miniemulsion polymerization

References

- [1] Pitto-Barry, A.; Barry, Nicolas P. E. *Polym. Chem.*, **2014**, *5*, 3291–3297.
- [2] Alakhova, D. Y.; Kabanov, A. V. *Mol. Pharmaceutics.*, **2014**, *11*, 2566–2578.
- [3] Stolnik, S.; Illum, L.; Davis, S. S. *Adv. Drug Delivery Rev.* **2012**, *64*, 290–301.
- [4] Chiappetta, D. A.; Sosnik, A. *Eur. J. Pharm. and Biopharm.* **2007**, *66*, 303–317.
- [5] Herzberger, J.; Niederer, K.; Pohlitz, H.; Seiwert, J.; Worm, M.; Wurm, F. R.; Frey, H. *Chem. Rev.* **2016**, *116*, 2170–2243.
- [6] Torcello-Gómez, A.; Wulff-Pérez, M.; Gálvez-Ruiz, M. J.; Martín-Rodríguez, A.; Cabrerizo-Vílchez, M.; Maldonado-Valderrama, J. *Adv. Colloid Interface Sci.* **2014**, *206*, 414–427.
- [7] Kozlov, M. Y.; Melik-Nubarov, N. S.; Batrakova, E. V.; Kabanov, A. V. *Macromolecules* **2000**, *33*, 3305–3313.
- [8] Durand, A.; Marie, E. *Adv. Colloid Interface Sci.* **2009**, *150*, 90–105.
- [9] Antonietti, M.; Landfester, K. *Prog. Polym. Sci.* **2002**, *27*, 689–757.
- [10] Bathfield, M.; Graillat, C.; Hamaide, T. *Macromol. Chem. Phys.* **2005**, *206*, 2284–2291.
- [11] Zanetti-Ramos, B. G.; Lemos-Senna, E.; Cramail, H.; Cloutet, E.; Borsali, R.; Soldi, V. *Mater. Sci. Eng. C* **2008**, *28*, 526–531.
- [12] Dingels, C.; Frey, H. *Adv. Polym. Sci.* **2013**, *262*, 167–190.
- [13] Tomlinson, R.; Klee, M.; Garrett, S.; Heller, J.; Duncan, R.; Brocchini, S. *Macromolecules* **2002**, *35*, 473–480.
- [14] Tehrani-Bagha, A.; Holmberg, K. *Curr. Opin. Colloid Interface Sci.* **2007**, *12*, 81–91.
- [15] Dan, K.; Ghosh, S. *Angew. Chem. Int. Ed.* **2013**, *52*, 7300–7305.
- [16] Akram, M.; Bhat, I. A.; Kabir-ud-Din. *J. Phys. Chem. B* **2015**, *119*, 3499–3509.
- [17] Aikawa, S.; Shrestha, R. G.; Ohmori, T.; Fukukita, Y.; Tezuka, Y.; Endo, T.; Torigoe, K.; Tsuchiya, K.; Sakamoto, K.; Sakai, K.; Abe, M.; Sakai, H. *Langmuir* **2013**, *29*, 5668–5676.
- [18] Basak, D.; Bej, R.; Ghosh, S. *Polym. Chem.* **2015**, *6*, 6465–6474.

- [19] Yurt, S.; Uche, K. A.; Scheintaub, J. R.; Coughlin, E. B.; Venkataraman, D. *Macromolecules*, **2006**, *39*, 1670-1672.
- [20] Lundberg, D.; Stjerndahl, M.; Holmberg, K. *Adv. Polym. Sci.* **2008**, *218*, 57-82.
- [21] Bieniecki, A.; Wilk, K. A. *J. Phys. Org. Chem.* **1995**, *8*, 71–76.
- [22] Rairkar, M. E.; Diaz, M. Elena; Torriggiani, M.; Cerro, R. L.; Harris, J. Milton; Rogers, S. E.; Eastoe, J.; Gomez del Rio, Javier A.; Hayes, D. G. *Colloids Surf. A Physicochem. Eng. Asp.* **2007**, *301*, 394–403.
- [23] Dingels, C.; Müller, S. S.; Steinbach, T.; Tonhauser, C.; Frey, H. *Biomacromolecules* **2013**, 448–459.
- [24] Pohlit, H.; Bellinghausen, I.; Schömer, M.; Heydenreich, B.; Saloga, J.; Frey, H. *Biomacromolecules* **2015**, *16*, 3103–3111.
- [25] Greenland, B. W.; Liu, S.; Cavalli, G.; Alpay, E.; Steinke, J. H. G. *Polymer* **2010**, *51*, 2984–2992.
- [26] Kabanov, A. V.; Nazarova, I. R.; Astafieva, I. V.; Batrakova, E. V.; Alakhov, V. Y.; Yaroslavov, A. A.; Kabanov, V. A. *Macromolecules* **1995**, *28*, 2303–2314.

Supporting Information

Acid-labile Amphiphilic PEO-*b*-PPO-*b*-PEO Copolymers:

Degradable Poloxamer Analogs

Matthias Worm,^{a,b} Biao Kang,^c Carsten Dingels,^a Frederik R. Wurm,^{b,c} and Holger Frey^{a*}

^aInstitute of Organic Chemistry, Johannes Gutenberg-University, Duesbergweg 10-14, 55128 Mainz, Germany.

^bMax Planck Graduate Center (MPGC), Staudinger Weg 9, 55128 Mainz, Germany.

^cMax Planck Institute for Polymer Research, Ackermannweg 10, 55128 Mainz, Germany.

Experimental Section

Materials and Characterization

Poly(propylene oxide) ($M_n = 3700$ g/mol) and p-toluenesulfonic acid mono hydrate (pTSA) were purchased from *Sigma Aldrich*. 2-Acetoxyethoxy vinyl ether was synthesized according to reported procedures.^[1] THF was dried over sodium/benzophenone. Dry dichloromethane (DCM) in a sealed bottle with molecular sieve was purchased from *Sigma Aldrich*. *Lutensol*[®] AT 25 Powder ($M_n = 1360$ g/mol) was purchased from *BASF*. Deuterated dichloromethane- d_2 was purchased from *Deutero GmbH*. All other chemicals were purchased from common commercial sources and used as received unless otherwise noted. ¹H NMR was measured on a Bruker AC 400 MHz with a 5 mm BBO probe at 294 K. GPC (SEC) data were obtained using Agilent 1100 Series endowed with a PSS HEMA-column ($10^6/10^4/10^2$ Å porosity), LiBr/DMF (1 g/L) as eluent and RI detector. Polydispersity indices ($\mathcal{D} = M_w/M_n$) were determined using monodisperse PEG standards from *Polymer Standard Service GmbH (PSS)*. MALDI-ToF mass spectrometry was conducted on an Axima CFR MALDI-ToF mass spectrometer using α -cyano-4-hydroxy-cinnamonic acid (CHCH) as matrix and potassium trifluoroacetate (KTFA) as a source for cations. Surface tension measurements to determine critical micelle concentrations (cmc) were performed on a DATA Physics DCAT 11 EC tensiometer with a TV 70 temperature control unit, a LDU 1/1 liquid dosing and refill unit as well as a RG 11 Du Noüy ring.

Miniemulsion systems were generated by ultrasonification using a Branson Sonifier W-450-Digital and a 1/8" tip, at 70% amplitude for 2 min. Afterwards the systems were placed in a thermal shaker at 72°C overnight. Dynamic Light Scattering (DLS). The size of the polystyrene particles was determined by DLS, using a PSS Nicomp Particle Sizer 380. The particle dispersion were diluted with MilliQ water to a solid content of 0.1%. The temperature is maintained at 25 °C while the scattered light is detected at an angle of 90°. Scanning Electron Microscopy (SEM) measurements were carried out by using a LEO (Zeiss) 1530 Gemini device (Oberkochen, Germany). The sample were diluted with MilliQ water, until the solid content was 0.01%. 20 µl of the dispersion were placed on the silica wafer, and dried at room temperature overnight. The images are obtained with an acceleration voltage of 350 V. Fourier transform infrared spectroscopy (FTIR) was proceeded using a BX spectrometer from Perkin-Elmer. 1.5 mg of the freeze dried sample was pressed with KBr to form a pellet, and the spectrum was recorded between 4000 and 400 cm⁻¹.

Di-(1-(2-acetoxyethoxy)-ethoxy)-α,ω-poly (propylene oxide) C. Poly (propylene oxide) ($M_n = 3700$ g/mol, 600 mg, 0.162 mmol), p-toluenesulfonic acid (pTSA) (4.2 mg, 0.022 mmol) were dissolved in benzene (6 mL), dried under vacuum and dissolved in dry DCM (12 mL). Subsequently, 2-acetoxyethoxy vinyl ether (297 mg, 2.23 mmol) was dissolved in toluene (6 mL) and the solvent was removed under reduced pressure. After adding DCM (6 mL) the solution was transferred into the reaction vessel the reaction mixture was stirred for 15 min under Ar atmosphere at ambient temperature and then quenched with triethylamine (10 mL). The solvent was evaporated under reduced pressure leaving a colorless residue that was dissolved in petroleum ether (50 mL) and rinsed with 1 N sodium hydroxide two times. The aqueous fractions were extracted with petroleum ether twice, the combined organic layers were dried over sodium sulfate and the solvent was evaporated under reduced pressure. After removing all volatiles in vacuum a colorless oil was obtained (635 mg, 0.160 mmol, 98 %). ¹H NMR (400 MHz, CD₂Cl₂): δ [ppm] = 4.89 (m, 1H, i), 4.81 (q, 1H, J = 5.3 Hz, d), 4.16-3.43 (m, 198H, b+c+f+g), 2.04 (s, 6H, a), 1.26 (d, 6H, J = 5.3 Hz, e+j), 1.28-1.25 (m, 190H, h)

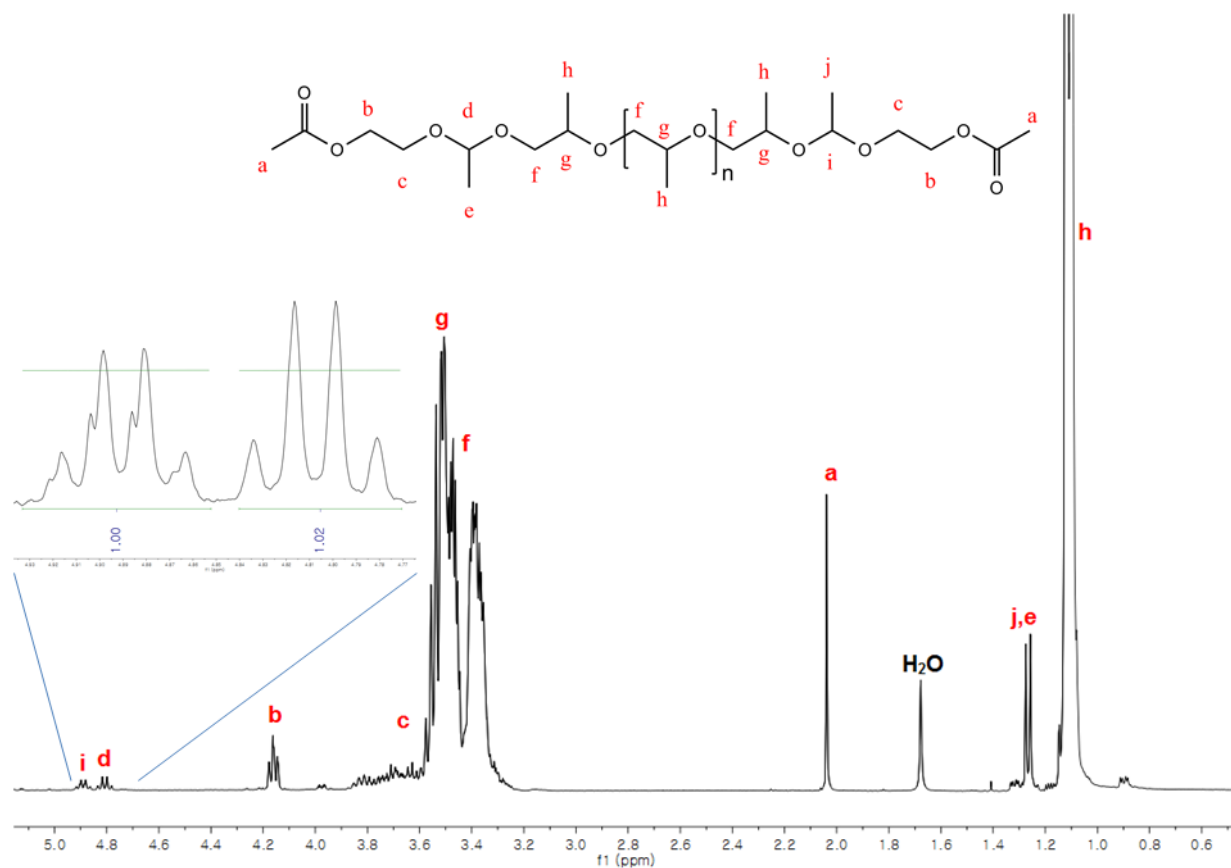


Figure S-1: ^1H NMR spectra of **C** measured in CD_2Cl_2 at 400 MHz.

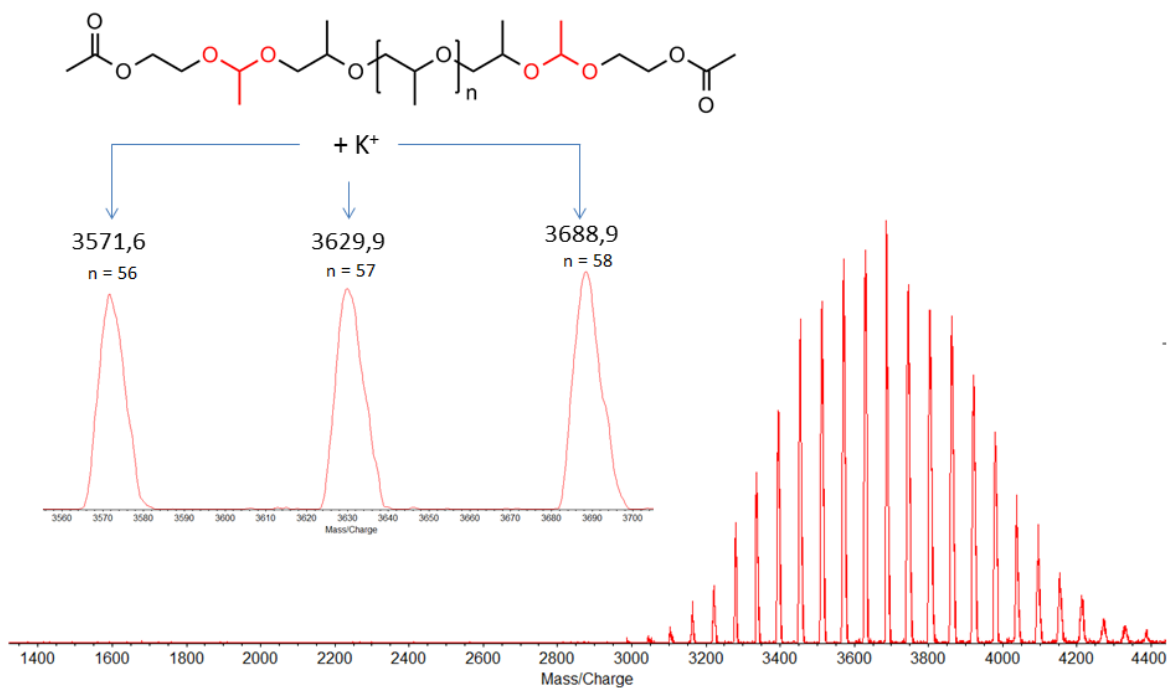


Figure S-2: MALDI-ToF MS of **C** using a CHCA matrix and KTFA as salt.

Di-(1-(2-hydroxyethyl)-ethoxy)- α,ω -poly(propylene oxide) D. Compound **C** (634 mg, 0,160 mmol) and KOH (360 mg, 6.43 mmol) were stirred under reflux in a mixture of ethanol (64 mL) and H₂O (3.8 mL, 0.21 mmol) for 2h. Ethanol was removed under reduced pressure to give a colorless residue that was dissolved in petroleum ether (100 mL), rinsed with 0.1 N NaOH two times and the aqueous layer was extracted with petroleum ether. After drying the combined organic layer over sodium sulfate, the solvent was removed and the viscous oil (536 mg, 0.138 mmol, 86 %) was dried in vacuum for 16 h. ¹H NMR (400 MHz, CD₂Cl₂): δ [ppm] = 4.89 (m, 1H, **i**), 4.82 (q, 1H, $J = 5.3$ Hz, **d**), 4.16-3.43 (m, 198H, **b+c+f+g**), 2.58 (m, 1H, **k/a**), 2.29 (m, 1H, **k/a**), 1.29 (d, 3H, $J = 5.3$ Hz, **j**), 1.27 (d, 3H, $J = 5.3$ Hz, **e**), 1.16-0.98 (m, 190H, **h**)

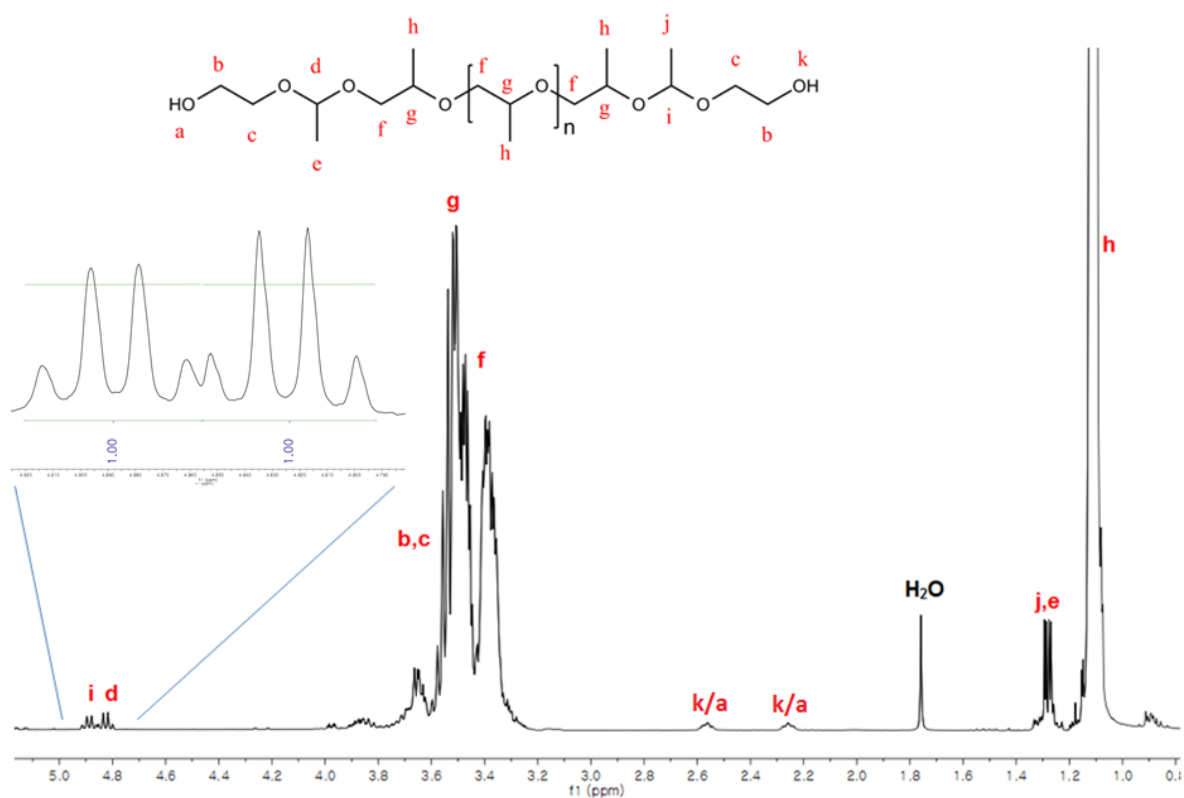


Figure S-3: ¹H NMR spectra of **D** measured in CD₂Cl₂ at 400 MHz.

SEC traces obtained after reaction with the vinyl ether **B** revealed a higher molecular weight species. (Supporting Information, Figure S-4) This observation is explained by a side reaction involving a transacetalization leading to the formation of symmetric acetals.^[21] SEC analysis indicates a molecular weight close to $7\text{ k g}\cdot\text{mol}^{-1}$ corresponding to a PPO homo-acetal. However, this undesired, high molecular weight byproduct was completely removed by precipitation of the final PEO-*b*-PPO-*b*-PEO copolymers in diethyl ether.

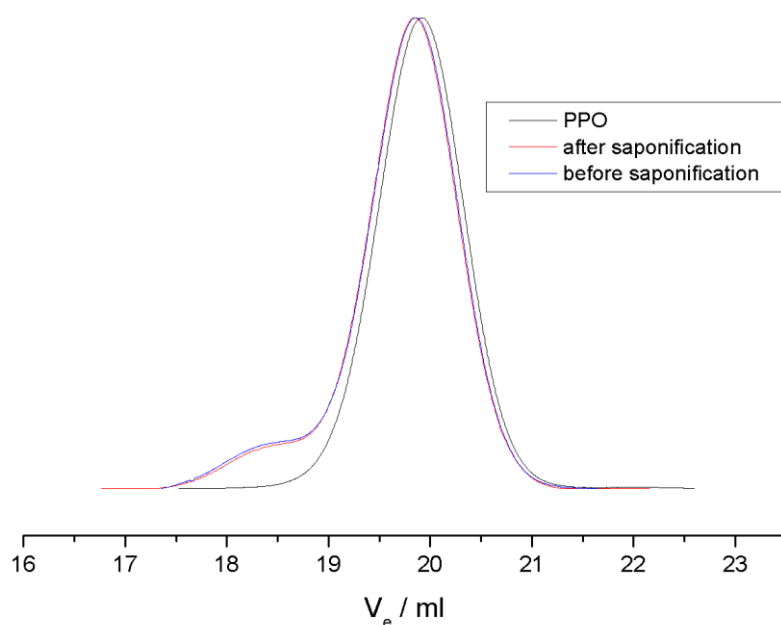


Figure S-4: SEC traces of PPO precursor **A** (black), **C** (blue) and **D** (red).

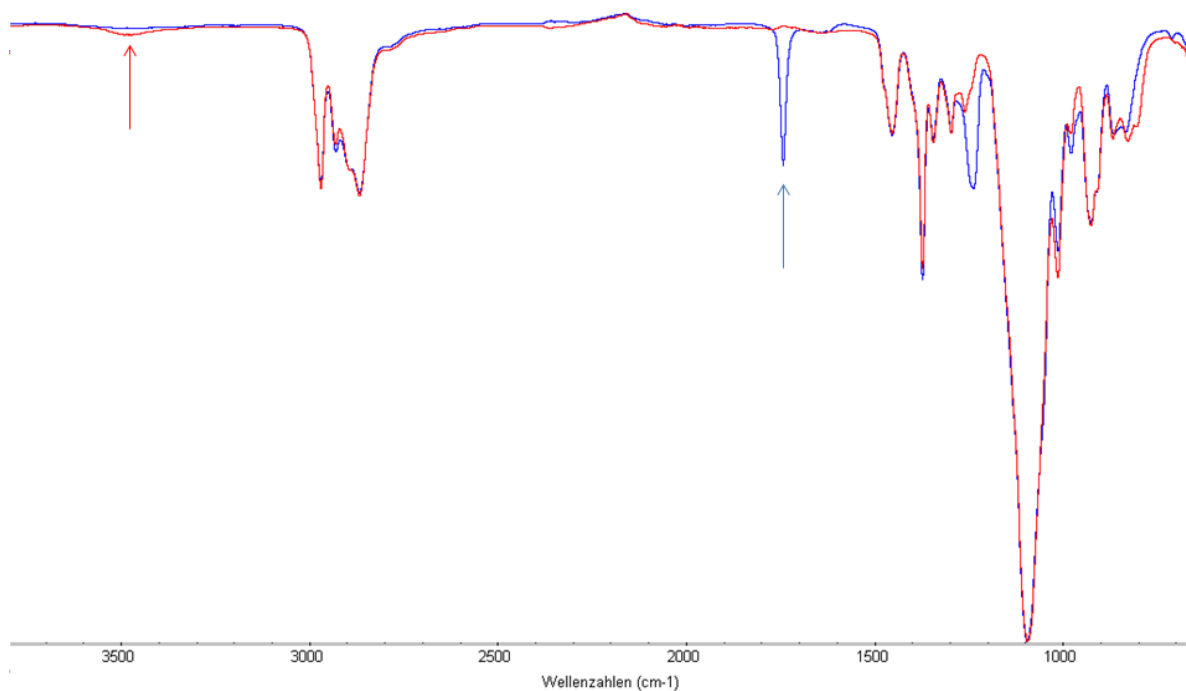


Figure S-5: FT-IR spectra of C (blue) and D (red).

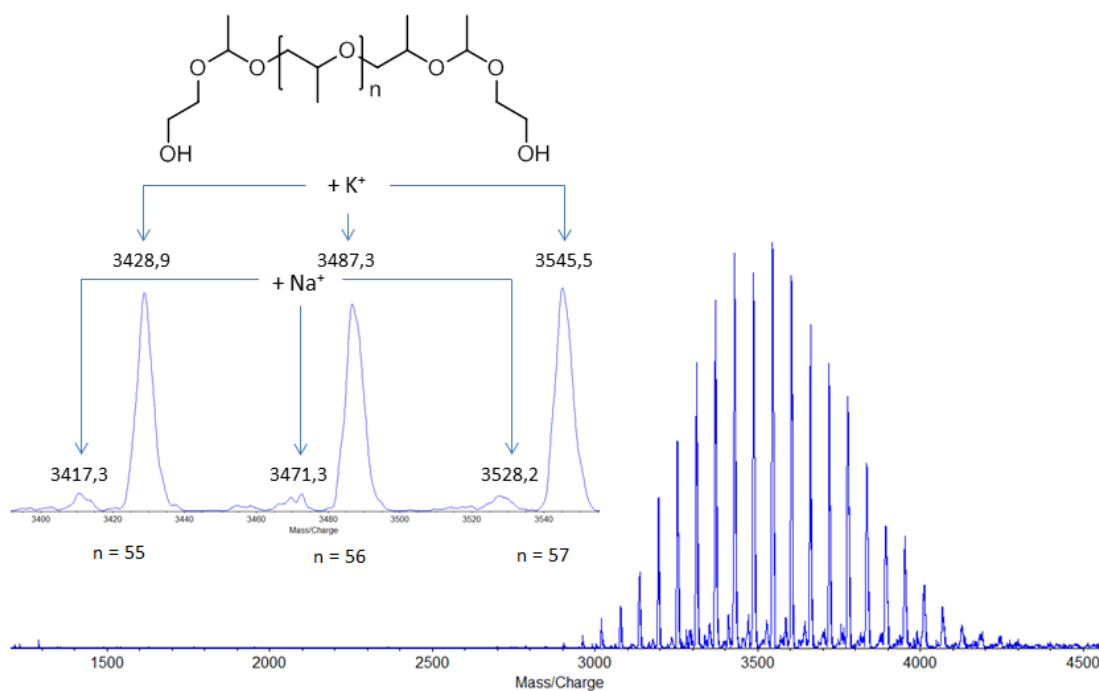


Figure S-6: MALDI-ToF MS of D using a CHCA matrix and KTFA as salt.

Synthesis of PEO-*b*-PPO-*b*-PEO copolymers.

The procedure is described for the synthesis of polymer sample **PA-3**, however was carried out accordingly for all PEO-*b*-PPO-*b*-PEO polymers discussed in this study. Compound **D** (520 mg, 0.134 mmol) was dissolved in benzene (20 mL) in a dry Schlenk flask. After stirring the solution at 70 °C for 30 min under slightly reduced keeping the stopcock closed moisture was removed by azeotropic distillation of benzene and drying under high vacuum for 16 h. The flask was then cooled to room temperature, dry THF was cryo-transferred into the Schlenk flask and potassium naphthalenide in THF (0.35 mL, $c = 0.5 \text{ mol/l}$, 0.176 mmol) was added via syringe. Potassium naphthalenide in THF solution ($c = 0.5 \text{ mol/l}$) was prepared under argon from potassium (235 mg, 6.0 mmol), naphthalene (770 mg, 6.0 mmol) and dry THF (12 mL) prior in a glovebox. Subsequently, the formed hydrogen and half of the THF was evaporated followed by the cryo-transfer of ethylene oxide (1.8 mL, 36 mmol) via a graduated ampule to the macroinitiator solution. The reaction mixture was stirred for 3 h at 40 °C and then allowed to react for 3 d at 60 °C. After quenching the reaction with methanol (5 mL) the polymer was precipitated from DCM in cold diethyl ether three times and dried in high vacuum. Yield: 740 mg (70 %). $^1\text{H NMR}$ (400 MHz, CD_2Cl_2): δ [ppm] = 4.89 (m, 1H, **i**), 4.82 (q, 1H, $J = 5.3 \text{ Hz}$, **d**), 3.65-3.55 (m, H_{PEO} , **b**), 3.91-3.20 (m, 568H, **b+c+f+g**), 1.26 (d, 6H, $J = 5.3 \text{ Hz}$, **j+e**) 1.16-0.98 (m, 190H, **h**)

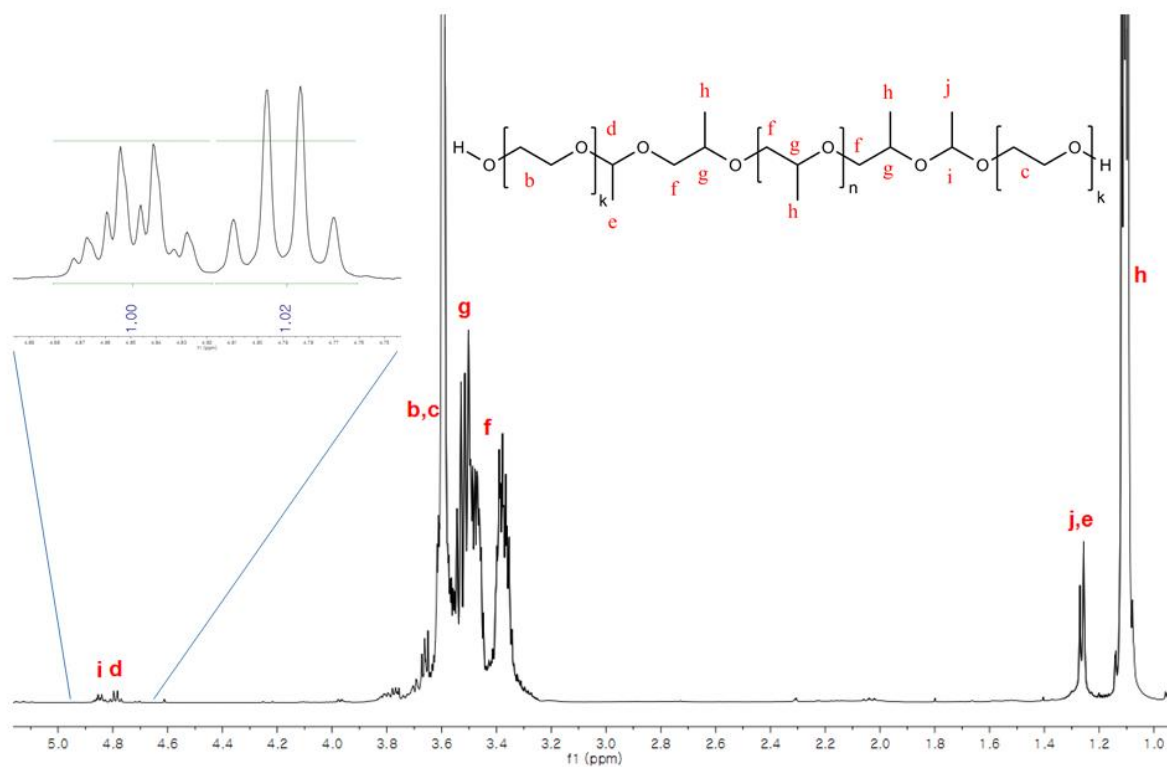


Figure S-7: ^1H NMR spectra of PA measured in CD_2Cl_2 at 400 MHz.

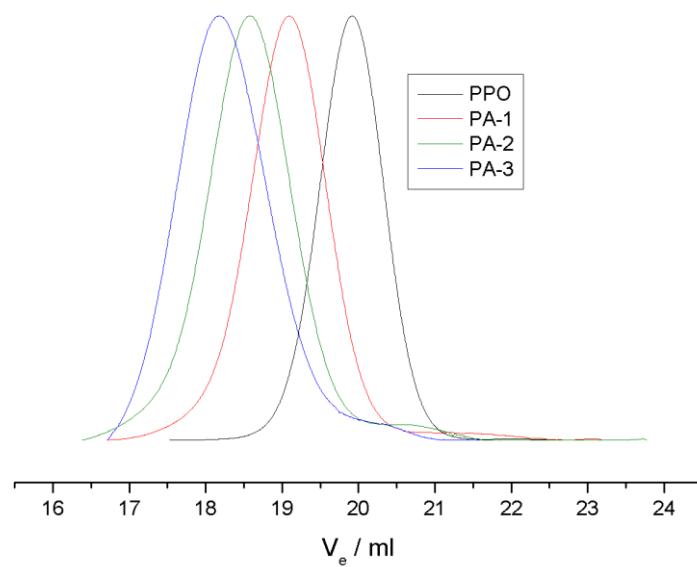


Figure S-8: SEC traces of PPO precursor A, PA-1, PA-2 and PA-3.

Hydrolysis studies of PEO-*b*-PPO-*b*-PEO copolymers. PEO-*b*-PPO-*b*-PEO samples (10 mg) were dissolved in mixture TFA / H₂O (5 mL, v/v: 2/1) and stirred for 1 d at ambient temperature. Solvent was evaporated under reduced pressure and moisture was removed by azeotropic distillation with benzene (2x3ml). Subsequently, the polymeric residue was analyzed by SEC measurements.

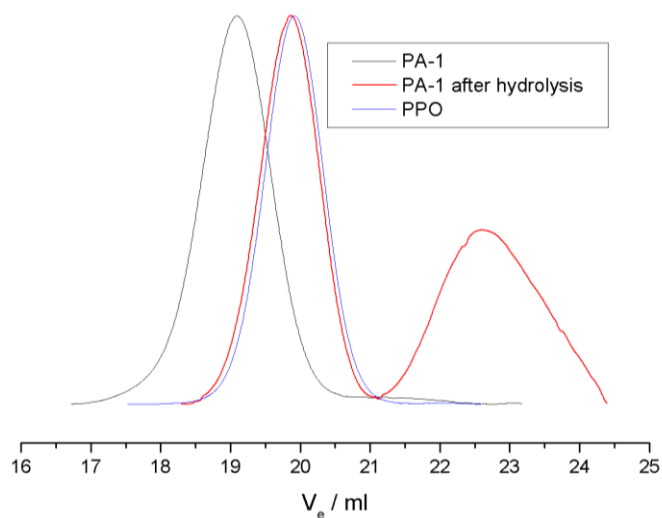


Figure S-9: SEC traces of PA-1 before and after hydrolysis in comparison with PPO precursor A.

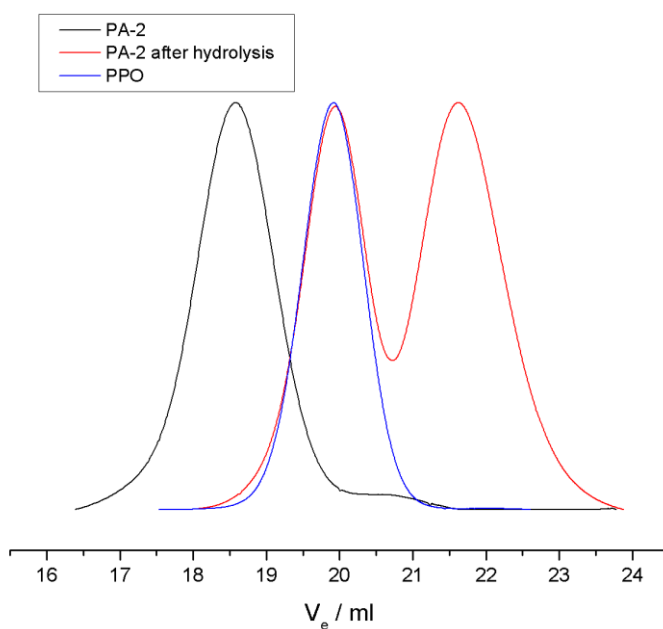


Figure S-10: SEC traces of PA-2 before and after hydrolysis in comparison with PPO precursor A.

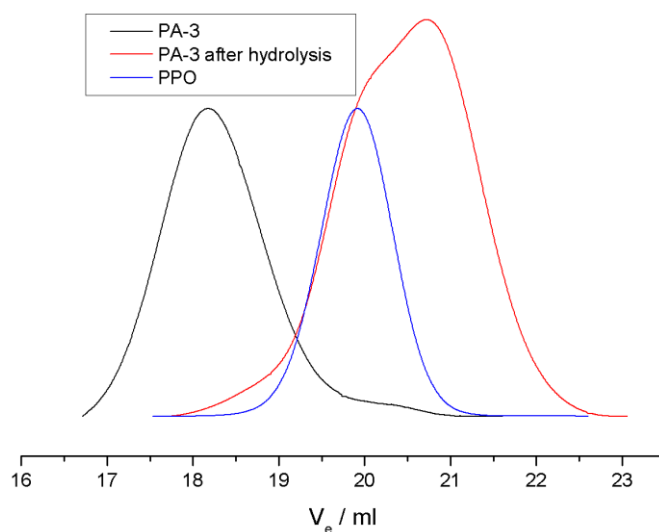


Figure S-11: SEC traces of **PA-3** before and after hydrolysis in comparison with PPO precursor **A**.

Note: The SEC traces of **PA-1,2,3** after hydrolysis do not reveal a third mode in lower elution volume region which had been present in the SEC traces of the PPO derivatives **C** and **D** (see Figure S-4). This demonstrates that the symmetric PPO acetal formed during functionalization of **A** was successfully removed.

Miniemulsion polymerizations. A stock solution of lutensol (respectively, **PA-3**) in water (2mg/ml) was prepared. Accordingly, an oil phase stock was prepared from AIBN (15 mg, 0.09 mmol), hexadecane (25 mg, 0.11 mmol), styrene (500 mg, 4.80 mmol) and aliquots of 50 mg of the oil stock were added into 2 ml of the water stock. The system was magnetically stirred for 1h at 1000 rpm, subsequently homogenized by indirect sonication (Branson 450W digital indirect sonifier), at 0°C, 90% amplitude, for 2 min to generate a miniemulsion system. Afterwards the system was placed in a thermal shaker at 72°C overnight.

Acidification of the nanoparticle dispersions. 400 μ l of the nanoparticle dispersion were mixed with MilliQ water (1600 μ l), and 1M HCl (20 μ l) was added. The final pH in both dispersions was determined to be ca. 1.5. Afterwards, the dispersion were magnetically stirred overnight, both of

them were purified by threefold centrifugation, at 7000 rpm for 30 min. The purified samples were freeze dried for further characterization.

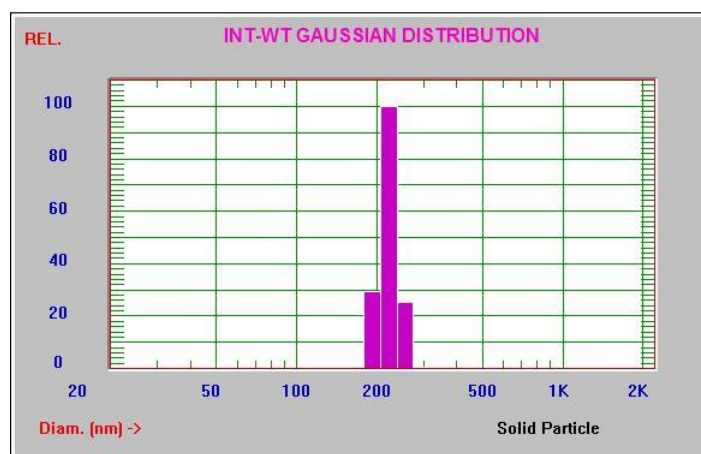


Figure S-12: Size distribution of polystyrene particles obtained with **PA-3** as a surfactant.

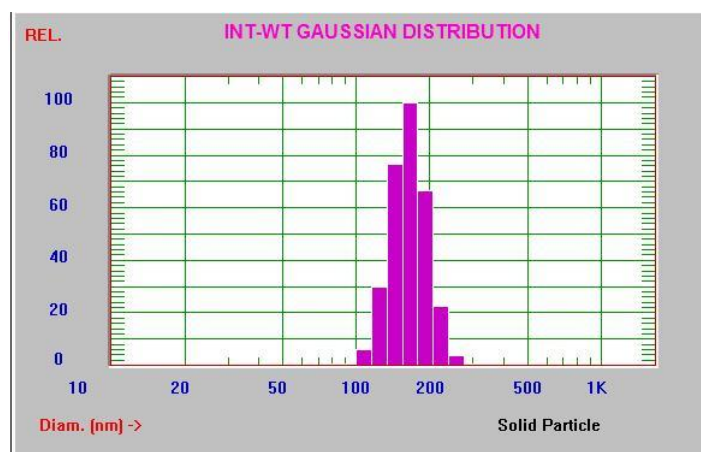


Figure S-13: Size distribution of nanoparticles obtained with Lutensol® as a surfactant.

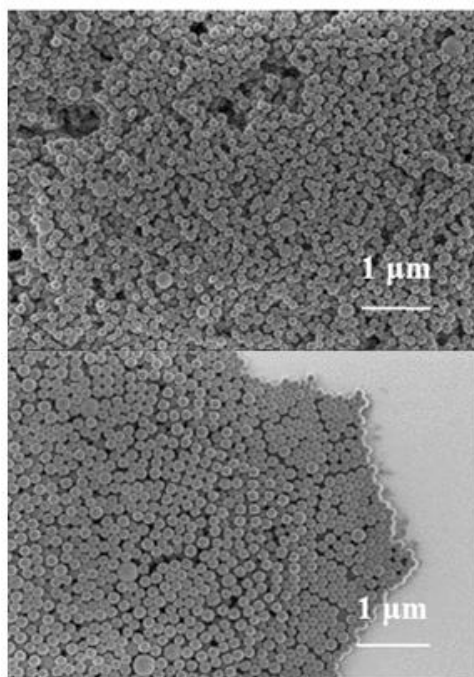


Figure S- 14: SEM Images of nanoparticles prepared using Lutensol® (top) and PA-3 (bottom).

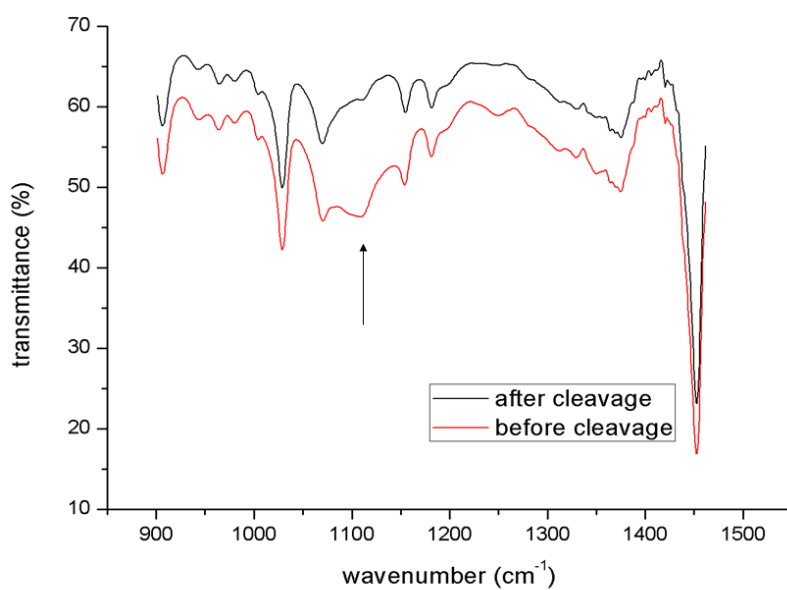


Figure S-15: FTIR spectra of PS particles before and after acidic cleavage of surfactants.

Reference

- [1] Greenland, B. W.; Liu, S.; Cavalli, G.; Alpay, E.; Steinke, J. H. G. *Polymer* **2010**, *51*, 2984–2992.

3 pH-Cleavable Poly(ethylene glycols)s

3.1 Cleavable Polyethylene Glycol (PEG): 3,4-Epoxy-1-butene (EPB) as a Comonomer to Establish Degradability at Physiologically Relevant pH

Matthias Worm,^a Daniel Leibig,^{a,b} Carsten Dingels,^a and Holger Frey^{a*}

^a Institute of Organic Chemistry, Johannes Gutenberg-University, Duesbergweg 10-14, D-55128 Mainz, Germany.

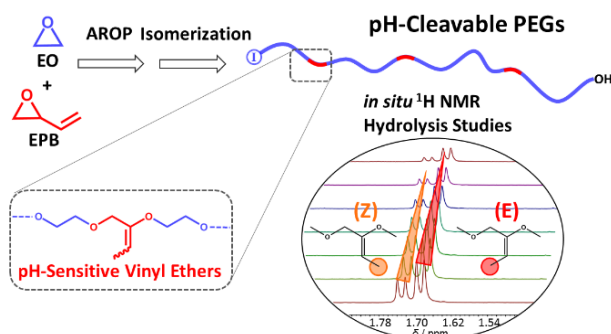
^b Graduate School Materials Science in Mainz, Staudinger Weg 9, D-55128 Mainz, Germany.

Submitted

Abstract

Polyethylene glycol (PEG) has been used for decades to improve the pharmacokinetic properties of protein drugs, and several PEG-protein conjugates are approved by the FDA. However, the non-degradability of PEG restricts its use to a limiting molecular weight to permit excretion via the kidney pathway. In this work, we introduce a simple strategy to overcome the non-degradability of PEG by incorporating multiple pH-sensitive vinyl ether moieties into the polyether backbone. Copolymerization of 3,4-epoxy-1-butene (EPB) with ethylene oxide via anionic ring-opening polymerization (AROP) provides access to allyl moieties that can be isomerized to yield pH-cleavable propenyl units (*iso*EPB). Well-defined P(EPB-*co*-EG) copolymers ($\bar{D} = 1.05 - 1.11$) with EPB contents of ~ 4 mol% were synthesized in a molecular weight range of 3000 to 10000 g mol⁻¹. ¹H NMR kinetic studies served to investigate acidic hydrolysis in a pH range of 4.4 to 5.4 and even allowed to distinguish between the hydrolysis rates of (E)- and (Z)-*iso*EPB units, demonstrating faster hydrolysis of the (Z)-isomer. SEC analysis of degradation products revealed moderate dispersities \bar{D} of 1.6 to 1.8 and consistent average molecular weights M_n of ~ 1000 g mol⁻¹. The presence of a defined hydroxyl end group permits the attachment to other functional molecules. The novel pH-degradable PEGs compile various desirable properties that render them promising candidates for biomedical application and can be cleaved in a physiologically relevant pH-range

Table of Contents Graphics



Introduction

Polyethylene glycol (PEG) is well-known to promote various favorable pharmacokinetic properties when linked to a bioactive agent. Numerous pharmaceuticals based on PEGylated drugs have been approved by the FDA.^[1–3] Covalent attachment of PEG chains to pharmaceutical agents effects higher aqueous solubility of the drug as well as decreased antigenic activity and proteolytic degradation.^[4,5] In addition, renal clearance is strongly reduced, leading to prolonged blood circulation times,^[6,7] hence therapeutic effects are strongly improved compared to the non-PEGylated drug. Due to these desirable properties and its ubiquitous presence in biomedicine,^[8] PEG has been termed the “gold standard polymer” for biomedical application.

Despite the abovementioned advantages, PEG suffers from a lack of biodegradability, limiting its use to a maximum molecular weight of about 40 kDa.^[9] Higher molecular weight polymers cannot be excreted via the kidneys and may accumulate in human tissue, potentially leading to storage diseases.^[10] However, the rate of glomerular filtration^[10] has been shown to inversely correlate with the molecular weight of the polymers,^[11] and, steric shielding of therapeutic drugs is clearly more efficient with increasing molecular weight,^[12,13] suggesting the use of high MW PEGs.

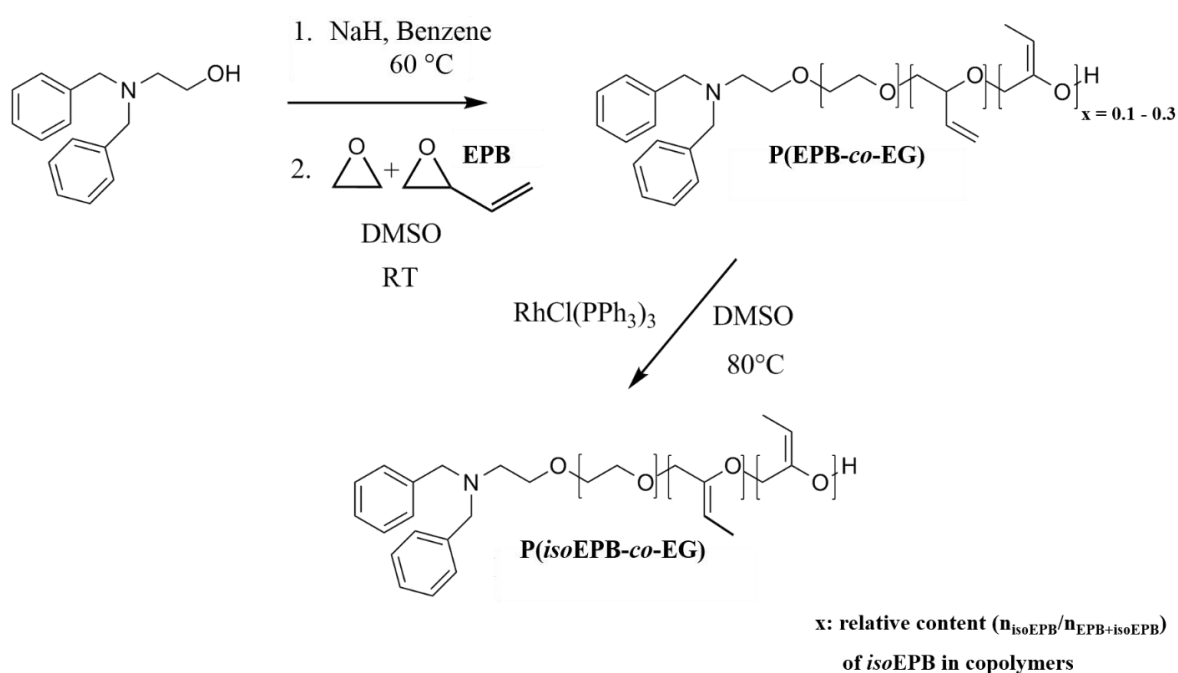
Several strategies have been proposed to circumvent these limitations. For instance, cleavable moieties can be introduced into PEG structures that allow for degradation of the polymers.^[14]

Polymer decomposition is expected to occur, either in physiological domains of lowered pH, such as endosomal/lysosomal compartments,^[15,16] and tumor tissue^[17,18] in case of acid-labile groups, or in reductive intracellular environments, if redox-responsive residues are employed.^[19] By using polycondensation or polyaddition reactions of telechelic PEGs with reactive end groups, degradable PEGs have been accessed. Examples of degradable units include pH-sensitive acetals,^[20] *cis*-aconitic acids,^[21] esters^[22,23] as well as, redox-responsive moieties such as disulfides.^[24] Although promising results have been demonstrated for some of the systems mentioned above with respect to degradation profiles and potential drug delivery, dispersities ($\mathcal{D} = M_w/M_n$) of these systems are generally high due to the unavoidable step-growth mechanism. Another innovative strategy involves partial oxidation of the PEG backbone to generate hydrolysable linkages. Elisseeff and coworkers used an iron-based oxidizing agent (Fenton's reagent) to form hemiacetal groups along the PEG backbone to ensure degradability. Unfortunately, no hydrolysis profiles of the polymers were reported to evaluate cleavage kinetics.^[25] Most recently, a similar approach was presented by Liu et al. who employed ruthenium oxide to oxidize PEG and thereby, introduced ester moieties to obtain acid-degradable poly((ethylene glycol)-co-(glycolic acid)) copolymers. The authors analyzed degradation rates and molecular weight distributions of the hydrolyzed polymer, however, the presence of different end groups at PEG after oxidation limits further modification and subsequent conjugation to biomolecules.^[26] Recently, our group reported a method to incorporate a pH-cleavable acetal unit at a precisely determinable position in a PEG chain, however, this approach is restricted to a single degradable moiety in PEG and its conjugates.^[27] Lately, an innovative strategy towards degradable PEGs was reported by Lynd, Hawker et al. Therein, copolymerization of ethylene oxide and epichlorohydrin followed by subsequent base treatment provided access to PEG containing vinyl ethers as cleavable linkages with dispersities of the copolymers below 1.4. Unfortunately, due to the trialkylaluminum-activated copolymerization, no defined end groups are

available to allow for bioconjugation and drug ligation strategies.^[28] Single vinyl ether groups have further been incorporated into PEG-based lipids for liposomal applications.^[29,30]

The use of vinyl ethers as pH-sensitive moieties is regarded as highly promising given that their rate of hydrolysis can be adjusted by the substitution pattern,^[31–33] offering perspectives to fine-tune cleavage kinetics with respect to the specific prerequisites of controlled drug release.

Although a variety of concepts has been reported to overcome limitations of PEG arising from its non-degradability, in our opinion, none of the aforementioned systems thoroughly matches the requirements for biomedical applications, i.e. well-defined structures, controlled hydrolysis profiles at physiological pH combined with possibilities to conjugate bioactive molecules.



Scheme 7: Synthesis procedure for P(isoEPB-co-EG) copolymers. The relative content of isoEPB was determined from ¹H NMR spectroscopy.

In this work we introduce a convenient, two-step procedure to incorporate multiple vinyl ether residues into the backbone of PEG to assure its degradability. By using anionic ring-opening copolymerization (AROP) of ethylene oxide and 3,4-epoxy-1-butene (EPB) as a comonomer, well-

defined copolymers ($\bar{D} = 1.05 - 1.11$) with tailorable molecular weights and tunable EPB content could be synthesized. The allyl moieties of EPB were subsequently isomerized utilizing Wilkinson's catalyst to yield pH-cleavable vinyl ethers (Scheme 1). ^1H NMR kinetic studies were performed to evaluate susceptibility of these copolymers towards acidic hydrolysis. The degradation products after complete hydrolysis were analyzed by size exclusion chromatography. The presence of defined terminal hydroxyl groups in all chains enables further bioconjugation and ligation. The novel P(EPB-co-EG) copolymers compile multiple favorable properties for biomedical applications and may be viewed as a promising pH-degradable PEG substitute.

Results and Discussion

We employed 3,4-epoxy-1-butene (EPB) as a comparatively inexpensive and readily available monomer and the well-established ethylene oxide (EO) for the AROP. This straightforward, one-step approach grants access to multiple allylic moieties distributed along the backbone of PEG that can be isomerized to yield pH-sensitive vinyl ether residues (*iso*EPB). To the best of our knowledge, anionic copolymerization of EPB and EO has not been reported to date. The synthesis of P(*iso*EPB-co-EG) polymers is illustrated Scheme 7.

N,N-Dibenzyl ethanolamine was used as an initiator to warrant distinguishable proton resonances of the polymer backbone and the initiator in NMR spectroscopy. Based on this initiator, accurate determination of molecular weights and comonomer content is possible via end group analysis. Copolymerization of EPB and EO was conducted in DMSO at room temperature using sodium hydride as a base. These mild reaction conditions proved necessary to suppress cleavage of copolymers during polymerization via β -elimination. This side reaction leads to the formation of butadiene fragments and has been observed in case of elevated temperatures and potassium or cesium alkoxides. (See SI, Scheme S-1) Presumably, the higher basicity of the alkoxide end groups for larger alkali metal ions such as potassium and cesium, promotes proton abstraction. A lack of *d*-

orbitals in sodium might, in addition, prevent interactions with the allylic system of EPB units. Similar behavior has been observed for the isomerization of *N*-allyl amino moieties in the presence of sodium and potassium/cesium alkoxides.^[34]

Conversion of the allyl residues (EPB) to pH-cleavable vinyl ether moieties (*iso*EPB) was conducted in presence of Wilkinson's catalyst $\text{RhCl}(\text{PPh}_3)_3$. Isomerization of α -substituted allyl ethers has been scarcely studied in the literature, however, some reports indicate that the catalytic activity of Wilkinson's catalyst in organic solvents is insufficient and suggest the use of more reactive catalytic systems.^[35,36] In the course of this study we found that isomerization of α -substituted allyl residues can be conveniently achieved using catalytic amounts of the conventional Wilkinson's catalyst in DMSO at elevated temperatures.

Table 4: Molecular Characteristics of P(EPB-*co*-EG) Copolymers.

Sample	$M_{n,\text{NMR}}$	$M_{n,\text{SEC}}$	\mathcal{D}^{SEC}	$\text{mol}\%$	(Z)/(E)	$M_{n,\text{SEC}}^{\text{a}}$	$\mathcal{D}_{\text{b}}^{\text{SEC}}$
	<i>before hydrolysis</i>					<i>after hydrolysis</i>	
	g mol ⁻¹	g mol ⁻¹				g mol ⁻¹	
P(EPB ₃ - <i>co</i> -EG ₆₄)	3200	2800	1.05	4.5	0.69	1100	1.62
P(EPB ₄ - <i>co</i> -EG ₈₈)	4400	3200	1.05	4.3	0.67	1000	1.57
P(EPB ₅ - <i>co</i> -EG ₁₄₃)	6900	5300	1.06	3.4	0.61	1100	1.71
P(EPB ₈ - <i>co</i> -EG ₂₁₁)	10000	7200	1.11	3.7	0.63	1200	1.76

$M_{n,\text{NMR}}$: Molecular weight of the copolymers obtained from ¹H NMR via end group analysis; $M_{n,\text{SEC}}$: Molecular weights of the copolymers determined via size exclusion chromatography in DMF using PSS PEG standards for calibration. $\mathcal{D}^{\text{SEC}} = M_w/M_n$: Dispersity of polymer samples obtained from SEC using PEG standards. $\text{mol}\%$ _{EPB}: Content of EPB calculated from ¹H NMR. (Z)/(E): Ratio of (Z)- to (E)-isomers after isomerization calculated from ¹H NMR. $M_{n,\text{SEC}}^{\text{a}}$: Molecular weight of polymer samples after acidic hydrolysis at pH 1 (MeOH/H₂O) determined via SEC in DMF using PEG calibration. $\mathcal{D}_{\text{b}}^{\text{SEC}}$: Dispersity of polymer samples after acidic hydrolysis at pH 1 (MeOH/H₂O) obtained from SEC via PEG calibration.

P(EPB-*co*-EG) copolymers with molecular weights M_n between 3200 and 10000 g mol⁻¹ were synthesized that exhibit narrow molecular weight distributions ($\mathcal{D} = 1.05 - 1.11$) and consistent EPB content of about 4 mol%.

Table 4 summarizes the molecular characteristics of the copolymers. Molecular weights and EPB content were calculated from ^1H NMR by comparing the integrals of initiator signals with the polyether backbone resonances and the vinyl proton signals of the comonomers. The values of the molecular weights obtained by size exclusion chromatography were generally underestimated with respect to results from NMR spectroscopy, which can be attributed to differences in the hydrodynamic volume of the copolymers and the PEG standards used for SEC calibration.

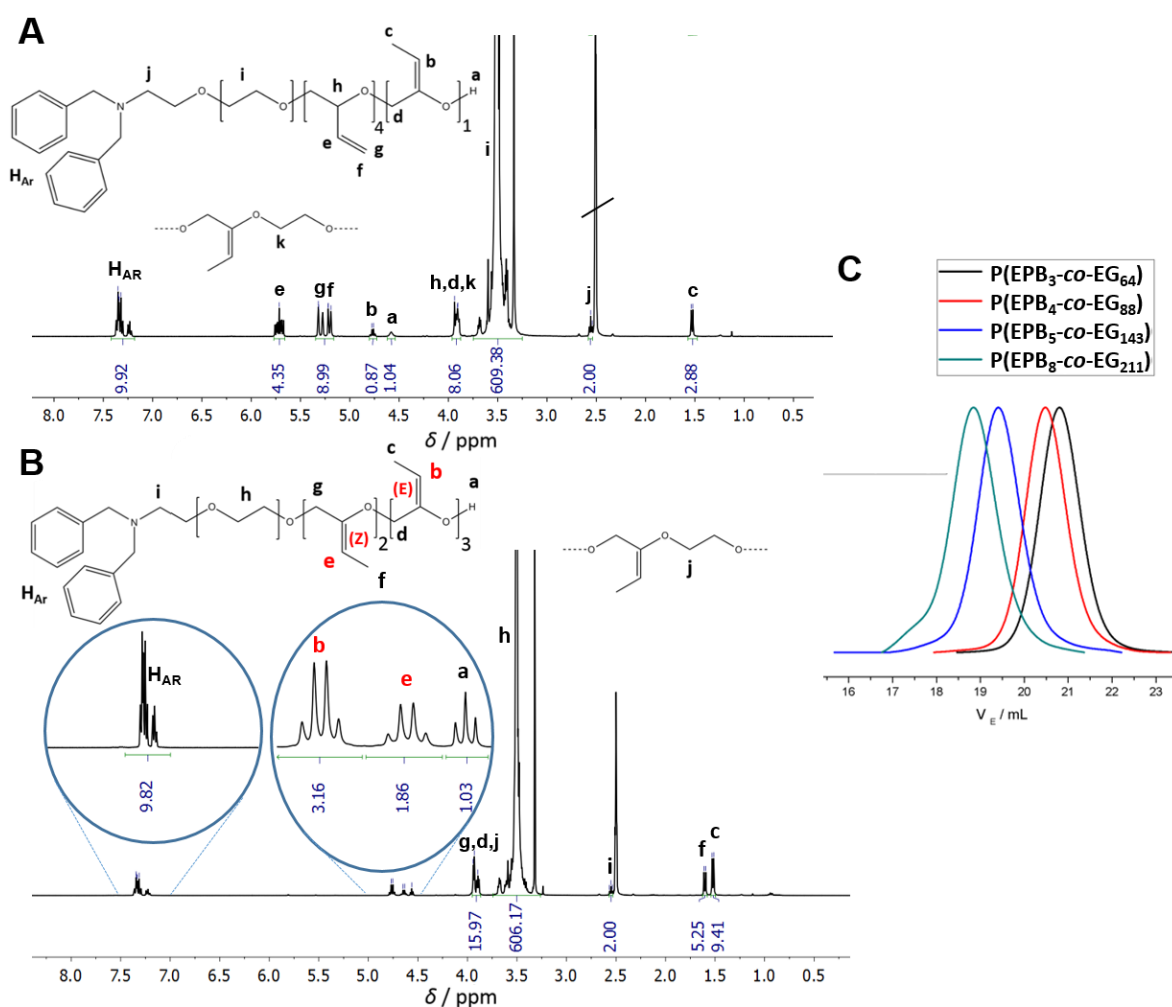


Figure 11: ^1H NMR Spectra of P(EPB₅-co-EG₁₄₃) before (A) and after (B) isomerization measured in DMSO- d_6 at 400 MHz. C: SEC traces of P(EPB-co-EG) copolymers using DMF as eluent and RI detection.

SEC traces of P(EPB-co-EG)s are presented in Figure 11 C, revealing monomodal molecular weight distributions for all polymer samples and shifts to lower elution volume with increasing molecular weights.

Figure 11 A displays the ^1H NMR of **P(EPB₅-co-EG₁₄₃)** as an example of a typical spectrum. Successful incorporation of EPB into the copolymers could be confirmed from the characteristic NMR signals of the allyl moieties in the olefinic region between 6.0 and 4.5 ppm. Furthermore, the spectra reveal already partial isomerization of allyl groups already during polymerization, which was observed for all polymer samples. The degree of isomerization varied between 11 and 28 %. Interestingly, only the (E)-isomer of the propenyl ether groups was formed spontaneously, as confirmed by ^{13}C and 2D NMR analysis. (See also Figures S-1 and S-2)

Catalytic isomerization of allyl residues to vinyl ether moieties could be monitored by ^1H NMR, relying on the disappearance of the EPB protons (5.7, 5.2 ppm), and the appearance of the typical *iso*EPB propenyl resonances at 4.7 - 4.6 ppm (methine protons) and 1.6 - 1.5 ppm (methyl protons, see Figure 11 B). In addition, ^{13}C and 2D NMR served to analyze the structures, and comparison of the integrals of the comonomers in ^1H NMR spectroscopy before and after isomerization proves quantitative conversion (spectra are included in SI). A mixture of (E)- and (Z)-isomers was obtained for the propenyl ether residues of *iso*EPB, though consistently higher amounts of the (E)-isomer were formed. The ratio of (Z)- to (E)-*iso*EPB was calculated from the relative integrals of the two characteristic quartets at 4.7 and 4.6 ppm revealing values of 0.61 to 0.69 (see

Table 4). A close-up view of the aromatic region in Figure 11 B verifies complete removal of the catalyst via precipitation as characteristic resonances of the PPh_3 ligands of Wilkinson's catalyst between 7.6 and 7.4 ppm are not observed in the spectra. The isomerized polymer samples were stable for several months without hydrolysis after solvent removal.

In order to evaluate degradation behavior of the pH-sensitive **P(*iso*EPB-co-EG)** copolymers in acidic environment, real-time ^1H NMR kinetic studies were performed in buffered D_2O at 37 °C. This technique permits direct monitoring of the chemical conversion in an NMR tube and has been employed to screen hydrolysis profiles of acid-hydrolyzable moieties in polymers.^[37] Figure 12 B

visualizes the results of *in situ* NMR kinetic measurements for the hydrolysis of **P(isoEPB₅-co-EG₁₄₃)** at pD 4.4 recorded for a period of time of 24 h.

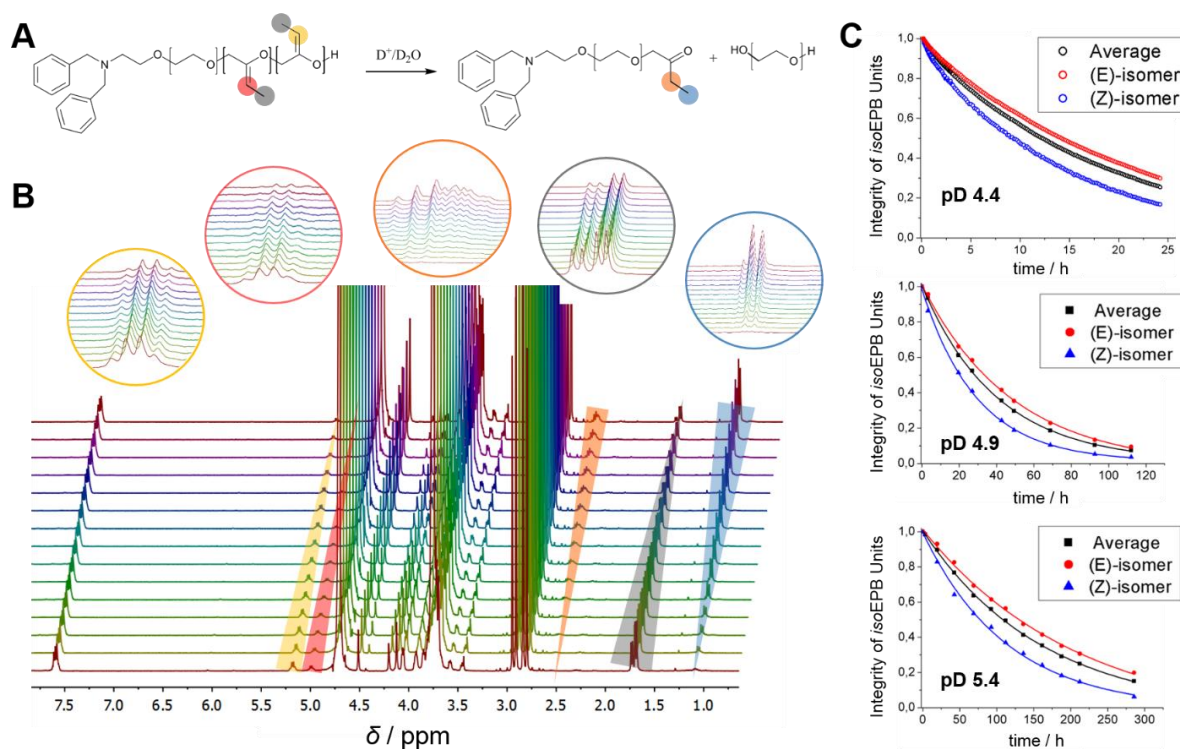


Figure 12: **A:** Expected reaction for the acidic hydrolysis of **P(isoEPB-co-EG)** copolymers showing the formation of ketone and PEG fragments; **B:** ^1H NMR kinetic studies on the hydrolysis of **P(isoEPB₅-co-EG₁₄₃)** in buffered D_2O (pD 4.4) at 37°C . The progression of signal intensities for characteristic resonances are presented in close-up and colored arrows visualize the development of respective peak intensities. **C:** Quantitative analysis of ^1H NMR hydrolysis studies for **P(isoEPB₅-co-EG₁₄₃)** showing the integrity (integral ratio $I(t)/I(t_0)$) of *iso*EPB units plotted vs. time for pD 4.4, 4.9 and 5.4. Individual plots are presented for the (E)-isomer (red), the (Z)-isomer (blue) and overall integrity of the propenyl ether moieties (black) revealing faster hydrolysis for the (Z)-*iso*EPB units. Exponential fits were used to calculate the rate constants of hydrolysis.

For illustrative purposes, an extract of 15 spectra is presented in Figure 12 (bottom), although 181 spectra have been recorded and used for the quantitative analysis. A continuous decrease in the signal intensities of *iso*EPB units (4.7, 4.6, 1.6 and 1.5 ppm), in conjunction with the appearance of resonances corresponding to ketone end groups (2.5 and 1.1 ppm) provides evidence for the hydrolysis according to the expected reaction shown in Figure 12 A. Regions of interest are highlighted to visualize the progression of signal intensities. Due to slower rates of degradation,

hydrolysis studies at higher pD values (4.9, 5.4) were conducted outside the NMR spectrometer by incubating the NMR sample tubes at 37 °C and manually recording NMR spectra after selected periods of time. pH values in a range of 4.3 to 5.8 have been reported in literature for endosomal and lysosomal cellular compartments,^[38,39] that match the pH range investigated in this study. Figure 12 C illustrates the hydrolysis profiles of **P(EPB₅-co-EG₁₄₃)** at pD 4.4, 4.9 and 5.4 obtained from ¹H NMR kinetic experiments. The integral ratio $I(t)/I(t_0)$ of the *iso*EPB methyl signals (denoted as integrity of *iso*EPB units) were plotted against time to assess the rate constant of hydrolysis k'_{D2O} and the half-life time $t_{1/2,D2O}$ of vinyl ether moieties in the copolymers. Half-lives of 12 h (pD 4.4), 28 h (pD 4.9) and 112 h (pD 5.4) for the average of *iso*EPB units were determined from exponential fits (Table 5). Here, real-time ¹H NMR kinetics proved to be a powerful technique as it allows to distinguish between the decay of (E)- and (Z)-propenyl ethers (see Figure S-7). Individual plots for the two geometric isomers consistently reveal faster cleavage of (Z)-*iso*EPB units (blue) and distinctly slower hydrolysis of (E)-*iso*EPB (red). (See Figure 12 C) This observation is reflected in the $t_{1/2,D2O}$ values of *iso*EPB units listed in Table 5, showing prolonged half-lives for the (E)-*iso*EPB residues.

For comparative purposes, we investigated the hydrolysis kinetics of **P(*iso*EPB₃-co-EG₆₄)** (M_n 3.2 kDa) at pD 4.4 as the lowest molecular weight polymer used in this study (see Figure S-10). Clearly, rates of hydrolysis are slower compared to **P(*iso*EPB₅-co-EG₁₄₃)** (M_n 6.9 kDa), however the values are on the same order of magnitude. Given that the amount of EPB and the (Z)/(E)-*iso*EPB ratio was approximately constant for the two copolymers, as shown in

Table 4, these discrepancies might be ascribed to the increased hydrophilicity of the higher molecular weight polymer, creating a more polar environment in the proximity of vinyl residues that promotes faster hydrolysis. Accelerated cleavage of (Z)-*iso*EPB compared to the (E)-*iso*EPB was reconfirmed in this measurement (see Figure S-11).

Table 5: Results of hydrolysis studies on **P(isoEPB₅-co-EG₁₄₃)** and **P(isoEPB₃-co-EG₆₄)** via NMR kinetics.

Sample	pD	k'_{D2O}	$k'_{D2O}(E)$	$k'_{D2O}(Z)$	$t_{1/2,D2O}$	$t_{1/2,D2O}(E)$	$t_{1/2,D2O}(Z)$
P(isoEPB₅-co-EG₁₄₃)	4.4	$1.64 \cdot 10^{-5}$	$1.35 \cdot 10^{-5}$	$2.10 \cdot 10^{-5}$	11.7	14.3	9.2
P(isoEPB₅-co-EG₁₄₃)	4.9	$6.72 \cdot 10^{-6}$	$5.52 \cdot 10^{-6}$	$9.13 \cdot 10^{-6}$	27.7	33.7	20.4
P(isoEPB₅-co-EG₁₄₃)	5.4	$2.16 \cdot 10^{-6}$	$1.70 \cdot 10^{-6}$	$3.18 \cdot 10^{-6}$	112.0	144.1	79.0
P(isoEPB₃-co-EG₆₄)	4.4	$1.19 \cdot 10^{-5}$	$9.67 \cdot 10^{-6}$	$1.49 \cdot 10^{-5}$	16.1	19.9	12.9

k'_{D2O} , $k'_{D2O}(E)$, $k'_{D2O}(Z)$ / s⁻¹: rate constants of hydrolysis for overall *iso*EPB units, and for the individual (E)-/(Z)-isomers calculated from exponential fits; $t_{1/2,D2O}$, $t_{1/2,D2O}(E)$, $t_{1/2,D2O}(Z)$ / h: half-lives of the overall *iso*EPB units, and the (E)-/(Z)-isomers.

These findings are in accordance with literature reports on the rate constants of hydrolysis for *cis*- and *trans*-propenyl ethers obtained from UV-Vis spectroscopy.^[40,41] One may envisage that control of the relative contents of the two hydrolyzable isomers would grant access to tailorable hydrolysis profiles of the PEG corona in biomedical formulations, e.g. for polymer-drug conjugates or stealth liposomes. Due to the kinetic deuterium isotope effect, these values are expected to differ to a certain extent from the rates of hydrolysis in H₂O. Depending on the substitution pattern of the vinyl ether, kinetic deuterium isotope effects k_H/k_D of 1.7 to 4.2 at 25 °C have been reported,^[41] suggesting faster hydrolysis of *iso*EPB units in aqueous medium compared to deuterium oxide.

Finally, we also investigated the degradation products of **P(isoEPB-co-EG)** copolymers after complete hydrolysis. To this end, aliquots of the polymers were treated with diluted hydrochloric acid (pH = 1) for 24 h to assure full hydrolysis of all cleavable vinyl ether linkages. Subsequently the hydrolysis fragments were analyzed by SEC.

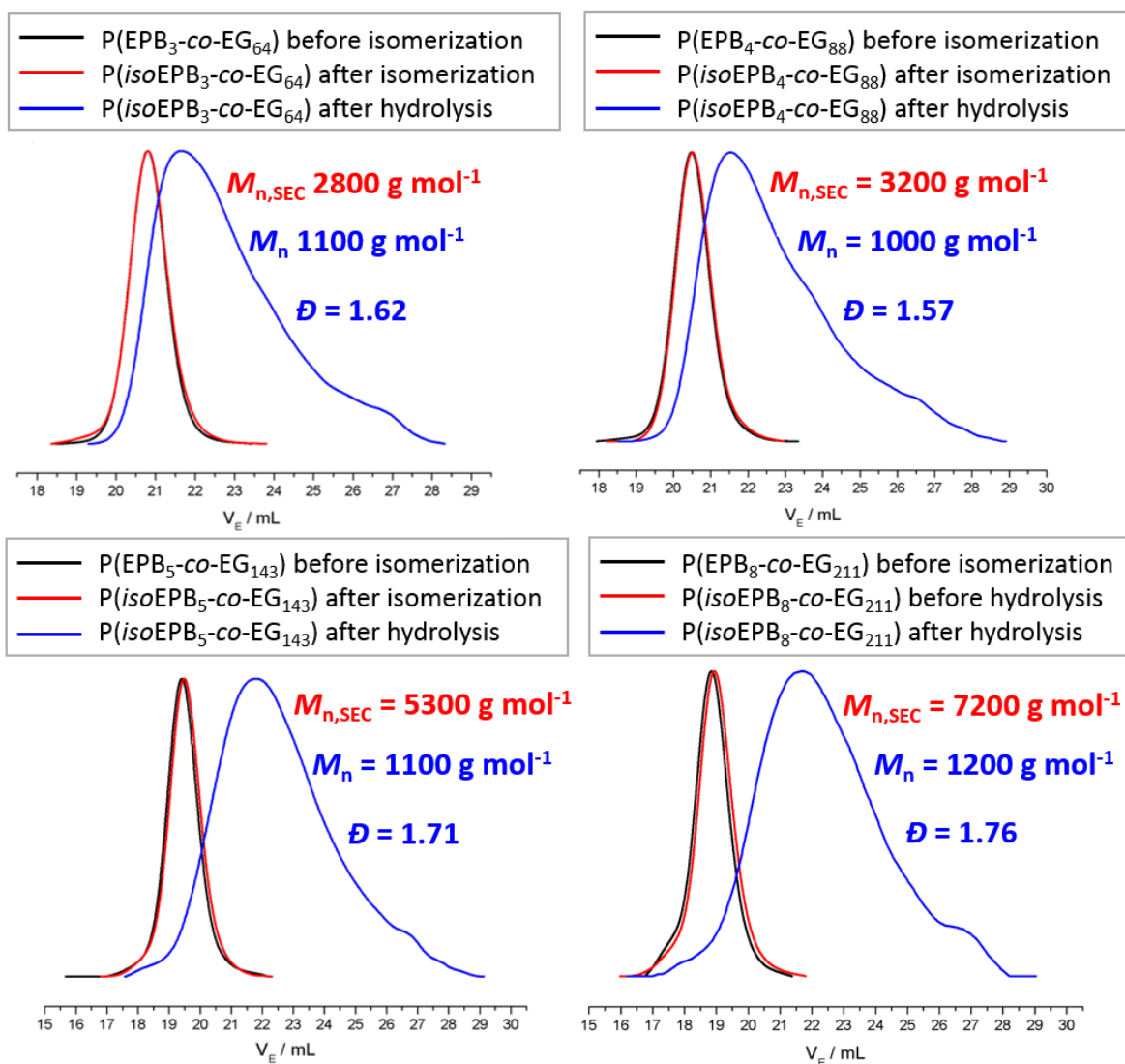


Figure 13: Overview of hydrolysis studies showing typical SEC traces of polymer samples before isomerization (black), after isomerization (red) and after acidic hydrolysis (blue) using DMF as eluent and RI detection. Molecular weights M_n and dispersities \mathcal{D} were determined via SEC (PEG calibration).

Figure 13 contains the SEC traces of the polymer samples before isomerization, after isomerization, and after acidic hydrolysis. Clearly, molecular weight distributions remained unaffected by the treatment with Wilkinson's catalyst in the isomerization step. As expected, significant shifts to lower molecular weights were observed after hydrolysis, accompanied by a broadening of the molecular weight distribution with moderate dispersities \mathcal{D} in a range of 1.6 to 1.8. Interestingly, the hydrolyzed copolymers concordantly exhibited average molecular weights M_n of $\sim 1000 \text{ g mol}^{-1}$ determined with PEG standards for SEC calibration. As the content of EPB was constant ($\sim 4 \text{ mol}\%$)

for all polymers, these results suggest a rather random distribution of EPB units along the backbone. The average molecular weights of hydrolysis products is therefore likely to be adjustable by the relative amount of EPB incorporated. With respect to a potential application in biomedicine, these findings are highly relevant as the size of degradation products is expected to affect rates of glomerular filtration and excretion from the body. This perspective may encourage the further development of P(EPB-*co*-EG) copolymers with molecular weights exceeding the renal filtration limit of ~ 40 kDa and low contents of EPB (< 4 mol %) to allow for exceptionally long-circulating PEG-drug conjugates that can be partially hydrolyzed to prevent accumulation in human tissue. Future experiments will focus on properties of polymer drug conjugates and their *in vivo* performance.

Conclusion

In this work, we introduce a simple strategy to circumvent the non-degradability of polyethylene glycol (PEG) by copolymerization of ethylene oxide with a minor amount of 3,4-epoxy-1-butene (EPB) and subsequent isomerization of EPB's allylic moieties to pH-degradable vinyl ether residues. Anionic ring-opening polymerization (AROP) was employed to access P(EPB-*co*-EG) copolymers with molecular weights M_n in a range of 3200 to 10000 g mol^{-1} and narrow molecular weight distributions ($\mathcal{D} = 1.05 - 1.11$). The structures were characterized by ^1H NMR, ^{13}C NMR spectroscopy and SEC revealing constant amounts of EPB (~ 4 mol%) for all copolymers. Isomerization of allyl moieties to propenyl ether groups (*iso*EPB) was achieved in the presence of Wilkinson's catalyst generating mixtures of (E)- and (Z)-isomers of the *in-chain* vinyl ether structures. Real-time ^1H NMR kinetic studies were performed in buffered deuterium oxide to monitor hydrolysis profiles of pH-sensitive *iso*EPB units. This technique served to elucidate crucial discrepancies in the hydrolysis rates of the two geometric isomers and displayed faster degradation of (Z)-*iso*EPB units. SEC analysis of the degradation products after complete hydrolysis of vinyl ether linkages consistently showed average

molecular weights M_n of 1000 g mol⁻¹ and moderate dispersities ($\mathcal{D} = 1.6 - 1.8$). The copolymers can further be readily derivatized at the chain end by conversion of the terminal hydroxyl group to facilitate the attachment of bioactive molecules for e.g. protein therapeutics. The novel P(EPB-co-EG) copolymers combine various desirable properties for biomedical application, such as well-defined structures, good control over the molecular weight of the degradation products and the possibility to conjugate drugs. By controlling the amounts of (E)- and (Z)-*iso*EPB formed in the isomerization step, precise tailoring of hydrolysis kinetics could be realized to match the specific requirements of biomedicine. These features render the new class of pH-degradable polyethers a potent candidate for PEG-analogous applications e.g. for PEGylation resulting in exceptionally long-circulating drug-conjugates that slowly hydrolyze in physiological environment, avoiding storage diseases.

Acknowledgements

M.W. is grateful for a fellowship of the Max Planck Graduate Center (MPGC). D. L. acknowledges a fellowship through the Excellence Initiative (DFG/GSC 266) in the context of MAINZ “Materials Science in Mainz”. The authors thank Dr. Johannes Liermann for scientific support and helpful discussion. This work was supported by funding of the DFG research center SFB 1066, project grant A7.

References

- [1] Alconcel, Steevens N. S.; Baas, A. S.; Maynard, H. D. *Polym. Chem.*, **2011**, *2*, 1442–1448.
- [2] Pfister, D.; Morbidelli, M. *J. Control. Release*, **2014**, *180*, 134–149.
- [3] Ivens, I. A.; Achanzar, W.; Baumann, A.; Brändli-Baiocco, A.; Cavagnaro, J.; Dempster, M.; Depelchin, B. Olympe; Irizarry Rovira, Armando R.; Dill-Morton, L.; Lane, J. H.; Reipert, B. M.; Salcedo, T.; Schweighardt, B.; Tsuruda, L. S.; Turecek, P. L.; Sims, J. *Toxicol. Pathol.*, **2015**, *43*, 959–983.
- [4] Khandare, J.; Minko, T. *Prog. Polym. Sci.*, **2006**, *31*, 359–397.
- [5] Ryan, S. M.; Mantovani, G.; Wang, X.; Haddleton, D. M.; Brayden, D. J. *Expert Opin. Drug Deliv.*, **2008**, *5*, 371–383.
- [6] Harris, J. Milton; Chess, R. B. *Nat Rev Drug Discov.*, **2003**, *2*, 214–221.
- [7] Roberts, M. J.; Bentley, M. D.; Harris, J. M., **2012**, *64*, 116–127.
- [8] Herzberger, J.; Niederer, K.; Pohlit, H.; Seiwert, J.; Worm, M.; Wurm, F. R.; Frey, H. *Chem. Rev.*, **2015**, *116*, 2170–2243.
- [9] Pasut, G.; Veronese, F. M. *Prog. Polym. Sci.*, **2007**, *32*, 933–961.
- [10] Markovsky, E.; Baabur-Cohen, H.; Eldar-Boock, A.; Omer, L.; Tiram, G.; Ferber, S.; Ofek, P.; Polyak, D.; Scomparin, A.; Satchi-Fainaro, R. *J. Control. Release*, **2012**, *161*, 446–460.
- [11] Yamaoka, T.; Tabata, Y.; Ikada, Y. *J. Pharm. Sci.*, **1994**, *83*, 601–606.
- [12] Yamaoka, T.; Tabata, Y.; Ikada, Y. *J. Pharm. Sci.*, **1995**, *84*, 349–354.
- [13] Caliceti, P.; Veronese, F. M. *Adv. Drug Delivery Rev.*, **2003**, *55*, 1261–1277.
- [14] Dingels, C.; Frey, H. *Adv. Polym. Sci.*, **2013**, *262*, 167–190.
- [15] Benjaminsen, R. V.; Sun, H.; Henriksen, J. R.; Christensen, N. M.; Almdal, K.; Andresen, T. L. *ACS Nano.*, **2011**, *5*, 5864–5873.
- [16] Sun, H.; Andresen, T. L.; Benjaminsen, R. V.; Almdal, K. *J. Biomed. Nanotechnol.*, **2009**, *5*, 676–682.

- [17] Gerweck, L. E.; Vijayappa, S.; Kozin, S. *AACR.*, **2006**, *5*, 1275–1279.
- [18] Patel, N. R.; Pattni, B. S.; Abouzeid, A. H.; Torchilin, V. P. *Adv. Drug Delivery Rev.*, **2013**, *65*, 1748–1762.
- [19] Jones, D. P.; Carlson, J. L.; Mody Jr, V. C.; Cai, J.; Lynn, M. J.; Sternberg Jr, P. *Free Radic. Biol. Med.*, **2000**, *28*, 625–635.
- [20] Tomlinson, R.; Klee, M.; Garrett, S.; Heller, J.; Duncan, R.; Brocchini, S. *Macromolecules*, **2002**, *35*, 473–480.
- [21] Clochard, M.-C.; Brocchini, S. *Macromol. Rapid Commun.* **2000**, *21*, 853-859.
- [22] Mero, A.; Schiavon, O.; Pasut, G.; Veronese, F. M.; Emilietri, E.; Ferruti, P. *J. Bioact. Compat. Polym.*, **2009**, *24*, 220–234.
- [23] Wang, N.; Dong, A.; Tang, H.; Van Kirk, Edward A.; Johnson, P. A.; Murdoch, W. J.; Radosz, M.; Shen, Y. *Macromol. Biosci.*, **2007**, *7*, 1187–1198.
- [24] Lee, Y.; Koo, H.; Jin, G.-w.; Mo, H.; Cho, M. Y.; Park, J.-Y.; Choi, J. S.; Park, J. S. *Biomacromolecules*, **2005**, *6*, 24–26.
- [25] Reid, B.; Tzeng, S.; Warren, A.; Kozielski, K.; Elisseeff, J. *Macromolecules*, **2010**, *43*, 9588–9590.
- [26] Di Liu; Bielawski, C. W. *Macromol. Rapid Commun.*, **2016**, *37*, 1587-1592.
- [27] Dingels, C.; Müller, S. S.; Steinbach, T.; Tonhauser, C.; Frey, H. *Biomacromolecules*, **2013**, *14*, 448–459.
- [28] Lundberg, P.; Lee, B. F.; van den Berg, S. A.; Pressly, E. D.; Lee, A.; Hawker, C. J.; Lynd, N. A. *ACS Macro Lett.*, **2012**, *1*, 1240–1243.
- [29] Shin, J.; Shum, P.; Grey, J.; Fujiwara, S.-i.; Malhotra, G. S.; González-Bonet, A.; Hyun, S.-H.; Moase, E.; Allen, T. M.; Thompson, D. H. *Mol. Pharmaceutics*, **2012**, *9*, 3266–3276.
- [30] Shin, J.; Shum, P.; Thompson, D. H. *J. Control. Release*, **2003**, *91*, 187–200.
- [31] Kresge, A. J.; Leibovitch, M. *J. Am. Chem. Soc.*, **1992**, *114*, 3099–3102.

- [32] Kresge, A. J.; Tobin, J. B. *J. Phys. Org. Chem.*, **1991**, *4*, 587–591.
- [33] Leibovitch, M.; Kresge, A. J.; Peterson, M. R.; Csizmadia, I. G. *Comp. Theor. Chem.*, **1991**, *230*, 349–385.
- [34] Reuss, V. S.; Obermeier, B.; Dingels, C.; Frey, H. *Macromolecules*, **2012**, *45*, 4581–4589.
- [35] Boons, G.-J.; Burton, A.; Isles, S. *Chem. Commun.*, **1996**, *2*, 141–142.
- [36] Boons, G.-J.; Isles, S. *J. Org. Chem.*, **1996**, *61*, 4262–4271.
- [37] Pohlit, H.; Bellinghausen, I.; Schömer, M.; Heydenreich, B.; Saloga, J.; Frey, H. *Biomacromolecules*, **2015**, *16*, 3103–3111.
- [38] Asokan, A.; Cho, M. J. *J. Pharm. Sci.*, **2002**, *91*, 903–913.
- [39] Lee, R. J.; Wang, S.; Low, P. S. *Biochim. Biophys. Acta, Biophys. Incl. Photosynth.*, **1996**, *1312*, 237–242.
- [40] Salomaa, P.; Nissi, P. *Acta Chem. Scand.*, **1967**, *21*, 1386–1389.
- [41] Kresge, A. J.; Sagatys, D. S.; Chen, H. L. *J. Am. Chem. Soc.*, **1977**, *99*, 7228–7233.

Supporting Information

Cleavable Polyethylene Glycol (PEG): 3,4-Epoxy-1-butene (EPB) as a Comonomer to Establish Degradability at Physiologically Relevant pH

Matthias Worm,^a Daniel Leibig,^{a,b} Carsten Dingels,^a and Holger Frey^{a*}

^aInstitute of Organic Chemistry, Johannes Gutenberg-University, Duesbergweg 10-14, D-55128 Mainz, Germany.

^bGraduate School Materials Science in Mainz, Staudinger Weg 9, D-55128 Mainz, Germany.

Experimentals

Materials and Methods

All chemicals were obtained from *Sigma Aldrich*, *TCl Europe*, or *Acros Organics* unless stated otherwise. Deuterated solvents (DMSO-*d*₆, D₂O) were purchased from *Deutero GmbH*. 3,4-Epoxy-1-butene (EPB) was obtained from *abcr GmbH* and was dried over CaH₂, and freshly distilled prior to use. Ethylene oxide was purchased from *Sigma Aldrich*. THF used for the anionic ring-opening polymerization (AROP) was dried and stored over sodium/benzophenone. A fresh and sealed bottle of dry DMSO purchased from *Acros Organics* stored over molecular sieve was used for each AROP. DMSO (purity (GC) > 99.98%) was obtained from *Fischer Scientific* and utilized for the isomerization step. Care must be taken when handle the flammable, toxic, and gaseous ethylene oxide. ¹H NMR spectra were measured on a Bruker Avance II 400 MHz (5 mm BBO probe, 256 Scans, and B-ACS 60 auto sampler) at 296 K. 2D NMR and ¹³C NMR spectra were recorded on a Bruker Avance II 400 (100.5 MHz, 5 mm BBO probe, and B-ACS 60 auto sampler) at 296 K, if not stated otherwise. All spectra were processed with MestReNova v9.0 software. GPC (SEC) data were obtained using Agilent 1100 Series endowed with a PSS HEMA-column (10⁶/10⁴/10² Å porosity), LiBr/DMF (1 g/L) as eluent using RI detection. Polydispersity indices ($\mathcal{D} = M_w/M_n$) were determined with monodisperse linear PEG standards from *Polymer Standard Service GmbH (PSS)*.

Handling of Ethylene Oxide (EO): EO must be stored in pressure-proof gas bottles and used only in an appropriate fume hood under respective safety precautions. Polymerizations of EO are carried out in flame-dried glassware, allowing secure handling by using cryo-transfer techniques to transport EO inside the evacuated and sealed glass apparatus. Batch-sizes must not exceed 5 g of EO in a 250 mL flask to prevent spontaneous detachment of the septum and evolution of EO.

Synthesis Procedures

Polymerization – P(EPB₃-co-EG₆₄): Sodium hydride (9.4 mg, 0.39 mmol) was transferred into a dry Schlenk flask and a solution of *N,N*-dibenzylethanolamine (100 mg, 0.414 mmol) in benzene (6 mL) was added. The solution was stirred under slightly reduced pressure at 60 °C for 30 min keeping the stopcock closed. Moisture was removed by azeotropic distillation of benzene and subsequent drying at 60 °C in high vacuum for 16 h. After cooling to RT, dry THF (3 mL) was cryo-transferred into the Schlenk flask to dissolve the initiator. A solution of EPB (0.10 mL, 1.24 mmol, EPB was stirred over CaH₂ for 30 min and freshly distilled prior to use) in dry DMSO (6 mL) was injected into the Schlenk flask via syringe at –80 °C. Ethylene oxide (1.32 mL, 26.5 mmol) was cryo-transferred via a graduated ampule and the polymerization was proceeded at RT for 3 d and was subsequently quenched with methanol (2 mL). After dialysis against methanol for 24 h (MWCO 500 DA), the polymer was dried *in vacuo*. (Yield: 80 %) ¹H NMR (400 MHz, DMSO-*d*₆): δ [ppm] 7.39–7.19 (m, 10H, H_{AR}), 5.71 (ddd, 2H, ³J_{AB} = 17.2 Hz, ³J_{AB} = 10.5 Hz, ³J_{AB} = 6.7 Hz, -CH=CH₂), 5.29 (ddd, 2H, ³J_{AB} = 17.2 Hz, ³J_{AB} = 2.1 Hz, ³J_{AB} = 1.1 Hz, -CH=HH_{trans}), 5.20 (ddd, 2H, ³J_{AB} = 10.5 Hz, ³J_{AB} = 2.1 Hz, ³J_{AB} = 1.1 Hz, -CH=HH_{cis}), 4.76 (q, 1H, J = 6.7 Hz, C=CH-CH₃ (*E* isomer)), 4.57 (bs, 1H, OH), 3.96–3.86 (m, 6H, CHO-CH=CH₂, OCH₂-C=CH-CH₃ and CH₂O-C=CH-CH₃), 3.71–3.35 (m, 264H, CH₂O and C_{AR}-CH₂N), 2.55 (t, 2H, J = 6.1 Hz, NCH₂-CH₂O), 1.52 (d, 3H, J = 6.7 Hz, C=CH-CH₃ (*E* isomer)). ¹³C NMR (100.6 MHz, DMSO-*d*₆): δ [ppm] 150.62 (1C, OCH₂-C=CH-CH₃ (*E* isomer)), 139.52 (1C, C_{AR}-CH₂-N), 136.28 (1C, CH₂=CH-CHO), 128.45 - 126.78 (3C, C_{AR}), 117.46 (1C, CH=CH₂), 106.35 (1C, C=CH-CH₃ (*E* isomer)),

79.53 (CH-CH=CH₂), 73.21-67.29 (131C, CH₂O), 60.21 (1C, NCH₂-CH₂O), 57.99 (1C, C_{AR}-CH₂-N), 52.09 (1C, NCH₂-CH₂O), 9.95 (1C, C=CH-CH₃ (*E* isomer)).

Isomerization - P(isoEPB₃-co-EG₆₄): In a Schlenk tube, **P(EPB₃-co-EG₆₄)** (200 mg, 0.063 mmol) was dissolved in DMSO and subjected to two freeze-pump-thaw cycles. Under argon atmosphere, Rh^ICl(PPh₃)₃ (10 mg, 0.011 mmol) was added and the solution was thoroughly degassed via two additional freeze-pump-thaw cycles. The light orange solution was stirred at 80 °C for 1d and was twice precipitated in acetone/diethyl ether (1:1). The pure polymer was obtained after drying in vacuum. (Yield: 94 %) ¹H NMR (400 MHz, DMSO-*d*₆): δ [ppm] 7.39–7.19 (m, 10H, H_{AR}), 4.76 (q, 2H, *J* = 6.7 Hz, C=CH-CH₃ (*E* isomer)), 4.64 (q, 1H, *J* = 7.0 Hz, C=CH-CH₃ (*Z* isomer)), 4.56 (t, 1H, OH), 3.96–3.86 (m, 12H, OCH₂-C=CH-CH₃ and CH₂O-C=CH-CH₃), 3.71–3.35 (m, 256H, CH₂O and C_{AR}-CH₂N), 2.55 (t, 2H, *J* = 6.1 Hz, NCH₂-CH₂O), 1.60 (d, 3H, *J* = 6.7 Hz, C=CH-CH₃ (*Z* isomer)), 1.52 (d, 6H, *J* = 6.7 Hz, C=CH-CH₃ (*E* isomer)). ¹³C NMR (100.6 MHz, DMSO-*d*₆): δ [ppm] 152.84 (1C, OCH₂-C=CH-CH₃ (*Z* isomer)), 151.07 (1C, OCH₂-C=CH-CH₃ (*E* isomer)), 139.97 (1C, C_{AR}-CH₂-N), 128.45 - 127.23 (3C, C_{AR}), 106.80 (1C, C=CH-CH₃ (*E* isomer)), 96.59 (1C, C=CH-CH₃ (*Z* isomer)), 72.81-67.34 (131C, CH₂O), 60.66 (1C, NCH₂-CH₂O), 58.44 (2C, C_{AR}-CH₂-N), 52.55 (1C, NCH₂-CH₂O), 11.81 (1C, C=CH-CH₃ (*Z* isomer)) 10.39 (1C, C=CH-CH₃ (*E* isomer)).

¹H NMR Kinetics

Deuterated phosphate/citrate phosphate buffer solutions were produced by mixing of two stock solutions and adjusting of the pH with a pH electrode. Stock solutions of citric acid (100 mmol L⁻¹) and K₂HPO₄ (100 mmol L⁻¹) in deuterium oxide were used for the citrate phosphate buffer at pD 4.4, 4.9 and 5.4. The respective pD values were obtained via the equation pD = pH + 0.4.^[1]

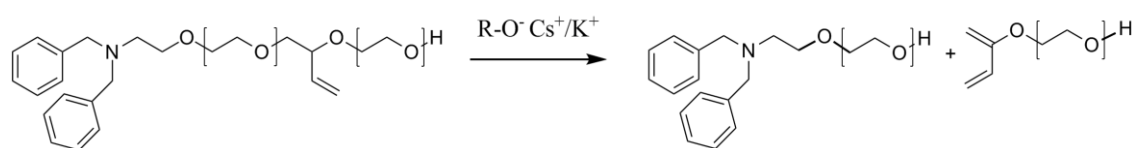
For *in-situ* ¹H NMR degradation kinetics at pD 4.4, 20 mg of the P(*iso*EPB-*co*-EG) copolymer were dissolved in 0.7 mL of deuterated buffer and transferred into a NMR tube immediately after dissolving. The NMR tube was placed in a preheated NMR spectrometer (37 °C) and the sample was locked to the solvent signal and shimmed after the sample temperature was constant (ΔT = 0.1 K)

for 2 min. Spectra were recorded with 16 scans at 2-minute intervals during the first hour, then at 5-minute intervals for 2 hours, and at 10-minute intervals within the next 5 hours due to a decrease in the reaction rate. The kinetic analysis was stopped after 24 h. For kinetic studies at pD 4.9 and 5.4, 20 mg of the respective polymer were dissolved in 0.7 mL of deuterated buffer and were transferred into a NMR tube immediately after dissolving. The NMR tube was placed in an oil bath at 37 °C and NMR spectra were recorded manually after selected periods of time, immediately returning the sample into the oil bath after each measurement.

SEC Hydrolysis Studies

Aliquots (8 mg) of the P(*iso*EPB-*co*-EG) copolymers were dissolved in a solution ($c_{\text{HCl}} = 0.1 \text{ mol L}^{-1}$) of hydrochloric acid (0.041 mL HCl_{conc}) in MeOH:H₂O (4:1, 5 mL) and stirred for 24 h under exposure to air. The solvent was evaporated in high *vacuo* and the residue was analyzed by size exclusion chromatography (SEC) using DMF as eluent and RI detection.

Synthesis and Characterization



Scheme S-1: Fragmentation reaction of P(EPB-co-EG) copolymers via β -elimination in the presence of potassium or cesium alkoxides.

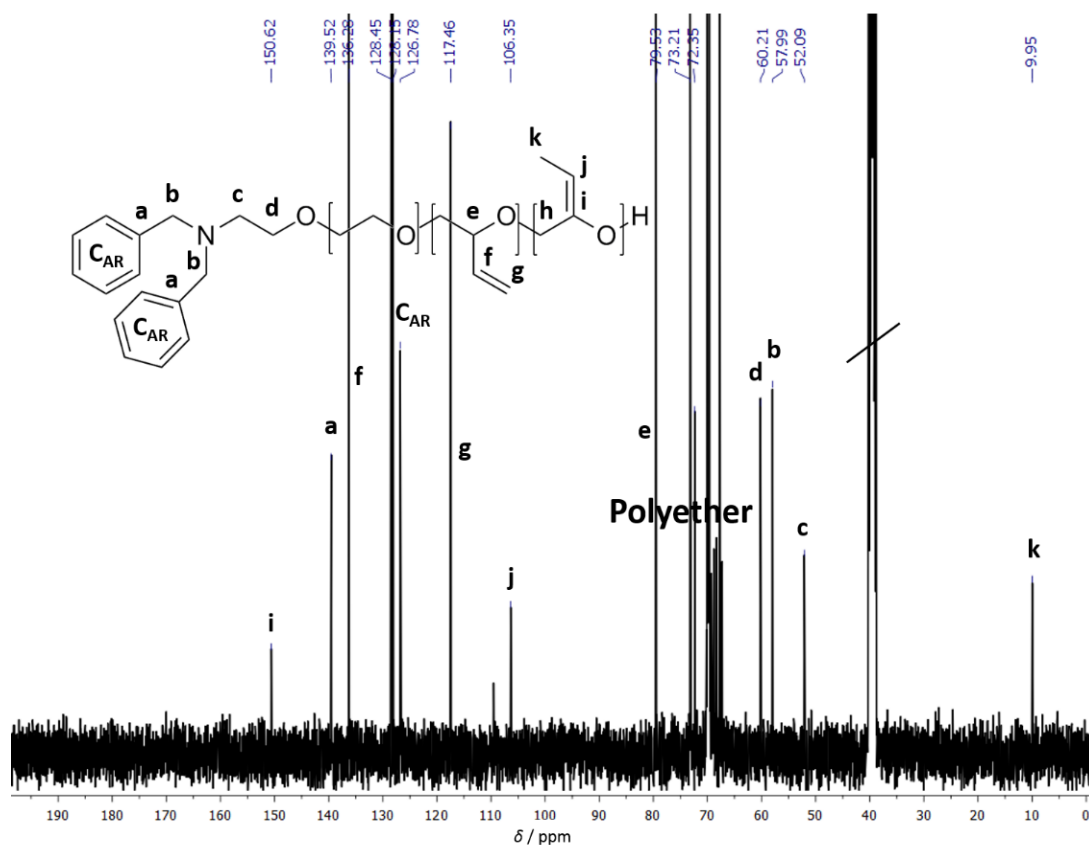


Figure S-16: ^{13}C NMR spectrum of P(EPB₅-co-EG₁₄₃) before isomerization measured in DMSO-d₆ at 100 MHz.

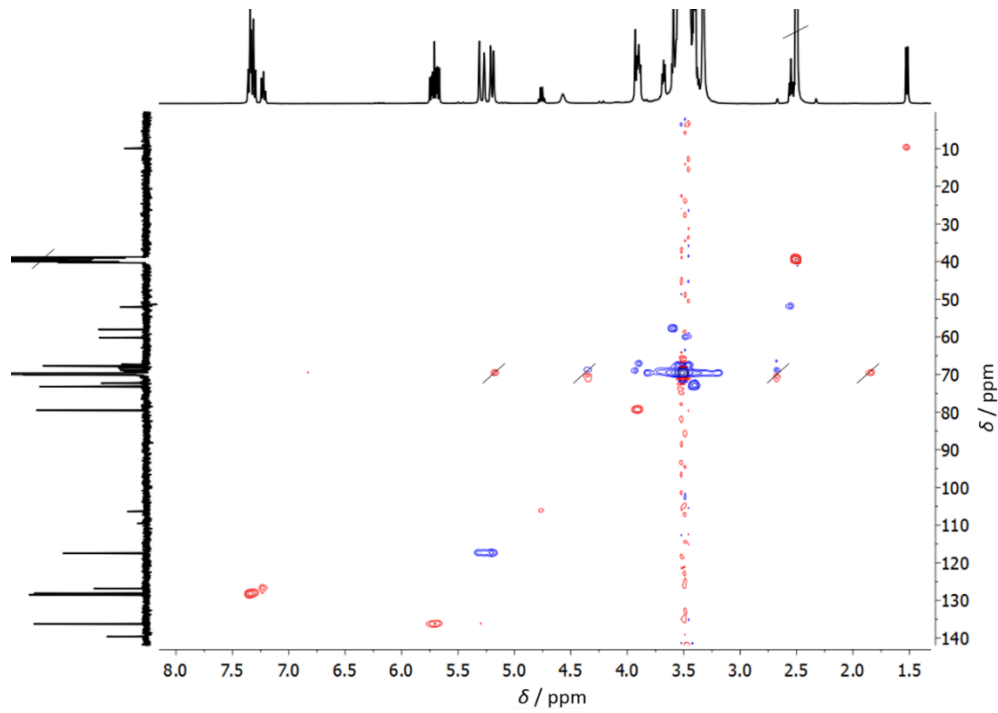


Figure S-17: H,C-HSQC NMR of P(EPB₅-co-EG₁₄₃) measured in DMSO-d₆. Methyl and methine groups appear as red correlation peaks, whereas blue correlation peaks correspond to the methylene groups in the polymer.

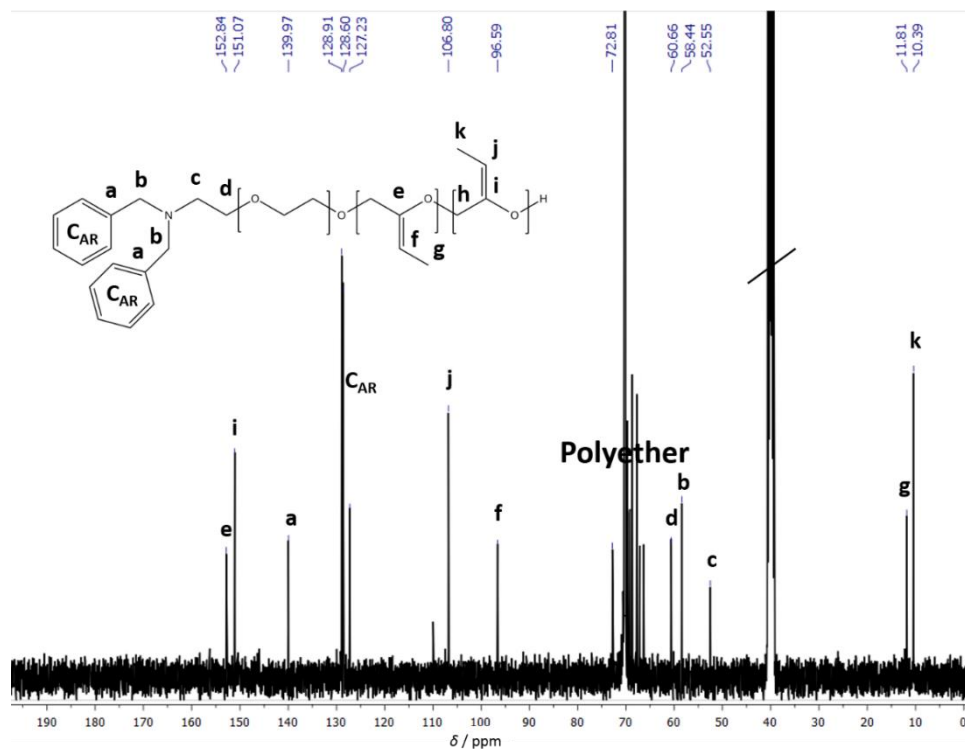


Figure S-18: ¹³C NMR spectrum of P(*iso*EPB₅-co-EG₁₄₃) after isomerization measured in DMSO-d₆ at 100 MHz.

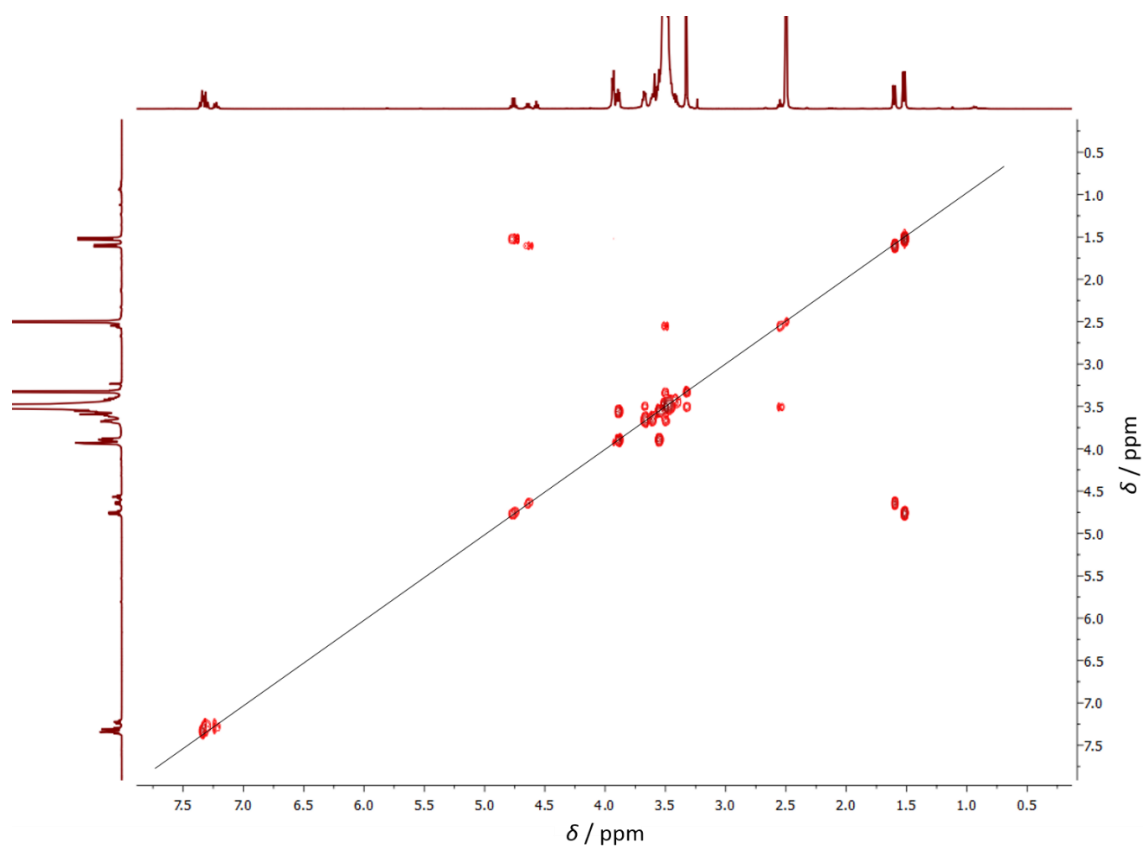


Figure S-19: H,H-COSY NMR of **P(isoEPB₅-co-EG₁₄₃)** measured in DMSO-d₆.

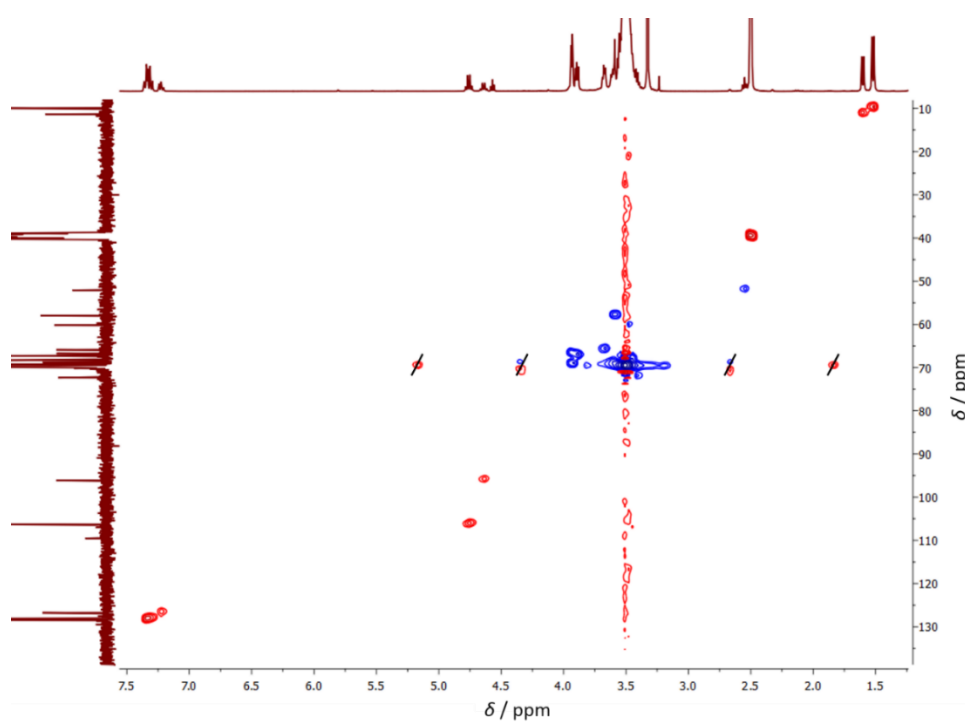


Figure S-20: H,C-HSQC NMR of **P(isoEPB₅-co-EG₁₄₃)** measured in DMSO-d₆. Methyl and methine groups appear as red correlation peaks, whereas blue correlation peaks correspond to the methylene groups in the polymer.

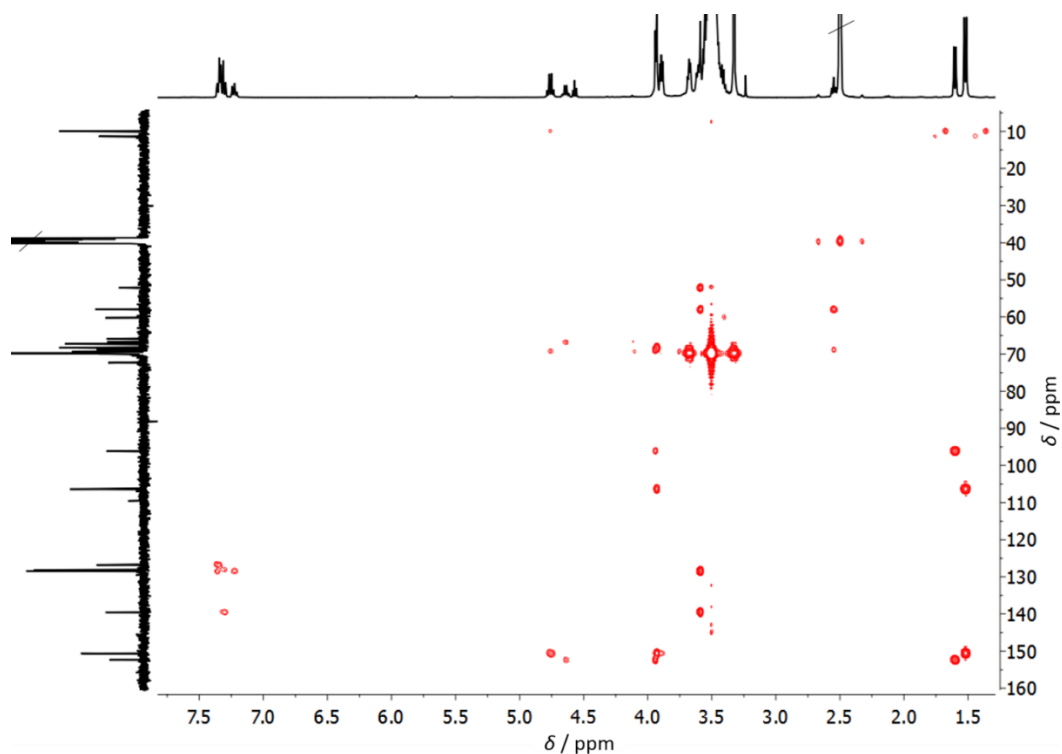


Figure S-21: H,C-HMBC NMR of $P(\text{isoEPB}_5\text{-co-EG}_{143})$ measured in DMSO-d_6 .

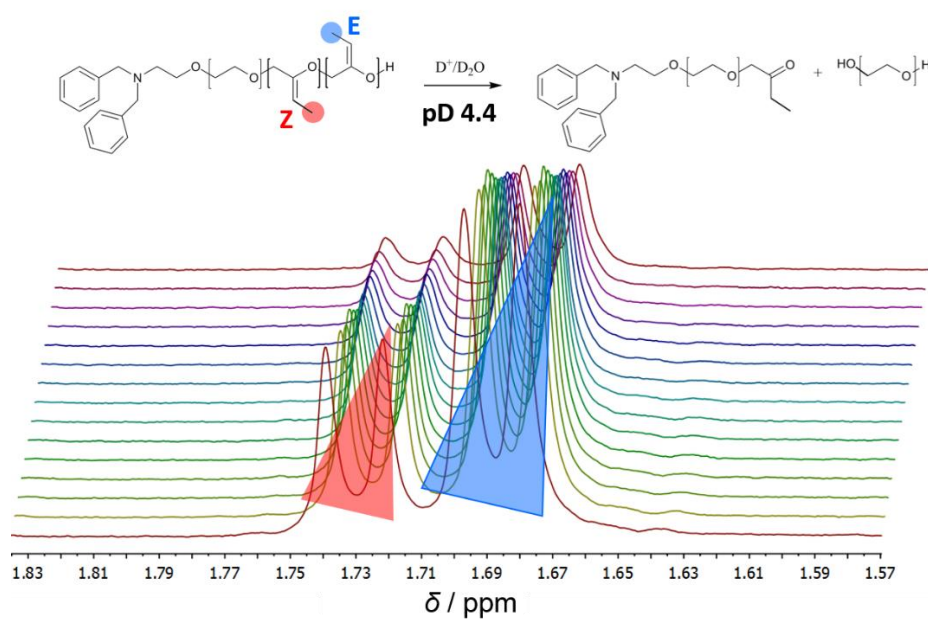


Figure S-22: Close-up of propenyl methyl resonances in the spectra obtained from ^1H NMR kinetics of $P(\text{isoEPB}_5\text{-co-EG}_{143})$ at $\text{pD } 4.4$, showing distinguishable proton signals for (E)- and (Z)-isomers of *isoEPB* that could be used to calculate individual rate constants of hydrolysis.

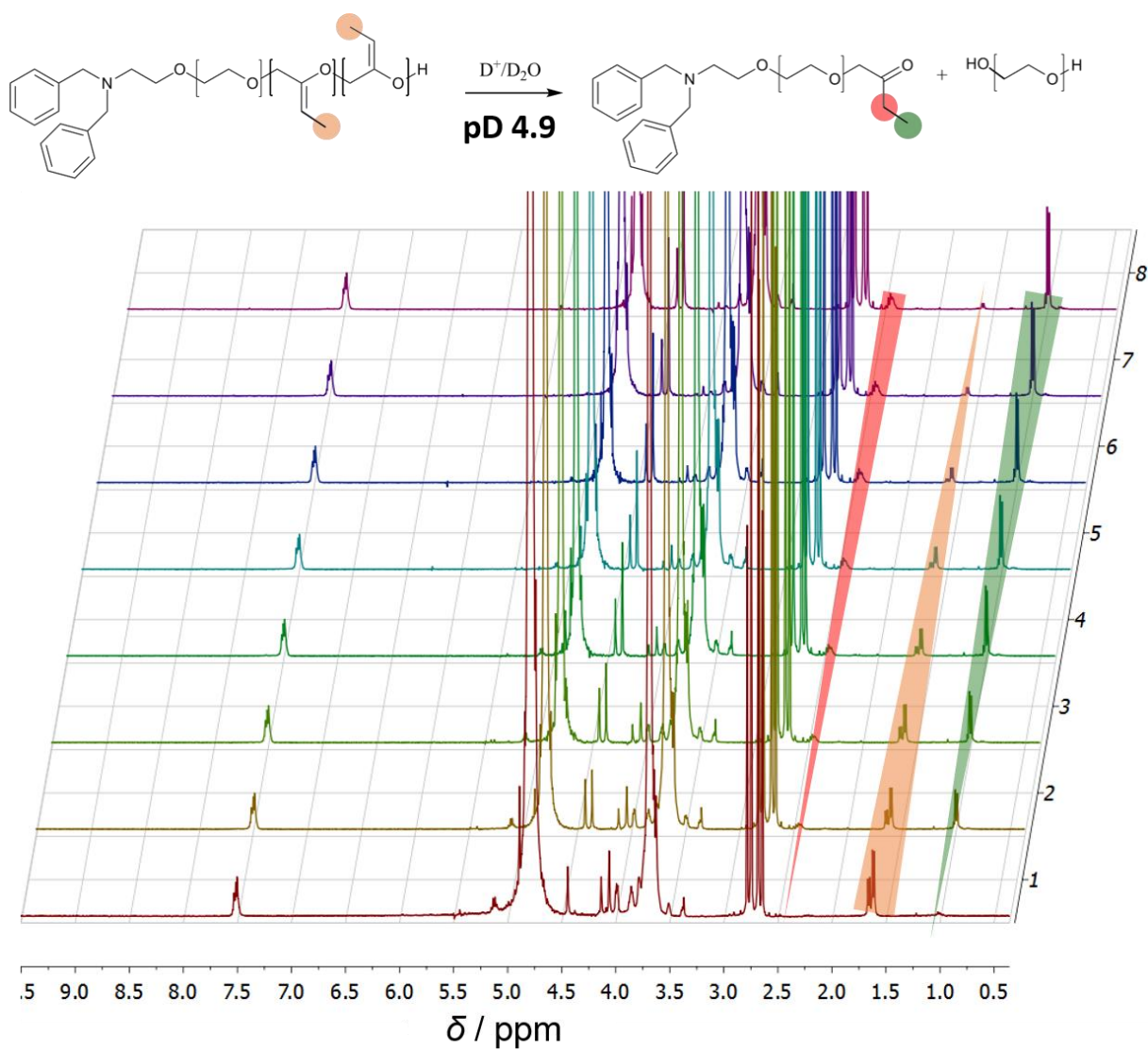


Figure S-23: 1H NMR Kinetic studies of $P(isoEPB_5-co-EG_{143})$ in deuterated citrate/phosphate buffer at $pD\ 4.9$ incubated at $37\ ^\circ C$ and spectra were recorded within a time period of 116 h.

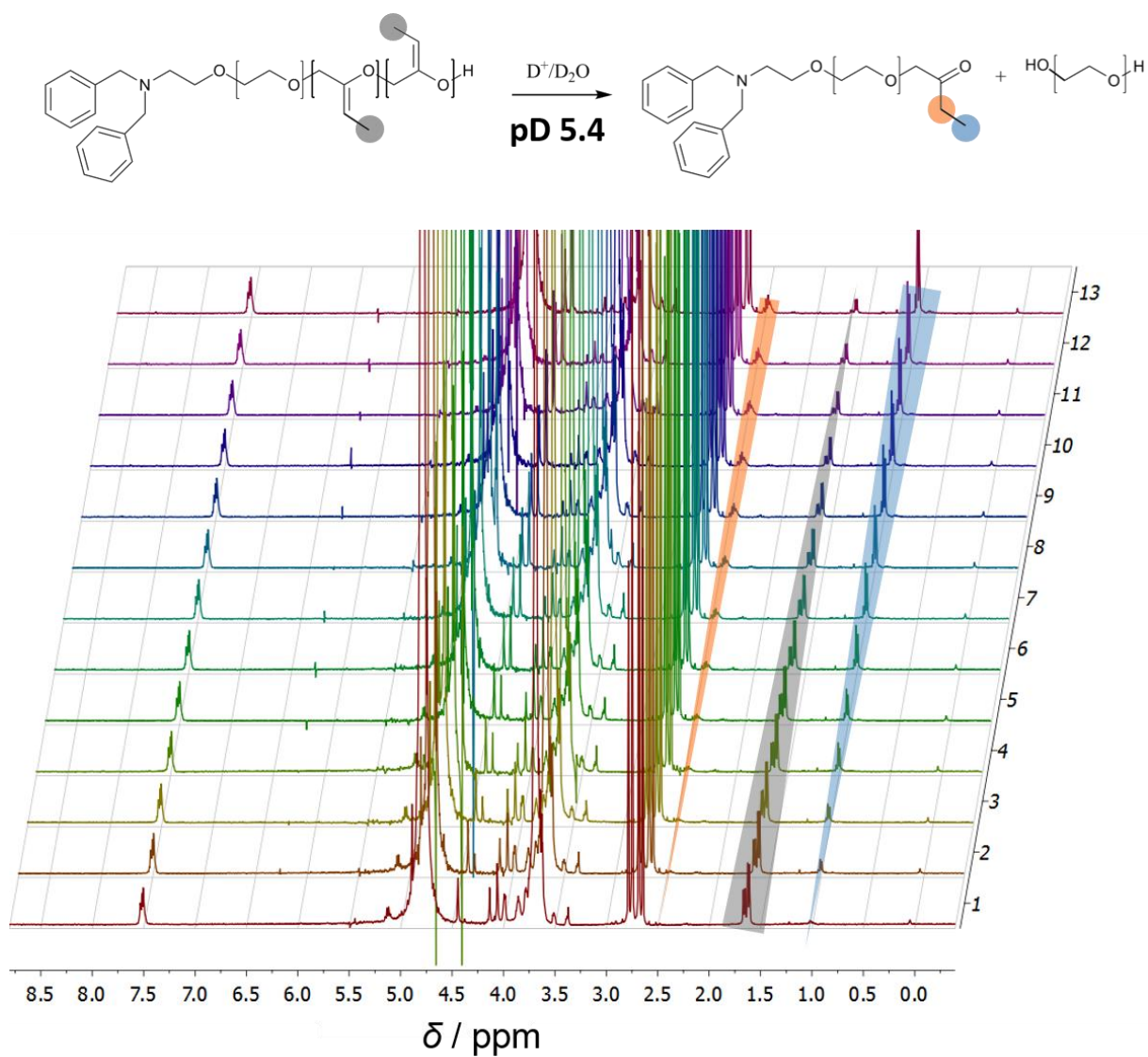


Figure S-24: 1H NMR Kinetic studies of $P(isoEPB_5-co-EG_{143})$ in deuterated citrate/phosphate buffer at pH 5.4 incubated at 37 °C and spectra were recorded within a time period of 290 h.

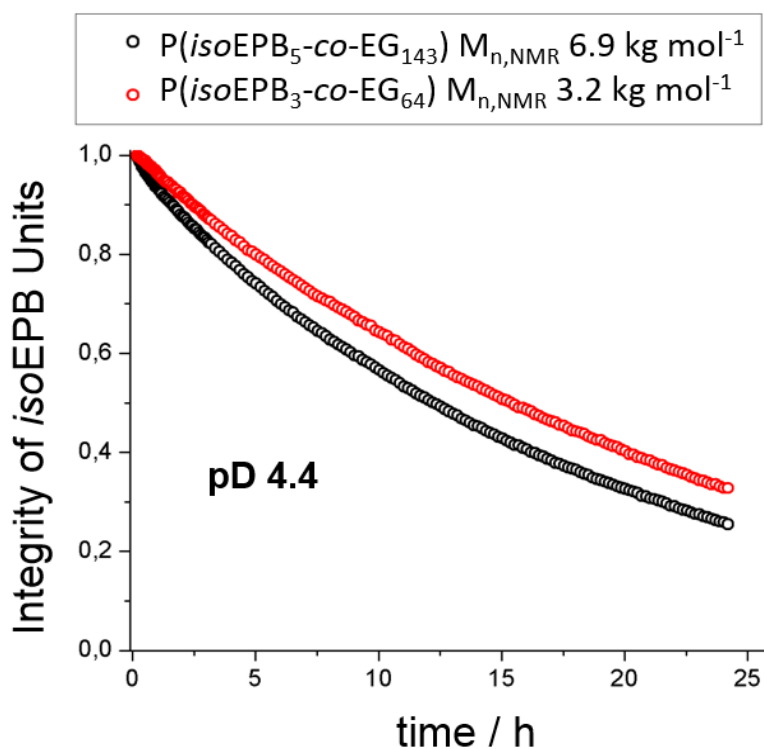


Figure S-25: Comparison of average hydrolysis profiles for P(*iso*EPB₅-co-EG₁₄₃) and P(*iso*EPB₃-co-EG₆₄) measured at pD 4.4 in D₂O determined by ¹H NMR kinetics.

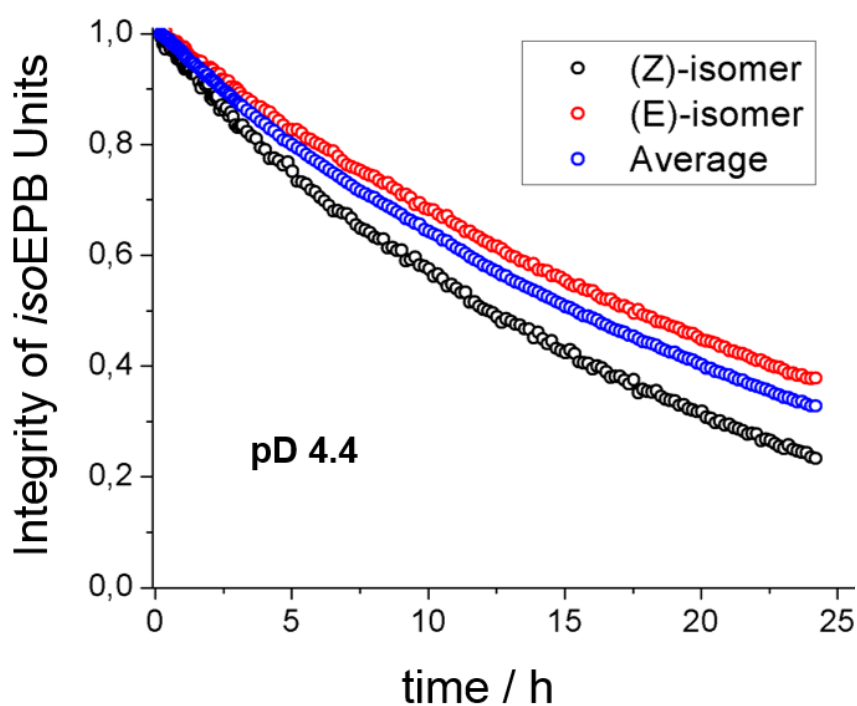


Figure S-26: Results of ¹H NMR Kinetics of P(*iso*EPB₃-co-EG₆₄) in buffered D₂O at pD 4.4 showing the integrity of *iso*EPB units plotted against time. The hydrolysis profiles of (Z)- (black), (E)- (red) geometric isomers and the average *iso*EPB units (blue) are presented in separate plots.

References

- [1] Glasoe, P. K.; Long, F. A. *J. Phys. Chem.*, **1960**, *64*, 188–190.

4 pH-Sensitive PEG-Lipids for Liposomal Applications

4.1 Ketal- and Acetal-functional Dialkyl-PEG Lipids for pH-Sheddable Liposomes

Matthias Worm,^a Thomas Fritz,^b Daniel Leibig,^{a,c} Fabian Jung,^b Eyleen Becker,^a Mark Helm,^b and Holger Frey^{a*}

^a Institute of Organic Chemistry, Johannes Gutenberg-University, Duesbergweg 10-14, D-55128 Mainz, Germany.

^b Institute of Pharmacy and Biochemistry, Johannes Gutenberg-University, Staudinger Weg 5, D-55128 Mainz, Germany.

^c Graduate School, Materials Science in Mainz, Staudinger Weg 9, D-55128 Mainz, Germany.

To be Submitted

Abstract

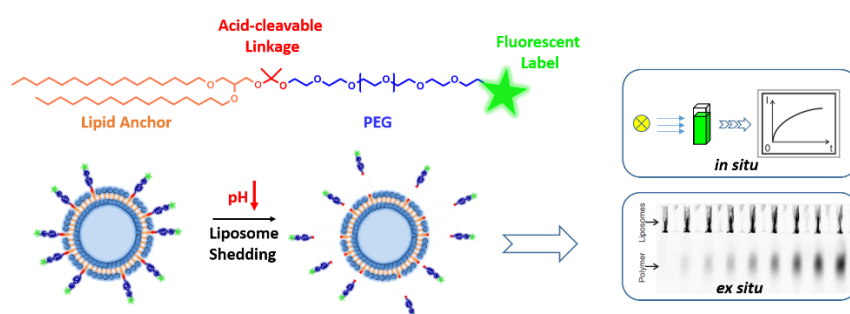
In nanomedicine, stealth liposomes with PEG-lipids entrenched in their membranes represent potent drug delivery systems for the treatment of tumors. However, in the presence of a PEG stealth layer, cellular uptake and intracellular drug release can be hampered. Here we introduce a novel class of pH-sensitive PEG-lipids containing ketals and acetals as cleavage linkages to facilitate shedding of the PEG shell inside the tumor tissue or in a cellular compartment. Acetals and ketals are highly versatile, as their hydrolysis kinetics can be adjusted by the respective substitution pattern. A prototype one-step synthesis towards ketals is introduced to conveniently incorporate asymmetric ketals into PEG-based block structures. Acetal- and ketal-functional bishexadecyl glycerol derivatives were used as initiators for the anionic ring-opening polymerization (AROP) of ethylene oxide to access well-defined PEG-lipids ($\bar{D} = 1.04 - 1.08$) with tunable molecular weights of PEG ($M_n = 2000 - 3500 \text{ g mol}^{-1}$). Online ^1H NMR kinetics served to evaluate susceptibility of these lipids towards acidic hydrolysis. Cell viability of liposomes containing the novel PEG-lipids was confirmed via MTT assays and post-modification of the lipids at the liposomal surface was demonstrated using copper(I)-catalyzed alkyne-azide click chemistry to attach fluorescent labels. Fluorescence spectroscopy experiments and agarose gel electrophoresis (PAGE) assays were employed to monitor pH-triggered shedding of liposomes, revealing highly promising cleavage

profiles for the ketal-functional lipids ($t_{1/2} \sim 4$ h, pH 6.4). The findings demonstrate the potential of functionalizable, pH-sensitive lipids for pH-triggered drug release strategies from liposomal carriers.

Keywords

liposomes, poly(ethylene glycol), PEG, lipids, pH-cleavable, ketals

Table of Contents Graphics



Introduction

In recent years, stimuli-responsive polymers have gained increasing attention in various fields of research due to their unique properties.^[1,2] Stimuli-responsive materials are sensitive to an external trigger, such as pH, oxidation/reduction, light or temperature, upon which a structural change is induced. Structural changes may encompass solubility switches due to temperature/light-induced conformational changes, protonation,^[3–5] or cleavage of pH-labile, redox-responsive, or light-sensitive moieties.^[6,7] Especially in nanomedicine, pH-responsive polymers have proven advantageous for the design of drug carrier systems, since acidic domains are present in various parts of human tissue. Lowered pH values have been reported for endosomal and lysosomal cellular compartments,^[8] as well as for the microenvironment of various tumor cell lines and for inflammatory tissue.^[9,10]

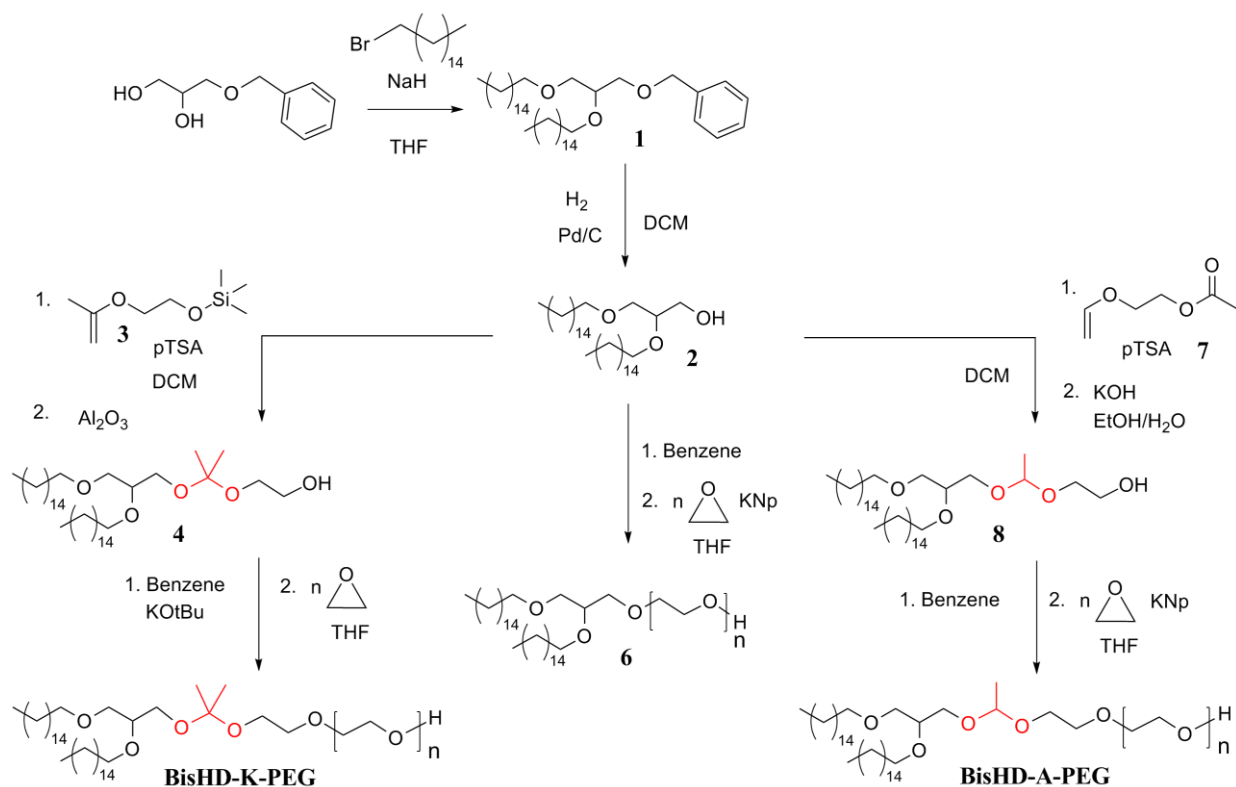
Poly(ethylene glycol) (PEG) is generally regarded as the gold standard polymer for medical applications due to its excellent biocompatibility and very low immunogenicity,^[11,12] and increasing

effort is devoted to incorporating pH-cleavable building blocks into PEG and its conjugates.^[13,14] In liposomal research, pH-sensitive PEG-lipids have recently become attractive, as they enable shedding of stealth liposomes inside the targeted tissue to enhance efficacy of the drug carriers. The presence of a PEG stealth layer can hamper cellular uptake of liposomes and drug release.^[15–17] Moreover, PEGylated nanoparticles can be subjected to accelerated blood clearance upon repetitive drug administration leading to an increased uptake by the liver.^[18–20] PEG-lipids bearing pH-cleavable linkages can be employed to avoid these drawbacks of PEG in liposomes.^[20,21] Examples of acid-cleavable moieties incorporated into pH-sensitive liposomes (PSL) include hydrazones,^[21–23] orthoesters,^[24–26] acetals,^[27] vinyl ethers,^[28,29] and cyclic ketals.^[30] The corresponding strategies are generally based on chemical modification of commercially available monomethoxy PEG (mPEG) and therefore lack the possibility to attach further functionalities such as dye labels or radioactive tracers, for instance to unravel the fate of the cleaved PEG chains. Also linking of targeting ligands to enable directed drug delivery is not possible. Furthermore, molecular compositions are restricted to the commercially available molecular weights of PEG, limiting precise tuning of lipid properties.

Within the class of acid-hydrolyzable moieties, acetals and ketals constitute highly potent representatives, as the substitution patterns provides a means of fine-tuning their susceptibility towards hydrolysis.^[31,32] Generally, acetals are hydrolyzed several orders of magnitude slower than respective ketals.^[33] These circumstances allow for the design of hydrolysis profiles to match the specific requirements for controlled release strategies. Increasing effort has been expended on incorporating acetals and ketals into polymeric structures.^[34–39] However, to date, no synthetic routes are available to conveniently access ketals composed of two different alcohol components without tedious purification or multi-step reactions. A straightforward approach to these asymmetric ketals may grant access to novel, pH-cleavable block-type structures and polymer conjugates, thereby extending the scope of pH-sensitive materials for triggered drug release

purposes. The design of lipids that combine well-defined pH-dependent hydrolysis with tailored molecular compositions and, in addition, facilitate the attachment of further functional groups remains a challenge.

Recent findings in liposomal research have elucidated higher membrane integrity of polyether-based lipids containing dialkyl-derived anchor groups compared to cholesterol-functional lipids.^[40] These results motivate a stronger focus on dialkyl-containing polyether-based lipids, since stable anchorage in the membrane can further enhance stability profiles of stealth liposomes and therefore prevent extracellular leakage of the cargo, while ligand-mediated targeting efficiencies are increased as well. In this work, we introduce a novel class of acid-cleavable dialkyl glycerol PEG-lipids containing ketals and acetals as scissile linkages and demonstrate their potential for pH-sensitive stealth liposomes. A prototype one-step strategy based on vinyl ether chemistry is presented, offering straightforward access to asymmetric ketals in polymers. Acetal- and ketal-containing dialkyl glycerol derivatives have been synthesized and used as initiators for the anionic ring-opening polymerization of ethylene oxide to obtain pH-cleavable lipids with precisely tunable molecular weights of PEG and narrow molecular weight distributions. The susceptibility of the PEG-lipids towards acidic hydrolysis has been evaluated via real-time ¹H NMR kinetic studies. Furthermore, functionalization of the lipids via copper(I)-catalyzed azide-alkyne click chemistry with fluorescent dyes has been demonstrated via a post-preparational approach at the liposomal surface. pH-triggered shedding of the liposomes endowed with the fluorescent-labeled PEG-lipids have been monitored by fluorescence spectroscopy and gel electrophoresis, revealing promising cleavage profiles for the ketal-functional lipid species.



Scheme 8. Synthesis of bishexadecyl glycerol-based lipids.

Experimental Section

Materials

All chemicals were obtained from *Sigma Aldrich*, *TCI Europe*, or *Acros Organics* unless stated otherwise. Deuterated solvents (C₆D₆, CD₂Cl₂, CDCl₃, DMSO-*d*₆, D₂O) were purchased from *Deutero GmbH*. Egg phosphatidylcholine (EPC, fully hydrogenated EPC3) was kindly provided by *Lipoid GmbH* (Ludwigshafen, Germany). Cholesterol was purchased from *Carl Roth* (Karlsruhe, Germany). Atto 488 azide was obtained from *Atto-Tec* (Siegen, Germany). 2-[2-[(Trimethylsilyl)oxy]ethoxy]propene (**3**)^[41] and 2-Acetoxyethoxy vinyl ether (**7**)^[42] were synthesized according to reported procedures. THF used for the anionic ring-opening polymerization was dried and stored over sodium/benzophenone. Care must be taken when handle the flammable, toxic, and gaseous ethylene oxide.

Methods

Characterization. ^1H NMR spectra were measured on a Bruker Avance II 400 MHz (5 mm BBO probe, 256 Scans, and B-ACS 60 auto sampler) at 294 K. 2D NMR and ^{13}C NMR spectra were recorded on a Bruker Avance II 400 (100.5 MHz, 5 mm BBO probe, and B-ACS 60 auto sampler) at 294 K, if not stated otherwise. ^{13}C inverse gated NMR spectra were recorded with 2048 scans and a relaxation delay of 10 s. Relaxation times T_1 for the ketal species were determined via saturation recovery methods. All spectra were processed with MestReNova v9.0 software. GPC (SEC) data were obtained using Agilent 1100 Series endowed with a PSS HEMA-column ($10^6/10^4/10^2$ Å porosity), LiBr/DMF (1 g/L) as eluent using RI detection. Molecular weights and dispersity ($\mathcal{D} = M_w/M_n$) were determined with monodisperse PEG standards from *Polymer Standard Service GmbH* (PSS). MALDI-ToF mass spectrometry was conducted on an Axima CFR MALDI-ToF mass spectrometer using pencil lead or α -cyano-4-hydroxy-cinnamic acid (CHCH) as matrix and potassium trifluoroacetate (KTFA) as a source for cations.

Liposome preparation was conducted via dual centrifugation (DC) according to a method previously described.^[43] Briefly, ethanolic solutions of hydrated egg phosphatidyl choline (EPC, Lipoid, Ludwigshafen, Germany), cholesterol (Carl Roth, Karlsruhe, Germany) and the respective polymeric amphiphile were combined to yield 85 μmol (~ 5 mg) in a molar ratio of 50:45:5, respectively, and dried *in vacuo*. Lipid samples were stored at -80 °C until use to prevent degradation of the ketal structures. 9.3 μL of Dulbecco's phosphate buffered saline (DPBS, Thermo-Fisher Scientific, Waltham, MA, USA) and 70 mg of ceramic beads (SiLyBeads ZY 0.3 – 0.4 mm) were added and the sample subjected to a 20 min dual centrifugation run at 2500 RPM, utilizing a customized Hettich Rotanta 400 centrifuge (Hettich, Tuttlingen, Germany) with a custom made inset. 28 μL DPBS were added and the obtained vesicular phospholipid gel subjected to two more 2 min DC runs, in between of which the sample orientation was reversed. Stock liposome suspensions were stored at 4 °C until usage, highly sensitive ketal compounds were used immediately.

Liposome functionalization was carried out according to a previously established protocol.^[44] For copper-catalyzed azide alkyne cycloaddition, the following reactants were added in the listed order: MilliQ water (to a total volume of 40 μL), phosphate buffer (5.3 mM NaH_2PO_4 , 94.7 mM Na_2HPO_4 , pH 8), THPTA (0.5 mM), CuSO_4 (0.1 mM), and sodium ascorbate (2.5 mM), Atto 488 azide (Atto-Tec, Siegen, Germany, 50 μM), liposome suspension (10 μL). After incubation for 2 h at 25 $^\circ\text{C}$, the reaction was stopped by addition of 1 μL of 50 mM EDTA (Carl Roth) solution. Liposome suspensions were purified via gel filtration over custom-made Sepharose 2B-CL (Sigma-Aldrich, St. Louis, MO, USA) columns, fluorimetric determination assured a complete removal of residual free fluorophore azide.

Liposome cleavage was quantified either via a fluorescence spectrometric *in situ* approach or via an *ex situ* approach, utilizing separation of cleavage products via polyacrylamide gel electrophoresis (PAGE). For the fluorimetric assay, quartz glass cuvettes (Hellma, Müllheim, Germany) with a 1 cm path length and tight PTFE plugs were used in a Jasco FP-6500 Fluorimeter (Jasco, Tokyo, Japan) equipped with an ETC-273T temperature controller, a Peltier element stage with a magnetic stirrer and a HAAKE WKL26 cooling unit (Thermo-Fisher Scientific). 2.5 μL of conventional liposomes, consisting only of EPC and cholesterol were combined with 3.8 mL DPBS for 24 h to saturate the glass surface in order to prevent adsorption of labeled amphiphiles. After removal, a liposome sample was added to the cuvette in PBS in a total volume of 2.53 mL, while the amount of liposomes was adjusted to yield Atto 488 in a concentration of 50 nM. After equilibration for 1 h, 1.26 mL of citric acid solutions were added to yield 3.8 mL total volume and no gas phase in the cuvette. Citric acid concentrations were previously determined to yield final pH values of 2.4, 3.4, 4.4, 5.4 and 6.4. For pH 7.4, DPBS was used. For pH 8.4, a sodium tetraborate buffer (12 mM $\text{Na}_2\text{B}_4\text{O}_7$, 126 mM NaCl) was used instead. Fluorescence emission (exc. 490 nm, em. 520 nm) was measured with data rates between 5 sec^{-1} and 7.5 h^{-1} under constant stirring and at 25 $^\circ\text{C}$. Other measurement parameters: em./exc. Bandwidth 5 nm, PMT voltage “high”. For the *ex situ* approach, samples of liposome

suspensions were combined with solutions of citric acid as described above, to obtain the previously determined pH values. Samples were taken at the intended timepoints and neutralized with Na₂HPO₄ solutions of specific and previously tested concentrations. As a gel loading buffer, 4 µL of a 60% (v/v) glycerol solution in DPBS was added and samples were stored at -80 °C until further analysis. PAGE was conducted with 10 cm x 20 cm x 2 mm 15% denaturing polyacrylamide gels (PAGE system, Carl Roth) for 2 h and 15 min at a constant power of 15 W, employing a CBS LSG-400-20 adjustable vertical electrophoresis stand (CBS Scientific, San Diego, USA) and a Consort EV232 power supply (Consort, Turnhout, Belgium). Gels were imaged with a Typhoon 9600 multimode imager with a blue laser unit (GE Healthcare), illuminated at 488 nm and analyzed with a 520 nm bandpass 40 nm filter. ImageJ was used for analysis and measurement of background-corrected band intensities.^[45] The data was fit with Origin (Origin-Lab, Northampton, MA; USA) to the first order exponential decay function $y = A_1 * e^{(-x/t_1)} + y_0$, while fluorescence intensities were normalized to target values y_0 obtained from a first order fit. The half-life time was calculated from $t_{1/2} = \ln(2) * t_1$.

Cytotoxicity: MTT Assay

Cytotoxicity of liposomal suspensions was assessed by a 3-(4,5-Dimethylthiazol-2-yl)-2,5-diphenyltetrazoliumbromid (MTT) assay. HeLa cells were seeded in a density of 10,000 per well in 96-well optical bottom plates (Greiner, Frickenhausen, Germany) 12 h before incubation. To test liposome toxicity, medium was replaced with fresh medium containing liposomes in total lipid concentrations of 100, 10, 1 and 0.1 mg/mL. After 24 h, 40 µL of a 5 mg/mL solution of MTT in DPBS (Thermo-Fisher Scientific, Waltham, MA, USA) were added to the cells and incubated for 1 hour. After careful removal of the medium, 225 µL of a 1:8 v/v mixture of glycine buffer pH 10 and DMSO were added and the cells shaken for 15 min to dissolve the precipitated crystals. 25 µL from each well diluted with 150 µL of glycine buffer pH 10-DMSO mixture (1:8 v/v) in a fresh 96-well plate. Absorbance of MTT was measured at 595 nm with background correction at 670 nm on a Tecan

M200 plate reader, values were normalized to untreated cells. All measurements were performed in technical triplicates.

¹H NMR Kinetics

Deuterated phosphate/citrate phosphate buffer solutions were produced by mixing of two stock solutions and adjustment of the pH with a pH electrode. Stock solutions of K₂HPO₄ (100 mmol L⁻¹) and KH₂PO₄ (100 mmol L⁻¹) in deuterated water were used for phosphate buffer at pD 6.4. Accordingly, stock solutions of citric acid (100 mmol L⁻¹) and K₂HPO₄ (100 mmol L⁻¹) in deuterated water were used for the citrate phosphate buffer at pD 3.4 and pD 5.4. The respective pD values were obtained via the equation $pD = pH + 0.4$.^[46]

For *in-situ* ¹H NMR degradation kinetics, 50 mg of the respective polymer were dissolved in 0.7 mL of deuterated buffer and transferred into a NMR tube immediately after dissolving. The NMR tube was placed in a preheated NMR spectrometer (37 °C) and the sample was locked to the solvent signal and shimmed after the sample temperature was constant ($\Delta T = 0.1$ K) for 2 min. Spectra were recorded with 16 scans at 2-minute intervals during the first hour, then at 5-minute intervals for 2 hours, at 10-minute intervals within the next 5 hours due to a decrease in the reaction rate. The kinetic analysis was stopped manually after complete cleavage was achieved.

Synthesis procedures

3-Benzyl-1,2-bis(hexadecyl)glycerol 1. In a 1000 mL three-necked round-bottom flask equipped with a reflux condenser and a mechanical stirrer 1-benzyl-*rac*-glycerol (5.0 g, 27.4 mmol) and sodium hydride (2.6 g, 109.7 mmol) were dissolved in dry THF (400 mL) under argon atmosphere. 1-Bromohexadecane (33.5 g, 109.7 mmol) was added via syringe and the reaction mixture was stirred at reflux for 6 d. The solvent was evaporated under reduced pressure and the resulting residue was dissolved in a 1/1-mixture of diethyl ether/water (500 mL). After stirring for 16 h, the aqueous phase was neutralized via addition of diluted sulfuric acid (1 mol L⁻¹) and the organic phase was

separated. The aqueous solution was extracted three times with diethyl ether and the combined organic layers were dried over sodium sulfate and filtrated. The solvent was evaporated under reduced pressure and excess 1-bromohexadecane was removed under high vacuum. The pure product (10.1 g, 16.0 mmol, 58 %) was obtained after column chromatography (eluent: petrol ether/ diethyl ether 30:1) over silica. ^1H NMR (400 MHz, CDCl_3): δ [ppm] 7.40–7.23 (m, 5H, CH_{Ar}), 4.56 (s, 2H, ArCH_2), 3.65–3.37 (m, 9H, $\text{CH}_2\text{-CH}_2\text{-O}$, $\text{CH-CH}_2\text{-O}$ and $\text{CH}_2\text{-CH-O}$), 1.66–1.48 (m, 4H, $\text{CH}_2\text{-CH}_2\text{-O}$), 1.43–1.15 (m, 52H, CH_2), 0.88 (t, 6H, $J_{\text{AB}} = 6.3$ Hz, $\text{CH}_3\text{-CH}_2$).

1,2-Bishexadecylglycerol **2. 1** (10.1 g, 16.0 mmol) was dissolved in DCM (200 mL) and stirred with 10wt%-palladium on activated charcoal (505 mg) under hydrogen atmosphere for 3 d. The residue was subsequently filtrated through Celite and the filter cake was washed with DCM. After evaporation of the solvent, the pure product was afforded as colorless crystals in quantitative yield. ^1H NMR (400 MHz, CDCl_3): δ [ppm] 3.78–3.36 (m, 9H, $\text{CH}_2\text{-CH}_2\text{-O}$, $\text{CH-CH}_2\text{-O}$ and $\text{CH}_2\text{-CH-O}$), 1.63–1.49 (m, 4H, $\text{CH}_2\text{-CH}_2\text{-O}$), 1.40–1.17 (m, 52H, CH_2), 0.88 (t, 6H, $J_{\text{AB}} = 6.6$ Hz, $\text{CH}_3\text{-CH}_2$).

2-[2-[(Trimethylsilyl)oxy]ethoxy]propene **3**. This compound was synthesized according to literature.^[41] Storage under argon atmosphere at 8 °C was essential to prevent decomposition.

2-(2-Hydroxyethoxy)-2-(1,2-bishexadecylglyceryloxy)-propane **4**. *p*-Toluenesulfonic acid monohydrate (9.6 mg, 0.056 mmol) and **2** (300 mg, 0.557 mmol) were dissolved in benzene (15 mL) in a dry Schlenk flask and stirred at 40 °C under slightly reduced pressure for 15 min keeping the stopcock closed. Moisture was removed via azeotropic distillation with benzene, and subsequent drying in high vacuum at 40 °C for 16 h. After cooling to RT, the residue was dissolved in dry DCM (15 mL) and 2-[2-[(trimethylsilyl)oxy]ethoxy]propene **3** (969 mg, 5.57 mmol) was added. The reaction was stirred for 90 min and quenched with triethylamine. After removing all volatiles in high vacuum, the pure product (147 mg, 41 %) was afforded via column chromatography over alox (neutral, 6wt% H_2O) applying a stepwise alteration of the eluent from petrol ether to petrol ether/ethyl acetate (20:1) to petrol ether/ethyl acetate (10:1). ^1H NMR (400 MHz, C_6D_6): δ [ppm]

3.77–3.43 (m, 11H, CH₂-O and CH₂-CH-O), 3.37 (t, 2H, $J_{AB} = 6.5$ Hz, CH₂-CH₂-O-CH₂), 1.71–1.54 (m, 4H, CH₂-CH₂-CH₂-O), 1.34–1.10 (m, 58H, CH₂ and CO₂-(CH₃)₂), 0.91 (t, 6H, $J_{AB} = 6.7$ Hz, CH₃-CH₂). ¹³C NMR (100.6 MHz, C₆D₆): δ [ppm] = 99.95 (1C, CO₂(CH₃)₂), 78.97 (1C, CH-CH₂O), 71.89 (1C, CH₂-CH₂O-CH₂), 71.46 (1C, CH-CH₂O-CH₂), 70.97 (1C, CH₂-CH₂O-CH), 62.82 (1C, CH-CH₂O-CO(CH₃)₂), 62.47 (1C, CH₂OH), 61.85 (1C, CH₂-CH₂OH), 32.38 (2C, CH₃-CH₂-CH₂), 30.79-29.88 (24C, CH₂), 26.74 (2C, CH₂), 25.11 (2C, CO₂(CH₃)₂), 23.16 (2C, CH₂-CH₃), 14.41 (2C, CH₂-CH₃).

α -(2-(1,2-bis-hexadecylglyceryl)-oxypropan-2'-yl) ω -hydro PEG **BisHD-K-PEG**. Compound **4** (100 mg, 0.155 mmol) and dry potassium *tert*-butoxide (15.6 mg, 0.139 mmol) were dissolved in benzene (10 mL) and stirred in a dry Schlenk flask under slightly reduced pressure at 50 °C for 15 min keeping the stopcock closed. Moisture and generated *tert*-butanol were removed by azeotropic distillation of benzene and subsequent drying at 50 °C in high vacuum for 16 h. After cooling to RT, dry THF (15 mL) was cryo-transferred into the Schlenk flask and ethylene oxide (1.11 mL, 22.3 mmol) was cryo-transferred via a graduated ampule into the initiator solution. The reaction was proceeded at 40 °C for 2 d and the polymerization was quenched with methanol (2 mL). After precipitation in cold diethyl ether, all volatiles were removed in vacuum and the pure polymer was obtained. (Yield: 81 %) ¹H NMR (400 MHz, C₆D₆): δ [ppm] 3.77–3.25 (m, 158H, CH₂O and CH₂-CHO), 1.71–1.53 (m, 4H, CH₂-CH₂-O), 1.51–1.10 (m, 58H, CH₂ and CO₂-(CH₃)₂), 0.90 (t, 6H, $J_{AB} = 6.7$ Hz, CH₃-CH₂). ¹³C NMR (100.6 MHz, C₆D₆): δ [ppm] = 100.00 (1C, CO₂(CH₃)₂), 78.97 (1C, CH-CH₂O), 73.17-60.74 (79C, CH₂O), 32.35 (2C, CH₃-CH₂-CH₂), 30.87-29.84 (24C, CH₂), 26.76 (2C, CH₂-CH₂-CH₂O), 25.12 (2C, CO₂(CH₃)₂), 23.12 (2C, CH₂-CH₃), 14.40 (2C, CH₂-CH₃).

1,2-Bis-hexadecylglycerol PEG **6**. Compound **2** (200 mg, 0.371 mmol) was dissolved in benzene (10 mL) and stirred in a dry Schlenk flask under slightly reduced pressure at 60 °C for 15 min keeping the stopcock closed. Moisture was removed by azeotropic distillation of benzene and subsequent drying at 70 °C in high vacuum for 16 h. After cooling to RT, dry THF (15 mL) was cryo-transferred into the Schlenk flask and potassium naphthalenide in THF (0.37 mL, 0.18 mmol, $c = 0.5$ mol L⁻¹,

prepared from potassium (235 mg, 6.0 mmol) and naphthalene (770 mg, 6.0 mmol) in dry THF (12 mL) in a glovebox under argon) was added via syringe. Generated hydrogen was removed in vacuum and ethylene oxide (1.11 mL, 22.3 mmol) was cryo-transferred via a graduated ampule into the initiator solution. The reaction was carried out at 40 °C for 3h and subsequently continued at 60 °C for 3 d. The polymerization was quenched with methanol (2 mL) and the polymer was precipitated in cold diethyl ether. After removing all volatiles under vacuum, the pure polymer was obtained. (Yield: 82 %) ^1H NMR (400 MHz, $\text{DMSO-}d_6$): δ [ppm] 3.70–3.20 (m, 250H, $\text{CH}_2\text{-O}$ and $\text{CH}_2\text{-CH-O}$), 1.50–1.38 (m, 4H, $\text{CH}_2\text{-CH}_2\text{-O}$), 1.34–1.10 (m, 52H, CH_2), 0.84 (t, 6H, $J_{AB} = 6.4$ Hz, $\text{CH}_3\text{-CH}_2$).

2-Acetoxyethoxy vinyl ether 7. This compound was synthesized according to prescriptions described in the literature.^[42]

1-(2-Hydroxy ethoxy)-1-(2,3-bis(hexadecyl)glyceryloxy) ethane BisHD-Acetal-Acetate. Compound **2** (600 mg, 1.11 mmol) and *p*-toluenesulfonic acid monohydrate (19 mg, 0.11 mmol) were dissolved in a dry Schlenk flask in benzene (15 mL) and stirred under slightly reduced pressure at 40 °C for 15 min keeping the stopcock closed. Moisture was removed by azeotropic distillation of benzene and subsequent drying at 40 °C in high vacuum for 2 h. After cooling to RT, the mixture was dissolved in dry DCM (15 mL) and a solution of 2-acetoxy ethoxy vinyl ether (**7**) (724 mg, 5.57 mmol) in dry DCM (15 mL) was added via syringe. The reaction was stirred for 15 min and subsequently quenched via addition of triethylamine (5 mL). After washing of the solution with 1N sodium hydroxide (100 mL), the aqueous phase was extracted with DCM (50 mL) and the combined organic layers were dried over sodium sulfate. The solvent was evaporated under reduced pressure and excess vinyl ether was removed in high vacuum for 16 h. The pure product (712 mg, 1.06 mmol, 96 %) was obtained by column chromatography (eluent: petrol ether/ethyl acetate, 10:1) over silica. ^1H NMR (400 MHz, C_6D_6): δ [ppm] 4.68 (q, 1H, $J_{AB} = 5.4$ Hz, O_2CHCH_3), 4.25–4.09 (m, 2H, $\text{CH}_2\text{-COOCH}_3$), 3.85–3.44 (m, 9H, $\text{CH}_2\text{-O}$ and $\text{CH}_2\text{-CH-O}$), 3.40 (t, 2H, $J_{AB} = 6.3$ Hz, $\text{CH}_2\text{-CH}_2\text{-O-CH}_2$), 1.72 (s, 3H, CH_3OOCH_2), 1.70–1.54 (m, 4H, $\text{CH}_2\text{-CH}_2\text{-CH}_2\text{-O}$), 1.52–1.27 (m, 52H, CH_2), 1.25 (d, 3H, $J_{AB} = 5.4$ Hz, $\text{O}_2\text{CH-CH}_3$), 0.92 (t,

6H, $J_{AB} = 6.7$ Hz, CH_3-CH_2). ^{13}C NMR (100.6 MHz, C_6D_6): δ [ppm] 170.11 (1C, $COOCH_3$), 100.19 (1C, O_2CH-CH_3), 78.73 (1C, $CH-CH_2O$), 71.88 (1C, $CH_2-CH_2O-CH_2$), 71.62 (1C, $CH-CH_2O-CH_2$), 70.97 (1C, CH_2-CH_2O-CH), 65.76 (1C, $CH-CH_2O-CHOCH_3$), 63.82 (1C, $CH_2O-COCH_3$), 63.03 (1C, $CH_2-CH_2O-COCH_3$), 32.38 (2C, $CH_3-CH_2-CH_2$), 30.79-29.88 (24C, CH_2), 26.77 (2C, $CH_2-CH_2-CH_2-O$), 23.16 (2C, CH_2-CH_3), 20.52 (2C, $CH_2O-COCH_3$), 19.73 (2C, O_2CH-CH_3), 14.40 (2C, CH_2-CH_3).

1-(2-Hydroxy ethoxy)-1-(2,3-bis-hexadecylglyceryloxy) ethane **8**. Potassium hydroxide (1.78 g, 31.8 mmol) and **BisHD-Acetal-Acetate** (712 mg, 1.06 mmol) were dissolved in a mixture of ethanol (320 mL)/water (19 mL, 1.06 mmol). The solution was stirred at reflux for 2 h and ethanol was removed under reduced pressure. The residue was dispersed in diethyl ether (300 mL) and washed with diluted sodium hydroxide (300 mL, 0.1 mol L^{-1}). Subsequently, the organic phase was dried over sodium sulfate and the solvent was evaporated in vacuum. The crude product was purified by column chromatography over silica (petrol ether/ethyl acetate, 6:1) yielding a ceraceous, yellowish solid (605 mg, 0.96 mmol, 91 %) as the pure product. 1H NMR (400 MHz, CD_2Cl_2): δ [ppm] 4.73 (q, 1H, $J_{AB} = 5.3$ Hz, O_2CHCH_3), 3.70–3.37 (m, 13H, CH_2O and CH_2-CH-O), 2.31 (s, 1H, OH), 1.58–1.47 (m, 4H, $CH_2-CH_2-CH_2-O$), 1.37–1.16 (m, 52H, CH_2), 1.29 (d, 3H, $J_{AB} = 5.3$ Hz, O_2CH-CH_3), 0.92 (t, 6H, $J_{AB} = 6.7$ Hz, CH_3-CH_2).

α -(1-(2,3-bis-hexadecylpropoxy)-1-ethoxy) ω -hydro PEG **BisHD-A-PEG**. Compound **8** (200 mg, 0.371 mmol) was dissolved in benzene (10 mL) and stirred in a dry Schlenk flask under slightly reduced pressure at 60 °C for 15 min keeping the stopcock closed. Moisture was removed by azeotropic distillation of benzene and subsequent drying at 70 °C in high vacuum for 16 h. After cooling to RT, dry THF (15 mL) was cryo-transferred into the Schlenk flask and potassium naphthalenide in THF (0.37 mL, 0.18 mmol, $c = 0.5$ mol L^{-1} , prepared from potassium (235 mg, 6.0 mmol) and naphthalene (770 mg, 6.0 mmol) in dry THF (12 mL) in a glovebox under argon) was added via syringe. Generated hydrogen was removed in vacuum and ethylene oxide (1.11 mL, 22.3 mmol) was cryo-transferred via a graduated ampule into the initiator solution. The reaction proceeded at 40 °C for 3 h and

subsequently continued at 60 °C for 3 d. The polymerization was quenched with methanol (2 mL) and the polymer was precipitation in cold diethyl ether. After removing all volatiles under vacuum, the pure polymer was obtained. (Yield: 82 %) ^1H NMR (400 MHz, C_6D_6): δ [ppm] 4.74 (q, 1H, $J_{AB} = 5.3$ Hz, O_2CHCH_3), 3.88–3.26 (m, 190H, CH_2O and $\text{CH}_2\text{-CH-O}$), 1.69–1.55 (m, 4H, $\text{CH}_2\text{-CH}_2\text{-O}$), 1.49–1.21 (m, 52H, CH_2), 1.29 (d, 3H, $J_{AB} = 5.3$ Hz, $\text{O}_2\text{CH-CH}_3$), 0.91 (t, 6H, $J_{AB} = 6.4$ Hz, $\text{CH}_3\text{-CH}_2$). ^{13}C NMR (100.6 MHz, C_6D_6): δ [ppm] = 100.46 (1C, $\text{O}_2\text{CH-CH}_3$), 78.86 (1C, $\text{CH-CH}_2\text{O}$), 73.24–61.89 (87C, CH_2O), 32.36 (2C, $\text{CH}_3\text{-CH}_2\text{-CH}_2$), 30.86–29.85 (24C, CH_2), 26.76 (2C, $\text{CH}_2\text{-CH}_2\text{-CH}_2\text{O}$), 23.14 (2C, $\text{CH}_2\text{-CH}_3$), 19.96 (1C, $\text{O}_2\text{CH-CH}_3$), 14.40 (2C, $\text{CH}_2\text{-CH}_3$).

General procedure applied to access alkyne-functional lipids. Example: BisHD-A-PEG Alkyne. In a dry Schlenk flask, compound **9** (300 mg, 0.115 mmol) was dissolved in dry THF (15 mL) under argon atmosphere. The solution was cooled to 0 °C, sodium hydride (8.3 mg, 0.34 mmol) was added and the mixture was stirred for 10 min. Propargyl bromide (51.1 mg, 0.34 mmol, 80 wt% in toluene) was injected via syringe and the reaction was carried out at RT for 20 h. After filtration, the solution was reduced to a small volume and the polymer was precipitated in cold diethyl ether. (280 mg, 92 %) ^1H NMR (400 MHz, C_6D_6): δ [ppm] 4.74 (q, 1H, $J_{AB} = 5.3$ Hz, O_2CHCH_3), 3.94 (d, 2H, $J_{AB} = 2.4$ Hz, $\text{OCH}_2\text{-CCH}$), 3.86–3.25 (m, 190H, CH_2O and $\text{CH}_2\text{-CH-O}$), 2.14 (m, 1H, $\text{OCH}_2\text{-CCH}$), 1.71–1.54 (m, 4H, $\text{CH}_2\text{-CH}_2\text{-O}$), 1.52–1.19 (m, 52H, CH_2), 1.29 (d, 3H, $J_{AB} = 5.3$ Hz, $\text{O}_2\text{CH-CH}_3$), 0.90 (t, 6H, $J_{AB} = 6.4$ Hz, $\text{CH}_3\text{-CH}_2$). ^{13}C NMR (100.6 MHz, C_6D_6): δ [ppm] 100.46 (1C, $\text{O}_2\text{CH-CH}_3$), 80.47 (1C, $\text{OCH}_2\text{-CCH}$), 78.86 (1C, $\text{CH-CH}_2\text{O}$), 74.70 (1C, $\text{OCH}_2\text{-CCH}$), 73.24–64.97 (87C, CH_2O), 58.38 (1C, $\text{OCH}_2\text{-CCH}$), 32.36 (2C, $\text{CH}_3\text{-CH}_2\text{-CH}_2$), 30.86–29.85 (24C, CH_2), 26.76 (2C, $\text{CH}_2\text{-CH}_2\text{-CH}_2\text{O}$), 23.14 (2C, $\text{CH}_2\text{-CH}_3$), 19.96 (1C, $\text{O}_2\text{CH-CH}_3$), 14.40 (2C, $\text{CH}_2\text{-CH}_3$).

Results and Discussion

A. Synthesis of Acid-Labile 1,2-Bis-*n*-hexadecyl Glycerol Macroinitiators

Recent findings confirmed superior membrane stability of 1,2-dialkyl-glycerol-based lipids compared in comparison to cholesterol-functional polyether-based lipids.^[40] Stable anchorage of lipids in the membrane of liposomes constitutes one crucial parameter contributing to the overall stability and serum half-life of stealth liposomes.^[47] Therefore, in this work we focused on designing PEG-lipids with dialkyl anchor units endowed with acetals and ketals as pH-sensitive linkages. An overview of the synthesis of lipids discussed in this study is depicted in Scheme 8. At first, 1,2-bis-*n*-hexadecyl glycerol **2** was synthesized in a two-step procedure by alkylation of 1-*O*-benzyl glycerol **1** and subsequent hydrogenation of the protecting group. This protocol has been reported in the literature before,^[48] however reaction conditions were slightly altered. 1,2-bis-*n*-hexadecyl glycerol **2** represents the key synthon in this reaction scheme and served as the precursor for further modification.

The first approach shown in Scheme 8 (left path) aims at incorporating acid-cleavable ketal moieties into dialkyl-based PEG-lipid. To this end, a novel synthetic route was introduced to access the ketal-functional alcohol **4** in a one-step protocol utilizing a TMS-protected vinyl ether **3** under acid catalysis. Cleavage of the TMS-protecting group was conveniently accomplished on a pre-hydrated alox-based chromatography column in the purification step. Compound **3** was synthesized according to reported protocols.^[41] Quenching of the reaction after 90 min prevented formation of a symmetric ketal compound (spectrum not shown). The structure of the macroinitiator **4** was verified by means of ¹H NMR and ¹³C NMR spectroscopy. (See Figure S-1 and S-2) In ¹H NMR spectra methyl proton signals of the ketal moiety overlapped with the resonances of the alkyl chains between 1.5 and 1.2 ppm as confirmed via 2D NMR (HSQC, HMBC) analysis (See SI Figure S-3, S-4).

Complete functionalization of the precursor **2** was concluded from the integration ratio of the terminal alkyl methyl proton signals (6H) compared to the superimposed resonances of the alkyl methylene protons and the ketal methyl protons (58H). The presence of the ketal moiety is evident from the ^{13}C NMR spectrum by the characteristic chemical shifts of 99.95 ppm for the quaternary carbon and 25.11 ppm for the methyl carbon atoms. In summary, this is, to the best of our knowledge, the first report on a one-step protocol to asymmetric, acyclic ketals in polymers.

The second approach provided access to acid-labile acetal-containing lipids (right path, Scheme 8). For this purpose, the acetate-protected vinyl ether **7** was used to derivatize 1,2-bis-*n*-hexadecyl glycerol **2** in an acid-catalyzed transformation, introducing an acetal moiety. Compared to the ketal synthesis described above, acetal formation proceeded at a faster rate, and the reaction was complete after 15 min. Reactivity of vinyl ethers towards acid-catalyzed electrophilic addition has been reported to occur at a faster rate in case of higher degrees of alkylation due to accelerated, rate-determining protonation of the olefin.^[29] The difference in reaction kinetics of the two vinyl ethers in this study towards addition of **2** might be a consequence of the bulkiness of the alcohol component and the more sterically hindered 2-propenyl ether moiety of **3**. Saponification of the acetate group liberated a terminal hydroxyl functionality forming the macroinitiator **8**. Figure S-7 contains the ^1H NMR spectrum of **8** revealing the acetal resonances at 4.73 ppm and 1.30 ppm, respectively. The loss of the acetate proton signals at 1.7 ppm confirmed successful hydrolysis of the ester protecting group (Compare Figure S-6 and S-7). This second approach builds upon a synthetic route previously reported by our group for other acetal-containing polymers.^[49–51] Herein, we extended the scope of the concept to dialkyl-based lipids.

B. Synthesis of Acid-Labile PEG-Lipid

Subsequently, the pH-sensitive, dialkyl-based alcohols were used as macroinitiators for the anionic ring-opening polymerization (AROP) of ethylene oxide to attach the lipids' hydrophilic PEG blocks. In case of the ketal-functional macroinitiator **4**, potassium *tert*-butoxide proved suitable to deprotonate the macroinitiator prior drying. Unexpectedly, drying of **4** in the non-deprotonated state led to partial decomposition of the ketal moieties. Furthermore, it is important to note that all AROPs were performed at ambient temperature to retain integrity of the ketal linkage. In this study, three ketal-functional polymers are presented in a range of molecular weights M_n from 2000 to 3600 g mol⁻¹ exhibiting narrow molecular weight distributions \mathcal{D} below 1.1.

Table 6: Molecular Characteristics of BisHD-K-PEG and BisHD-A-PEG Lipids Prepared

	$M_{n,NMR}/\text{g mol}^{-1}$	$M_{n,SEC}/\text{g mol}^{-1}$	\mathcal{D}_{SEC}
BisHD-K-PEG ₃₇	2230	2000	1.06
BisHD-K-PEG ₄₀	2350	2100	1.07
BisHD-K-PEG ₆₈	3590	3400	1.08
BisHD-A-PEG ₄₆	2650	2400	1.05
BisHD-A-PEG ₆₀	3140	3100	1.04
BisHD-A-PEG ₆₈	3560	3400	1.07
BisHD-PEG ₆₂	2870	2200	1.05

$M_{n,NMR}$: molecular weights of the lipids calculated from ¹H NMR spectroscopy via end group analysis; $M_{n,SEC}$: molecular weights of the lipids determined from SEC analysis using PEG standards. $\mathcal{D}_{SEC} = M_w/M_n$ (dispersity).

Table 6 summarizes the molecular characteristics of the pH-sensitive PEG-lipids discussed in this work. Molecular weights M_n were calculated from ¹H NMR spectroscopy considering the integration ratio of the polyether backbone signals and the terminal methyl proton resonances of the alkyl chains. Apparently, molecular weights obtained from SEC analysis were generally underestimated compared to the molecular weights determined from NMR which could be ascribed to differences in hydrodynamic radii of the lipids and the PEG standards used for calibration. Figure 14 shows the

SEC traces of the polymers synthesized in this study, revealing monomodal molecular weight distributions for all samples and shifts to lower elution volume with increasing molecular weights.

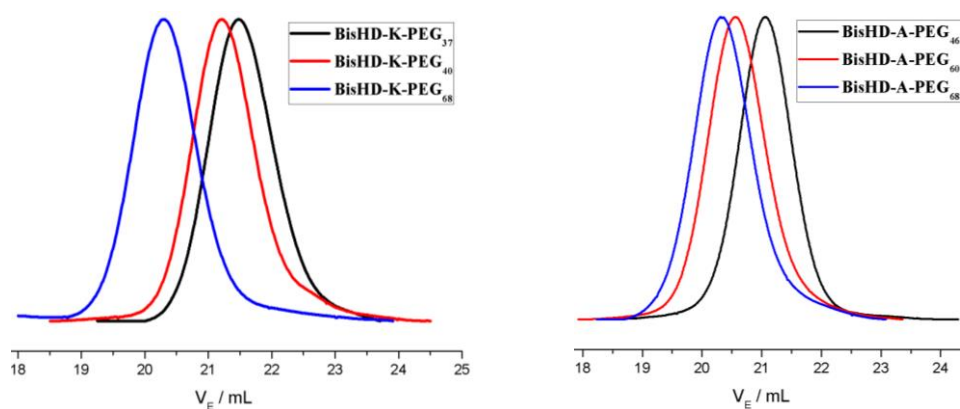


Figure 14. SEC traces (RI detector signal/eluent: DMF) of **BisHD-K-PEGs** and **BisHD-A-PEGs** with varying degrees of polymerization.

As an example, the ^1H NMR spectrum of **BisHD-K-PEG₃₇** is given in Figure 15. As stated above for the macroinitiator, an overlap of the ketal and the alkyl proton signals was observed for the ketal-functional lipids as well (See 2D NMR analysis, Figure S-3, S-4).

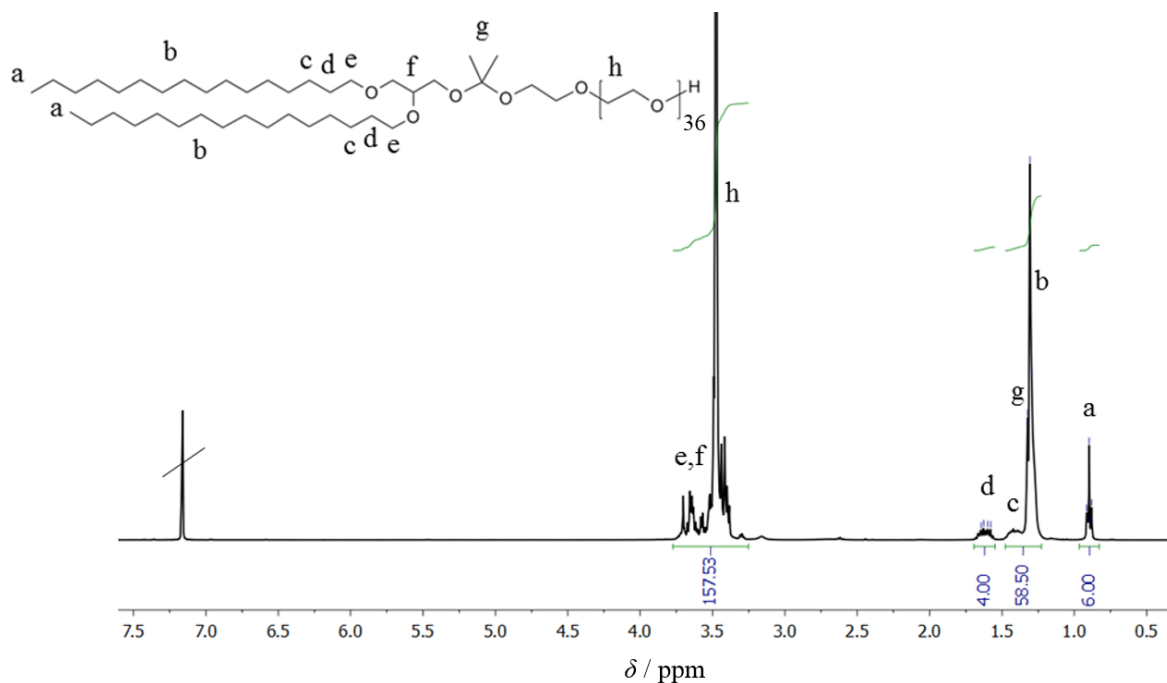


Figure 15. ^1H NMR spectrum of **BisHD-K-PEG₃₇** measured in C_6D_6 at 400 MHz.

In order to confirm incorporation of the ketal moiety in the lipid structure, inverse gated ^{13}C NMR spectroscopy (IG ^{13}C NMR) and MALDI ToF mass spectrometry were conducted. The IG ^{13}C NMR spectrum of **BisHD-K-PEG** is given in Figure 16 including the integration ratios for a set of characteristic carbon atoms normalized to alkyl methyl carbon signals. Herein, a comparison of the integrals for the alkyl methyl carbon at 14.40 ppm, the methyl ketal carbon at 25.12 ppm and the quaternary ketal carbon at 100.00 ppm, respectively provided evidence for the complete integrity of the ketal linkages. It is noteworthy that IG ^{13}C NMR analysis was performed under customized parameters of the measurements, including a relaxation delay d_1 of 10 s and 2048 scans in order to record accurate signal intensities. These prerequisites proved necessary due to the long relaxation time T_1 of the quaternary ketal carbon of 7.10 s in C_6D_6 determined via saturation recovery.

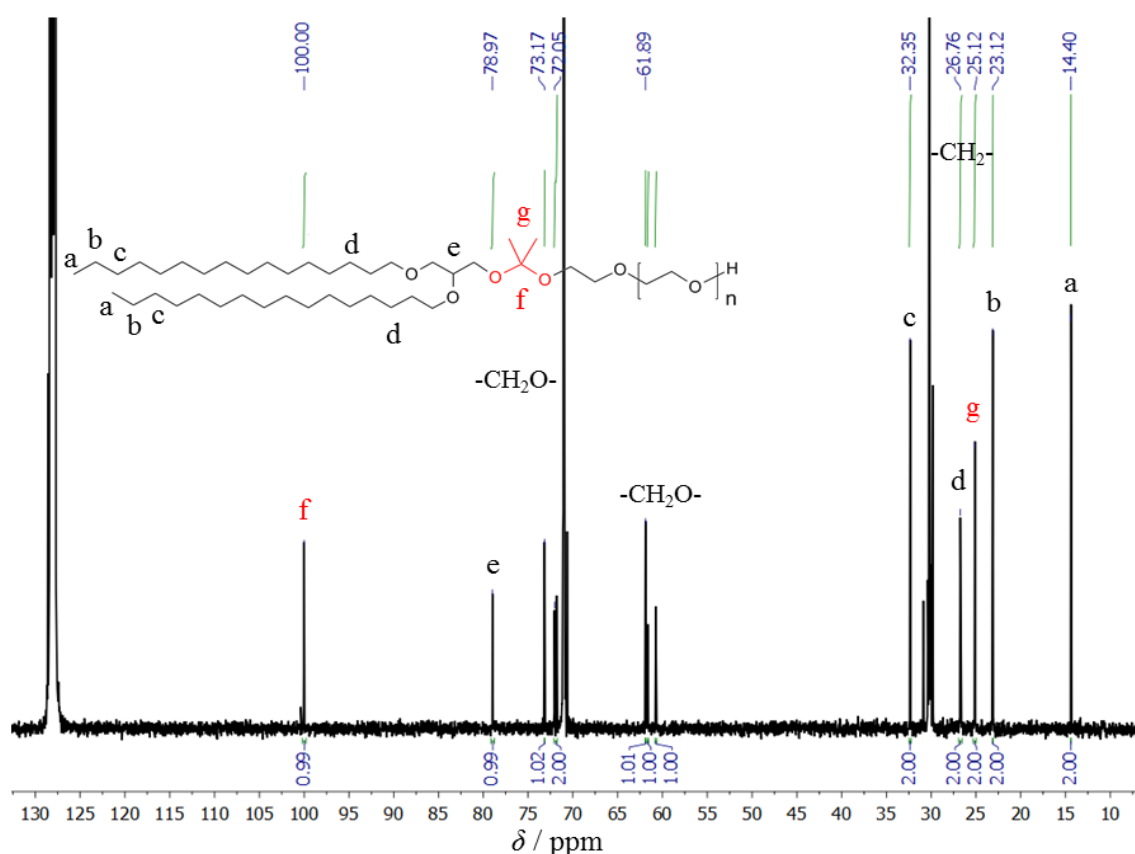


Figure 16. Inverse gated ^{13}C NMR spectrum of **BisHD-K-PEG**₃₇ measured in C_6D_6 at 100 MHz.

Figure 17 depicts a MALDI ToF mass spectrum of the ketal-functional PEG-lipid detected as an ionized potassium complex, using a pencil lead matrix. The use of a non-acidic matrix prevented decomposition of the ketal during sample preparation. Apparently, no PEG diol was observed in the spectra, which could be formed in the presence of water during the polymerization or cleavage of the lipid in the work-up process. The two methods retrospectively demonstrate stability of the ketal-functional macroinitiator **4** under the strongly basic conditions of AROP and further on, prove the absence of non-cleavable PEG-lipids.

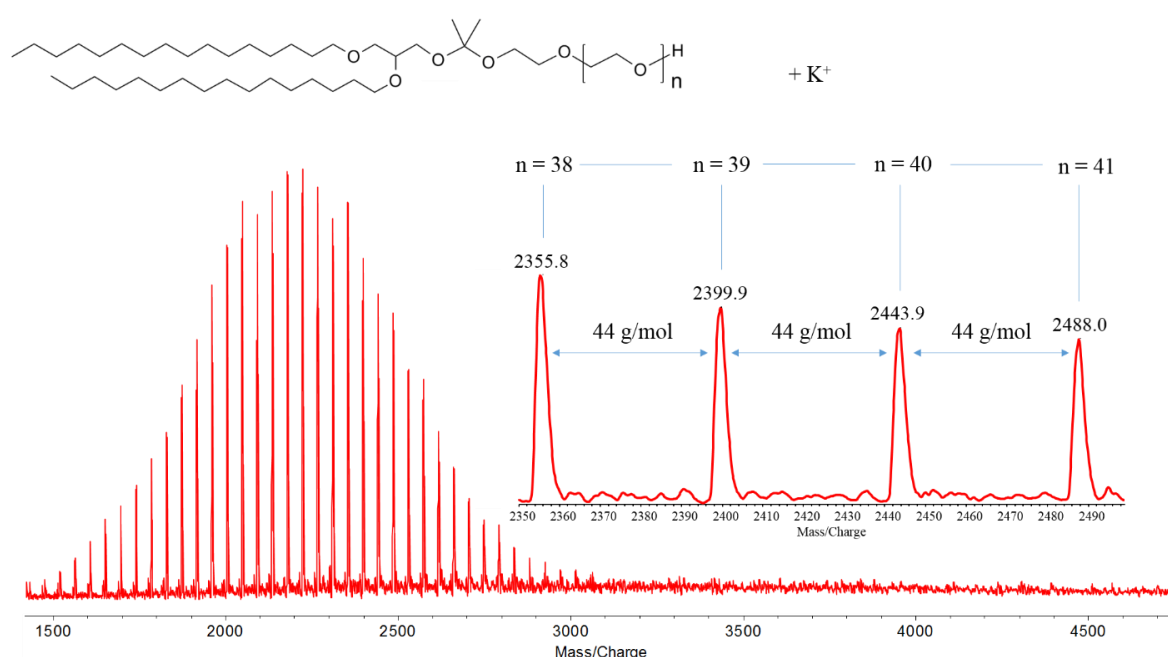


Figure 17. MALDI-ToF mass spectrum of **BisHD-K-PEG₃₇** using pencil lead as a matrix recorded in reflectron mode.

In an analogous manner, the acetal-functional alcohol **8** was utilized as a macroinitiator for the AROP of ethylene oxide. In contrast, however, the integrity of the acetals remained unaffected by drying of the macroinitiator without prior deprotonation. Three acetal-containing PEG-lipids are presented in this study covering a molecular weight range of 2400 to 3600 g mol⁻¹ comparable to the ketal-functional lipids discussed above. SEC analysis revealed narrow, monomodal molecular weight distributions with dispersities \mathcal{D} below 1.1 (see Table 6). As an example, Figure 18 shows the

^1H NMR spectrum of **BisHD-A-PEG₄₆** measured in C_6D_6 . The characteristic multiplet between 4.77 and 4.69 ppm corresponds to the acetal proton and verifies complete incorporation of the pH-cleavable moiety into the lipid structure. The complex splitting pattern of the signal derives from two diastereoisomers of the lipid and was observed for all polymer samples. As stated above for the ketal-functional lipids, molecular weights obtained from SEC were consistently underestimated compared to the values determined by NMR spectroscopy, however, results of both methods were in good agreement. Molecular weights were calculated from ^1H NMR spectra considering the integral of the polyether backbone in relation to the alkyl methyl resonances.

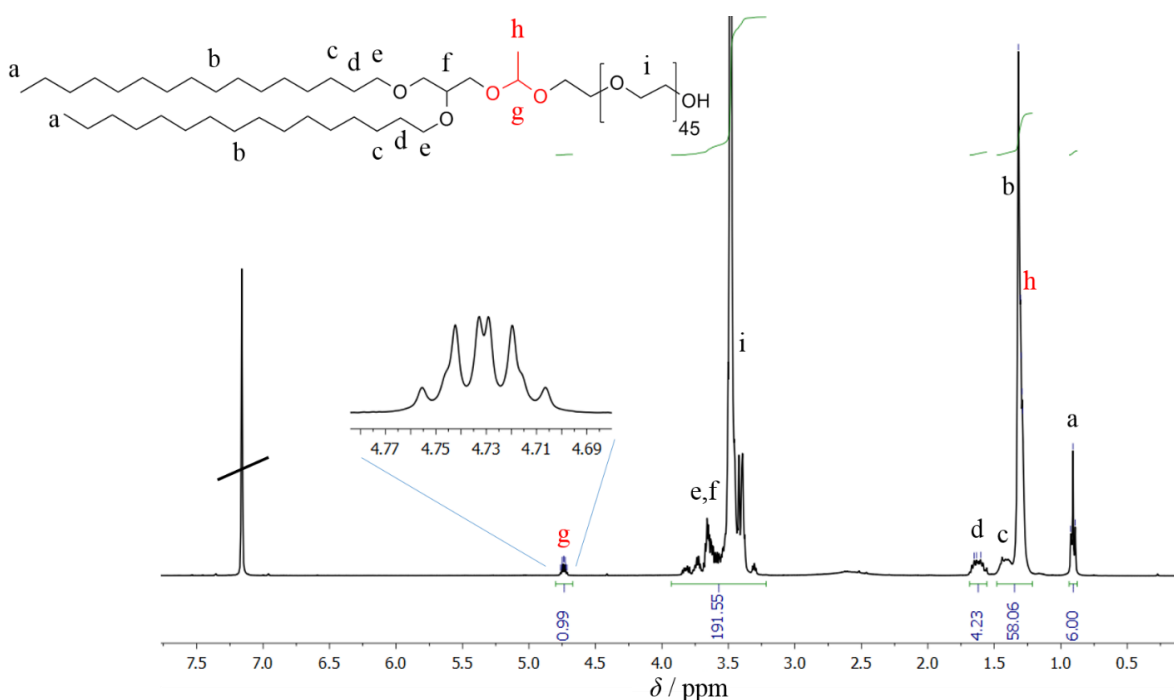


Figure 18: ^1H NMR spectrum of **BisHD-A-PEG₄₆** measured in C_6D_6 at 400 MHz. The region between 4.77 and 4.69 ppm was magnified to clarify the splitting pattern of the acetal signal.

Furthermore, MALDI ToF mass spectroscopy served to prove the proposed lipid structure, revealing two sub-distributions in the spectrum of **BisHD-A-PEG₆₀** corresponding to sodium and potassium counterions of the polymer (See Figure S-9). Although α -cyano-4-hydroxycinnamic acid (CHCA) and potassium trifluoroacetate (KTFA) were used as matrix/salt with slight acidity, no sign of acetal hydrolysis was apparent from the spectra. For comparative purposes, we additionally synthesized

a non-cleavable PEG-lipid **6** with a molecular weight M_n of 2870 g mol⁻¹ by implementing 1,2-bis-*n*-hexadecyl glycerol **2** as a macroinitiator (middle path, Scheme 8). The molecular characteristics of this polymer are given in Table 6. The straightforward access to a portfolio of structurally varied lipids discussed in the section above allows for a systematic investigation of the effect of different acid-labile moieties on the overall lipid properties. In the following section, we focus on kinetic studies with respect to pH-dependent hydrolysis of the novel acetal- and ketal-containing, dialkyl-derived PEG-lipids.

C. Online ¹H NMR Kinetics

In order to evaluate susceptibility of the pH-sensitive lipids towards acidic hydrolysis, time-resolved ¹H NMR spectroscopy in deuterated buffer was employed. This technique enables online monitoring of reaction kinetics in an NMR tube by examining time-dependent intensity changes of characteristic NMR signals and has been utilized recently to screen cleavage profiles of acetals and ketals.^[51] Since slightly acidic conditions (pH 5.5 to 6.5) have been reported for the tumor microenvironment of various cancer cells lines and inflammatory tissue,^[9] we studied the behavior of the lipids in a physiologically relevant pH range. To this end, cleavage profiles of **BisHD-K-PEG₆₈** and **BisHD-A-PEG₆₈** were investigated in buffered solutions of deuterium oxide with pD 5.4 (citrate-phosphate buffer) and 6.4 (phosphate buffer) at 37°C recording a set of 105 spectra in a time period of 8 h and 24 h, respectively. An excerpt of the spectra obtained for the cleavage of **BisHD-K-PEG₆₈** at pD 6.4 is illustrated in Figure 19, revealing a consistent increase of the signal intensity at 2.3 ppm corresponding to acetone formed by hydrolysis of the ketal. (See expected reaction equation in Figure 19) To assess the respective half-life $t_{1/2-D2O}$ of the lipid according to pseudo-first order kinetics, the integral of the acetone signal was plotted against time t and analyzed by means of an exponential fit function. (See Figure 19) Table 7 summarizes the results for the ketal-functional lipid exhibiting half-lives of ~ 40 min at pD 5.4, and ~ 4.5 h at pD 6.4, respectively.

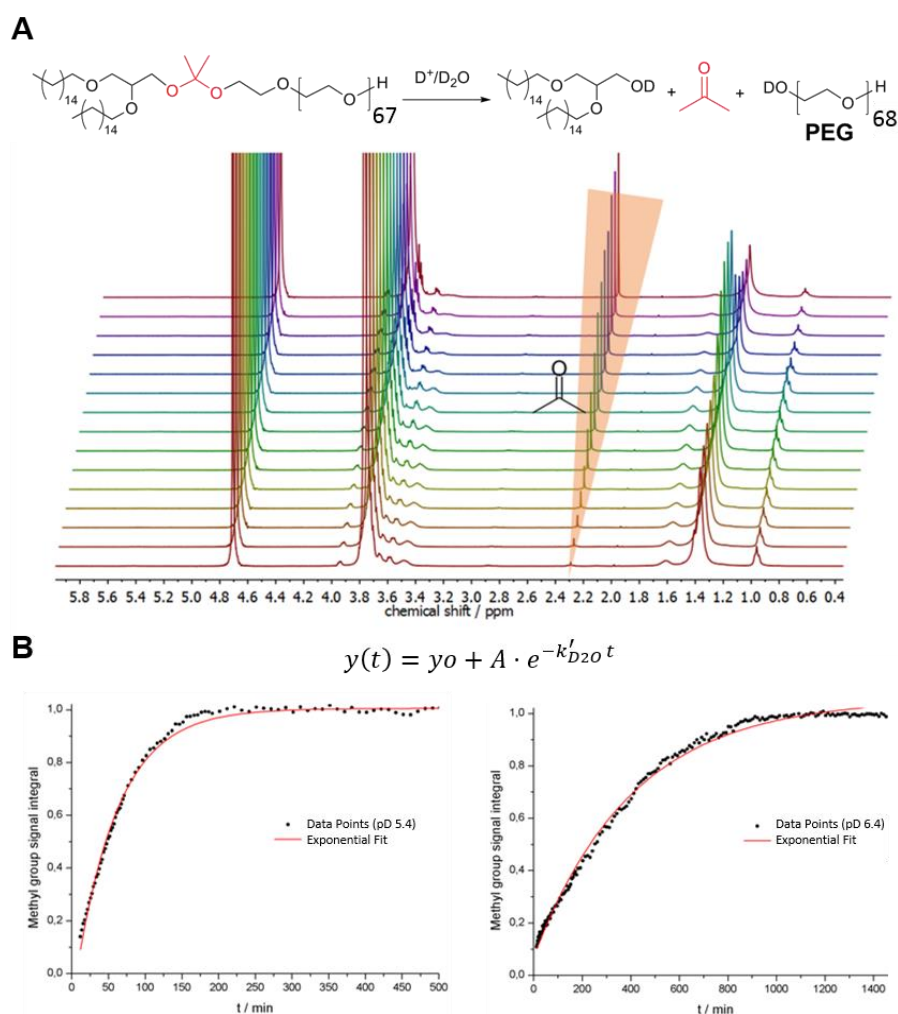


Figure 19: A: Reaction equation for the hydrolysis of ketals (top). Online ^1H NMR kinetic study monitoring ketal cleavage of the lipid in phosphate buffered D_2O at 37°C . For illustrative purposes, an excerpt of 16 spectra is shown for the measurement of **BisHD-K-PEG₆₈** at pD 6.4. However, a series of 105 spectra was recorded and analyzed for the study (bottom). **B:** Experimental results from ^1H NMR kinetic studies for the hydrolysis of **BisHD-K-PEG₆₈** at pD 5.4 and 6.4. The integrals of the acetone signal at 2.3 ppm are plotted against time t using an exponential fit of the general form given above to determine $t_{1/2-D2O}$.

Closer examination of the cleavage profile reveals that the signal intensity of the PEG backbone remains constant, whereas alkyl resonances roughly prevail unaltered first, but gradually decrease after a certain degree of decomposition. This observation might be explained by the presence of micelles in the NMR tube, causing solubilization of the cleaved alkyl chains in the micellar cores, thereby keeping their magnetic environment unchanged. As hydrolysis of the lipids progressed, stability of the micelles decreased, effecting an assembly of the hydrophobic fragments at the air-

D₂O interface that led to a drop in the signal intensity. Kim et al. performed NMR kinetic studies in buffered D₂O by manual analysis of aliquots to determine the half-life of an acetone ketal-containing PEG dimethacrylate and found values ~ 14 min at pH 5.0. Given the structural difference and the slightly lower pH, these reports are consistent with our findings.^[52]

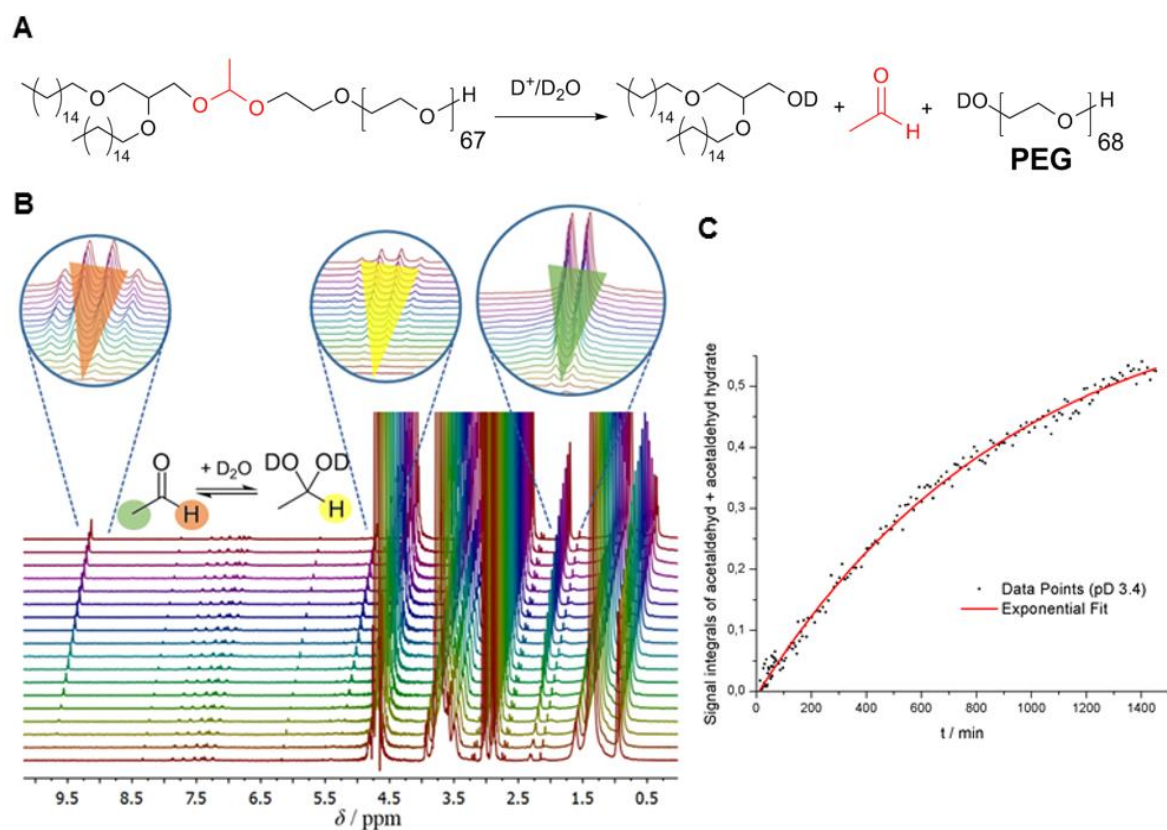


Figure 20: **A:** Expected reaction for the hydrolysis of acetals. **B:** Online ¹H NMR kinetic study monitoring acetal cleavage of the lipid in citrate-phosphate buffered D₂O at 37°C. For illustrative purposes, an excerpt of 18 spectra is shown for the measurement of **BisHD-A-PEG₆₈** at pD 3.4, though a series of 105 spectra was recorded and analyzed for the study. **C:** Experimental results of ¹H NMR kinetic studies for the hydrolysis of **BisHD-A-PEG₆₈** at pD 3.4. The combined integrals of the acetaldehyde signal (9.8 ppm) and acetaldehyde hydrate (5.4 ppm) are plotted vs. time *t*, using an exponential fit to determine *t*_{1/2-D₂O}.

In case of the acetal-functional lipid **BisHD-A-PEG₆₈**, no sign of acetal hydrolysis was observed within a time period of 24 h at pD 5.4. Thereupon, the experiment was repeated at pD 3.4. A selection of the spectra is presented in Figure 20, indicating the formation of acetaldehyde and acetaldehyde hydrate as hydrolysis products. Due to an overlap of the acetal proton signals with the NMR solvent

peak, direct monitoring of acetal cleavage was not possible. Instead, combined signal intensities of the two hydrolysis products were considered to determine the half-life $t_{1/2-D2O}$ of ~ 11 h.

Table 7: Results of ^1H NMR hydrolysis studies for **BisHD-K-PEG₆₈**.

BisHD-K-PEG₆₈	$t_{1/2-D2O} / \text{h}$
pD 5.4	0.67 ± 0.01
pD 6.4	4.68 ± 0.08
BisHD-A-PEG₆₈	$t_{1/2-D2O}$
pD 3.4	10.98 ± 0.34

$t_{1/2-D2O}$: half-life of the lipid in buffered D₂O at a given pD value.

The results of the NMR kinetics indicate that cleavage of ketals occurs at a rate several orders of magnitude higher than the hydrolysis rate of acetal. These findings have motivated us to take a closer look at the behavior of the pH-sensitive lipids in liposomal formulations via alternative techniques.

D. pH-Triggered Liposome Shedding

In this section we aim at elucidating the behavior of liposomes modified with the pH-sensitive lipids introduced in the sections above to evaluate their potential for pH-responsive drug carriers. For this purpose, two parallel experiments were designed to investigate shedding of the PEG stealth layer from the liposomal surface. To monitor the cleavage profiles, fluorescent dyes (Atto 488 azide) were covalently attached to the pH-sensitive PEG-lipids using copper(I)-catalyzed azide-alkyne click chemistry (CuAAC), and PEG shedding from liposomes was analyzed by fluorescence spectroscopy (FS) and polyacrylamide gel electrophoresis (PAGE). The *in situ* fluorescence spectroscopy assay has been introduced in a previous study,^[53] however, has so far not been used to quantify rates of hydrolysis. Liposomes were prepared by means of dual centrifugation (DC) replacing 5 mol% of the total amount of lipids (egg phosphatidylcholine EPC, and cholesterol) with the novel pH-sensitive

PEG-lipids. Cell viability of liposomes containing alkyne-functional lipids was evaluated via MTT assays, revealing high cellular compatibility comparable to conventional liposomes (CL) and sterically stabilized liposomes (SSL, DSPE-mPEG2000).

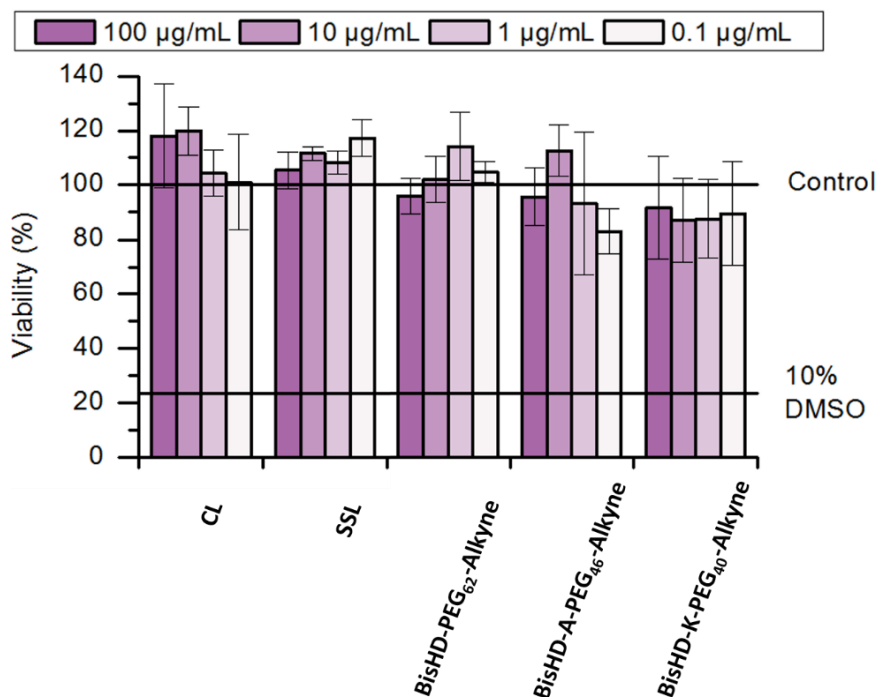


Figure 21: Cell viability test (MTT assay) for liposomes containing alkyne-functional PEG-lipids (**BisHD-PEG₆₂**, **BisHD-A-PEG₄₆**, **BisHD-K-PEG₄₀**) in comparison to conventional liposomes (CL) and sterically stabilized liposomes (SSL, DSPE-mPEG2000).

The post-preparational dye-labelling of stealth liposomes via CuAAC has been demonstrated in previous works.^[44] In case of FS analysis, fluorescently labeled liposomes were studied in buffered solutions in a pH range of 2.4 to 5.4. Prior to use, cuvette surfaces were incubated with plain EPC/cholesterol liposomes to prevent amphiphile adsorption. At first, susceptibility of acetal-containing PEG-lipids in liposomes towards acidic hydrolysis was pursued, as slower rates of hydrolysis could be expected. Figure 22 B illustrates the results of time-dependent FS analysis for dye-labeled liposomes prepared from **BisHD-A-PEG₄₆-Alkyne**. The fluorescence intensities are plotted vs. time t for spectra recorded within a period of 24 h at 37 °C.

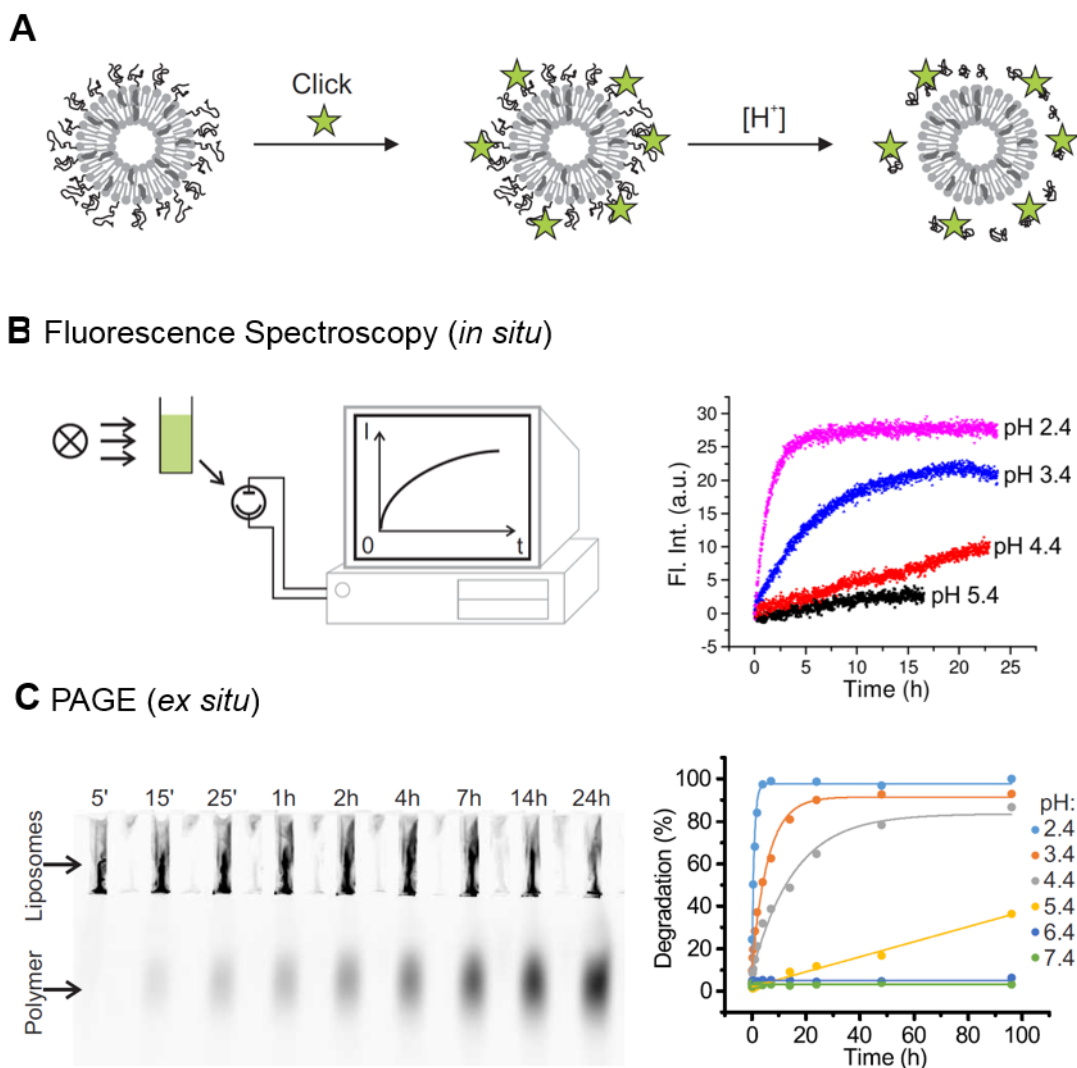


Figure 22: **A:** Schematic post-preparational dye-labelling of liposomes and subsequent pH-triggered shedding **B:** Fluorescence spectroscopy analysis of pH-dependent shedding for dye-labeled **BisHD-A-PEG₄₆** liposomes at 37 °C **C:** Example of a PAGE fluorescence scan for the cleavage analysis of **BisHD-A-PEG₄₆** in liposomes at pH 3.4.(left) pH-dependent cleavage profiles for **BisHD-A-PEG₄₆** liposomes analyzed via PAGE analysis (right) at 37 °C.

A systematic increase of the fluorescence signal was detected for pH values of 2.4 to 4.4, whereas at higher pH, intensities remained approximately constant throughout the time of measurement (see Figure 22 B). Control measurements assured that the fluorescence increase was not due to reaction of the fluorophore itself and that compounds without a cleavable group (**BisHD-PEG₆₂-Alkyne**) did not show this fluorescence increase (compare SI Figure S-12). The incline of fluorescence intensities can be associated with the cleavage of acetal moieties and consequently

the detachment of dye-labeled PEGs from the liposomes. Presumably, in case of unscathed acetal linkages, dyes were located in proximity to the liposomal surface, promoting thermal relaxation of excited fluorophores that lead to quenching of the fluorescence intensity. After acidic cleavage of acetals, the weakened interactions of fluorophores with the vesicles' surfaces effected an increased fluorescence emission. In addition, inner filter effects were expected to lower fluorescence emission while fluorophores were bound to the surfaces. Half-lives $t_{1/2}$ were determined via an exponential fit revealing values of ~ 1 h (pH 2.4) and ~ 4 h (pH 3.4). (See Table 8) At pH 4.4, a slow gradual increase was observed, albeit unsuitable for quantitative analysis.

Table 8: Half-lives of **BisHD-A-PEG₄₆** and **BisHD-K-PEG₄₀** liposomes at different pH values.

Half-life	$t_{1/2}$ / h					
	pH	2.4	3.4	4.4	5.4	6.4
BisHD-A-PEG₄₆						
FS	1.04 ± 0.01	4.48 ± 0.32	n.d.	n.d.	s.h.	s.h.
PAGE	0.59 ± 0.08	4.16 ± 0.45	10.72 ± 1.47	21.09 ± 2.83	s.h.	s.h.
BisHD-K-PEG₄₀						
FS	r.h.	r.h.	0.01	0.17 ± 0.02	4.01 ± 0.70	19.50 ± 0.28
PAGE	r.h.	r.h.	0.01	0.15 ± 0.01	3.11 ± 0.28	13.10 ± 0.80

r.h.(rapid hydrolysis): $t_{1/2} < 10$ s; n.d.: not determinable; s.h.(slow hydrolysis): half-life exceeds 24 h.

As a reference experiment, polyacrylamide gel electrophoresis (PAGE) was conducted to evaluate the results from FS and furthermore to investigate the cleavage profiles on a longer time scale. To this end, dye-labeled liposomes of **BisHD-A-PEG₄₆-Alkyne** were prepared as discussed above and incubated at 37 °C in buffered solutions (pH 2.4 to 7.4). Samples were taken within a period of 96 h, neutralized in PBS buffer (pH 7.4) to prevent further acetal hydrolysis and subsequently analyzed on an agarose gel by measuring the fluorescence intensity of the cleaved PEG-dye fractions (See Figure 22 C). The data suggest that intact liposomes showed no migration, whereas cleaved polymers migrated through the gel effecting increased emission intensities with longer times of incubation. Figure 22 C (right) shows the time-dependent fluorescence signal for different pH values revealing a continuous increase of the signal intensities at pH values below 6.4. As expected, faster

cleavage rates were observed at lower pH values. Half-lives $t_{1/2}$ were determined from an exponential fit ranging from 1 h (pH 2.4) to 21 h (pH 5.4). (See Table 8) A comparison of the half-lives at pH 2.4 and 3.4 obtained from FS and PAGE reveals that results of both methods are in good agreement. At pH values exceeding 5.4, the rates of acetal hydrolysis were too slow to be detected by the two techniques.

In an analogous manner, liposomes were prepared from the ketal-functional PEG-lipid **BisHD-K-PEG₄₀-Alkyne** and subsequently, their susceptibility towards acidic hydrolysis was analyzed via FS and PAGE, as described above in a pH range from 3.4 to 7.4 at 37 °C. (See Figure 23) Due to significant differences in the rates of hydrolysis at different pH values, separate plots were chosen for each set of data points. Half-lives $t_{1/2}$ were calculated from exponential fits and values are summarized in Table 8. Both techniques consistently demonstrated rapid cleavage of ketals at pH 4.4 ($t_{1/2} \sim 40$ s) and 5.4 ($t_{1/2} \sim 10$ min), whereas at pH 6.4 slower rates of hydrolysis with values of $t_{1/2}$ in the order of ~ 3.5 h were determined. As observed above, results obtained via FS fit well with the results from PAGE analysis. Figure 23 visualizes the concordant curve profiles for the two measurements. At pH 7.4, small discrepancies between the two techniques are visible, however values are in the same order of magnitude. Below pH 4.4, complete scission of the PEG-lipids occurred in less than 10 s and was beyond the time resolution of the techniques employed in this study. Slow hydrolysis of ketals at pH 7.4 might require storage of the liposomal formulations at higher pH values after preparation. Therefore, we investigated the stability of ketal residues at pH 8.4 and found half-lives (PAGE analysis) exceeding 130 h (data not shown) that account for the high stability of the liposomes under slightly basic storage conditions.

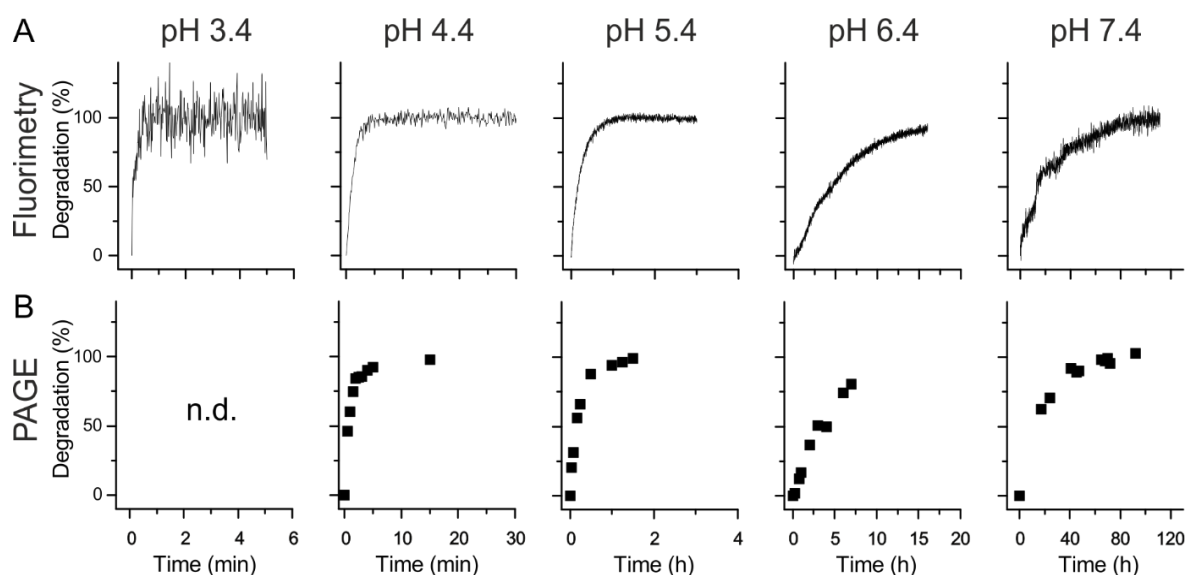


Figure 23: **A:** Fluorimetric analysis of liposome disintegration at 37 °C for dye-labeled **BisHD-K-PEG₄₀** liposomes at different pH. Data points are visualized in separate plots as time scales differ significantly. **B:** PAGE analysis of the dye-labeled **BisHD-K-PEG₄₀** liposomes in a pH range of 4.4 to 7.4 at 37 °C.

Clearly, values obtained for the half-life $t_{1/2}$ of acetal- and ketal-containing lipids in liposomes via FS/PAGE were generally lower than values calculated from online ^1H NMR kinetics for the pure lipids (Compare Table 7 and Table 8). Several factors might contribute to these differences. For instance, the liposomal surface contains multiple, negatively charged moieties, creating a more polar environment in closer proximity to the cleavable linkages that might lead to accelerated rates of hydrolysis. Similar findings have been observed for lipids containing vinyl ethers as pH-cleavable units in the presence of negatively charged phosphates.^[28] Another influence might derive from the different hydrolysis kinetics of acetals and ketals in D_2O and H_2O , respectively due to the kinetic deuterium isotope effect.^[54] It is noteworthy that discrepancies were more pronounced for acetal-based lipids, whereas, in case of ketals, values were of the same order of magnitude. This might be due to the transition of volatile acetaldehyde into the gas phase, rendering it undetectable by NMR, and hence, causing a drop in signal intensities. These findings suggest great potential for these functionalizable, pH-sensitive lipids in liposomal research, as they allow for pH-triggered release strategies combined with active cell targeting and/or simultaneous polymer/carrier trafficking. The *in vivo* behavior of the PSLs discussed in this study is under current investigation.

Conclusion

In this work, we introduce a novel class of pH-sensitive PEG-lipids based on bis-hexadecyl glycerol anchor groups containing acetal and ketal moieties as cleavable linkages. The use of polyether-based lipids with dialkyl chains in liposomes has recently been proven particularly advantageous, as dialkyl anchors are stably entrenched in liposomal membranes.^[40] A prototype synthesis route has been developed that provides straightforward access to asymmetric ketals in PEG-lipids. Acetal- and ketal-functional dialkyl glycerol derivatives were utilized as macroinitiators for the anionic ring-opening polymerization (AROP) of ethylene oxide to obtain amphiphilic PEG-block structures in a molecular weight range of 2000 to 3500 g mol⁻¹ with narrow molecular weight distributions ($\mathcal{D} = 1.04 - 1.08$). Integrity of the acid-cleavable moieties was proven by ¹H, IG ¹³C NMR spectroscopy and MALDI ToF mass spectrometry.

In order to evaluate susceptibility of the lipids towards acidic hydrolysis, real-time ¹H NMR kinetic studies were performed in D₂O revealing rapid cleavage of the ketals $t_{1/2-D_2O} \sim 1$ h (pD 5.4), ~ 5 h (pD 6.4) and significantly slower hydrolysis for the acetals. Furthermore, pH-responsiveness of the scissile PEG-lipids in liposomes at physiologically relevant pH was investigated by means of fluorescence spectroscopy and agarose gel electrophoresis. In accordance with the results from NMR kinetic studies, acetal hydrolysis occurs at a distinctly slower rate with half-lives of ~ 21 h (pH 5.4) compared to the fast cleavage of ketals with half-lives $t_{1/2}$ of ~ 10 min (pH 5.4), ~ 3.5 h (pH 6.4). These cleavage profiles, in particular, render the ketal-functional PEG-lipids promising candidates for pH-triggered drug release strategies from liposomes. Due to lowered pH values in the microenvironment of various tumor cell lines,^[9] pH-sensitive stealth liposomes represent a promising class of drug carrier systems for anticancer treatment. A combination of the slowly hydrolyzing acetal PEG-lipid species endowed with target moieties such as folate or mannose to achieve active cell targeting, and the rapidly hydrolyzing ketal PEG-lipid ensuring pH-triggered shedding of the liposome inside the tumor tissue, might further improve cellular uptake and may

reduce accelerated blood clearance (ABC phenomenon). These results demonstrate the great potential of the pH-sensitive lipids enabling further post-functionalization strategies and render them an innovation for pH-triggered release strategies from liposomal drug carriers. Future experiments will focus on the *in vivo* performance of these acid-sensitive PEG-dialkyl-lipids in liposomal formulations.

Acknowledgements

The authors thank Dr. J. Liermann for customized NMR measurements, Dr. E. Berger-Nicoletti for MALDI-ToF mass spectrometry, and Monika Schmelzer for technical support. Furthermore, we thank Hannah Pohlit for scientific input and Tobias Bauer for technical assistance. M.W. and T.F. are grateful for a fellowship by the Max Planck Graduate Center (MPGC). D.L. acknowledges a fellowship through the Excellence Initiative (DFG/GSC 266) in the context of MAINZ “Materials Science in Mainz”. The Rotanta 400 DC prototype was kindly provided by Andreas Hettich GmbH, Tuttlingen, Germany. This work was supported by funding of the DFG research center SFB 1066, project grant A7.

References

- [1] Gil, E. S.; Hudson, S. M. *Prog. Polym. Sci.*, **2004**, *29*, 1173–1222.
- [2] Guragain, S.; Bastakoti, B. P.; Malgras, V.; Nakashima, K.; Yamauchi, Y. *Chem. Eur. J.*, **2015**, *21*, 13164–13174.
- [3] Vancoillie, G.; Frank, D.; Hoogenboom, R. *Prog. Polym. Sci.*, **2014**, *39*, 1074–1095.
- [4] Moon, H. J.; Du Ko, Y.; Park, M. H.; Joo, M. K.; Jeong, B. *Chem. Soc. Rev.*, **2012**, *41*, 4860–4883.
- [5] Schattling, P.; Jochum, F. D.; Theato, P. *Polym. Chem.*, **2014**, *5*, 25–36.
- [6] Gohy, J.-F.; Zhao, Y. *Chem. Soc. Rev.*, **2013**, *42*, 7117–7129.
- [7] Wei, H.; Zhuo, R.-X.; Zhang, X.-Z. *Prog. Polym. Sci.*, **2013**, *38*, 503–535.
- [8] Asokan, A.; Cho, M. J. *J. Pharm. Sci.*, **2002**, *91*, 903–913.
- [9] Gerweck, L. E.; Vijayappa, S.; Kozin, S. *AACR*, **2006**, *5*, 1275–1279.
- [10] Patel, N. R.; Pattni, B. S.; Abouzeid, A. H.; Torchilin, V. P. *Adv. Drug Delivery Rev.*, **2013**, *65*, 1748–1762.
- [11] Pasut, G.; Veronese, F. M. *Prog. Polym. Sci.*, **2007**, *32*, 933–961.
- [12] Herzberger, J.; Niederer, K.; Pohlitz, H.; Seiwert, J.; Worm, M.; Wurm, F. R.; Frey, H. *Chem. Rev.*, **2015**, *116*, 2170–2243.
- [13] Hatakeyama, H.; Akita, H.; Harashima, H. *Adv. Drug Delivery Rev.*, **2011**, *63*, 152–160.
- [14] Dingels, C.; Frey, H. *Adv. Polym. Sci.*, **2013**, *262*, 167–190.
- [15] Dufort, S.; Sancey, L.; Coll, J.-L. *Adv. Drug Delivery Rev.*, **2012**, *64*, 179–189.
- [16] Legendre, J.-Y.; Szoka Jr, Francis C. *Pharm. Res.*, **1992**, *9*, 1235–1242.
- [17] Ishiwata, H.; Sato, S. B.; Vertut-Doi, A.; Hamashima, Y.; Miyajima, K. *BBA-Mol. Cell Res.*, **1997**, *1359*, 123–135.
- [18] Dams, Els T. M.; Laverman, P.; Oyen, Wim J. G.; Storm, G.; Scherphof, G. L.; van der Meer, Jos W. M.; Corstens, Frans H. M.; Boerman, O. C. *J. Pharm. Exp. Ther.*, **2000**, *292*, 1071–1079.

- [19] Laverman, P.; Carstens, M. G.; Boerman, O. C.; Th. M. Dams, Els; Oyen, Wim J. G.; van Rooijen, N.; Corstens, Frans H. M.; Storm, G. *J. Pharm. Exp. Ther.*, **2001**, *298*, 607–612.
- [20] Abu Lila, Amr S.; Kiwada, H.; Ishida, T. *J. Control. Release*, **2013**, *172*, 38–47.
- [21] Chen, D.; Liu, W.; Shen, Y.; Mu, H.; Zhang, Y.; Liang, R.; Wang, A.; Sun, K.; Fu, F. *J. Nanomed.*, **2011**, *6*, 2053–2061.
- [22] Daquan Chen; Xiaoqun Jiang; Yanyu Huang; Can Zhang; Qineng Ping *J. Bioact. Compat. Polym.*, **2010**, *25*, 527–542.
- [23] Zhang, L.; Wang, Y.; Yang, Y.; Liu, Y.; Ruan, S.; Zhang, Q.; Tai, X.; Chen, J.; Xia, T.; Qiu, Y.; Gao, H.; He, Q. *ACS Appl. Mater. Interfaces*, **2015**, *7*, 9691–9701.
- [24] Guo, X.; Szoka, F. C. J., *Bioconjugate Chem.*, **2001**, *12*, 291–300.
- [25] Li, W.; Huang, Z.; MacKay, J. A.; Grube, S.; Szoka, F. C. *J. Gene Med.*, **2005**, *7*, 67–79.
- [26] Masson, C.; Garinot, M.; Mignet, N.; Wetzler, B.; Mailhe, P.; Scherman, D.; Bessodes, M. *J. Control. Release*, **2004**, *99*, 423–434.
- [27] Wong, J. B.; Grosse, S.; Tabor, A. B.; Hart, S. L.; Hailes, H. C. *Mol. Biosyst.*, **2008**, *4*, 532–541.
- [28] Shin, J.; Shum, P.; Thompson, D. H. *J. Control. Release*, **2003**, *91*, 187–200.
- [29] Shin, J.; Shum, P.; Grey, J.; Fujiwara, S.-i.; Malhotra, G. S.; González-Bonet, A.; Hyun, S.-H.; Moase, E.; Allen, T. M.; Thompson, D. H. *Mol. Pharmaceutics*, **2012**, *9*, 3266–3276.
- [30] Luvino, D.; Khiati, S.; Oumzil, K.; Rocchi, P.; Camplo, M.; Barthélémy, P. *J. Control. Release*, **2013**, *172*, 954–961.
- [31] Nakamura, N.; Suzuki, K. *J. Polym. Sci. Pol. Chem.*, **1996**, *34*, 3319–3328.
- [32] Nakamura, N.; Suzuki, K. *J. Polym. Sci. A Polym. Chem.*, **1997**, *35*, 1719–1731.
- [33] St. Pierre, T.; Chiellini, E. *J. Bioact. Compat. Polym.*, **1986**, *1*, 467–497.
- [34] Gillies, E. R.; Goodwin, A. P.; Fréchet, Jean M. J. *Bioconjugate Chem.*, **2004**, *15*, 1254–1263.

- [35] Gillies, E. R.; Fréchet, Jean M. J. *Bioconjugate Chem.*, **2005**, *16*, 361–368.
- [36] Shenoi, R. A.; Lai, Benjamin F. L.; Imran ul-haq, M.; Brooks, D. E.; Kizhakkedathu, J. N. *Biomaterials*, **2013**, *34*, 6068–6081.
- [37] Binauld, S.; Stenzel, M. H. *Chem. Commun.*, **2013**, *49*, 2082–2102.
- [38] Chen, D.; Wang, H. J. *Nanosci. Nanotechnol.*, **2014**, *14*, 983–989.
- [39] Zhang, S.; Zhao, Y. *Bioconjugate Chem.*, **2011**, *22*, 523–528.
- [40] Fritz, T.; Voigt, M.; Worm, M.; Negwer, I.; Müller, S. S.; Kettenbach, K.; Ross, T. L.; Roesch, F.; Koynov, K.; Frey, H.; Helm, M. *Chem. Eur. J.*, **2016**, *22*, 11578–11582.
- [41] Gassman, P. G.; Burns, S. J.; Pfister, K. B. *J. Org. Chem.*, **1993**, *58*, 1449–1457.
- [42] Greenland, B. W.; Liu, S.; Cavalli, G.; Alpay, E.; Steinke, J. H. G. *Polymer*, **2010**, *51*, 2984–2992.
- [43] Massing, U.; Cicko, S.; Ziroli, V. *J. Control. Release*, **2008**, *125*, 16–24.
- [44] Fritz, T.; Hirsch, M.; Richter, F. C.; Müller, S. S.; Hofmann, A. M.; Rusitzka, Kristiane A. K.; Markl, J.; Massing, U.; Frey, H.; Helm, M. *Biomacromolecules*, **2014**, *15*, 2440–2448.
- [45] Abràmoff, M. D.; Magalhães, P. J.; Ram, S. J. *Photonics International*, **2004**, *11*, 36–41.
- [46] Glasoe, P. K.; Long, F. A. *J. Phys. Chem.*, **1960**, *64*, 188–190.
- [47] Pattni, B. S.; Chupin, V. V.; Torchilin, V. P. *Chem. Rev.*, **2015**, *115*, 10938–10966.
- [48] Stauch, O.; Uhlmann, T.; Fröhlich, M.; Thomann, R.; El-Badry, M.; Kim, Y.-K.; Schubert, R. *Biomacromolecules*, **2002**, *3*, 324–332.
- [49] Dingels, C.; Müller, S. S.; Steinbach, T.; Tonhauser, C.; Frey, H. *Biomacromolecules*, **2013**, *14*, 448–459.
- [50] Worm, M.; Kang, B.; Dingels, C.; Wurm, F. R.; Frey, H. *Macromol. Rapid Commun.*, **2016**, *37*, 775–780.
- [51] Pohlit, H.; Bellinghausen, I.; Schömer, M.; Heydenreich, B.; Saloga, J.; Frey, H. *Biomacromolecules*, **2015**, *16*, 3103–3111.

- [52] Kim, S.; Linker, O.; Garth, K.; Carter, K. R. *Polym. Degrad. Stab.*, **2015**, *121*, 303–310.
- [53] Muller, S. S.; Fritz, T.; Gimnich, M.; Worm, M.; Helm, M.; Frey, H. *Polym. Chem.*, **2016**, *7*, 6257–6268.
- [54] Cordes, E. H., *Prog. Phys. Org. Chem.*, **2007**, *4*, 1–44.

Supporting Information

Ketal- and Acetal-Functional Dialkyl-PEG Lipids for pH-Sheddable Stealth Liposomes

Matthias Worm,^a Thomas Fritz,^b Daniel Leibig,^{a,c} Fabian Jung,^b Eyleen Becker,^a Mark Helm,^b and Holger Frey^{a*}

^a Institute of Organic Chemistry, Johannes Gutenberg-University, Duesbergweg 10-14, D-55128 Mainz, Germany.

^b Institute of Pharmacy and Biochemistry, Johannes Gutenberg-University, Staudinger Weg 5, D-55128 Mainz, Germany.

^c Graduate School Materials Science in Mainz, Staudinger Weg 9, D-55128 Mainz, Germany.

Characterization

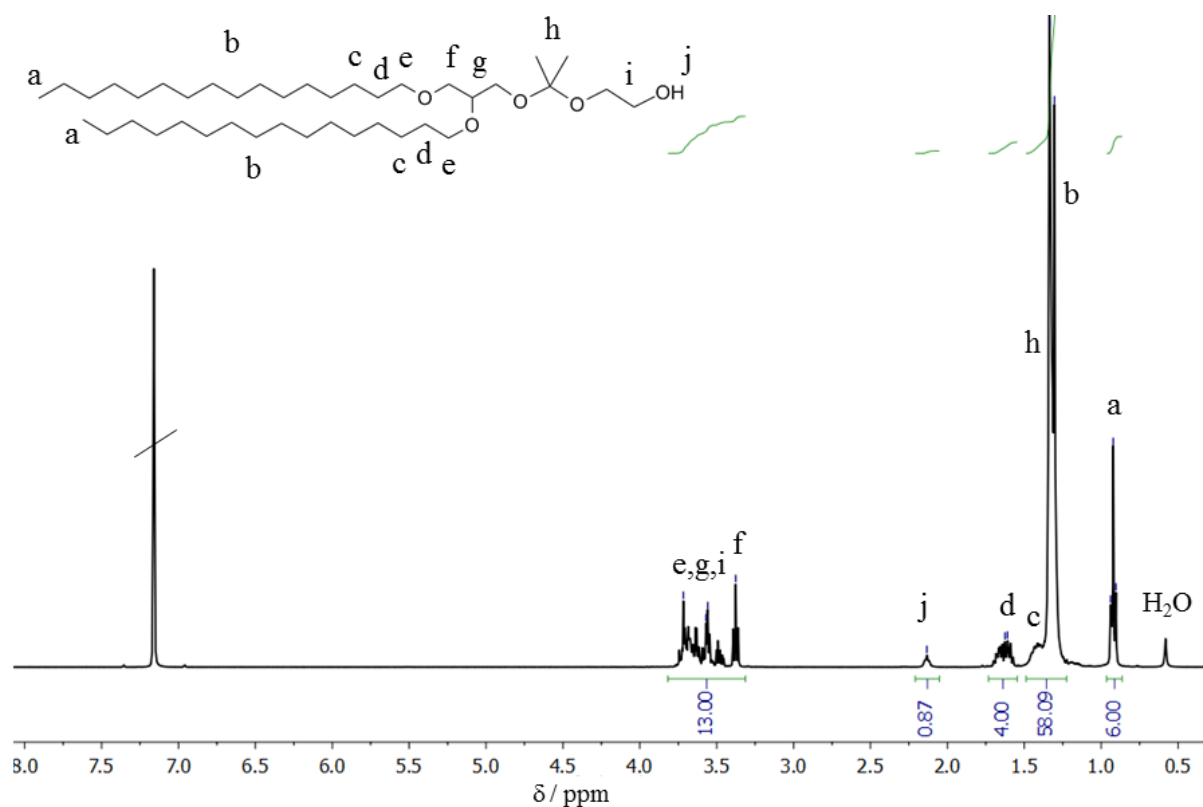


Figure S-27. ¹H NMR spectrum of the macroinitiator **4** measured in C₆D₆ at 400 MHz.

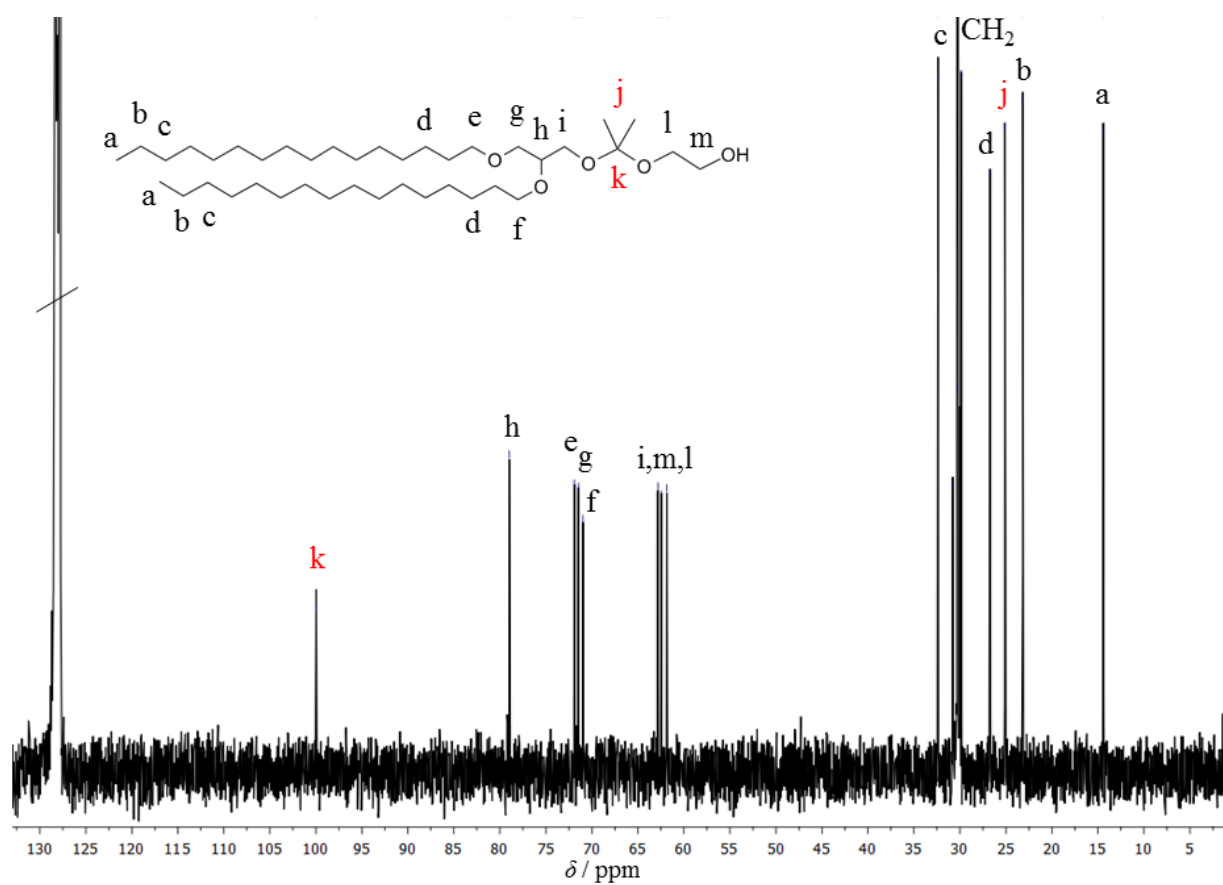


Figure S-28. ^{13}C NMR spectrum of the macroinitiator **4** measured in C_6D_6 at 100 MHz.

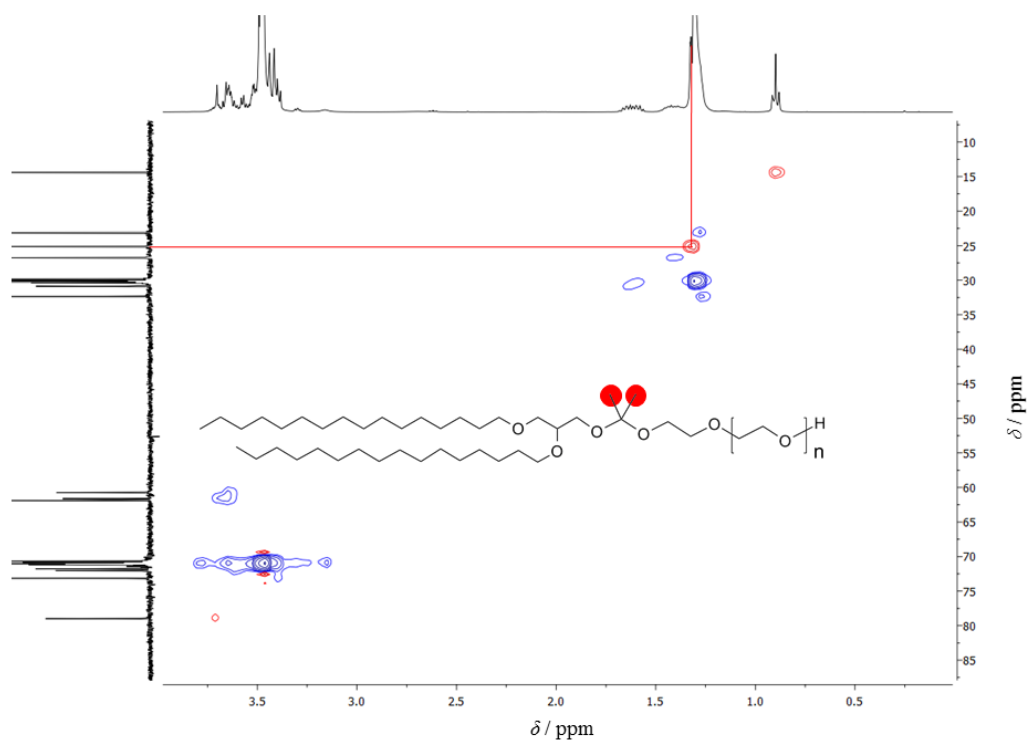


Figure S-29. HSQC 2D NMR spectrum of BisHD-K-PEG measured in C_6D_6 .

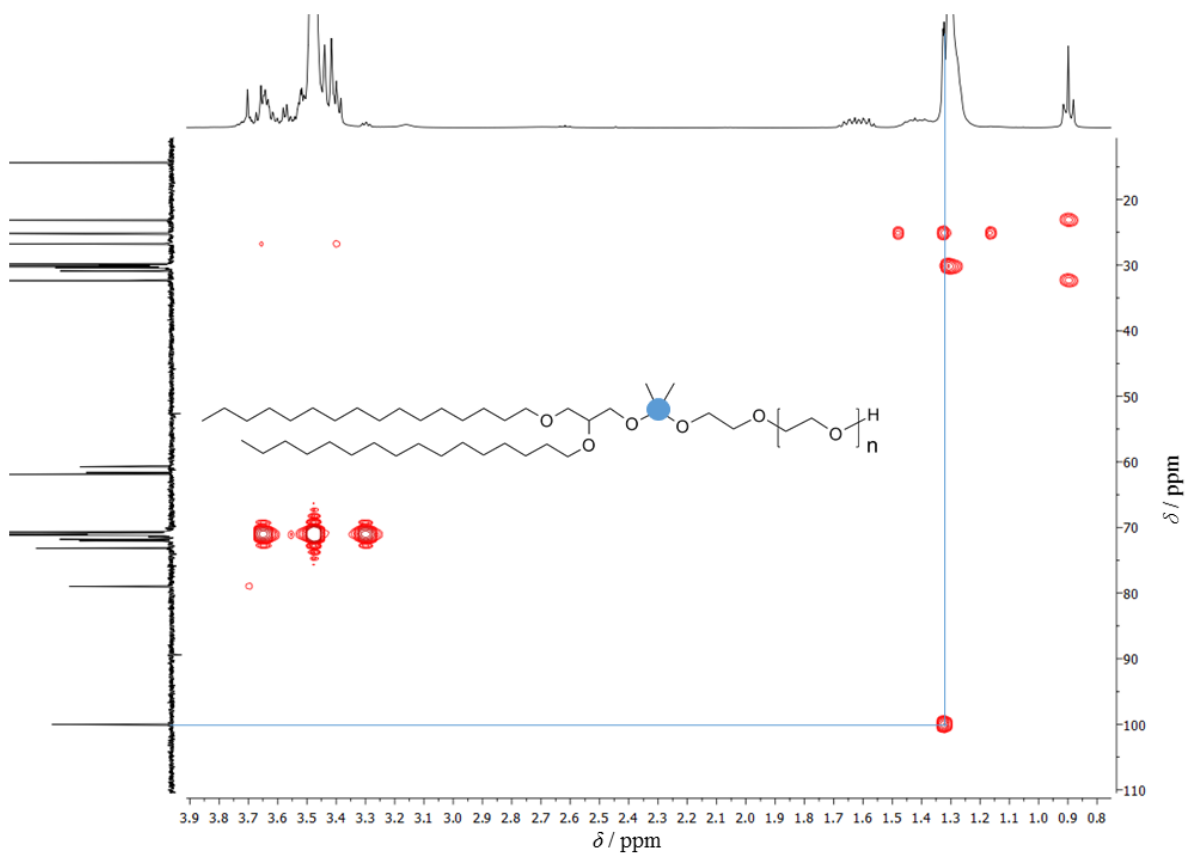


Figure S-30. HMBC 2D NMR spectrum of BisHD-K-PEG measured in C_6D_6 .

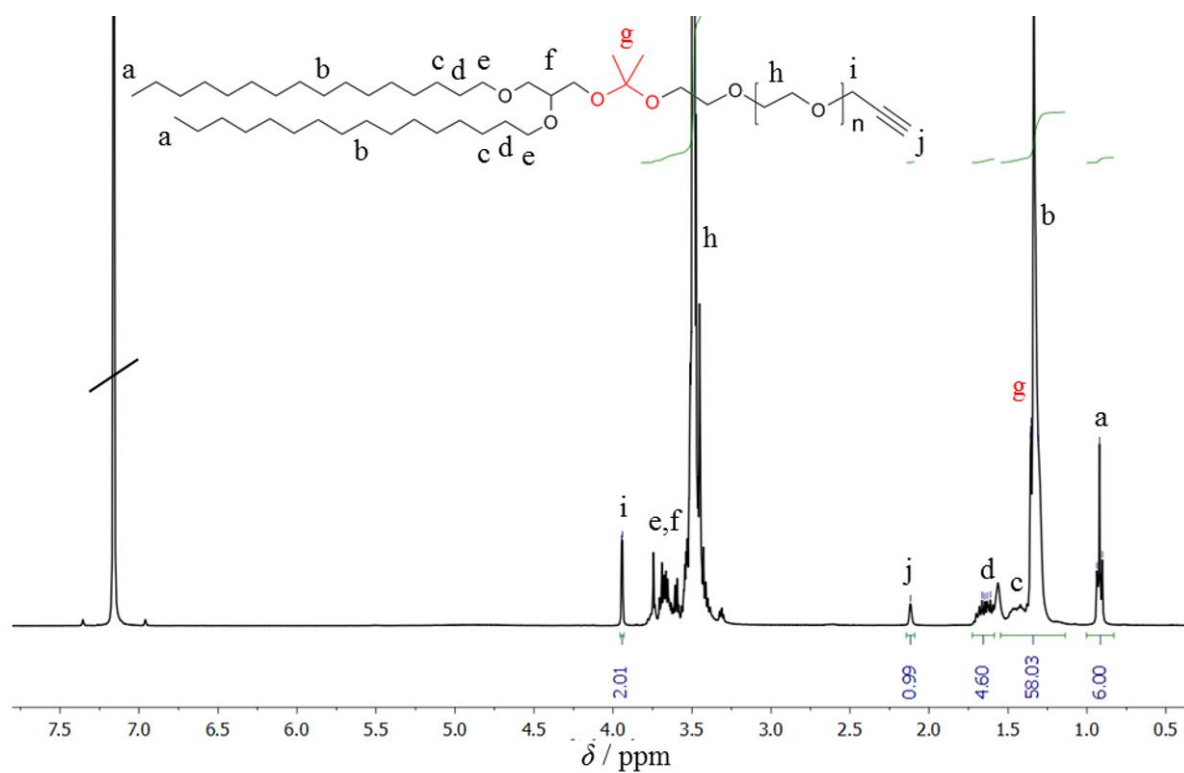


Figure S-31. ^1H NMR Spectrum of BisHD-K-PEG₄₀-Alkyne in C_6D_6 measured at 400 MHz.

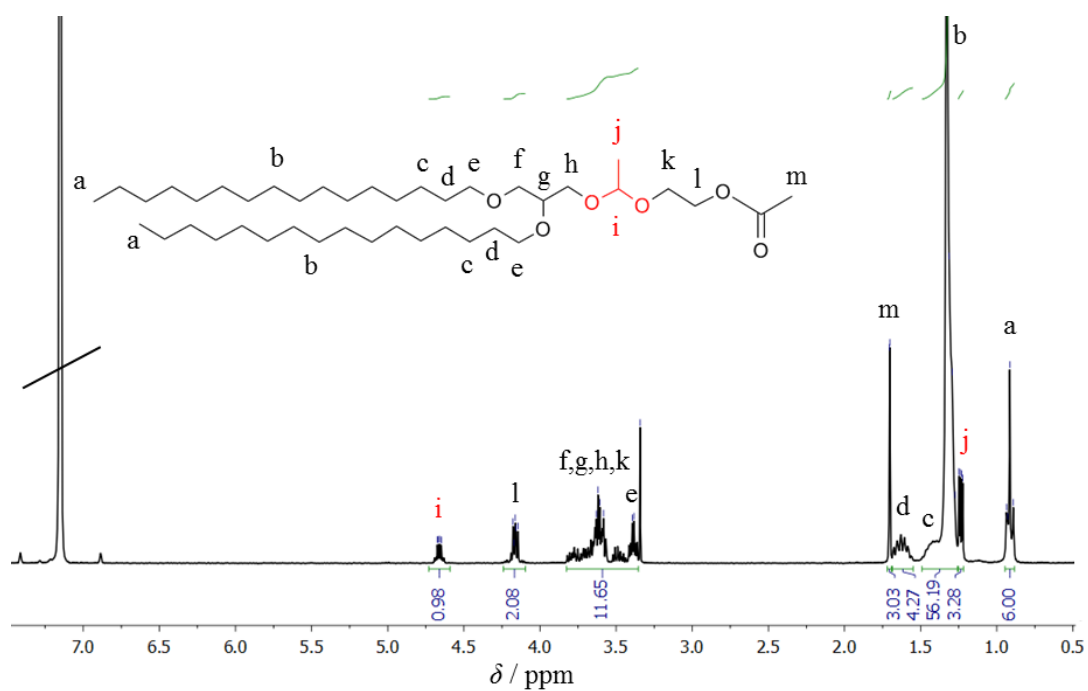


Figure S-32: ^1H NMR spectrum of **BisHD-Acetal-Acetate** measured in C_6D_6 at 400 MHz.

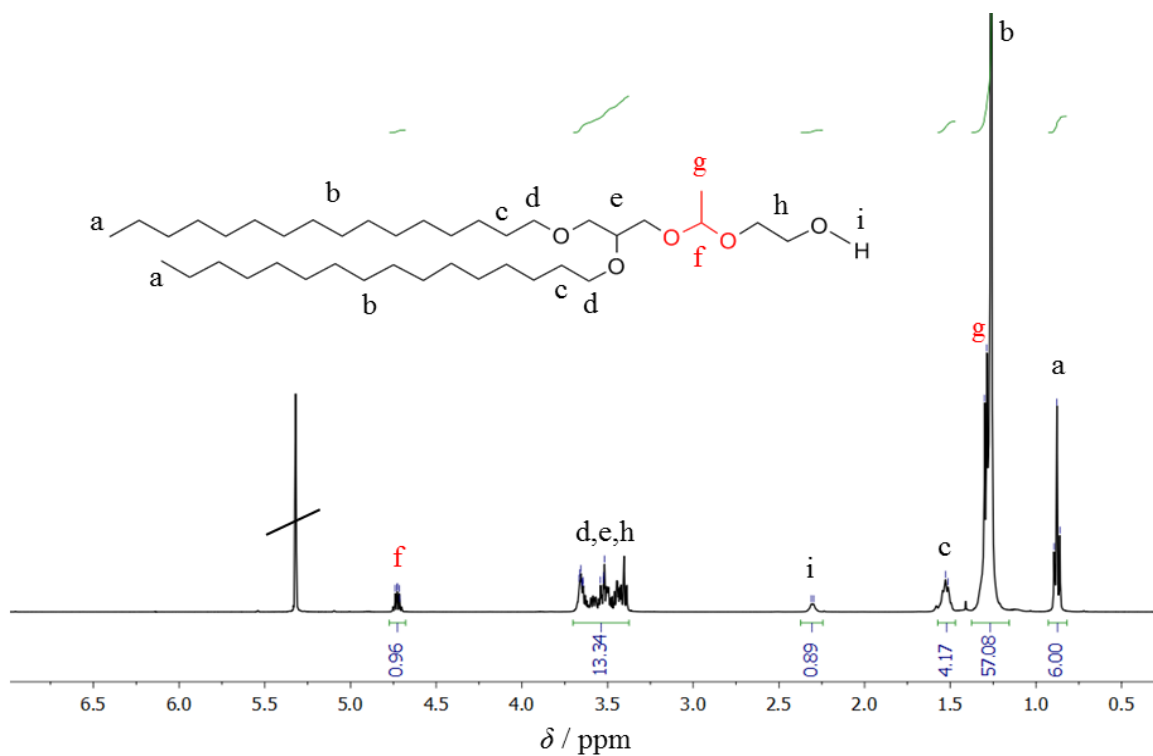


Figure S-33. ^1H NMR spectrum of the macroinitiator **8** measured in CD_2Cl_2 at 400 MHz.

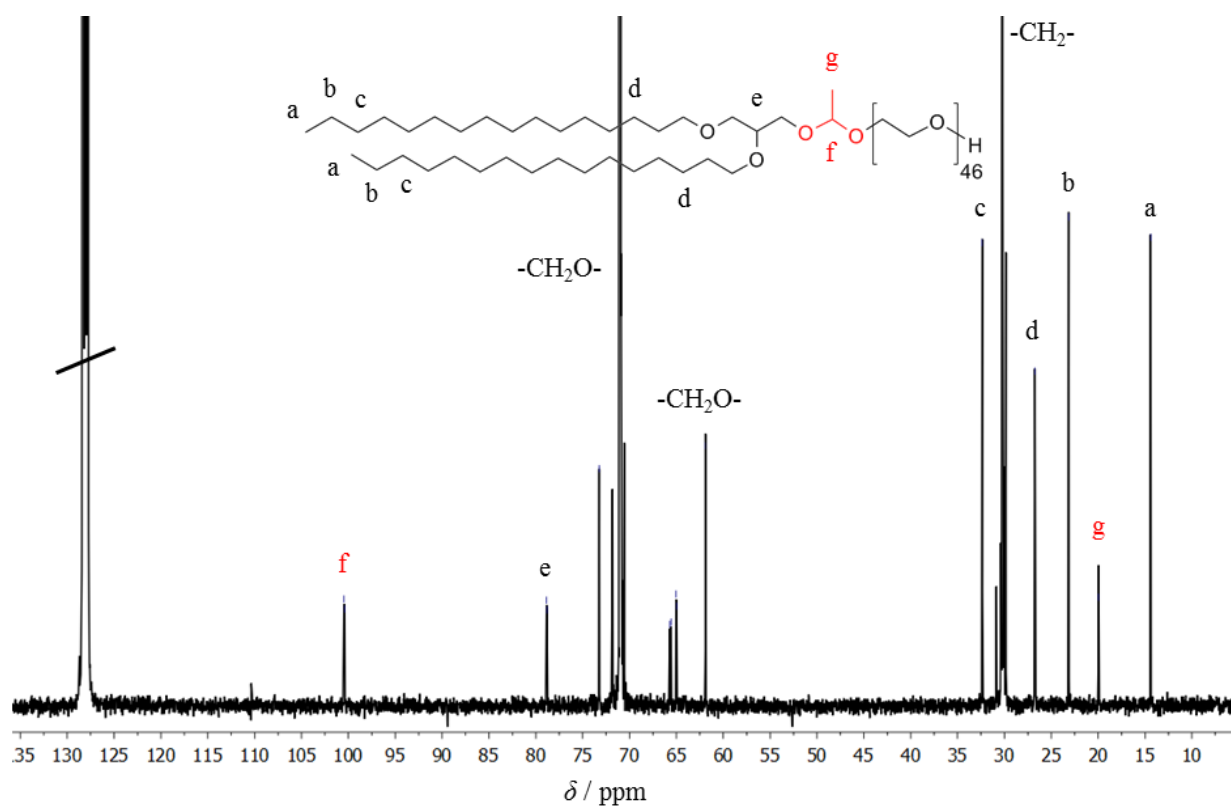


Figure S-34. ^{13}C NMR spectrum of BisHD-A-PEG₄₆ measured in C_6D_6 at 100 MHz.

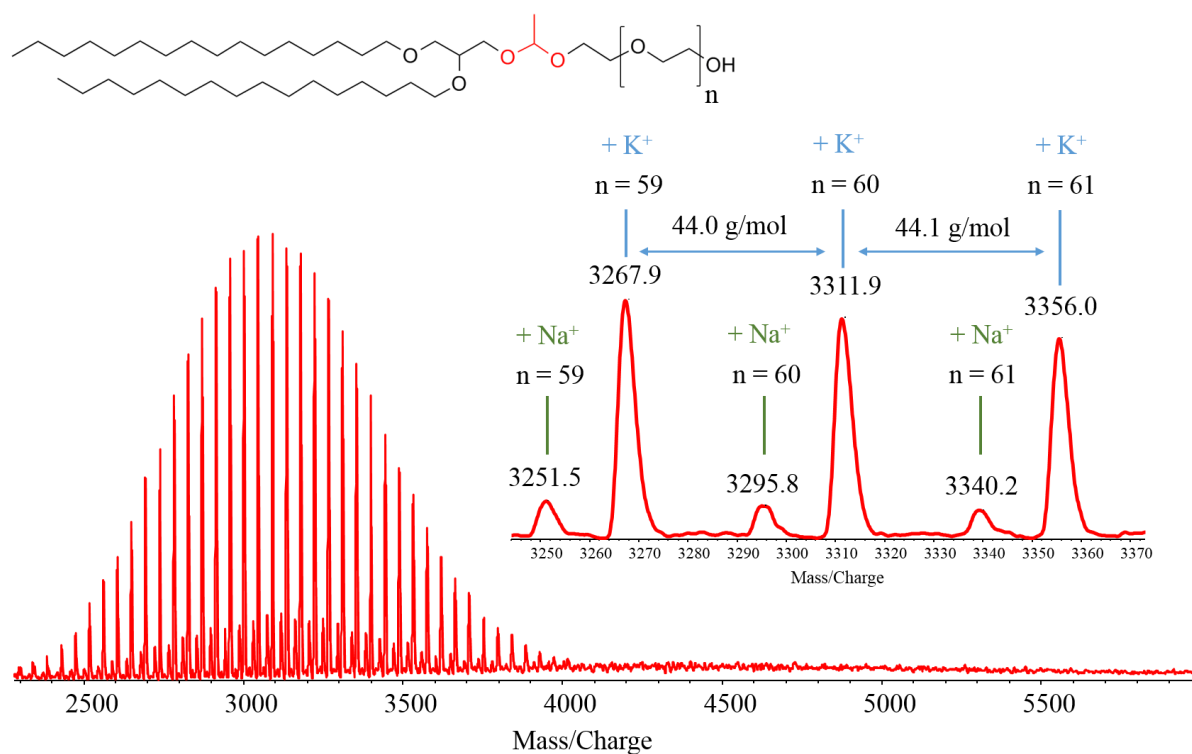


Figure S-35. MALDI-ToF mass spectrum of BisHD-A-PEG using a KTFA/CHCA matrix recorded in reflectron mode.

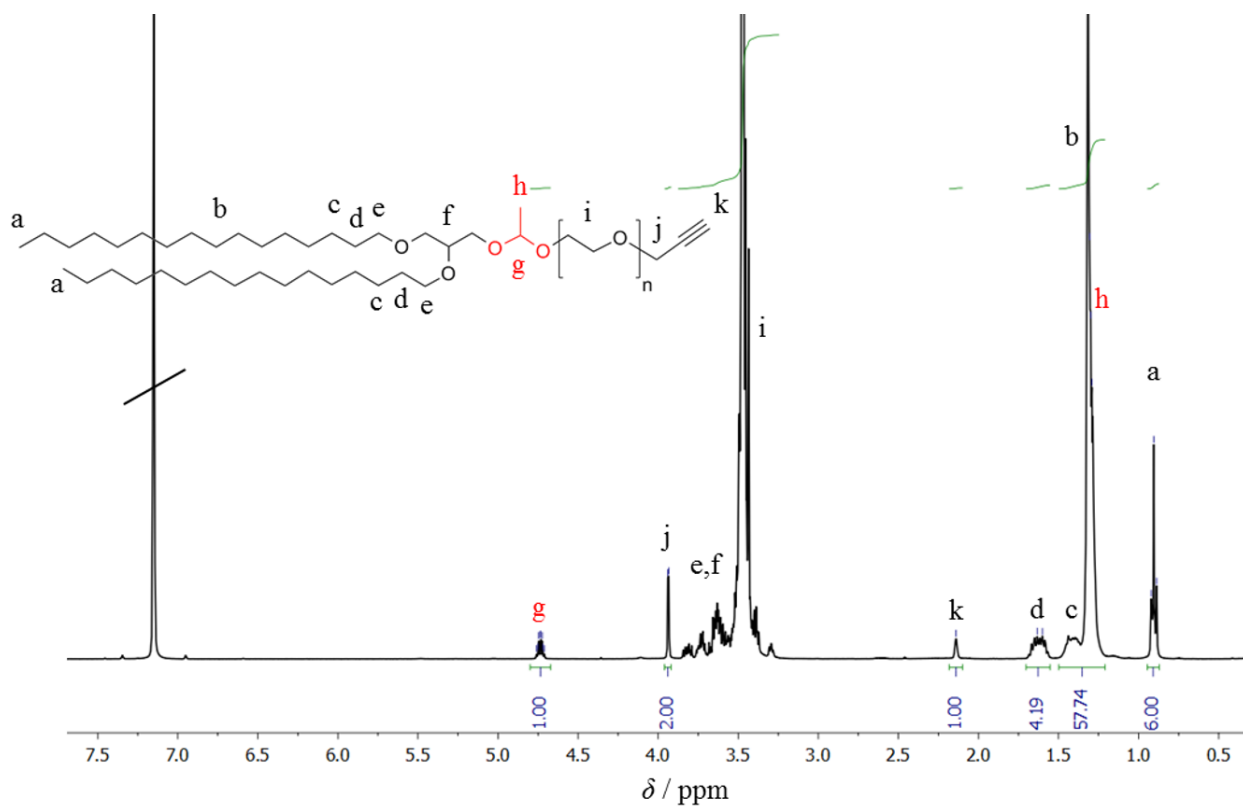


Figure S-36. ¹H NMR spectrum of BisHD-A-PEG₄₆-Alkyne measured in C₆D₆ at 400 MHz.

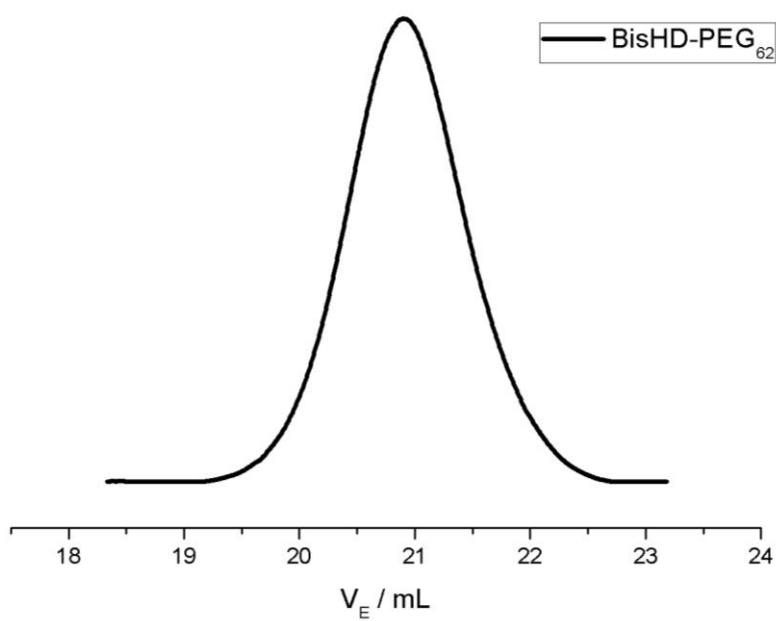


Figure S-37: SEC trace of BisHD-PEG₆₂ measured in DMF using RI detection.

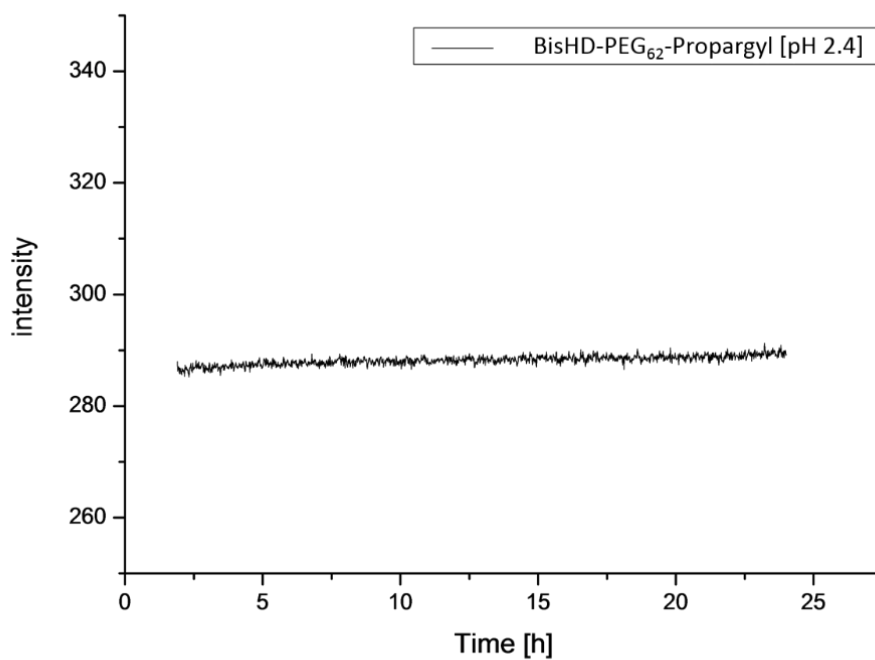


Figure S-38. Fluorescence trace of amphiphile without a cleavable group at pH 2.4. No increase in fluorescence was measurable.

5 Hyperbranched Polyglycerol-based Lipids in Liposomes

5.1 Hyperbranched Polyglycerol- and PEG-Lipids – Synthesis and Characterization

Matthias Worm,^{a,*} Matthias Voigt,^{b,#} Karolin Wagener,^{c,§} Maïke Schinnerer,^{d,£} Ulrike Kemmer-Jonas,^a Frank Roesch,^c Mark Helm,^b and Holger Frey.^a

^a Institute of Organic Chemistry, Johannes Gutenberg-University, Duesbergweg 10-14, D-55128 Mainz, Germany.

^b Institute of Pharmacy and Biochemistry, Johannes Gutenberg-University, Staudinger Weg 5, D-55128 Mainz, Germany.

^c Institute of Nuclear Chemistry, Johannes Gutenberg-University, Fritz Strassmann Weg 2, D-55128 Mainz, Germany.

^d Institute of Physical Chemistry, Johannes Gutenberg-University Mainz, Jakob Welder Weg 11, D-55128 Mainz, Germany.

* Synthesis, alkyne-functionalization and characterization of the polyether-lipids was performed by M.W.

Liposome preparation *via* dual centrifugation and characterization was carried out by M.V.

§ Radio-labelling, liposome preparation *via* membrane extrusion and characterization was conducted by K.W.

£ Dynamic light scattering experiments were performed by M. S.

Unpublished results

Abstract

Polyether-lipids based on poly(ethylene glycol) (PEG) are often employed in liposomal formulations to improve their pharmacokinetic properties. However, due to the low number of functional groups, PEG-lipids provide limited possibilities for post-modification to attach other molecules such as target units, dyes or radioactive tracers. Hyperbranched polyglycerol (*hbPG*)-lipids represent promising multifunctional alternatives. In this study, we report a novel synthesis pathway towards dialky-*hbPG*-lipids by utilizing a linear polyglycerol precursor as a macrinitiator for the slow monomer addition of glycidol. Thereby, bishexadecyl glycerol *hbPG*-lipids with molecular weights in the range of 3 to 7 kg mol⁻¹ and dispersities \mathcal{D} below 1.3 were obtained. For comparative purposes, well-defined PEG-lipids with similar molecular weights were synthesized. The lipids were incorporated into liposomes *via* dual centrifugation to study the effect of the polyether architecture and the molecular weight on the size of liposomes. A control of the liposome diameters below 100

nm could be achieved, while retaining high encapsulation efficiencies above 50 % of a model cargo. Positron emission tomography (PET) imaging served to investigate the *in vivo* biodistribution of ^{18}F -radiolabeled polyether-lipids and *hbPG*-modified liposomes in mice. While the pure polyether-lipids were rapidly excreted by renal filtration, liposomes containing the *hbPG*-lipids exhibit blood circulation times of more than 1 h. These findings reveal enhanced *in vivo* stability of liposomes modified with dialkyl-based *hbPG*-lipids and provide evidence for a *hbPG*-mediated “stealth” behavior of liposomes.

Introduction

In biomedicine, liposomes constitute a prominent class of drug carrier systems routinely used in clinical practice. Since they are composed of natural phospholipids, liposomes display excellent biocompatibility profiles that discriminate them from other nanoscopic drug carriers.^[1] In order to improve pharmacokinetic properties of liposomes, PEGylated lipids can be incorporated into the membrane with the polyethylene glycol (PEG) chains covering the liposomal surface. These sterically-stabilized liposomes or ‘stealth’ liposomes exhibit enhanced serum half-lives and reduced undesired effects of the therapeutic cargo compared to the free drug rendering them particularly interesting for anticancer therapy.^[1–3] It is a widely held view that liposomes passively accumulate in the tumor tissue due to the ‘enhanced permeability and retention effect’ (EPR effect).^[4,5] To further improve the efficacy of a liposomal drug carrier, target units such as antibodies,^[6] cell-penetrating peptides,^[7,8] or aptamers,^[9] have been attached to the surface of liposomes to enable directed drug delivery (active targeting). In case of PEG-lipids, mostly, a single methoxy or hydroxyl end group is present at the chain end, limiting possibilities for post-modification reactions to conjugate functional molecules.^[10] A promising strategy to overcome this limitation involves substitution of PEG as polyether segment by hyperbranched polyglycerol (*hbPG*). Aside from an excellent biocompatibility and water-solubility,^[11] *hbPG* exhibits multiple hydroxyl functionalities that allow for ligation of e.g. targeting moieties or radioactive tracers. Recently, the synthesis of

hbPG-lipids has been reported by our group,^[12] and increasing effort has been devoted to elucidating their effect on liposomal properties.^[13,14] For instance, in-depth studies on the influence of different hydrophobic anchor moieties of the lipid revealed significantly higher membrane integrity of dialkyl-derived *hbPG*-lipids opposed to cholesterol-based lipids, the latter of which are more commonly used in liposomal formulations.^[15] These findings are in accordance with results obtained from *in vivo* positron emission tomography (PET) imaging for ¹⁸F-radiolabeled cholesterol-lipids in liposomes.^[16] As stable anchorage of polyether-lipids in the liposomal bilayer is crucial to enable active targeting and to assure stability of the drug carrier in the blood stream, these findings suggest a more detailed study of liposomes containing multifunctional, dialkyl-anchored *hbPG*-lipids. Although, recent studies suggested reduced protein adsorption and aggregation of *hbPG*-modified liposomes in human blood serum,^[14] no *hbPG*-mediated ‘stealth’ properties of liposomes could be demonstrated *in vivo*.

Moreover, tuning the size of the liposomes in a range below 100 nm is necessary to allow for an effective use in tumor therapy.^[17] However, the effect of the molecular weight and the polyether architecture, i.e. linear or hyperbranched of dialkyl-lipids on the size of liposomes has not been explored yet.

In this study, we address these aspects of liposomal research by comparing the properties of dialkyl-based PEG- and *hbPG*-lipids with similar molecular weights. To this end, *rac*-bishexadecyl glycerol was used as an initiator for the anionic ring-opening polymerization (AROP) of ethoxy ethyl glycidyl ether (EEGE) to generate a linear polyglycerol (*linPG*) precursor after removal of EEGE’s acetal protecting groups. The *linPG*-lipid was employed for the hypergrafting of glycidol *via* slow monomer addition to yield *hbPG*-lipids in a molecular weight range of 3 – 7 kDa. For comparative purposes, bishexadecyl glycerol PEGs of similar molecular weights were synthesized by using bishexadecyl glycerol as an initiator for the AROP of ethylene oxide. New strategies were explored to control the size of liposomes containing PEG/*hbPG*-lipids by dual centrifugation. As an alternative method,

liposomes were generated by membrane extrusion and their temperature-dependent stability was analyzed by dynamic light scattering (DLS). In addition, results of *in vivo* PET studies in mice are presented.

Experimental Section

Materials

All chemicals were obtained from *Sigma Aldrich*, *TCl Europe*, or *Acros Organics* unless stated otherwise. Deuterated solvents (DMSO- d_6 , Pyridin- d_5) were purchased from *Deutero GmbH*. THF used for the anionic ring-opening polymerization was dried and stored over sodium/benzophenone. Care must be taken when handle the flammable, toxic, and gaseous ethylene oxide.

Methods

^1H NMR spectra were measured on a Bruker Avance II 400 MHz (5 mm BBO probe, 256 Scans, and B-ACS 60 auto sampler) at 294 K. ^{13}C NMR spectra were recorded on a Bruker Avance II 400 (100.5 MHz, 5 mm BBO probe, and B-ACS 60 auto sampler) at 294 K, if not stated otherwise. All spectra were processed with MestReNova v9.0 software. GPC (SEC) data were obtained using Agilent 1100 Series endowed with a PSS HEMA-column ($10^6/10^4/10^2$ Å porosity), LiBr/DMF (1 g/L) as eluent using RI detection. Polydispersity indices ($\mathcal{D} = M_w/M_n$) were determined with monodisperse PEG standards from *Polymer Standard Service GmbH (PSS)*. MALDI-ToF mass spectrometry was conducted on an Axima CFR MALDI-ToF mass spectrometer using pencil lead or α -cyano-4-hydroxycinnamic acid (CHCH) as matrix and potassium trifluoroacetate (KTFA) as a source for cations.

Synthesis Procedures

1,2-Bishexadecylglycerol (**1**). The synthesis has been described in previous reports.^[12]

Ethoxyethyl glycidyl ether EEGE (**2**). This compound has been synthesized according to known literature protocols.^[18]

1,2-Bishexadecylglycerol linPG₁₈ (**3**). Compound (**1**) (100 mg, 0.155 mmol) and cesium hydroxide mono hydrate (15.6 mg, 0.139 mmol) were dissolved in benzene (6 mL) and stirred in a dry Schlenk flask under slightly reduced pressure at 60 °C for 15 min keeping the stopcock closed. Moisture was removed by azeotropic distillation of benzene and subsequent drying at 60 °C in high vacuum for 16 h. Under argon atmosphere, dry dioxane (10 mL) was added via syringe and the solution was heated to 40 °C. EEGE (**2**) (1.09 mL, 7.42 mmol) was injected and the reaction mixture was stirred at 80 °C for 3 d. After removal of the solvent in vacuum, the resulting polymer was dissolved in a mixture of methanol (20 mL) and hydrochloric acid (2 mL, 2 mol L⁻¹) and stirred for 2 d at 40 °C. The solvent was partially removed under reduced pressure and the polymer was precipitated two times in cold diethyl ether. The pure polymer was obtained after drying in high vacuum. (Yield: 82 %) ¹H NMR (400 MHz, DMSO-*d*₆): δ [ppm] 4.85–4.20 (m, 18H, OH), 3.70–3.10 (m, 99H, CH₂-O and CH₂-CH-O), 1.50–1.38 (m, 4H, CH₂-CH₂-O), 1.34–1.10 (m, 52H, CH₂), 0.84 (t, 6H, *J*_{AB} = 6.4 Hz, CH₃-CH₂).

1,2-Bishexadecylglycerol hbPG₉₅ (**4**). In a dry Schlenk flask, the *linPG* precursor (**3**) (600 mg, 0.321 mmol) and cesium hydroxide mono hydrate (102 mg, 0.61 mmol) were dissolved in benzene (6 mL) and stirred at 60 °C for 1 h. The macroinitiator was freeze-dried in vacuo for 16 h, dissolved in dry NMP (0.5 mL) and heated to 100 °C. A solution of glycidol in dry NMP (6.8 mL, 5 wt%) was added within 8 h via a syringe pump and subsequently stirred for 2 h. After cooling to RT, the polymerization was terminated with methanol (0.5 mL). The crude polymer was dialyzed (MWCO 500 Da) against methanol for 24 h and dried under vacuo. (Yield: 740 mg, 80 %) ¹H NMR (400 MHz, Pyridin-*d*₅): δ [ppm] 6.66–5.76 (m, , OH) 4.61–3.28 (m, 529H, CH₂-O and CH₂-CH-O), 1.78–1.59 (m, 4H, CH₂-CH₂-O), 1.54–1.20 (m, 52H, CH₂), 0.88 (t, 6H, *J*_{AB} = 6.4 Hz, CH₃-CH₂). ¹³C NMR (100 MHz, Pyridin-*d*₅): δ [ppm] 79.92–62.73 (285C, CH₂O), 32.48 (2C, O-CH₂-CH₂-CH₂), 31.01–29.97 (22C, CH₂), 26.96 (2C, -CH₂-CH₂-CH₃), 23.30 (2C, CH₂-CH₃), 14.65 (2C, CH₂-CH₃).

1,2-Bishexadecylglycerol hbPG₃₂-Alkyne (**6**). Compound (**4**) (300 mg, 0.102 mmol) was dissolved in dry DMF (10 mL) under argon atmosphere. The solution was cooled to 0 °C, sodium hydride (18.0

mg, 0.75 mmol) was added and the mixture was stirred for 10 min. Propargyl bromide (31.7 mg, 0.21 mmol, 80 wt% in toluene) was injected via syringe and the reaction proceeded for 20 h at RT. After the suspension was diluted with water (1 mL), the solvent was removed *in vacuo* and the final polymer was obtained via dialysis (MWCO 500 Da) against methanol for 5 h. (267 mg, 89 %) ^1H NMR (400 MHz, $\text{DMSO-}d_6$): δ [ppm] 4.98–4.37 (m, 32H, OH), 4.29–4.09 (m, 2H, $\text{OCH}_2\text{-CCH}$), 3.80–3.04 (m, 169H, CH_2O and $\text{CH}_2\text{-CH-O}$), 2.89 and 2.72 (s, 1H, $\text{OCH}_2\text{-CCH}$), 1.53–1.38 (m, 4H, $\text{CH}_2\text{-CH}_2\text{-O}$), 1.35–1.11 (m, 52H, CH_2), 0.85 (t, 6H, $J_{AB} = 6.4$ Hz, $\text{CH}_3\text{-CH}_2$).

1,2-Bishexadecylglycerol PEG (5). Compound **(1)** (200 mg, 0.371 mmol) was dissolved in benzene (10 mL) and stirred in a dry Schlenk flask under slightly reduced pressure at 60 °C for 15 min keeping the stopcock closed. Moisture was removed by azeotropic distillation of benzene and subsequent drying at 70 °C in high vacuum for 16 h. After cooling to RT, dry THF (15 mL) was cryo-transferred into the Schlenk flask and potassium naphthalenide in THF (0.37 mL, 0.18 mmol, $c = 0.5 \text{ mol}\cdot\text{L}^{-1}$, prepared from potassium (235 mg, 6.0 mmol) and naphthalene (770 mg, 6.0 mmol) in dry THF (12 mL) in a glovebox under argon) was added via syringe. Generated hydrogen was removed in vacuum and ethylene oxide (1.11 mL, 22.3 mmol) was cryo-transferred via a graduated ampule into the initiator solution. The reaction was proceeded at 40 °C for 3h and subsequently continued at 60 °C for 3 d. The polymerization was quenched with methanol (2 mL) and the polymer was precipitation in cold diethyl ether. After removing all volatiles under vacuum, the pure polymer was obtained. (Yield: 82 %) ^1H NMR (400 MHz, $\text{DMSO-}d_6$): δ [ppm] 3.70–3.20 (m, 250H, $\text{CH}_2\text{-O}$ and $\text{CH}_2\text{-CH-O}$), 1.50–1.38 (m, 4H, $\text{CH}_2\text{-CH}_2\text{-O}$), 1.34–1.10 (m, 52H, CH_2), 0.84 (t, 6H, $J_{AB} = 6.4$ Hz, $\text{CH}_3\text{-CH}_2$).

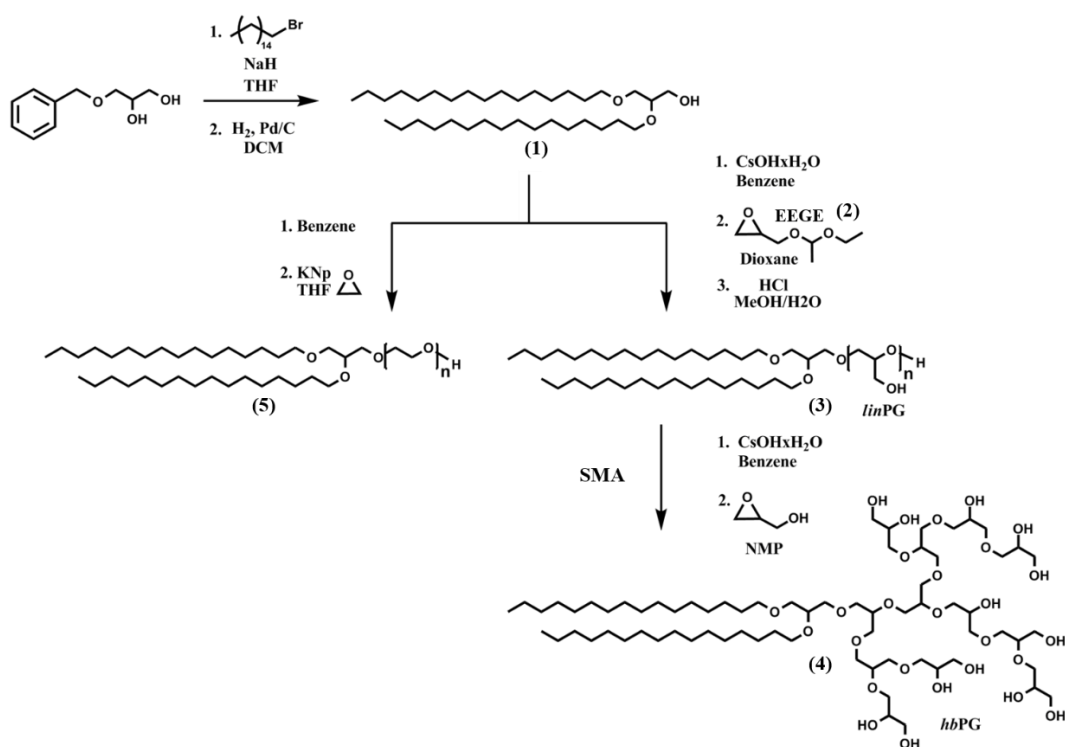
1,2-Bishexadecylglycerol PEG Alkyne (7). In a dry Schlenk flask, compound **9** (300 mg, 0.115 mmol) was dissolved in dry THF (15 mL) under argon atmosphere. The solution was cooled to 0 °C, sodium hydride (8.3 mg, 0.34 mmol) was added and the mixture was stirred for 10 min. Propargyl bromide (51.1 mg, 0.34 mmol, 80 wt% in toluene) was injected via syringe and the reaction was proceeded at RT for 20 h. After filtration, the solution was reduced to a small volume and the polymer was

precipitated in cold diethyl ether. (280 mg, 92 %) ^1H NMR (400 MHz, C_6D_6): δ [ppm] 3.94 (d, 2H, $^4J_{AB}$ = 2.4 Hz, $\text{OCH}_2\text{-CCH}$), 3.86–3.25 (m, 190H, CH_2O and $\text{CH}_2\text{-CH-O}$), 2.14 (m, 1H, $\text{OCH}_2\text{-CCH}$), 1.71–1.54 (m, 4H, $\text{CH}_2\text{-CH}_2\text{-O}$), 1.52–1.19 (m, 52H, CH_2), 0.90 (t, 6H, J_{AB} = 6.4 Hz, $\text{CH}_3\text{-CH}_2$). ^{13}C NMR (100.6 MHz, C_6D_6): δ [ppm] 100.46 (1C, $\text{O}_2\text{CH-CH}_3$), 80.47 (1C, $\text{OCH}_2\text{-CCH}$), 78.86 (1C, $\text{CH-CH}_2\text{O}$), 74.70 (1C, $\text{OCH}_2\text{-CCH}$), 73.24–64.97 (87C, CH_2O), 58.38 (1C, $\text{OCH}_2\text{-CCH}$), 32.36 (2C, $\text{CH}_3\text{-CH}_2\text{-CH}_2$), 30.86–29.85 (24C, CH_2), 26.76 (2C, $\text{CH}_2\text{-CH}_2\text{-CH}_2\text{O}$), 23.14 (2C, $\text{CH}_2\text{-CH}_3$), 19.96 (1C, $\text{O}_2\text{CH-CH}_3$), 14.40 (2C, $\text{CH}_2\text{-CH}_3$).

Results and Discussion

A. Synthesis of 1,2-Bis-*n*-hexadecyl glycerol *hbPG*- and PEG-lipids

To access dialkyl-based lipids containing hyperbranched polyglycerol (*hbPG*) as hydrophilic polyether segment, first, bishexadecyl glycerol (**1**) was synthesized from 1-*O*-benzyl glycerol via Williamson etherification with hexadecyl bromide and subsequent hydrogenation to remove the benzyl protective group. The synthesis has been described in the literature.^[12]



Scheme 9: Synthesis of bishexadecyl (BisHD) glycerol PEG/*hbPG* lipids.

Bis-hexadecyl glycerol (**1**) was then employed as an initiator for the anionic ring-opening polymerization (AROP) of ethoxyethyl glycidyl ether (EEGE) (**2**) using cesium hydroxide as a base to generate a bis-hexadecyl glycerol-PEEGE prepolymer. The PEEGE precursor could be converted into BisHD-*lin*PG (**3**) by acidic hydrolysis of the acetal protecting groups. By using the *lin*PG precursor (**3**) as a macroinitiator for the slow monomer addition (SMA) of the AB₂ monomer glycidol, BisHD-*hb*PG lipids (**4**) could be synthesized containing a hydrophilic hyperbranched polyglycerol (*hb*PG) segment and a hydrophobic dialkyl anchor moiety (See Scheme 9, right path).

The synthesis of *hb*PG-lipid based on dialkyl anchor groups has been reported in a previous work that employed a deprotected poly(isopropylidene glyceryl glycidyl ether) lipid (IGG) precursor as an initiator for the hypergrafting of glycidol.^[12] In this study, we employed deprotected EEGE precursors as an alternative macroinitiators and aimed for a precise tailoring of the *hb*PG molecular weight in a range of 3000 to 7000 g mol⁻¹. Thereby, we extended the scope of dialkyl-derived *hb*PG-lipids to allow for a detailed investigation of their properties in liposomes. For comparative purposes, PEG-functional bis-hexadecyl glycerol-lipids (**5**) in the same molecular weight range were synthesized by utilizing bis-hexadecyl glycerol (**1**) to initiate the AROP of ethylene oxide. In this case, the polymerization was conducted in THF using potassium naphthalenide to deprotonate the initiator (See Scheme 9, left path).

Table 9 summarizes the molecular characteristics of the polymers discussed in this study. First, a *lin*PG lipid (**3**) was synthesized with a molecular weight of $M_n = 1800$ g mol⁻¹ exhibiting a narrow molecular weight distribution ($\mathcal{D} = 1.06$). ¹H NMR spectroscopy proved complete removal of the EEGE acetal protective groups and incorporation of the lipophilic anchor (See SI Figure S-1). Average molecular weights were determined by ¹H NMR spectroscopy via end group analysis and size exclusion chromatography (SEC) in DMF using PEG calibration with good agreement of the two values.

Table 9: Molecular characteristics of hyperbranched and linear bishexadecyl glycerol lipids.

Sample	M_n (NMR) / g mol ⁻¹	M_n (SEC) / g mol ⁻¹	\mathcal{D}
BisHD- <i>lin</i> PG ₁₉	1950	1800	1.06
BisHD- <i>hb</i> PG ₃₂	2910	2200	1.21
BisHD- <i>hb</i> PG ₆₆	5420	2600	1.29
BisHD- <i>hb</i> PG ₉₆	7640	2900	1.30
BisHD- <i>lin</i> PG ₂₄	2320	2300	1.17
BisHD- <i>hb</i> PG ₇₇	6240	4300	1.27
BisHD-PEG ₆₂	3290	2200	1.05
BisHD-PEG ₁₁₂	5470	4900	1.08
BisHD-PEG ₁₆₀	7560	6400	1.08

M_n (NMR): Molecular weights of polymers calculated from ¹H NMR via end group analysis. M_n (SEC): Molecular weights of polymers obtained from SEC using PEG standards for calibration. $\mathcal{D} = M_w/M_n$: Molecular weight distribution determined from SEC using PEG standards.

Figure 24 includes SEC traces of the PEEGE- (black trace) and the *lin*PG polymer (red trace) revealing narrow, monomodal molecular weight distributions and a significant shift to higher elution volume upon acidic hydrolysis of the acetals. The structure of BisHD-*lin*PG₁₉ was further verified by MALDI-ToF mass spectrometry showing the polymer as potassium and cesium species (See SI Figure S-2).

Subsequently, BisHD-*lin*PG₁₉ was used for the hypergrafting of glycidol to generate three *hb*PG-functional lipids with molecular weights of about 3000, 5000 and 7000 g mol⁻¹ as calculated from ¹H NMR spectroscopy (See Table 9). Molecular weight distributions are monomodal with moderate dispersities \mathcal{D} below 1.3 showing minor shifts to lower elution volume with increasing molar masses. Clearly, deviation of molecular weights obtained from SEC and ¹H NMR is more pronounced for higher degrees of polymerization. This observation can be explained by the rather globular structure of *hb*PGs.^[19] Therefore, the hydrodynamic volume only slightly increases with higher molecular weights of BisHD-*hb*PG resulting in similar elution volumes of the three polymers in SEC (See Figure 24).

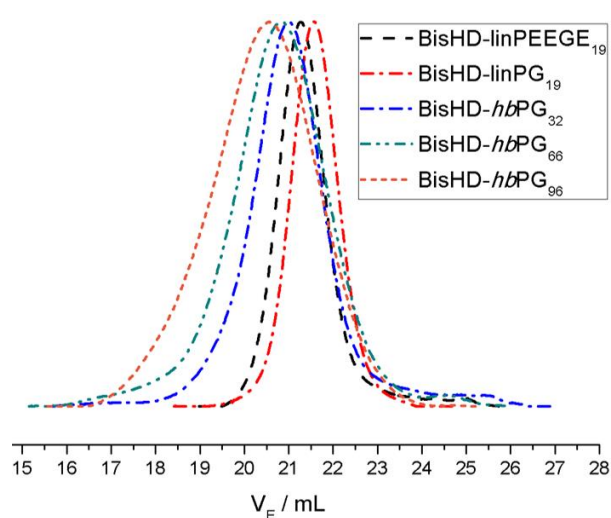


Figure 24: SEC traces of **BisHD-PEGEE₁₉**, **BisHD-linPG₁₉**, **BisHD-hbPGs** using DMF as eluent and RI detection.

As an example, Figure 25 contains the ^1H NMR spectrum of **BisHD-hbPG₉₆** showing the characteristic resonances of the lipophilic anchor in the aliphatic region of 0.8 – 1.7 ppm. The proton signals of the initiator are clearly separated from the polyether backbone ($\delta = 3.1 - 3.7$ ppm) and the multiple hydroxyl groups ($\delta = 4.3 - 4.7$ ppm).

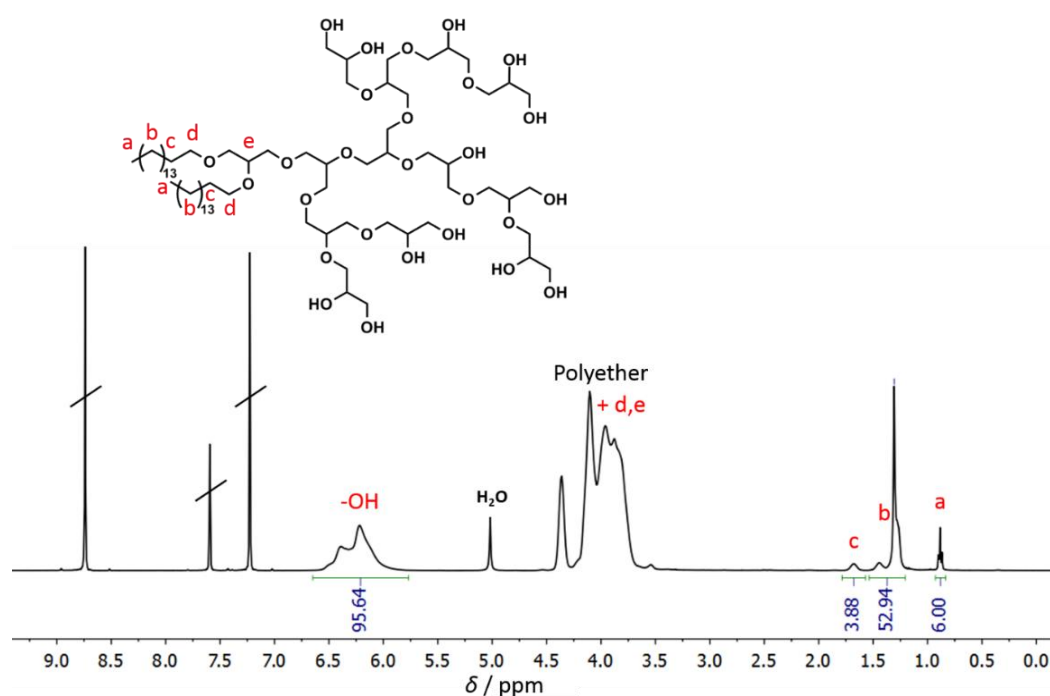


Figure 25: ^1H NMR spectrum of **BisHD-hbPG₉₅** measured in pyridine- d_5 at 400 MHz.

By comparing the integrals of the backbone resonances and the hydroxyl groups with the methyl proton signals of the dialkyl chains ($\delta = 0.91$ ppm), molecular weights could be calculated.

^{13}C NMR provided additional evidence for the purity of the lipids and served to verify their structure (See Figure 26). It is worth noting that NMR measurements were performed in deuterated pyridine to assure well-resolved signals for the hydrophilic polyether segment as well as the hydrophobic anchor group and to avoid an overlap of the water residual peak with the polyether backbone as observed for spectra measured in $\text{DMSO-}d_5$ leading to an inaccurate determination of molecular weights.

Following the above-described procedure, a **BisHD-*lin*PG₂₄** macroinitiator was synthesized and used to generate a **BisHD-*hb*PG₇₇**-lipid with a molecular weight of around 6000 g mol^{-1} and monomodal molecular weight distributions ($\mathcal{D} = 1.27$) filling the molecular weight gap between **BisHD-*hb*PG₆₆** ($M_n \sim 5000\text{ g mol}^{-1}$) and **BisHD-*hb*PG₉₆** ($M_n \sim 7000\text{ g mol}^{-1}$) as given in Table 9. (SEC traces of the **BisHD-*lin*PG₂₄** included in the SI Figure S-3)

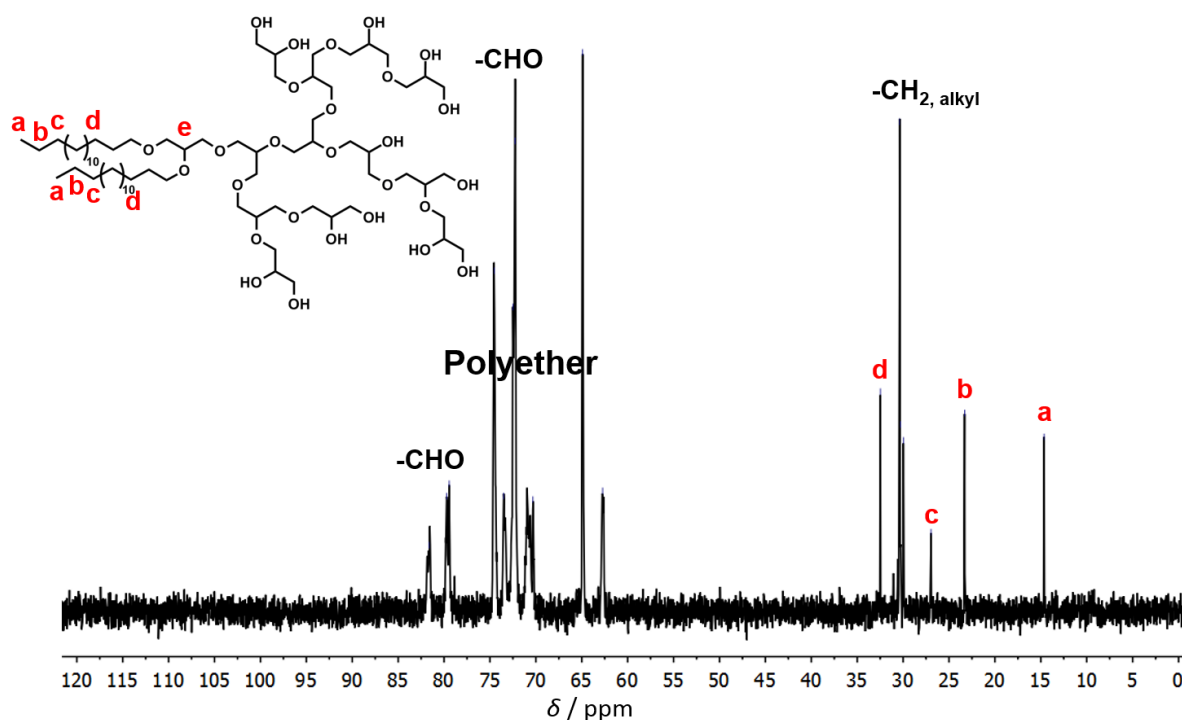


Figure 26: ^{13}C NMR spectrum of **BisHD-*hb*PG₉₅** measured in pyridine- d_5 at 100 MHz.

In order to enable structure-property correlation between dialkyl-based *hb*PG- and PEG-lipids in liposomal formulations, **BisHD-PEGs** with molecular weights in the range of 3300 to 7600 g mol^{-1}

comparable to the **BisHD-hbPG** lipids (see Table 9) were prepared. Molecular weights from SEC are consistently underestimated compared to values calculated from ^1H NMR spectroscopy via end group analysis.

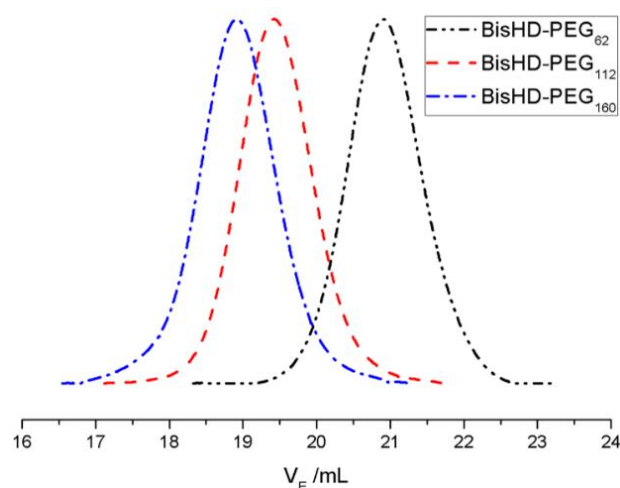


Figure 27: SEC traces of **BisHD-PEGs** using DMF as eluent and RI detection.

These discrepancies can be attributed to difference in the hydrodynamic volume of the PEG-lipids and the PEG standards used for SEC calibration. Narrow, monomodal molecular weight distributions ($\mathcal{D} < 1.1$) were found for the three polymers with consistent shifts to lower elution volume for higher molecular weight polymers as shown in Figure 27.

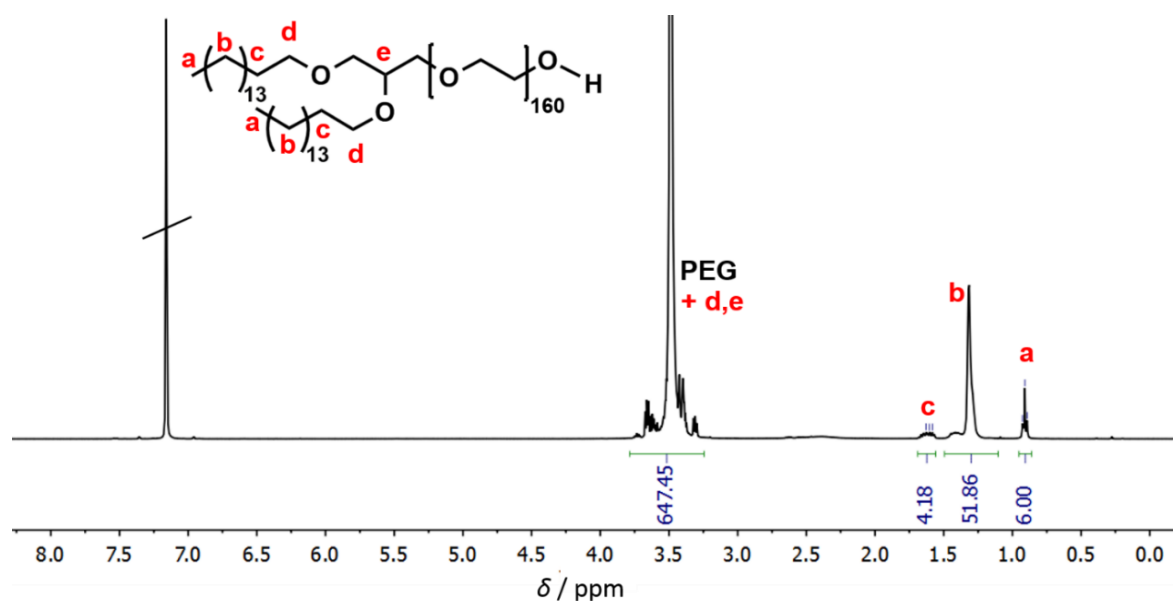
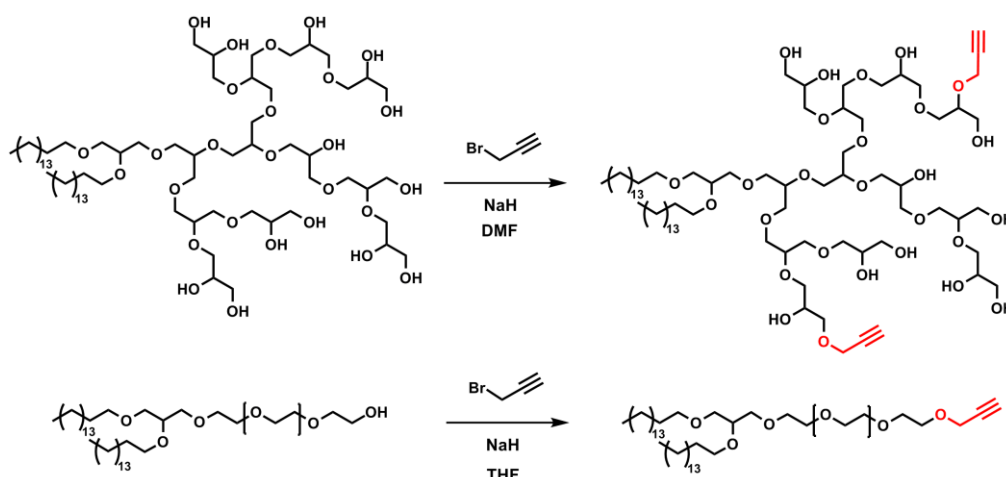


Figure 28: ^1H NMR spectrum of **BisHD-PEG₁₆₀** measured in C_6D_6 at 400 MHz.

A typical ^1H NMR spectrum of **BisHD-PEG** lipids is presented in Figure 28 for **BisHD-PEG₁₆₀**. Molecular weights were determined by comparing the integrals of the methyl initiator signals (0.91 ppm) with the backbone resonances ($\delta = 3.25\text{--}3.80$ ppm) of PEG.

B. Alkyne-Functionalization of Lipids

In order to enable attachment of functional molecules to the polyether end groups via copper(I)-catalyzed azide alkyne cycloaddition click chemistry (CuAAC), alkyne moieties were introduced. To this end, PEG- and *hbPG*-lipids were functionalized by conversion of terminal hydroxyl groups with propargyl bromide as depicted in Scheme 10. This reaction has been reported in the literature,^[16] and was adapted for the dialkyl-based lipids used in this study.



Scheme 10: Functionalization of **BisHD-hbPG₃₂** (top) and **BisHD-PEG₆₂** (bottom) with propargyl bromide in order to attach alkyne functionalities.

Successful functionalization of lipids could be confirmed by ^1H NMR spectroscopy and the appearance of the characteristic resonances for the methylene protons ($\delta = 4.0\text{--}4.2$ ppm) and the alkyne protons ($\delta = 2.5\text{--}3.0$ ppm) as shown in Figure 29 and Figure 30. In addition, diffusion-ordered NMR spectroscopy (DOSY) provided evidence for the attachment of alkyne residues to the polymers (See SI, Figure S-42 and Figure S-43).

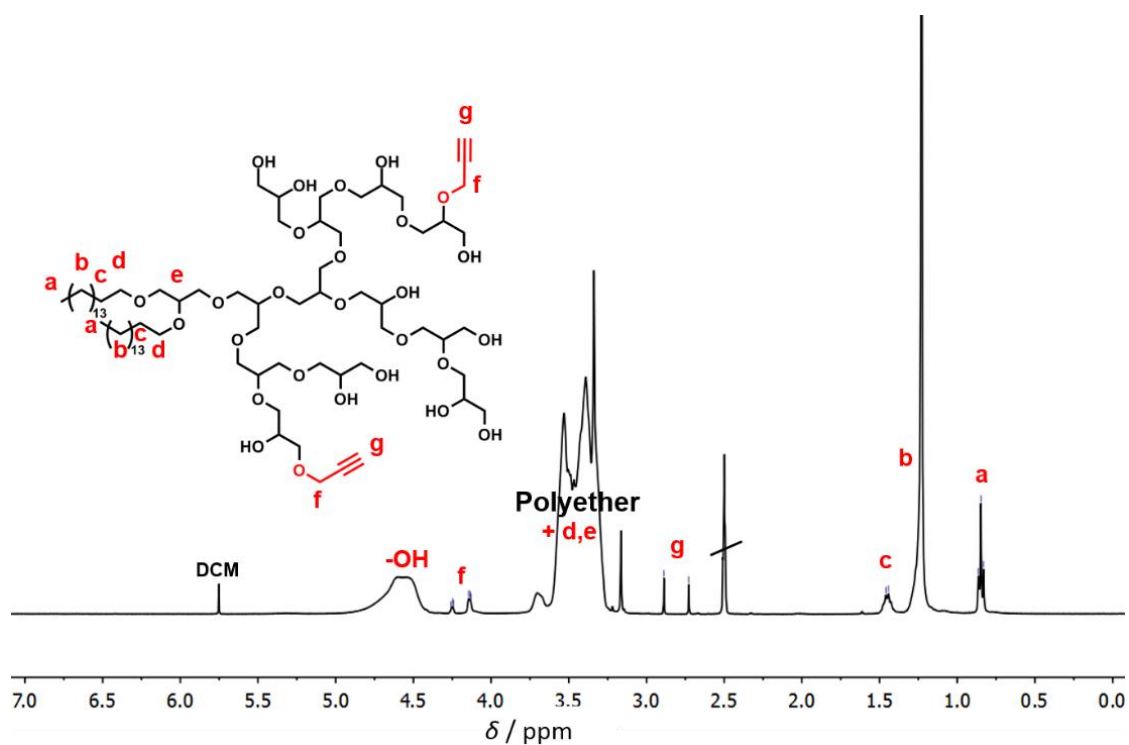


Figure 29: ^1H NMR spectrum of BisHD-hbPG₃₂-Alkyne measured in DMSO-d₆ at 400 MHz.

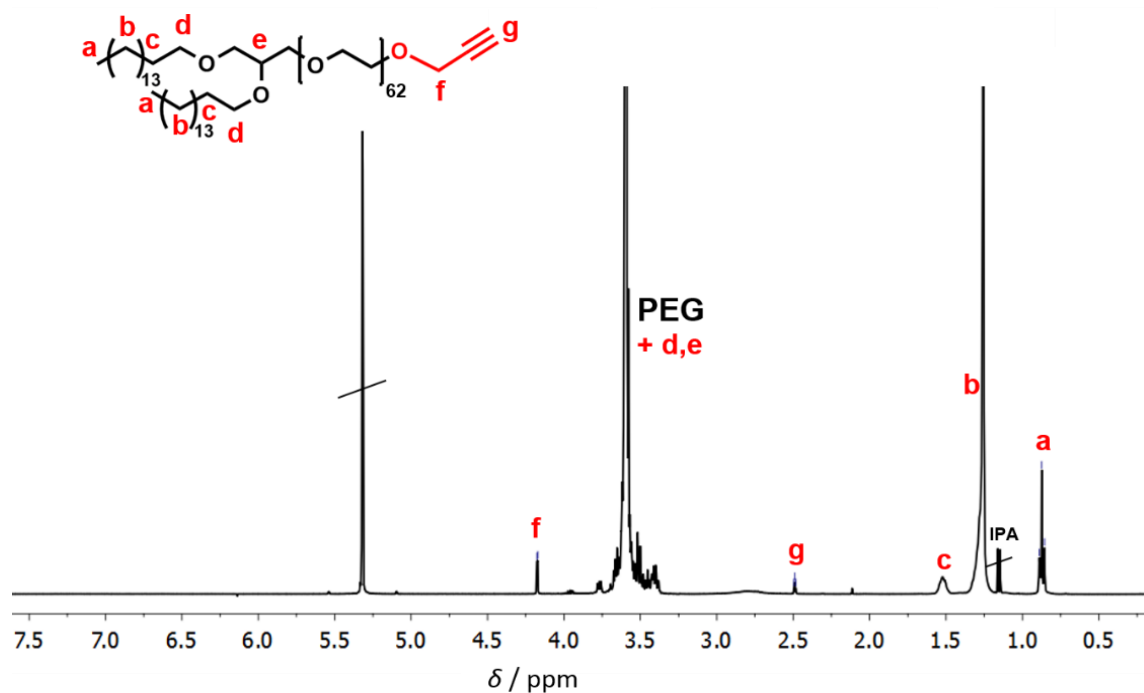


Figure 30: ^1H NMR spectrum of BisHD-PEG₆₂-Alkyne measured in CD₂Cl₂ at 400 MHz.

5.2 Size Control of *hbPG*-modified Liposomes *via* Dual Centrifugation

This section briefly illustrates recent findings that have been obtained in a collaboration with the research group of Prof. Mark Helm (Institute of Pharmacy and Biochemistry, Johannes Gutenberg-University Mainz). Experiments were performed by Matthias Voigt.

Dual centrifugation (DC) represents a modern and convenient method to generate liposomes of variable lipid compositions that enables liposome preparation in small batch-sizes and with high encapsulation efficiencies (EE) of the cargo.^[20,21] Polyether-based lipids composed of PEG and *hbPG* have been incorporated into liposomes using DC,^[13] however, so far, no particular attention was drawn towards the effect of the polymer architecture and the molecular weights on the size of liposomes. Notably, the size of a nanocarrier is known to have crucial implications on cellular uptake.^[22] In anti-cancer research, nanoparticles below 100 nm in diameter have been reported as optimum for tumor cell targeting.^[17] Stealth liposomes obtained *via* DC typically exhibit diameters in the range of 120 to 250 nm,^[13,15] that are above the aforementioned size threshold.

For the purpose of this work, liposomes composed of egg phosphatidylcholine (EPC) and cholesterol were prepared using DC as described before,^[13] containing small amounts of the polyether-lipids introduced in the previous chapter. Ceramic beads are routinely added to the centrifuge vials to ensure efficient mixing.

At first, the influence of the molecular weight and the molar content of the polyether-lipids on the size of liposomes was investigated for the hyperbranched lipids. To this end, **BisHD-*hbPG*₃₂(3k)**, **BisHD-*hbPG*₆₆(5k)**, **BisHD-*hbPG*₉₆(7k)** were incorporated into liposomes and dynamic light scattering (DLS) was performed *via* zeta-sizer to determine the z-averaged hydrodynamic radius. In Figure 31, diameters of liposomes are plotted versus the molar content of *hbPG*-lipids in the composition (0 - 8 mol%) for different molecular weights of the lipids ($M_n \sim 3, 5$ and 7 kg mol^{-1}). With low amounts of the polyether-lipids (1 – 3 mol%), a drop in the diameters of liposomes is apparent for *hbPG*-lipids regardless of the molecular weights. If the molar content of *hbPG*-lipids is

further increased, a continuous decline in the size of liposomes could be detected for **BisHD-hbPGs** with molecular weights of 5000 (red) and 7000 g mol⁻¹ (green), while a gradual size incline is observed for liposomes containing **BisHD-hbPG3k** ($M_n \sim 3000$ g mol⁻¹).

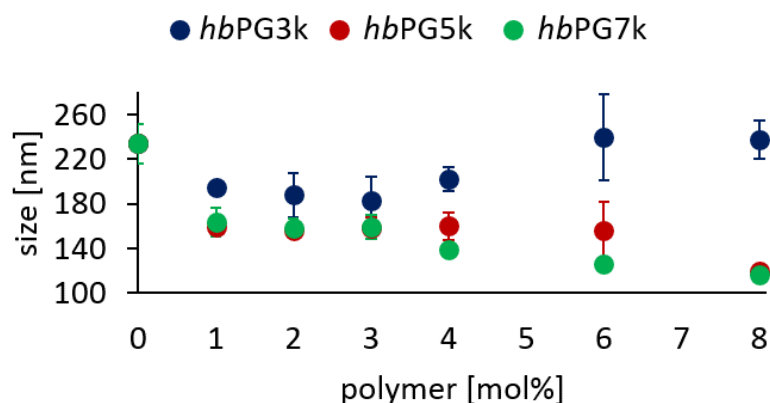


Figure 31: Effect of molecular weight and content of hyperbranched polyether-Lipids **BisHD-hbPG3k**, **BisHD-hbPG5k**, **BisHD-hbPG7k** on the size of liposomes measured by dynamic light scattering (DLS) *via* zeta-sizer. Liposomes were prepared *via* dual centrifugation (DC) with lipid compositions of egg phosphatidyl choline (EPC, 50 mol% - x), cholesterol (50 mol%) and **BisHD-PEGs/BisHD-hbPGs** (x = 0 – 8 mol%).

Interestingly, similar liposome sizes were obtained for **BisHD-hbPG5k** and **BisHD-hbPG7k**, albeit the differences in molecular weight. These first results suggested perspective to passively influence the size of liposomes by choosing polyether-based lipids with different molecular weights and served as motivation to take a closer look at the effect of the higher molecular weight lipids ($M_n > 5000$ g mol⁻¹).

In order to evaluate the influence of the polyether architecture of the lipids, i.e. linear or hyperbranched on the size of liposomes, additional liposomal formulations were prepared *via* DC as described above containing varying amounts (1 – 8 mol%) of **BisHD-PEG7k**. For illustrative purposes, the diameters of a series of liposomes modified with **BisHD-PEG7k** or **BisHD-hbPG7k** lipids are presented in Figure 32 revealing comparable values for the diameters of both classes of liposomes. Apparently, the drop in size with increasing molar content of the polyether-lipid is also observed in case of the linear polyether architecture of **BisHD-PEG7k**.

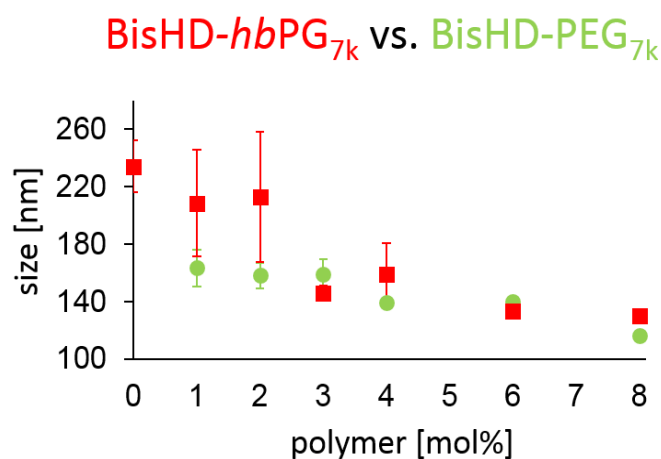


Figure 32: Influence of the architecture (linear PEG or hyperbranched PG) and the molar content (0 - 8 mol%) of polyether lipids on the size of liposomes for **BisHD-PEG_{7k}** and **BisHD-*hb*PG_{7k}** with molecular weights around 7000 g mol⁻¹. Diameters of liposomes were measured by DLS using a zeta-sizer.

Within the scope of these experiments, smallest diameters of liposomes were obtained for molar contents of polyether-lipids of 8 mol% and molecular weights above 5000 g mol⁻¹ which was considered in the follow-up experiments. Based on these exploratory findings, it is not possible to unravel the origin of this trend behavior. However, a possible reason might be the increased steric demand of the polyethers with higher molecular weights, thereby promoting higher curvatures of the liposomal surface and hence, larger surface areas. Consequently, small liposome sizes are favored if larger amounts of high molecular weight lipids are employed to reduce interactions between polymer chains on the liposomal surface. Additional experiments are in progress to further analyze this behavior and to establish a more comprehensive understanding of the phenomenon.

Although, a consistent drop in the size of liposomes could be achieved by varying the molecular weight of the lipids and their molar content in the composition, so far diameters were above the designated size threshold of 100 nm. Therefore, additional studies were performed to optimize experimental parameters for the preparation of liposomes *via* DC by capitalizing on the findings discussed above. Figure 33 graphically displays physical characteristics of a series of liposomes containing 8 mol% of **BisHD-*hb*PG_{6k}** (left columns) and **BisHD-PEG_{7k}** (right columns) prepared *via* DC with different dilutions of lipids in buffer and varying amounts ceramic beads. Three

experimental settings (standard, diluted, optimized) have been investigated and are distinguished in the chart below.

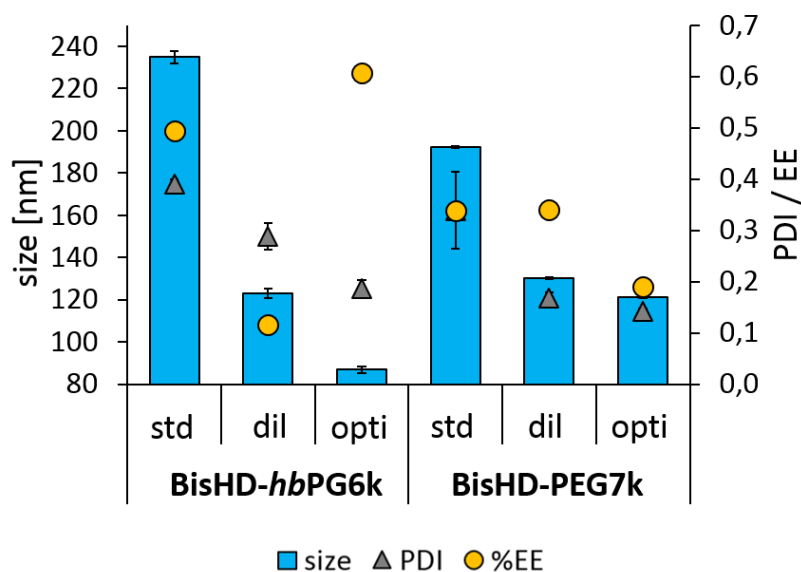


Figure 33: Dependency of liposome properties, i.e. size (diameter), PDI (polydispersity index), EE (encapsulation efficiency) on different experimental parameters for DC preparation ($n = 3$) of liposomes composed of egg phosphatidyl choline (EPC, 42 mol%), cholesterol (50 mol%) and **BisHD-*hbPG6k*** or **BisHD-PEG7k** (8 mol%) with total lipid amounts of 9.6 mg for PEG liposomes and 8.5 mg for *hbPG* liposomes and different amounts of ceramic beads (\varnothing 0.4 mm). Experimental parameters include std (standard): $V_{\text{Buffer}}^s = 2 \cdot V_{\text{Beads}}^s = 38 \mu\text{L}$, dil (diluted): $V_{\text{Buffer}}^d = 2 \cdot V_{\text{Beads}}^d = 66 \mu\text{L}$, opti (optimized): $V_{\text{Buffer}}^o = V_{\text{Beads}}^o = 66 \mu\text{L}$. The volume of beads was determined from their hydrostatic displacement. Size and PDI of liposomes were determined *via* zeta-sizer and EE was obtained from SEC using UV detection.

Apparently, higher dilution and increased amounts of ceramic beads lead to a significant drop in the size of liposomes. This effect is more pronounced for the *hbPG*-lipids showing minimum diameters of approx. 90 nm for optimized parameters of DC preparation. In addition, encapsulation efficiencies (EE) of calcein as a model cargo could be assessed by size exclusion chromatography using UV detection. Interestingly, lower PDIs (around 0.2) and increased EEs (> 50%) were determined for liposomes prepared under optimized conditions which is desirable as well.

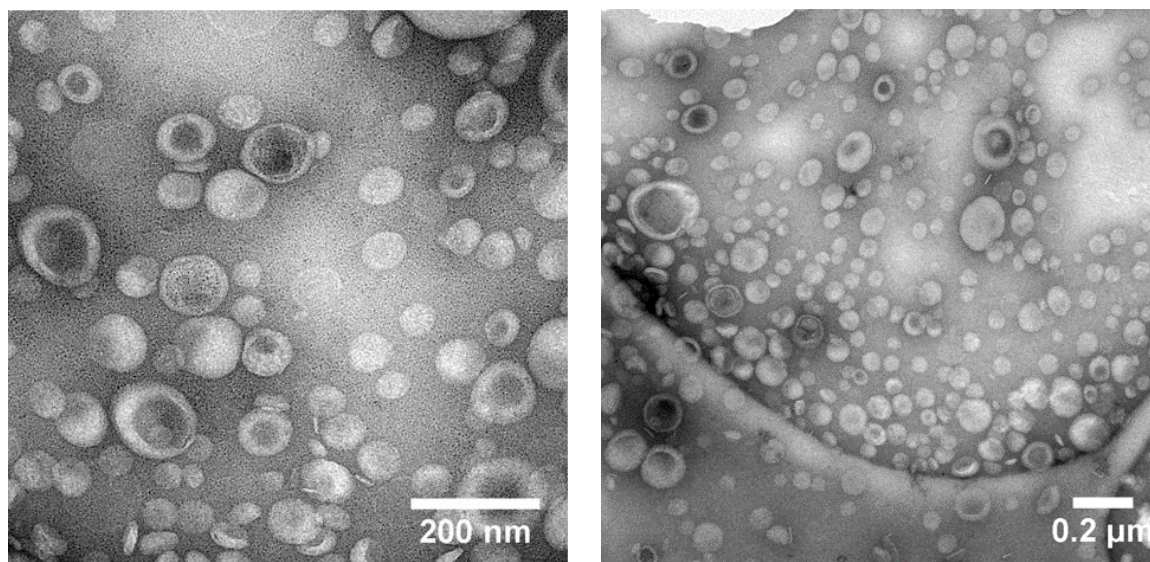


Figure 34: Transmission electron microscopy (TEM) images of liposomes containing **BisHD-*hbPG6k*** lipids embedded in trehalose using negative staining with uranyl acetate and performing measurements on a lacey carbon grid.^[23]

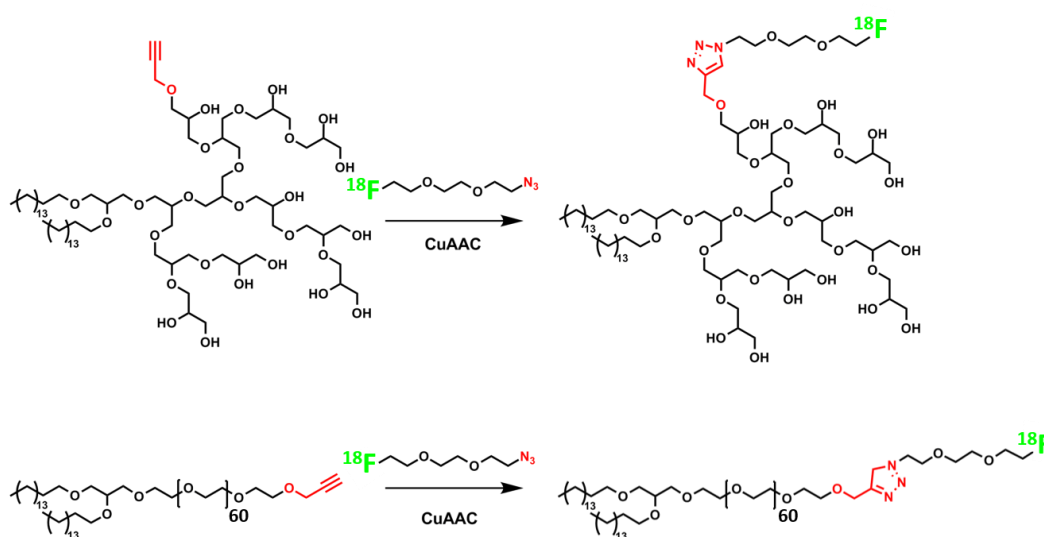
To visualize the physical appearance of liposomes prepared *via* DC under the above-described optimized parameters, transmission electron microscopy (TEM) images were recorded for liposomes containing 8 mol% of **BisHD-*hbPG6k***. This sample preparation technique has been employed before for TEM imaging of other nanoparticles.^[23] Figure 34 depicts TEM images of liposomes that reveal average diameters below 100 nm confirming the results from DLS.

Although the findings discussed in this chapter express exploratory character, they suggest promising perspective for preparational strategies *via* dual centrifugation to control the size of liposomes below 100 nm, by using polyether-lipids with molecular weights exceeding 5000 g mol^{-1} , which is regarded as the desirable size range of nanoparticles for antitumor therapy. These results may serve as incentive for future experiments in this area.

5.3 *In Vivo* Biodistribution Studies of ^{18}F -Radiolabeled Lipids and Liposomes by Positron Emission Tomography Imaging

In this chapter, a short overview of recent results is presented that have been obtained in collaboration with the research group of Prof. Frank Roesch (Institute of Nuclear Chemistry, University of Mainz). Radiolabeling of lipids and liposome preparation were conducted by Karolin Wagener (Research Group Prof. Frank Roesch). Animal studies in mice were carried out by Karolin Wagener and Dr. Stefanie Pektor (Clinic and Polyclinic of Nuclear Medicine, University Medical Center Mainz). Dynamic light scattering was performed by Meike Schinnerer (Research Group Prof. Manfred Schmidt).

Positron emission tomography (PET) is a versatile imaging technology in nuclear medicine that allows *in vivo* visualization of biodistributions of nanoparticles and liposomes, by attaching radioactive tracers to their surfaces.^[24,25] The most frequently used radioisotope in PET is fluorine-18 (^{18}F) with a comparatively short half-life of $t_{1/2} = 109.7$ min, which can be produced on a large scale and, in contrast to positron emitting metal nuclides, can be introduced without the use of chelating agents.^[26] In liposomal research, PET imaging with ^{18}F -labeled lipids has been reported in the literature.^[16,27,28]



Scheme 11: ^{18}F -Radiolabeling of alkyne-functional **BisHD-hbPG3k** (top) and **BisHD-PEG3k** (bottom) via copper(I)-catalyzed azide-alkyne cycloaddition click chemistry (CuAAC) using [^{18}F]F-TEG-azide as a radioactive synthon.

In order to facilitate PET imaging, alkyne-functional **BisHD-PEG₆₂(3k)** and **BisHD-hbPG₃₂(3k)** lipids introduced in Chapter 5.1 were radiolabeled with [^{18}F]F-TEG-azide using copper(I)-catalyzed alkyne-azide cycloaddition click chemistry (CuAAC) as shown in Scheme 11. ^{18}F -Radiolabeling of polyether amphiphiles has been described for cholesterol-lipids in previous reports,^[16] and has been adapted for dialkyl-functional lipids in this study. Polyether-lipids with molecular weights of around 3000 g mol⁻¹ were chosen to be in line with molecular weights of cholesterol-lipids investigated in the previous studies.

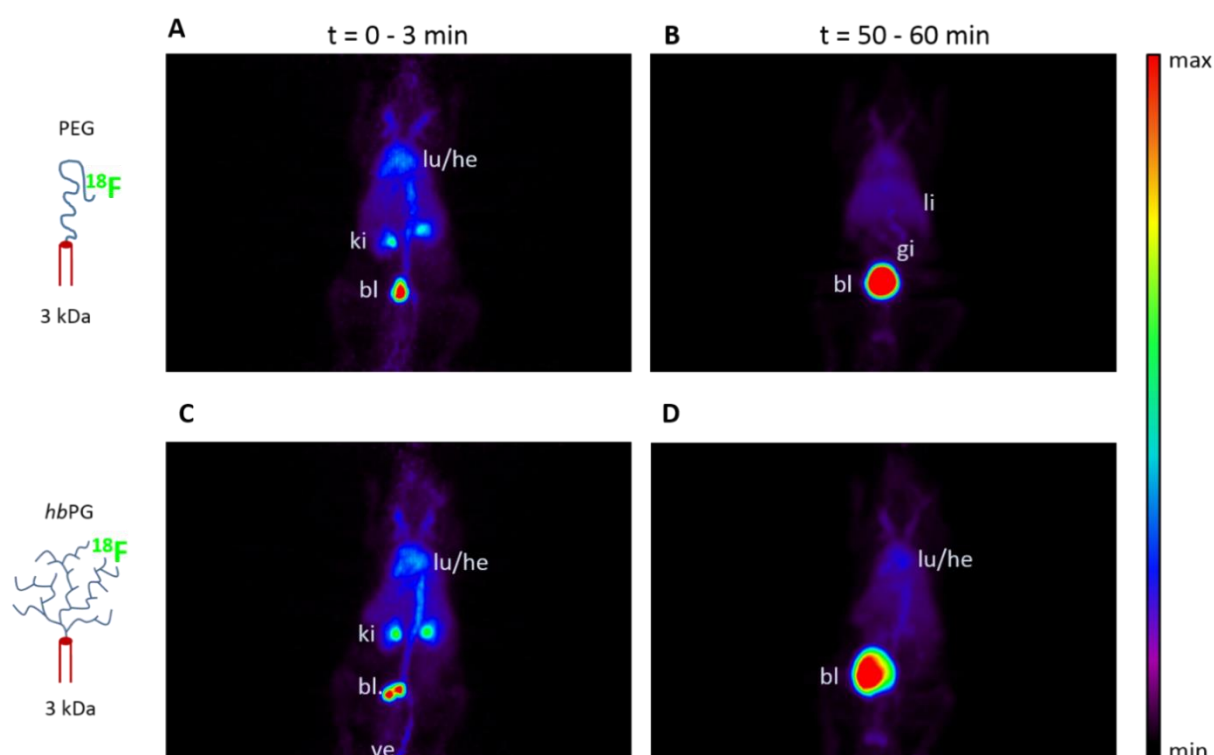


Figure 35: MIPs (coronal views) of whole body biodistributions for ^{18}F -labeled **BisHD-PEG3k** (top) and **BisHD-hbPG3k** (bottom) lipids in mice, recording images in time periods of 0 – 3 min (**A, C**) and 50 – 60 min (**B, C**) after injection. Abbreviation of organs include lu = lung, he = heart, ki = kidneys, bl = bladder, ve = vena, gi = gastrointestinal tract.

To analyze the behavior of the BisHD-polyether lipids *in vivo*, μPET experiments of the ^{18}F -labeled polymers in healthy C57BL/6 mice were conducted.

Figure 35 presents coronal views of maximum intensity projections (MIPs) for the PET images of hyperbranched and linear polyether-lipids recorded in time periods of 0 – 3 min (**A, C**) and 50 – 60

min (**B**, **D**) after injection. In early phases (0 – 3 min), increased uptake was recorded in organs of high blood supply such as the heart and the lung, whereas maximum intensities were observed in the kidneys and the bladder for both lipids. In later timeframes (50 – 60 min), predominant uptake was detected in the bladder of the mice.

These results suggest rapid clearance of ^{18}F -labeled *hbPG*- and PEG-lipids by glomerular filtration leading to an accumulation in the bladder which is in accordance with findings obtained for cholesteryl polyether-lipids of comparable molecular weights.^[16] Small differences in the biodistribution of the two lipids are apparent from images **B** and **D** indicating minor uptake of the PEG-lipids in the liver and the gastrointestinal tract, which is less pronounced for the hyperbranched polymers. With respect to a potential application in liposomal formulations, efficient renal clearance of the lipids is highly desirable to assure excretion after successful drug delivery and decomposition of liposomes, to avoid accumulation in the tissue or uptake by the MPS.

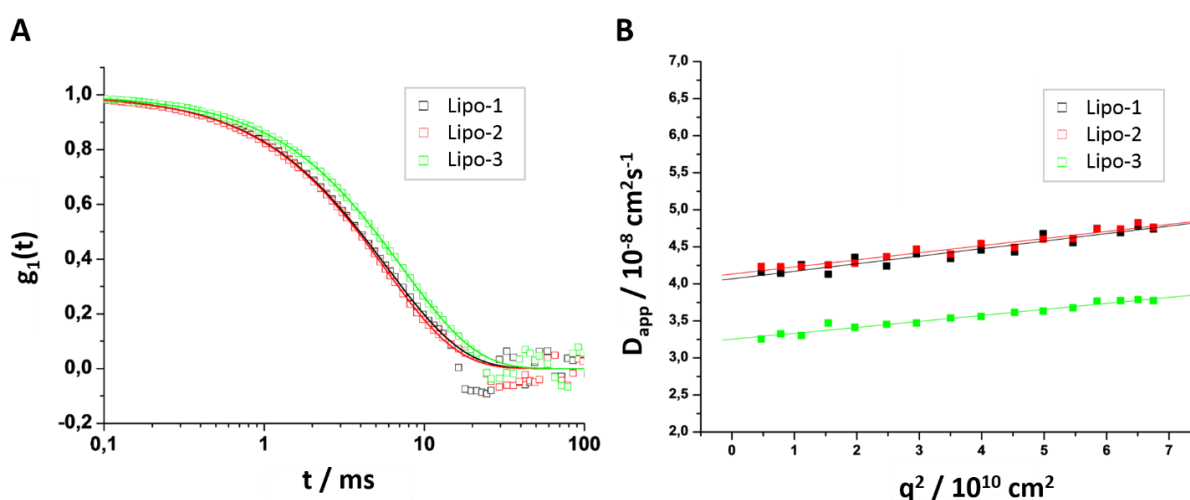


Figure 36: **A:** Autocorrelation function $g_1(t)$ of three liposome formulations (Lipo-1, Lipo-2, Lipo-3) prepared via membrane extrusion obtained from dynamic light scattering (DLS) at a scattering angle of 30° . **B:** Plots of the apparent diffusion coefficient D_{app} vs. scattering vector q for Lipo-1, Lipo-2 and Lipo-3 to assess the z-averaged diffusion coefficient $\langle D \rangle_z$ by extrapolation to $q = 0$.

Furthermore, liposomes composed of **BisHD-PEG3k** (5 mol%), 1,2-dioleoyl-glycero-*sn*-3-phosphocholine DOPC (55 mol%) and cholesterol (40 mol%) were prepared by successive extrusion

through polycarbonate membranes with pore sizes of 400 nm and 100 nm. Subsequently, dynamic light scattering (DLS) was performed to determine the hydrodynamic radius R_h and the size distributions of liposomes (μ^2). Figure 36 compiles experimental results from DLS measured at multiple angles for three liposome formulations Lipo-1 (black), Lipo-2 (red), Lipo-3 (green). The autocorrelation functions $g_1(t)$ (A) recorded for liposomes at a scattering angle of 30° are shown as an example. Apparent diffusion coefficients $D_{\text{app}}(q)$ could be calculated from $g_1(t)$ and plotting of D_{app} against the respective scattering vector q allowed determination of the z-averaged diffusion coefficient $\langle D \rangle_z$ via extrapolation to $q = 0$.

By calculating the hydrodynamic radius R_h of liposomes from $\langle D \rangle_z$ using the Stokes–Einstein equation, values of 53 nm (Lipo-1, Lipo-2) and 67 nm (Lipo-3) were determined with narrow size distributions ($\mu^2 < 0.13$) of the liposomes. These results are in agreement with DLS data obtained for cholesterol–PEG-liposomes prepared by membrane extrusion,^[16] and are close to the proposed optimum size for nanoparticles in tumor therapy.^[17] Deviations in the size of liposomes are likely to be due to different extrusion speeds during sample preparation.

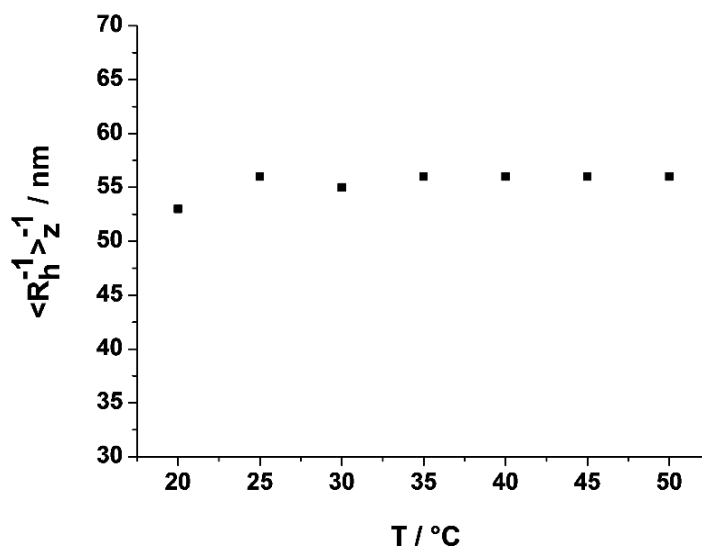


Figure 37: Z-averaged hydrodynamic radius R_h of Lipo-1 at different temperatures determined by DLS.

In addition, temperature-dependency of R_h was measured for Lipo-1 in a temperature range of 20 - 50 $^\circ\text{C}$ in PBS buffer, to evaluate the stability of the stealth liposomes upon heating. Clearly, the

hydrodynamic radius of the liposomes remained almost unaffected by the temperature increase as visualized in Figure 37. Changes in the size of liposomes could be expected in case of inter-liposomal lipid exchange or aggregation. The temperature range examined in this experiment by far exceeded the physiological range, yet, these results suggest steric stabilizing of the surface-modified liposomes to a certain degree that prevents aggregation in solution.

Finally, liposomes were prepared via membrane extrusion containing ^{18}F -radiolabeled **BisHD-hbPG3k** lipids (5 mol%) and their *in vivo* biodistribution was investigated in healthy C57BL/6 mice *via* μPET imaging in time periods of 0-3 min, 50-60 min and 3.5-4 h after injection. The preparation of liposomes has been adapted from previous reports on PET imaging of cholesterol-based *hbPG*-lipids.^[16] Coronal views of MIPs for liposomes modified with ^{18}F -radiolabeled **BisHD-hbPG3k** lipids are presented in Figure 38.

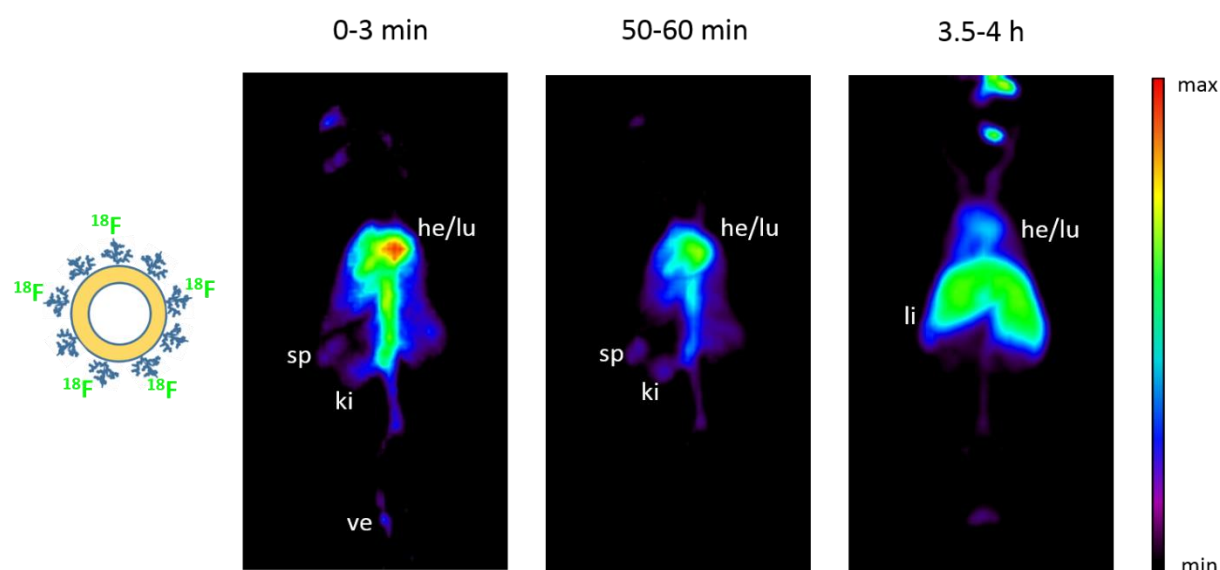


Figure 38: MIPs (coronal views) of whole body biodistributions for liposomes containing ^{18}F -labeled **BisHD-hbPG3k** lipids (5 mol%) in healthy C57BL/6 mice, recording images in time periods of 0 – 3 min, 50 – 60 min and 3.5 – 4.0 h after injection. Abbreviation of organs include lu = lung, he = heart, ki = kidneys, sp = spleen, bl = bladder, ve = vene.

In early (0-3 min) to medium (50-60 min) phases, maximum signal intensities were observed in organs of high blood supply especially the heart and the lung, while minor uptake by the kidneys

and the spleen could be detected. In later timeframes (3.5-4 h), increased uptake by the liver was recorded, while lower emission intensities were observed in the heart and the lung. In contrast to the results from PET imaging of the pure lipids presented in Figure 35, no uptake by the bladder and thus no excretion *via* the kidney pathway was observed for radiolabeled lipid components.

The PET results indicate blood circulation of the *hbPG*-modified liposomes for more than 1h without renal excretion of labeled lipid components suggesting *in vivo* stability of the liposomal carriers in this time period. In comparison to previous *in vivo* studies of liposomes containing cholesterol-based *hbPG*-lipids that revealed rapid disintegration of liposomal carriers in the blood stream,^[16] improved *in vivo* performance can be concluded for the liposomes modified with dialkyl-derived *hbPG*-lipids. Furthermore, these results are in accordance with recently elucidated insights on the *in vitro* membrane stability of polyether-functional lipids that showed a more stable anchorage for dialkyl-based lipids compared to cholesterol-functional lipids.^[15] To the best of our knowledge, this is the first report that provides evidence for a *hbPG*-mediated 'stealth shielding' of liposomes *in vivo* motivating a stronger emphasis on multifunctional hyperbranched polyglycerol in liposomal applications.

Conclusion

In this work, we envisaged to investigate the properties of *hbPG*- and PEG-functional dialkyl-lipids with respect to their performance in liposomal formulations. By using bishexadecyl glycerol (BisHD) as an initiator for the anionic ring-opening polymerization (AROP) of ethoxyethyl glycidyl ether (EEGE), a novel linear polyglycerol (*linPG*) lipid was obtained after acidic hydrolysis of acetal protecting groups. The *linPG* precursor served as a macroinitiator for the slow monomer addition of glycidol to yield **BisHD-*hbPGs*** with molecular weights of 3 to 7 kg mol⁻¹ exhibiting moderate molecular weight distributions ($\mathcal{D} \leq 1.3$). For comparative purposes, **BisHD-PEGs** of similar molecular weights and with low dispersities ($\mathcal{D} < 1.1$) were synthesized using BisHD as an initiator for the AROP of ethylene oxide. The structures were analyzed by SEC, ¹H NMR and ¹³C NMR spectroscopy. Studies on the properties of liposomes containing the **BisHD-*hbPG*** and **BisHD-PEG** lipids prepared *via* dual centrifugation (DC) suggest promising perspectives to control the size of liposomes in the range of 100 nm for BisHD-lipid molecular weights above 5 kg mol⁻¹, while retaining high encapsulation efficiencies of the model cargo calcein. *In vivo* biodistribution data of the radio-labeled lipids obtained by positron emission tomography (PET) imaging are presented confirming rapid clearance of *hbPG*- and PEG-lipids *via* the kidney pathway. Furthermore, PET imaging of liposomes modified with ¹⁸F-labeled **BisHD-*hbPG***-lipids was performed revealing blood circulation times of more than 1h. Aside from extending the scope of hyperbranched lipids in terms of architectures, molecular weights and synthetic accessibility from a novel EEGE precursor, these findings suggest promising perspective regarding size control of liposomes in DC preparation. Most notably, the PET studies provide evidence for ‘stealth’ properties of *hbPG*-modified liposomes *in vivo* that may serve as additional incentive for the application of hyperbranched polyglycerols in liposomal formulations as multifunctional alternatives to PEG.

References

- [1] Pattni, B. S.; Chupin, V. V.; Torchilin, V. P. *Chem. Rev.*, **2015**, *115*, 10938–10966.
- [2] Torchilin, V. P. *Nat Rev Drug Discov*, **2005**, *4*, 145–160.
- [3] Dawidczyk, C. M.; Kim, C.; Park, J. H.; Russell, L. M.; Lee, K. H.; Pomper, M. G.; Searson, P. *C. J. Control. Release*, **2014**, *187*, 133–144.
- [4] Matsumura, Y.; Maeda, H. *Cancer Res.*, **1986**, *46*, 6387.
- [5] Hobbs, S. K.; Monsky, W. L.; Yuan, F.; Roberts, W. Gregory; Griffith, L.; Torchilin, V. P.; Jain, R. K. *PNAS*, **1998**, *95*, 4607–4612.
- [6] Sofou, S.; Sgouros, G. *Expert Opin. Drug Deliv.*, **2008**, *5*, 189–204.
- [7] Gupta, B.; Levchenko, T. S.; Torchilin, V. P. *Oncology Research Featuring Preclinical and Clinical Cancer Therapeutics*, **2006**, *16*, 351–359.
- [8] Pappalardo, J. S.; Quattrocchi, V.; Langellotti, C.; Di Giacomo, S.; Gnazzo, V.; Olivera, V.; Calamante, G.; Zamorano, P. I.; Levchenko, T. S.; Torchilin, V. P. *J. Control. Release*, **2009**, *134*, 41–46.
- [9] Baek, S. E.; Lee, K. H.; Park, Y. S.; Oh, D.-K.; Oh, S.; Kim, K.-S.; Kim, D.-E. *J. Control. Release*, **2014**, *196*, 234–242.
- [10] Sawant, R. R.; Torchilin, V. P. *AAPS*, **2012**, *14*, 303–315.
- [11] Kainthan, R. K.; Janzen, J.; Levin, E.; Devine, D. V.; Brooks, D. E. *Biomacromolecules*, **2006**, *7*, 703–709.
- [12] Hofmann, A. M.; Wurm, F.; Hühn, E.; Nawroth, T.; Langguth, P.; Frey, H. *Biomacromolecules*, **2010**, *11*, 568–574.
- [13] Fritz, T.; Hirsch, M.; Richter, F. C.; Müller, S. S.; Hofmann, A. M.; Rusitzka, Kristiane A. K.; Markl, J.; Massing, U.; Frey, H.; Helm, M. *Biomacromolecules*, **2014**, *15*, 2440–2448.
- [14] Mohr, K.; Müller, S. S.; Müller, L. K.; Rusitzka, K.; Gietzen, S.; Frey, H.; Schmidt, M. *Langmuir*, **2014**, *30*, 14954–14962.

- [15] Fritz, T.; Voigt, M.; Worm, M.; Negwer, I.; Müller, S. S.; Kettenbach, K.; Ross, T. L.; Roesch, F.; Koynov, K.; Frey, H.; Helm, M. *Chem. Eur. J.*, **2016**, *22*, 11578–11582.
- [16] Reibel, A. T.; Müller, S. S.; Pektor, S.; Bausbacher, N.; Miederer, M.; Frey, H.; Rösch, F. *Biomacromolecules*, **2015**, *16*, 842–851.
- [17] Nagayasu, A.; Uchiyama, K.; Kiwada, H. *Adv. Drug Delivery Rev.*, **1999**, *40*, 75–87.
- [18] Fitton, A. O.; Hill, J.; Jane, D. E.; Millar, R. *Synthesis*, **1987**, *1987*, 1140–1142.
- [19] Seiwert, J.; Leibig, D.; Kemmer-Jonas, U.; Bauer, M.; Perevyazko, I.; Preis, J.; Frey, H. *Macromolecules*, **2016**, *49*, 38–47.
- [20] Massing, U.; Cicko, S.; Ziroli, V. *J. Control. Release*, **2008**, *125*, 16–24.
- [21] Meier, S.; Pütz, G.; Massing, U.; Hagemeyer, C. E.; Elverfeldt, D. von; Meißner, M.; Ardipradja, K.; Barnert, S.; Peter, K.; Bode, C.; Schubert, R.; von zur Muhlen, C. *Biomaterials*, **2015**, *53*, 137–148.
- [22] Allen, T. M.; Everest, J. M. *J. Pharmacol. Exp. Ther.*, **1983**, *226*, 539.
- [23] Renz, P.; Kokkinopoulou, M.; Landfester, K.; Lieberwirth, I. *Macromolecular Chemistry and Physics*, **2016**, *217*, 1879–1885.
- [24] Cole, J. T.; Holland, N. B. *Drug Deliv. Transl. Res.*, **2015**, *5*, 295–309.
- [25] Kunjachan, S.; Ehling, J.; Storm, G.; Kiessling, F.; Lammers, T. *Chem. Rev.*, **2015**, *115*, 10907–10937.
- [26] Jacobson, O.; Kiesewetter, D. O.; Chen, X. *Bioconjugate Chem.*, **2015**, *26*, 1–18.
- [27] Marik, J.; Tartis, M. S.; Zhang, H.; Fung, J. Y.; Kheirrolomoom, A.; Sutcliffe, J. L.; Ferrara, K. *W. Nucl. Med. Biol.*, **2007**, *34*, 165–171.
- [28] Oku, N.; Yamashita, M.; Katayama, Y.; Urakami, T.; Hatanaka, K.; Shimizu, K.; Asai, T.; Tsukada, H.; Akai, S.; Kanazawa, H. *Int. J. Pharm.*, **2011**, *403*, 170–177.

Supporting Information

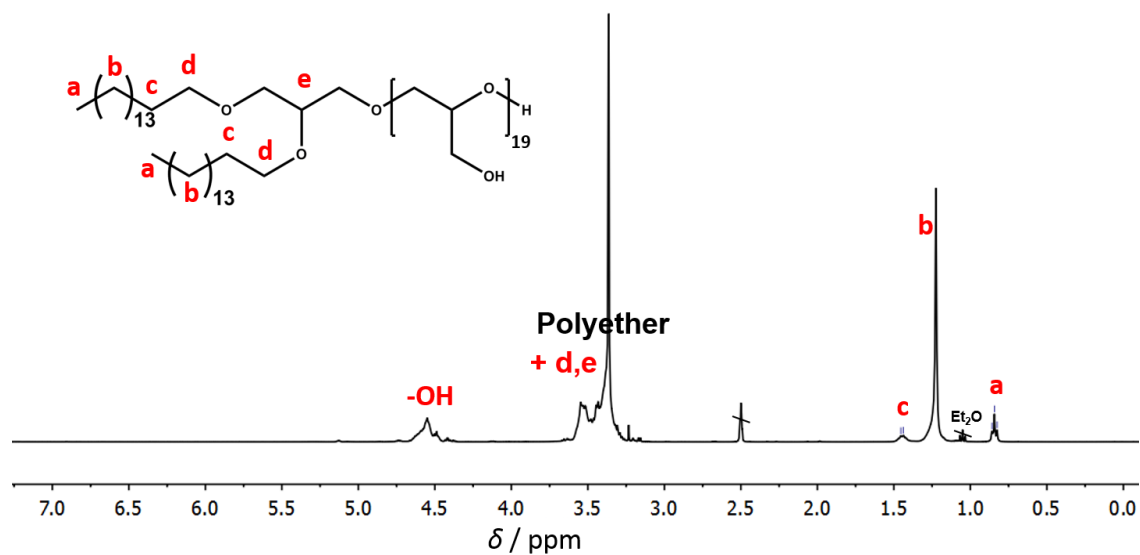


Figure S-39: ^1H NMR spectrum of BisHD-*linPG* macroinitiator (**3**) measured in DMSO-d_6 at 400 MHz.

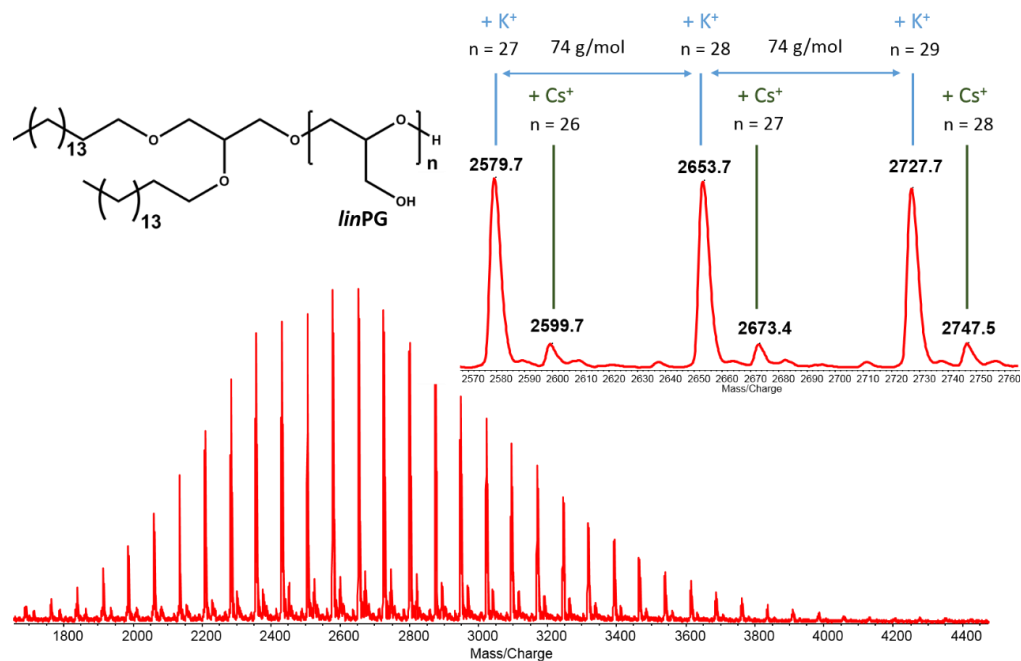


Figure S-40: MALDI ToF MS spectrum of BisHD-*linPG* recorded using KTFA as salt and CHCA as matrix.

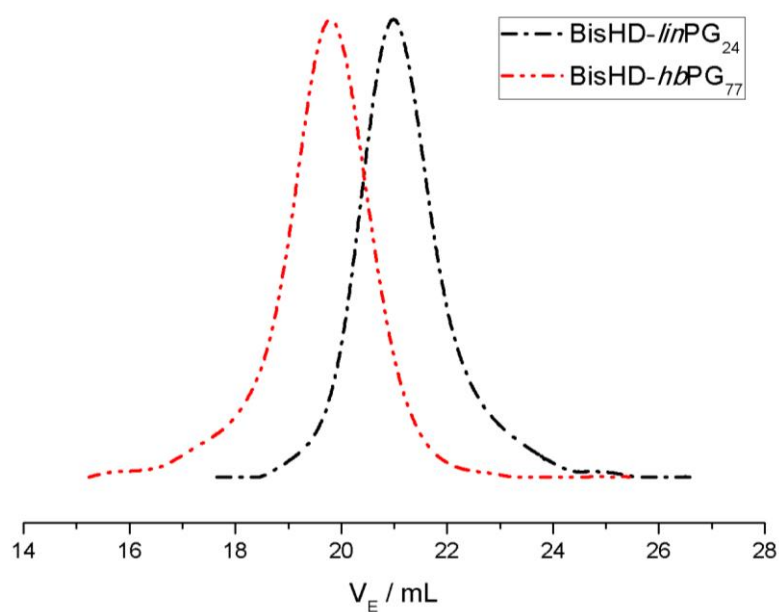


Figure S-41: SEC traces of the macroinitiator **BisHD-*lin*PG₂₄** and **BisHD-*hb*PG₇₇** measured in DMF using RI detection.

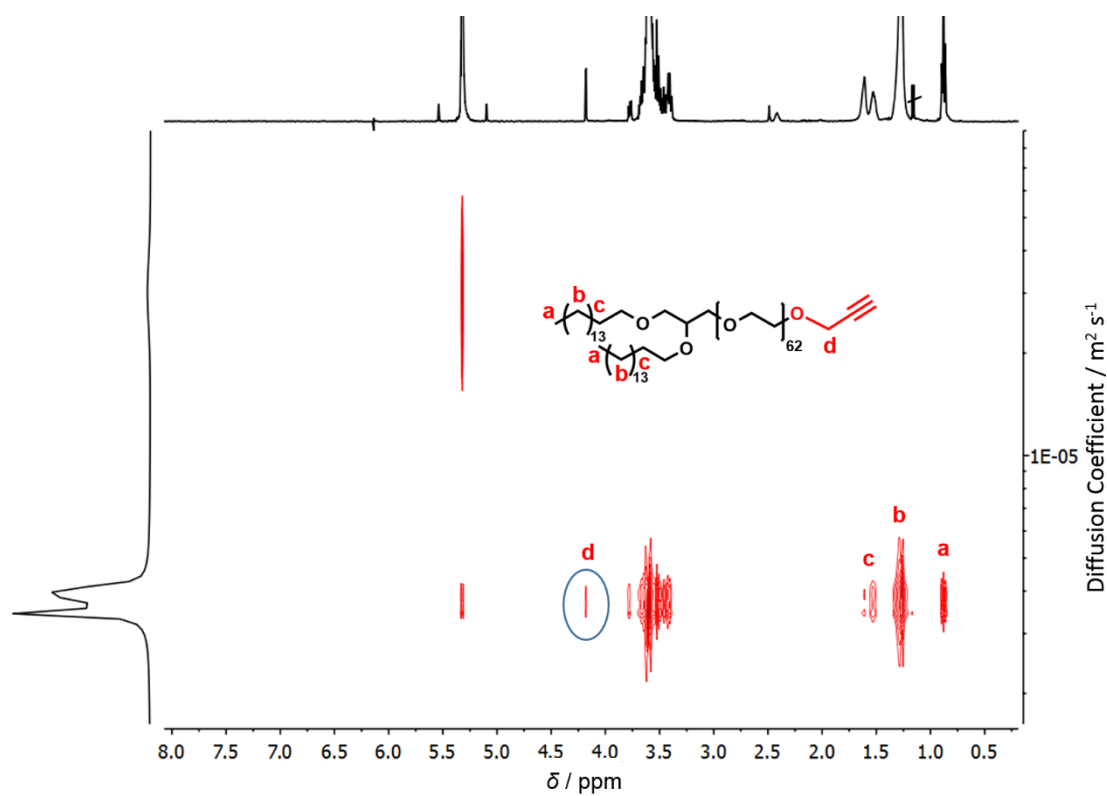


Figure S-42: Diffusion-Ordered NMR spectrum (DOSY) of alkyne-functional **BisHD-PEG₆₂** measured in CD_2Cl_2 .

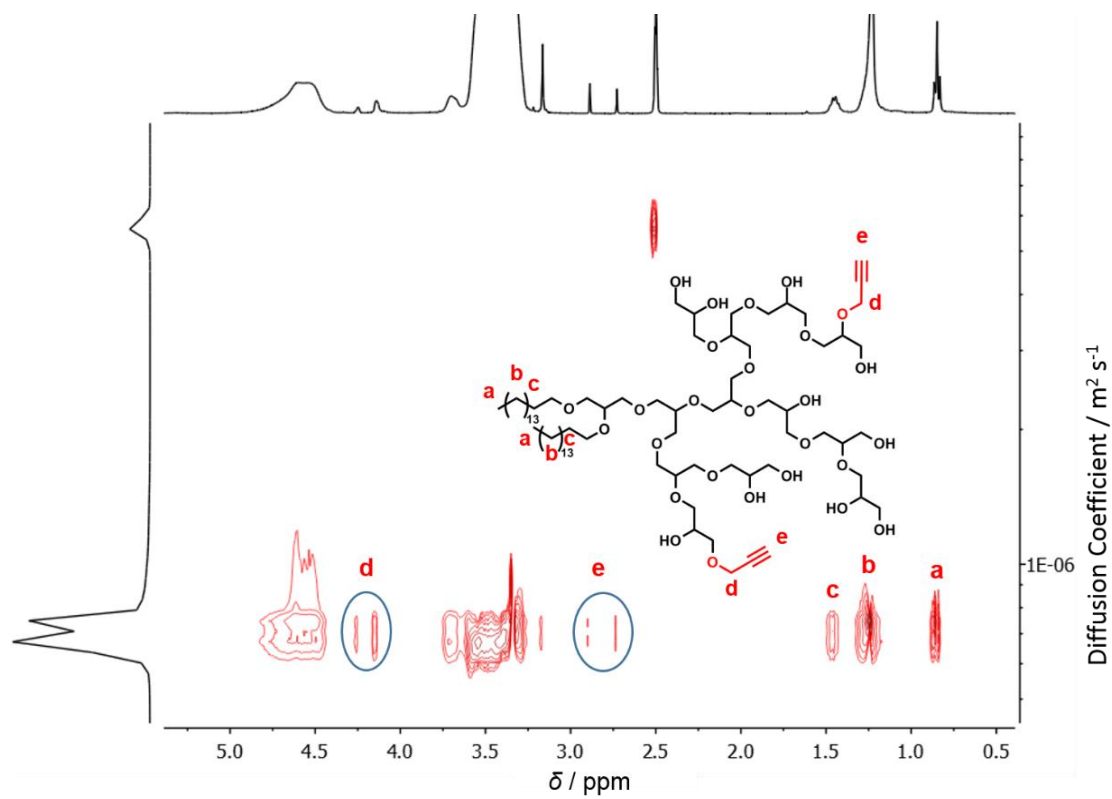


Figure S-43: Diffusion-ordered NMR spectrum (DOSY) of alkyne-functional **BisHD-hbPG₃₂** measured in DMSO-d₆

Outlook

i) pH-Degradable Poloxamer Analogs

In **chapter 2**, the usefulness of acid-cleavable poloxamer analogs **PA** (PEO-*b*-PPO-*b*-PEO copolymers) in miniemulsion polymerization (MEP) was demonstrated, suggesting great potential for the preparation of surfactant-free nanoparticles. MEPs can be employed for the polymerization of numerous monomers to generate nanoparticles comprised of e.g. polyvinyl acetate, polyurethanes or polyacrylonitrile.^[1] By using the acid-sensitive poloxamer analogs it could be possible to further enhance the purity of the resulting nanoparticles and render them suitable for high performance applications. It is well-known that the molecular composition of the surfactant, i.e. the block lengths, crucially influences the emulsification properties, which was also confirmed for **PAs** in the course of this study.

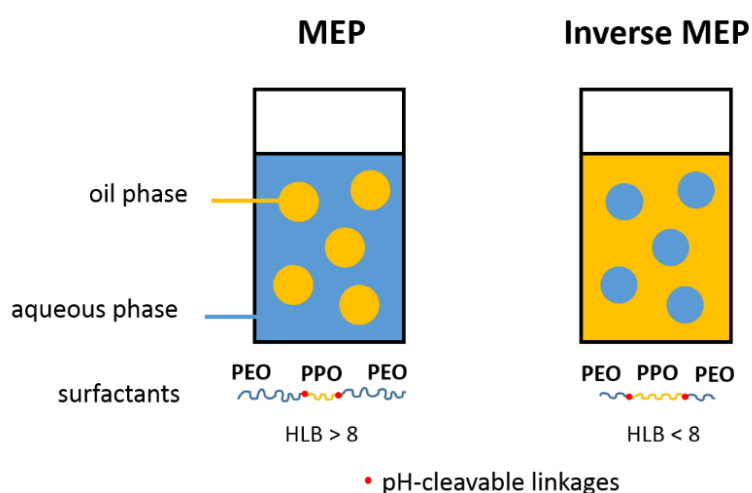


Figure 39: Schematic illustration of oil-in-water miniemulsion polymerization (MEP) and water-in-oil inverse miniemulsion polymerization (inverse MEP), using pH-cleavable poloxamer analogs of different molecular composition with HLB (hydrophilic-lipophilic balance) values below or above 8 to stabilize the respective miniemulsions.

To further extend the scope of the novel surfactants, polymeric amphiphiles with HLB values (hydrophilic-lipophilic balance) below 8, i.e. with high molecular weights of the lipophilic PPO block and low molecular weights of the hydrophilic PEO segments could be synthesized and applied in

inverse MEP techniques (water-in-oil) as illustrated in Figure 39. Consequently, water-soluble monomers such as hydroxyethyl methacrylate, acrylamides or acrylic acid could be polymerized to generate hydrophilic nanoparticles. Since MEP further allows to encapsulate cargo molecules inside of nanoparticles or nanocapsules, drug-loaded, water-soluble, and most importantly, surfactant-free nanostructures could be prepared by **PA**-assisted inverse MEPs. These structures are promising as drug carrier systems for biomedical applications. In case of pH-sensitive therapeutic cargo, it might be necessary to modify the **PA** structures by incorporating cleavable linkages with higher susceptibility towards acid hydrolysis, such as ketals or orthoesters. Drawing benefit from the achievements in **chapter 4**, the synthesis route introduced for asymmetric ketals could provide access to ketal-functional PEO-*b*-PPO-*b*-PEO copolymers for 'burst' pH-responsive behavior of the particle emulsions in mildly acidic media.

ii) pH-cleavable PEGs

The synthesis of poly(ethylene glycol)s (PEG) with in-chain pH-cleavable vinyl ether moieties that are hydrolyzable in a physiologically relevant pH range was developed in **chapter 3**. By capitalizing on the anionic ring-opening copolymerization of ethylene oxide (EO) and 3,4-epoxy-1-butene (EPB) followed by subsequent catalytic isomerization of the double bonds, well-defined and hydroxyl-functional copolymers were accessible. To allow for an application of the pH-cleavable P(EPB-*co*-EG) copolymers as PEG substitutes for polymer-drug conjugates, common bioconjugation routes could be employed, for instance by attaching amino-reactive moieties such as succinimidyl carbonates,^[2] squaric acids,^[3] and 3-thioazolidin-2-thiones,^[4] or thiol-reactive groups like orthopyridyl disulfide,^[5] to the polymers' chain ends. In this manner, ligation of proteins to the degradable, isomerized form of P(EPB-*co*-EG) via their lysine or cysteine residues could be achievable.

Another interesting future objective is the development of a catalyst system that permits control over the content of EPB (E)- and (Z)-isomers in the isomerization step. *In situ* ¹H NMR kinetic studies

detailed in **chapter 3** revealed significantly faster hydrolysis of the (Z)-isomeric form providing perspectives for a fine-tuning of hydrolysis profiles and the respective half-lives in the blood stream. In particular, the design of long-circulating conjugates with molecular weights of the pH-cleavable PEG exceeding the renal filtration limit, appears to be a promising perspective (See Figure 40). The attachment of radioactive tracers or fluorescent labels to the cargo or the polymer, can permit studies on the *in vivo* biodistribution and blood circulation times of the polymer-drug conjugates.

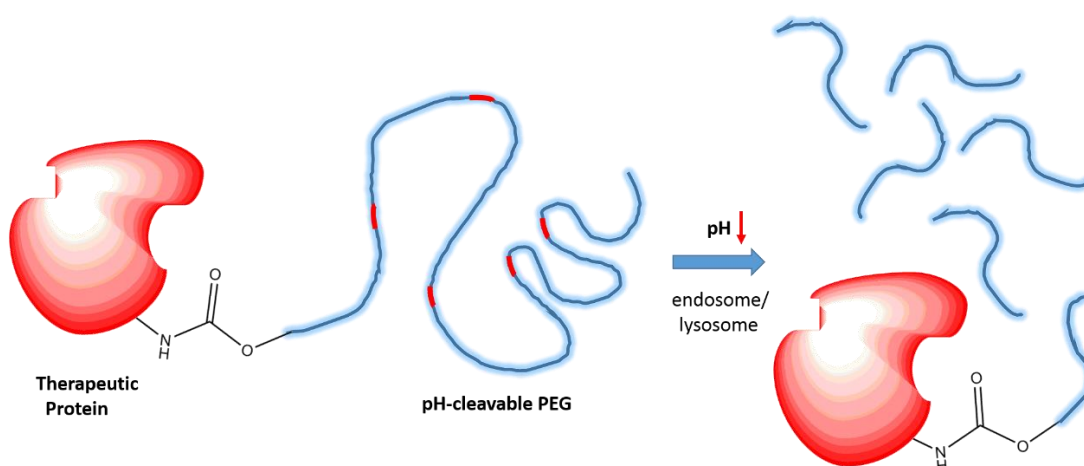


Figure 40: Illustration of a polymer-drug conjugate tethered via a urethane linkage for pH-induced intracellular cleavage and decomposition of PEG chains.

By using lipophilic initiators for the copolymerization of EO and EPB, pH-responsive amphiphilic structures with cleavable hydrophilic polyether blocks could be accessible that might serve as an innovation both for liposomal research and the development of pH-triggered release strategies.

iii) pH-cleavable PEG-Lipids

In **chapter 4**, the development of novel ketal- and acetal-functional dialkyl-PEG lipids was reported with a strong emphasis on elucidating pH-dependent cleavage profiles of the pure lipids as well as evaluating the shedding properties of the lipids in liposomal formulations.

The promising hydrolysis profiles found for the ketal-functional PEG-lipids in liposomes motivate further research activities in this area. A potential next step could be the combination of pH-sheddable liposomes with active targeting strategies. Due to the hydroxyl functionality of the lipids

and the well-established post-modification chemistry of PEG,^[6] attachment of targeting molecules such as folates or aptamers to the PEG-lipids appears achievable. To warrant presentation of the target units on the liposomal surface in order to permit interaction with cellular receptors, post-preparational conjugation of target units to lipids might be necessary. This has already been established for dye-labeling of liposomes.^[7] Furthermore, it appears reasonable to link the target unit to the less rapidly hydrolyzing acetal-containing PEG-lipid in order to avoid premature cleavage of the target function from the carrier. The use of lipid compositions comprised of low amounts of acetal-PEG lipids functionalized with targeting moieties and higher contents of ketal-PEG lipids could be beneficial to induce an effective PEG shedding in the slightly acidic tumor microenvironment in order to promote receptor-mediated uptake into the targeted cells. A certain amount of fusogenic lipids,^[8] e.g. DOPE could further assist destabilization of the liposomal membranes and could induce membrane fusion in endosomal compartments after detachment of the PEG stealth layer. A schematic representation of a stealth liposome including the above-mentioned modifications is shown in Figure 41. The efficacy of the modified stealth liposomes could be evaluated in *in vivo* experiments with tumor-bearing mice.

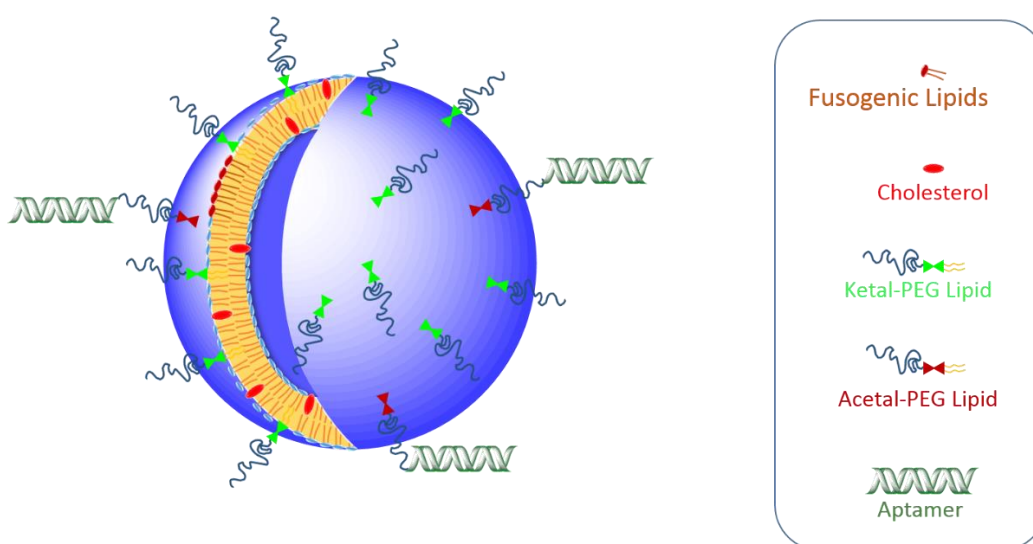


Figure 41: Schematic illustration of an aptamer-modified, pH-sheddable stealth liposome with fusogenic lipids containing fusogenic lipids.

To further extend the scope of the newly developed synthesis strategy of asymmetric ketals in polymers, different alcohol precursors could be employed to synthesize various pH-cleavable PEG-based polymeric architectures that e.g. could serve as an innovation in the design of pH-responsive polymersomes.

Combining the essence of **chapter 3** and **4**, another state-of-the-art approach would be the use of a suitable ketal-containing, functional initiator for the copolymerization of EO and EPB and subsequent conjugation of the copolymers to a therapeutic agent. Thereby, pH-induced “burst dePEGylation” behavior could be triggered in physiological domains of lowered pH values, such as tumor or inflammatory tissues, and different cellular compartments, while assuring partial degradability of the detached PEGs due to the in-chain cleavable vinyl ether linkages.

iv) hbPG-Lipids in Liposomes

The influence of the polyether architecture on the properties of liposomes was studied in **chapter 5** for dialkyl-lipids containing hyperbranched polyglycerol (*hbPG*) or linear PEG of similar molecular weights.

A possible next step would be to further exploit the multifunctionality of *hbPG* by attaching multiple functional substrates onto the surface of liposomes to achieve high local concentrations of the targeting structures that may effectuate a so-called multivalence effect in active targeting. This could be interesting when addressing recognition sites of low binding affinity on cellular surfaces. Here, positron emission tomography (PET) imaging of radiolabeled liposomes could serve to screen the *in vivo* biodistribution of liposomes in mice and allow to unravel the fate of lipid components after receptor-mediated uptake. By using different ligation chemistries, attachment of radioactive tracers as well as targeting ligands to the same lipid could enable simultaneous therapeutic treatment and imaging in terms of a “theranostic” application.

References

- [1] Antonietti, M.; Landfester, K. *Prog. Polym. Sci.*, **2002**, *27*, 689–757.
- [2] Miron, T.; Wilchek, M. *Bioconjugate Chem*, **1993**, *4*, 568–569.
- [3] Dingels, C.; Wurm, F.; Wagner, M.; Klok, H.-A.; Frey, H. *Chem. Eur. J.*, **2012**, *18*, 16828–16835.
- [4] Greenwald, R. B.; Pendri, A.; Martinez, A.; Gilbert, C.; Bradley, P. *Bioconjugate Chem*, **1996**, *7*, 638–641.
- [5] Howorka, S.; Movileanu, L.; Lu, X.; Magnon, M.; Cheley, S.; Braha, O.; Bayley, H. *J. Am. Chem. Soc.*, **2000**, *122*, 2411–2416.
- [6] Thompson, M. S.; Vadala, T. P.; Vadala, M. L.; Lin, Y.; Riffle, J. S. *Polymer*, **2008**, *49*, 345–373.
- [7] Fritz, T.; Hirsch, M.; Richter, F. C.; Müller, S. S.; Hofmann, A. M.; Rusitzka, Kristiane A. K.; Markl, J.; Massing, U.; Frey, H.; Helm, M. *Biomacromolecules*, **2014**, *15*, 2440–2448.
- [8] Deshpande, P. P.; Biswas, S.; Torchilin, V. P. *Nanomedicine*, **2013**, *8*, 1509–1528.

Appendix

A.1 Biodegradable Hyperbranched Polyether-lipids with In-chain pH-sensitive Linkages

S. S. Müller,^{a, b} T. Fritz,^c M. Gimnich,^a M. Worm,^a M. Helm^c and H. Frey^{*a}

^a Institute of Organic Chemistry, Johannes Gutenberg University Mainz, Duesbergweg 10-14, 55128 Mainz, Germany.

^b Graduate School Materials Science in Mainz (MAINZ), Staudingerweg 9, 55128 Mainz, Germany.

^c Institute of Pharmacy and Biochemistry, Johannes Gutenberg University Mainz, Staudingerweg 5, 55128 Mainz, Germany.

Published in Polymer Chemistry, **2016**, 7, 6257–6268.

Reproduced from Müller, S. S.; Fritz, T.; Gimnich, M.; Worm, M.; Helm, M.; Frey, H. *Polym. Chem.*, **2016**, 7, 6257–6268 with permission from The Royal Society of Chemistry 2016.



Cite this: *Polym. Chem.*, 2016, **7**, 6257

Biodegradable hyperbranched polyether-lipids with in-chain pH-sensitive linkages

S. S. Müller,^{a,b} T. Fritz,^c M. Gimnich,^a M. Worm,^a M. Helm^c and H. Frey^{*a}

Hyperbranched polyether-based lipids with cleavable acetal units were obtained via copolymerization of the epoxide inimer 1-(glycidyl)oxyethyl ethylene glycol ether (GEGE) and glycidol, using anionic ring-opening polymerization. Cholesterol-linear polyglycerol (Ch-*lin*PG) was used as a macroinitiator, resulting in branched polyethers with an adjustable amount of acid-cleavable units. Random copolymerization led to Ch-P(GEGE_x-co-G_y) copolymers, whereas sequential copolymerization provided access to Ch-P(GEGE_x-*b*-G_y) amphiphiles. The amount of GEGE was varied between 8–49 mol% of the total amount of monomer units. In addition, hyperbranched polyethers with a single acetal unit were prepared using glycol-1-(cholesteryloxy)ethylether as an initiator for the polymerization of allyl glycidyl ether (AGE) in bulk. Subsequent thiol–ene coupling of mercaptoethanol resulted in the hydroxyl functional macroinitiator used for the polymerization of glycidol. The novel polyether-based lipids were characterized in detail by ¹H NMR spectroscopy and size exclusion chromatography, revealing narrow to moderate molecular weight distributions. Degradation was achieved at pH 2 in a proof-of-principle experiment. Acid-triggered shedding of liposomes was proven using the linear analogue α-(1-(cholesteryloxy)ethoxy)-ω-hydro-PEG-CH₂-C≡CH with one cleavable group and a fluorescence label, Atto 488 azide. Investigation of the acetal-cleavage under neutral and acidic pH (7.4–2.0) via fluorescence spectroscopy was carried out.

Received 27th July 2016.
Accepted 16th September 2016
DOI: 10.1039/c6py01308b

www.rsc.org/polymers

Introduction

Drug delivery vehicles, such as liposomes, are well known carriers, especially in anti-cancer treatment.^{1,2} Liposomes consist of amphiphilic phospholipids that form spherical vesicles in aqueous solution. Effective delivery systems enable an important step towards minimizing undesired effects of extremely toxic drugs, such as doxorubicin, on healthy tissue. Disadvantages like cardiotoxicity of doxorubicin and short circulation times can be avoided. The use of poly(ethylene glycol) (PEG) as a polymer shell at the liposome surface has become a popular approach to create long-circulating liposomes.^{3,4} These systems are also called sterically stabilized or “stealth” liposomes, since the PEGylated liposomes obtain extraordinary properties due to the water-soluble and flexible polymer chains. The presence of PEG results in prolonged blood circulation times,^{5,6} reduced mononuclear phagocyte system (MPS) uptake,⁷ reduced aggregation of the carriers and increasing colloidal stability.⁸ Nevertheless, the gold standard PEG pos-

sesses drawbacks that need to be overcome in advanced drug delivery systems. Having reached the target tissue and cells, the PEG shell can prevent the liposome from penetrating into cells or escaping from the endosome after endocytosis (PEG dilemma).^{9,10} Currently established drug delivery systems that are based on such liposomes fail to release the drug actively and rely on passive diffusion or slow and non-specific liposome degradation. Ideally, PEGylated liposomes profit from the enhanced permeability and retention (EPR) effect,¹¹ and are stable under physiological pH (pH 7.4). Preferentially, the polymer coating would be detached under local pathological conditions such as low pH, leading to destabilization and release of the cargo. The slightly acidic environment in endosomes, tumor tissues, or inflammatory tissue is one of the main differences to healthy tissue. Endocytic pathways lead to a drop from a neutral pH to pH 6 in late endosomes and pH 4 in lysosomes.^{12,13} Cancer and inflammatory tissue also exhibit acidic pH around pH 6.5.¹⁴ A perfectly tuned pH-sensitive nanoparticle would shed the polymer coating and thus enable membrane-membrane fusion and internalization. Fusion with the endosomal membrane is especially important for the release of a cargo into the cytoplasm.^{15,16} This escape is crucial for acid-degradable cargo such as small interfering RNA (siRNA), proteins or acid-labile drugs.¹⁷ The need for “stealth” liposomes that are stable under physiological conditions, but release their content at decreased pH at the site of

^aInstitute of Organic Chemistry, Johannes Gutenberg University Mainz, Duesbergweg 10-14, 55128 Mainz, Germany. E-mail: hfrey@uni-mainz.de

^bGraduate School Materials Science in Mainz (MAINZ), Staudingerweg 9, 55128 Mainz, Germany

^cInstitute of Pharmacy and Biochemistry, Johannes Gutenberg University Mainz, Staudingerweg 5, 55128 Mainz, Germany

action is proposed in an increasing number of publications in this field. Several examples have been reported for controlled release including acetals,^{18,19} vinyl ethers,^{20–22} (di-*ortho* esters,^{23–25} hydrazones,^{26–28} and esters (*e.g.* succinates).^{29,30} The second drawback of PEG is its lack of functional groups. Methoxypoly(ethylene glycol) (mPEG), that is commonly used for the linkage to phospholipids or cholesterol, does not possess additional functional groups for derivatization. However, functional groups are important for the attachment of markers, antibodies or proteins for “active” tumor targeting.³¹ Our group has introduced multifunctional polyether-based lipids synthesized from an epoxide “construction kit”.^{32–34} By using cholesterol directly as the initiator for the oxyanionic ring-opening polymerization (ROP) of various epoxides (ethylene oxide (EO), ethoxyethyl glycidyl ether (EEGE), isopropylidene glycidyl glyceryl ether (IGG), and glycidol), a variety of tailor-made architectures like linear, hyperbranched or linear-hyperbranched polyether amphiphiles can be obtained. The hyperbranched structures can be realized by using glycidol in the ring-opening multibranching polymerization technique *via* slow monomer addition (SMA) of the AB₂ monomer to a multihydroxy-precursor. With this method reproducible and narrowly distributed hyperbranched polyglycerol (*hbPG*) derivatives can be obtained.³⁵ Furthermore, the number of hydroxyl groups can be accurately tuned by the amount of glycidol utilized. *HbPG* has been extensively studied in drug delivery applications and as a biorepellent material due to its extraordinary biocompatibility,^{36–38} multifunctionality and water-solubility.³⁹ Similar to the abovementioned PEG-lipids, its non-biodegradability can be an issue in special applications. To overcome this drawback, pH-sensitive polyether polyketals with tunable degradation in solution were synthesized by Kizhakkedathu and coworkers.^{40–42}

Hyperbranched acetal-containing polyethers were introduced by our group using the epoxide inimer 1-(glycidyoxy)ethyl ethylene glycol ether (GEGE) in a copolymerization reaction with glycidol.⁴³

In the present study, we combine the benefits of multifunctional polyether-based lipids with the degradability of pH-sensitive acetal-containing polyglycerol. In all cases, cholesterol moieties were employed as the hydrophobic part of the amphiphilic structure, ensuring strong interaction with the phospholipid bilayer of liposomes. In the first strategy, we show the synthesis of hyperbranched acetal-containing polyglycerol using GEGE and glycidol in a random copolymerization or a sequential polymerization (Fig. 1a and Scheme 1). In the second approach, we expand the concept of glycol-1-(cholesteryloxy)ethylether recently presented by our group.¹⁸ This initiator is used for the polymerization of AGE, and subsequent thiol-ene coupling with 2-mercaptoethanol followed by the polymerization of glycidol. This pathway results in either linear multihydroxy-functional polyethers or hyperbranched polyethers having exactly one acetal group between the cholesterol anchor and the polymer chain (Fig. 1b and Scheme 2). In the third case, the scope of α -(1-(cholesteryloxy)ethoxy)- ω -hydro-PEG is extended by the functionalization with propargyl bromide followed by copper-catalyzed cycloaddition with Atto 488 azide. Acidic cleavage of the acetal group in functionalized liposomes was investigated *via* fluorescence spectroscopy. The shedding process could be monitored by fluorescence emission of the dye Atto 488 (Fig. 1c and 8).

With these different polymer systems comprising multiple or single acetal groups in hand, we introduce a platform of lipids that combine desired lipid pH-responsiveness with multifunctionality for drug delivery applications.

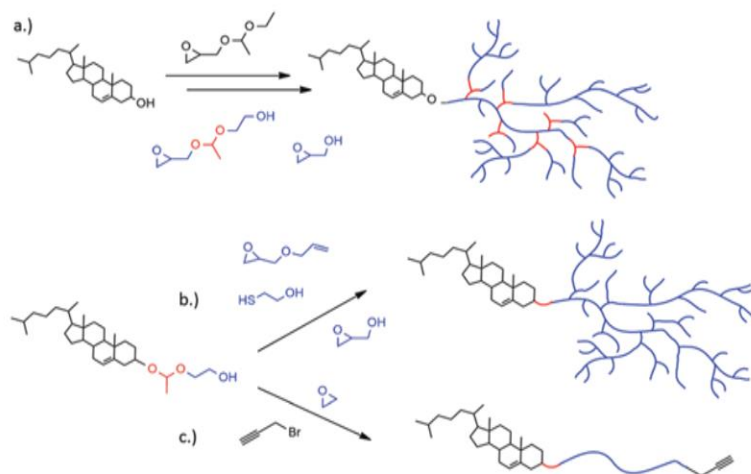
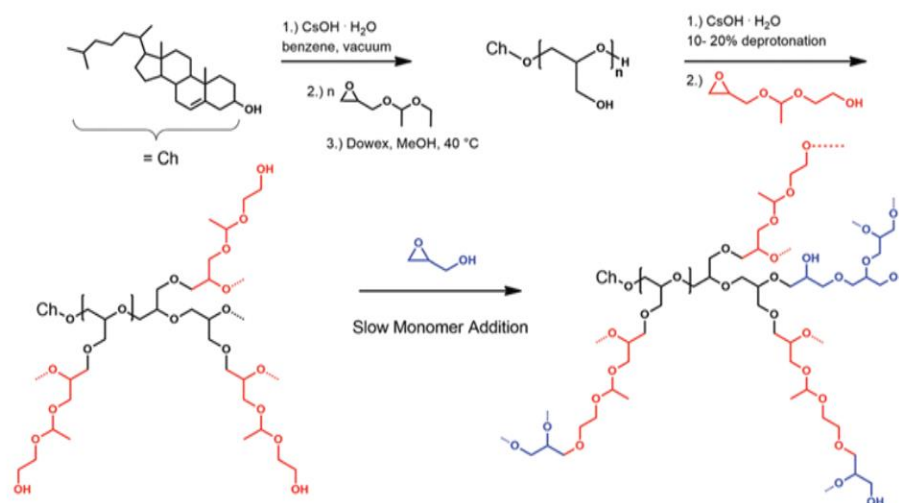
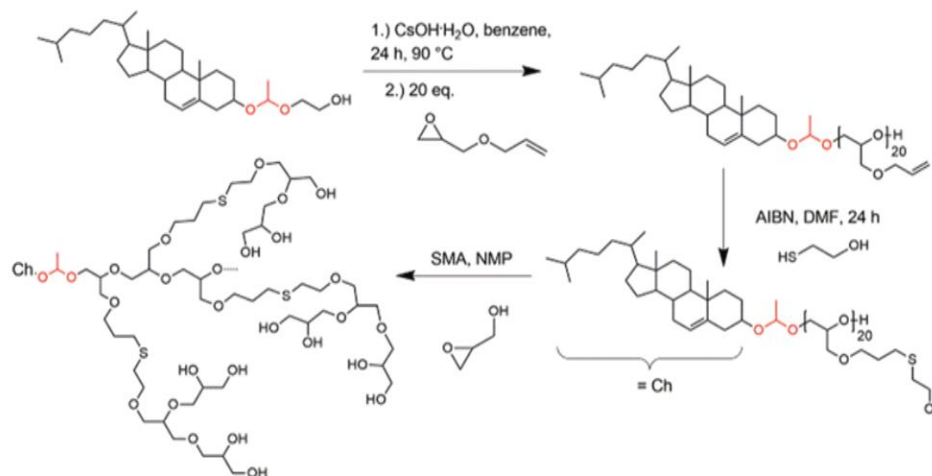


Fig. 1 Synthesis of (a) hyperbranched polyglycerol lipids containing multiple acetal groups by using GEGE and glycidol in a random copolymerization or a sequential polymerization (b) hyperbranched polyether lipids with exactly one acetal group at the block junctions utilizing glycol-1-(cholesteryloxy)ethylether as an initiator (c) linear PEG lipids with one cleavable group functionalized with the fluorescent dye Atto 448.



Scheme 1 Reaction scheme for the synthesis of the macroinitiator *Ch-linPG_n*, followed by the slow monomer addition of GEGE and glycidol, which can be carried out simultaneously or sequentially as depicted here.



Scheme 2 Synthesis of hyperbranched cholesterol-lipids with exactly one acetal group starting from glycol-1-(cholesteryloxy)ethylether (Ch-acetal); (SMA = slow monomer addition).

Experimental

Methods

^1H NMR spectra (300 MHz and 400 MHz) were recorded using a Bruker AC300 or a Bruker AMX400, employing CD_2Cl_2 , MeOD, or $\text{THF-}d_8$ as solvent. All spectra were referenced internally to residual proton signals of the deuterated solvent. Size exclusion chromatography (SEC) measurements were carried out in dimethylformamide (DMF) with 0.25 g L^{-1} LiBr on PSS

HEMA columns (300/100/40). For SEC measurements UV (275 nm) and RI detectors were used. Calibration was carried out using poly(ethylene glycol) (PEG) standards provided by Polymer Standards Service (PSS). Matrix-assisted laser desorption/ionization time-of-flight mass spectrometry (MALDI-ToF MS) measurements were performed on a Shimadzu Axima CFR MALDI-ToF mass spectrometer equipped with a nitrogen laser delivering 3 ns laser pulses at 337 nm. Dithranol was used as a matrix. The sample was prepared by dissolving the polymer in

methanol at a concentration of 10 g L^{-1} . A $10 \mu\text{L}$ aliquot of this solution was added to $10 \mu\text{L}$ of a 10 g L^{-1} solution of the matrix and $1 \mu\text{L}$ of a solution of potassium trifluoroacetate (KTFA) (0.1 M in methanol as a cationization agent). A $1 \mu\text{L}$ aliquot of the mixture was applied to a multistage target, methanol evaporated and a thin matrix/analyte film created.

Liposome preparation

Liposomes bearing acetal-containing cholesterol-based amphiphiles were prepared as described previously.^{44,45} Briefly, $32.5 \mu\text{L}$ of phosphate buffered saline (PBS) (137 mM NaCl , 2.7 mM KCl , $10 \text{ mM Na}_2\text{HPO}_4$, $2 \text{ mM KH}_2\text{PO}_4$, pH 7.4) was added to 17.5 mg of a dried lipid film consisting of cholesterol (Carl Roth), egg phosphatidyl choline (EPC, kindly provided by Lipoid) and α -(1-(cholesteryloxy)ethoxy)- ω -Hydro-PEG₄₆-CH₂-C \equiv CH ($40:55:5$ molar ratio) and 250 mg ceramic beads (SiLiBeads ZY $0.6\text{--}0.8 \text{ mm}$, kindly provided by Sigmund Lindner, Warmensteinach, Germany). Non-cleavable liposomes were prepared with an equivalent cholesterol-PEG-CH₂-C \equiv CH compound. After dual centrifugation in a Rotanta 400 centrifuge (customized with a prototype DC-rotor, Hettich, Tuttlingen, Germany) for 20 min at 2500 RPM and dilution with $100 \mu\text{L}$ PBS, $5 \mu\text{L}$ of the liposome suspension were exposed to click-modification with $50 \mu\text{M}$ Atto 488 azide (Atto-Tec, Siegen, Germany) in Milli-Q water (to a total volume of $40 \mu\text{L}$), phosphate buffer ($5.3 \text{ mM NaH}_2\text{PO}_4$, $94.7 \text{ mM Na}_2\text{HPO}_4$, pH 8), Tris(hydroxypropyltriazolylmethyl)amine (THPTA) (0.5 mM), CuSO₄ (0.1 mM) and sodium ascorbate (2.5 mM) and subsequent gel filtration through Sepharose 2B. Liposome size was obtained *via* dynamic light scattering (DLS) on a Malvern Zetasizer Nano ZS, using disposable poly(styrene) cuvettes (Sarstedt, Germany). $1 \mu\text{L}$ of liposome stock suspension was diluted in 1 mL PBS. After equilibration to $25 \text{ }^\circ\text{C}$, three measurements were performed, using the internal measurement optimization for both attenuator and measurement position. Refractive index (RI) and viscosity of the dispersant was set to 1.330 and 0.8872 cP , the RI of the particle to 1.59 . The absorption of the particle was set to 0.01 and all measurements were performed at a scattering angle of 173° . Cleavage of the polymeric liposome shell was observed *via* fluorescence spectroscopy on a FP-6500 spectrofluorimeter (Jasco, Tokyo, Japan) at 488 nm excitation wavelength and 523 nm emission wavelength during a time course measurement with a data interval of 1 min . $50 \mu\text{L}$ of purified liposomes were combined with 3 mL PBS in a 1 cm^3 quartz glass cuvette (Hellma Analytics, Müllheim, Germany) with a magnetic stirrer. After equilibration for 12 h at $37 \text{ }^\circ\text{C}$, the pH of the suspension was adjusted by addition of $50 \mu\text{L}$ 2 M hydrochloric acid (HCl) (pH 2), $20 \mu\text{L}$ 2 M HCl (pH 3) or $15 \mu\text{L}$ 2 M HCl (pH 5.5). Fluorescence intensity was normalized to the intensity at the beginning of acidification.

Syntheses and reagents

All reagents and solvents were purchased from Acros and used as received, unless otherwise mentioned. Anhydrous solvents were stored over molecular sieves and were purchased from

Aldrich. Deuterated solvents were purchased from Deutero GmbH, and stored over molecular sieves. Cholesterol was purchased from Acros and stored at $8 \text{ }^\circ\text{C}$. Ethoxyethyl glycidyl ether (EEGE) was synthesized as described in the literature,⁴⁶ dried over CaH₂ and cryo-transferred prior to use. Glycidol and *N*-methyl-2-pyrrolidone (NMP) were purified by distillation from CaH₂ directly prior to use. 1-(Glycidyl)ethyl ethylene glycol ether (GEGE) was synthesized according to the literature.⁴³ To release the hydroxyl group in the final reaction step, the benzyl protecting group was removed using catalytic hydrogenation (Pd(OH)₂/C, $10 \text{ wt}\%$). The product was purified by column chromatography in ethyl acetate. Glycol-1-(cholesteryloxy)ethyl-ether and α -(1-(cholesteryloxy)ethoxy)- ω -Hydro-PEG₄₆ were synthesized following reported procedures.¹⁸ Propargyl bromide (0.8 M in toluene) was stored at $4 \text{ }^\circ\text{C}$ and used as received. Allyl glycidyl ether (AGE) was purchased from Acros Organics, dried over CaH₂ and cryo-transferred prior to use. Azobisisobutyronitrile (AIBN, Acros) was recrystallized from MeOH. 2-Mercaptoethanol (Acros) was stored at $5 \text{ }^\circ\text{C}$ and was used as received.

Macroinitiator: cholesterol initiated linear poly(glycerol) (Ch-*lin*PG₂₀; Ch-*lin*PG₁₃). Cholesterol (2.0 g , 5.2 mmol), CsOH monohydrate (0.782 g , 4.7 mmol , 90% of deprotonation), and benzene (8 mL) were placed in a Schlenk flask. The mixture was stirred at $60 \text{ }^\circ\text{C}$ for about 30 min to generate the cesium alkoxide. The salt was then dried under vacuum at $90 \text{ }^\circ\text{C}$ for 24 h . The salt was suspended in 60 mL anhydrous dioxane, the monomer EEGE was added (5.5 mL , 36 mmol , 7 eq.) and the mixture was heated up to $80 \text{ }^\circ\text{C}$ for 24 h . A sample was removed for NMR and SEC analysis, the polymerization was stopped *via* addition of an excess of methanol and the acetal protecting groups of PEEGE were cleaved by the addition of an acidic ion-exchange resin (Dowex 50WX8) and 2 N HCl , stirring at $40 \text{ }^\circ\text{C}$ for 24 h . The solution was filtered, concentrated, and the crude product was precipitated twice in cold diethyl ether. The block copolymer was dried under vacuum. Yield: $\sim 80\%$. No ¹H NMR spectrum was measured before the deprotection step, because residual cholesterol was detected in SEC diagrams, leading to incorrect integration of the resonances. ¹H NMR (300 MHz , MeOD-*d*₄): δ (ppm) = 5.37 (C=CH cholesterol), $3.80\text{--}3.40$ (polyether backbone; CHO cholesterol), $2.40\text{--}0.82$ (CH₂, CH cholesterol), 0.72 (-CH₃ cholesterol).

Ch-Poly(1-(glycidyl)oxy)ethyl ethylene glycol ether-co-glycerol Ch-P(GEGE_{*x*}-co-G_{*y*}). For random copolymerization of GEGE and glycidol Ch-*lin*PG₂₀ was used, and for sequential copolymerization (block copolymers) Ch-*lin*PG₁₃ was used as the macroinitiator. General procedure for the copolymerization of glycidol and GEGE: Ch-*lin*PG₁₃ (0.20 g , 0.15 mmol), CsOH monohydrate (10% of OH groups, 0.035 g , 0.21 mmol), and 1.2 mL of benzene were placed in a Schlenk flask and stirred at $60 \text{ }^\circ\text{C}$ for 30 min . All solvents were removed under reduced pressure, and the initiator salt was dried at $90 \text{ }^\circ\text{C}$ for at least 4 h under high vacuum. The initiator salt was dissolved in NMP and a mixture of glycidol in NMP and GEGE in NMP was slowly added under argon atmosphere using a syringe pump. For random copolymerization the monomers were mixed in

NMP and slowly added, whereas for block copolymers, GEGE in NMP was added before glycidol in NMP was added. The reaction was terminated by the addition of an excess of methanol. The mixture was concentrated and precipitated (2–4 times) into an excess of cold diethyl ether. Yield: 60–75%. ^1H NMR (300 MHz, $\text{MeOD}-d_4$): δ (ppm) = 5.38 (C=CH cholesterol), 4.79 ($\text{H}_3\text{C}-\text{CHO}_2$, GEGE acetal group), 3.80–3.40 (polyether backbone; CHO cholesterol), 2.36–0.87 (CH_2 , CH cholesterol), 1.32 ($\text{H}_3\text{C}-\text{CHO}_2$, GEGE), 0.72 ($-\text{CH}_3$ cholesterol).

α -(1-(cholesteryloxy)ethoxy)- ω -hydro-poly(allyl glycidyl ether) in bulk. Glycol-1-(cholesteryloxy)ethylether (0.3 g, 0.63 mmol), CsOH monohydrate (0.095 g, 0.57 mmol; degree of deprotonation 90%), and benzene (8 mL) were placed in a Schlenk flask. The mixture was stirred for about 30 min at 60 °C to generate the cesium alkoxide. The salt was then dried under vacuum at 90 °C for 3 h. The monomer AGE was added (1.45 mL, 12.6 mmol, 20 eq.) and the mixture was heated up to 65 °C for 24 h. The polymerization was stopped using an excess of methanol. Yield: ~98%. Ch-OCHCH₃O-PAGE₂₀: ^1H NMR (300 MHz, CD_2Cl_2): δ (ppm) = 5.93 ($-\text{CH}_2\text{CH}=\text{CH}_2$, allyl), 5.39 (C=CH cholesterol), 5.33–5.17 ($-\text{CH}_2\text{CH}=\text{CH}_2$, allyl), 4.82 ($\text{H}_3\text{C}-\text{CHO}_2$, acetal group), 4.01 ($-\text{CH}_2\text{CH}=\text{CH}_2$), 3.80–3.39 (polyether backbone; CHO cholesterol), 2.32–0.88 (CH_2 , CH cholesterol), 1.30 ($\text{H}_3\text{C}-\text{CHO}_2$), 0.72 ($-\text{CH}_3$ cholesterol).

Thiol-ene coupling of Ch-OCHCH₃O-PAGE₂₀ with 2-mercaptoethanol. Ch-OCHCH₃O-PAGE₂₀ (0.3 g, 0.1 mmol), 270 mg AIBN (0.75 eq. for each allyl group), and 2-mercaptoethanol (1.55 mL, 22 mmol, 10 eq. of allyl groups) were dissolved in 10 mL DMF. After three freeze–pump–thaw cycles, the mixture was stirred at 75 °C for 24 h. For purification, the reaction mixture was dialyzed against MeOH (MWCO = 1000 g mol⁻¹) for two days and dried under vacuum to give the polymer with a sticky appearance. Yield: 83%. ^1H NMR (400 MHz, $\text{THF}-d_8$): δ (ppm) = 5.34 (C=CH cholesterol), 4.81 ($\text{H}_3\text{C}-\text{CHO}_2$, acetal group), 4.00–3.30 (polyether backbone; CHO cholesterol), 2.72–2.40 ($-\text{CH}_2\text{SCH}_2$), 1.83 ($-\text{CH}_2\text{CH}_2\text{S}$), 2.37–0.87 (CH_2 , CH cholesterol), 0.72 ($-\text{CH}_3$ cholesterol).

Hypergrafting of glycidol onto Ch-OCHCH₃O-thiol-coupling₂₀. The macroinitiator Ch-OCHCH₃O-thiol-coupling₂₀ (0.2 g, 0.05 mmol), CsOH monohydrate (20% of OH groups, 0.033 g, 0.19 mmol), and benzene were placed in a Schlenk flask and stirred at 60 °C for 30 min. All solvents were removed under reduced pressure and the initiator salt was dried at 90 °C for 24 h under vacuum. The initiator salt was dissolved in 0.5 mL NMP and glycidol in NMP (0.5 mL, 20 wt%) was slowly added under argon atmosphere using a syringe pump. The reaction was terminated by the addition of excess of methanol. The mixture was concentrated and precipitated into an excess of cold diethyl ether. Residual NMP could be removed by drying under vacuum and washing with CH_2Cl_2 . Yield: 80%.

^1H NMR (400 MHz, $\text{DMSO}-d_6$): δ (ppm) = 5.32 (C=CH cholesterol), 5.11 ($-\text{OH}$) 4.81 ($\text{H}_3\text{C}-\text{CHO}_2$, acetal group), 3.90–3.20 (polyether backbone; CHO cholesterol), 2.65–2.52 ($-\text{CH}_2\text{SCH}_2$), 1.74 ($-\text{CH}_2\text{CH}_2\text{S}$), 2.40–0.84 (CH_2 , CH cholesterol), 0.65 ($-\text{CH}_3$ cholesterol).

Etherification of α -(1-(cholesteryloxy)ethoxy)- ω -hydro-PEG₄₆ with propargyl bromide. α -(1-(cholesteryloxy)ethoxy)- ω -hydro-PEG₄₆ (0.4 g, 0.16 mmol) was dissolved in anhydrous THF (7 mL), and sodium hydride (9.6 mg, 0.4 mmol) was slowly added under an argon stream at 0 °C. The reaction mixture was stirred for 30 min and after slow addition of propargyl bromide (0.17 mL, 0.6 mmol) allowed to warm up to room temperature. The reaction was stirred at room temperature for 24 h and was filtered. Removal of the solvent *in vacuo* and precipitation in cold diethyl ether resulted in the pure product. Yield: 90%. ^1H NMR (400 MHz, CD_2Cl_2): δ (ppm) = 5.34 (C=CH cholesterol), 4.79 ($\text{H}_3\text{C}-\text{CHO}_2$, acetal group), 4.18 ($-\text{OCH}_2-\text{C}\equiv\text{CH}$), 3.80–3.40 (polyether backbone; CHO cholesterol), 2.49 ($-\text{C}\equiv\text{CH}$), 2.27–0.82 (CH_2 , CH cholesterol), 0.68 ($-\text{CH}_3$ cholesterol).

Results and discussion

Synthesis of amphiphilic hyperbranched lipids with multiple acid-cleavable moieties

Hyperbranched polyether-lipids with multiple pH-responsive acetal groups were prepared by the oxyanionic ring-opening polymerization using cholesterol as an initiator. After deprotonation with cesium hydroxide, the alkoxide was used for the polymerization of ethoxyethyl glycidyl ether (EEGE) with subsequent acidic hydrolysis of the EEGE protecting groups (Scheme 1). Molecular weights for the macroinitiators were in the range of 1300 to 1900 g mol⁻¹ (Table 1) according to ^1H NMR spectroscopy, with an expected underestimation by size exclusion chromatography (SEC). The linear polyglycerol repeating units were calculated by comparing the methyl group of cholesterol (0.72 ppm) and the polyether backbone resonances after acidic cleavage of the acetal protecting groups from the EEGE moieties. Molecular weights calculated by ^1H NMR spectroscopy for both macroinitiators were higher than the theoretical values. We aimed at seven glycerol units per macroinitiator, however, 20 and 13 units were obtained,

Table 1 Characterization data of the macroinitiators (Ch-*lin*PG₂₀; Ch-*lin*PG₁₃) and the pH-responsive copolymers (random: Ch-P(GEGE_x-*co*-G_y); block: Ch-P(GEGE_x-*b*-G_y))

Composition	M_n^{theo}	M_n^{NMR}	M_n^{SEC}	D^{SEC}	GEGE mol%
	g mol ⁻¹				
Ch- <i>lin</i> PG ₂₀	904	1870	830	1.05	—
Ch-P(GEGE ₄ - <i>co</i> -G ₁₈)	4160	4600	1600	1.57	8
Ch-P(GEGE ₂₀ - <i>co</i> -G ₁₉)	5040	7200	2100	1.60	29
Ch- <i>lin</i> PG ₁₃	904	1350	980	1.14	—
Ch-P(GEGE ₁₀ - <i>b</i> -G ₃₆)	4220	4700	2500	1.24	22
Ch-P(GEGE ₁₈ - <i>b</i> -G ₃₆)	4660	6000	3000	1.29	33
Ch-P(GEGE ₁₇ - <i>b</i> -G ₁₈)	4600	4500	2200	1.22	49

M_n^{theo} : theoretical molecular weights; M_n^{NMR} : molecular weights calculated from ^1H NMR *via* end group analysis; M_n^{SEC} : molecular weights obtained from size exclusion chromatography using PEG standards for calibration; $D^{\text{SEC}} = M_w/M_n$: dispersity determined from SEC *via* PEG calibration; GEGE mol%: molar content of GEGE calculated from ^1H NMR.

Paper

respectively. Fast proton exchange results in the protonated form of cholesterol and deprotonated adducts of initiator and the first monomer unit.^{47–49} This leads to different kinetics in the initiation step and the propagation step, since the ethoxylated cholesterol exhibits higher reactivity than the cholesterol alkoxide. Hence, significant amounts of free initiator are found in the reaction mixture when oligomers are targeted.⁵⁰ After acidic hydrolysis of the acetal groups, the polymer was precipitated multiple times in cold diethyl ether to remove excess cholesterol. This led to reduced yields and an enhanced concentration of longer polymer chains.

The resulting linear polyglycerol amphiphiles (Ch-*lin*PG₂₀; Ch-*lin*PG₁₃) functioned as a macroinitiator for the slow monomer addition of 1-(glycidyoxy)ethyl ethylene glycol ether (GEGE) and glycidol. Partial deprotonation and slow monomer addition allows good control over the alkoxide concentration resulting in equal growth of the polymer chain ends. This technique narrows the molecular weight distribution and prevents undesired homopolymerization of the cyclic imers.⁵¹ Deprotonation of the macroinitiator was adjusted to 10% (relative to the total amount of hydroxyl groups) in order to ensure solubility in *N*-methyl-2-pyrrolidone (NMP). Both monomers, *i.e.* GEGE and glycidol, can be copolymerized randomly or sequentially. The reaction route is shown in Scheme 1 (*vide supra*). The advantage of a sequential addition of the monomers, in which GEGE is polymerized first, derives from the proximity of the cleavable acetal group to the cholesterol anchor group. Acidic cleavage would lead to scission near the phospholipid bilayer in the final liposomes, which could enhance shedding of the polymer and drug release.

This approach enabled the synthesis of a series of copolymers bearing multiple acetal groups distributed in the hyperbranched polymer or located near the cholesterol anchor (Table 1).

The random copolymers were prepared from a macroinitiator consisting of 20 linear glycerol units, whereas for the sequentially synthesized copolymers the macroinitiator Ch-*lin*PG₁₃ was used. Molecular weights of the hyperbranched lipids were approx. 5000 g mol⁻¹, again with an underestimation in SEC due to differences in the hydrodynamic radius compared to the linear PEG polymer used for calibration. On the other hand, we assume a slight overestimation of the molecular weights in ¹H NMR spectroscopy, since residual solvent resonances can overlap with the polyether backbone signals. Molecular weight distributions ($D = M_w/M_n$) below 1.15 were found for the two macroinitiators, whereas for the hyperbranched copolymers D_s below 1.60 could be achieved. The last column of Table 1 summarizes the mol% of GEGE, which were successfully tuned between 8 mol% and 49 mol% (in relation to the total amount of monomer units).

Fig. 2 depicts SEC traces for a selection of copolymers that were synthesized from Ch-*lin*PG₁₃ (black solid line, Fig. 2). All distributions were monomodal and molecular weights for the Ch-P(GEGE-*b*-G_{*y*}) copolymers were shifted to lower elution volumes compared to the macroinitiator. Due to the underestimation of molecular weights in SEC, absolute molecular

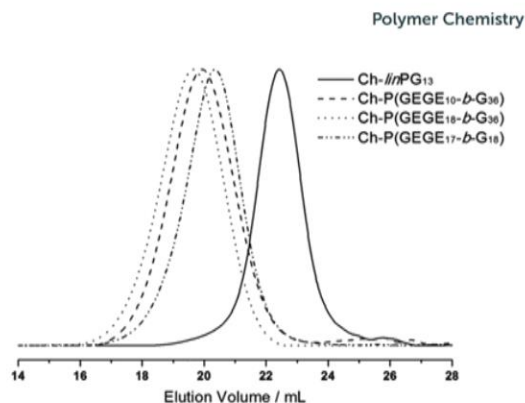


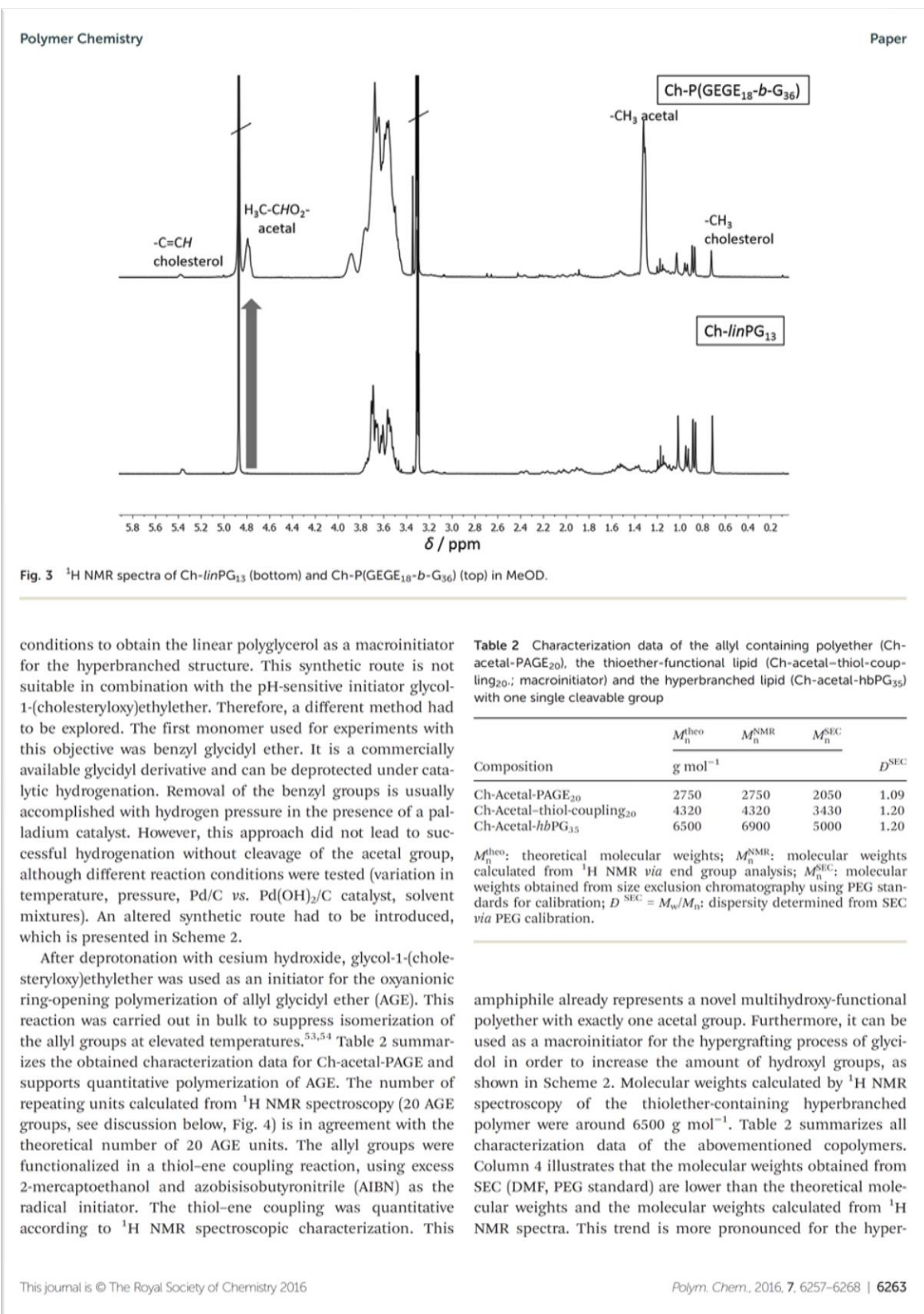
Fig. 2 SEC traces (RI detection; DMF) for selected copolymer samples that were synthesized from Ch-*lin*PG₁₃ (black solid line).

weights were calculated from ¹H NMR integration ratios of the resonances for the methyl group of cholesterol at 0.72 ppm and the polyether signals between 4.00–3.27 ppm (Fig. 3). The number of GEGE units was calculated by comparing the integration of the initiator signals (–CH₃; 0.72 ppm) with the acetal resonance at 4.79 ppm (arrow in Fig. 3). The methyl group of the acetal moieties is observed at 1.32 ppm. As an example, Fig. 3 illustrates the ¹H NMR spectra of Ch-*lin*PG₁₃ (bottom) and Ch-P(GEGE₁₈-*b*-G₃₆) (top) in MeOD.

Synthesis of amphiphilic hyperbranched lipids with exactly one acid-cleavable moiety

In a previous publication, we presented the synthesis of glycol-1-(cholesteryloxy)ethylether (Ch-acetal) as a pH-sensitive initiator for the anionic ring-opening polymerization of ethylene oxide.¹⁸ This initiator can be accessed *via* a three-step procedure by, first, synthesizing 2-acetoxyethyl vinyl ether⁵² which can then be converted with commercially available cholesterol under acid catalysis to introduce the acetal group. After saponification of the acetate protecting group, the hydroxyl-functional initiator glycol-1-(cholesteryloxy)ethylether was obtained, which can be used in the anionic polymerization of various epoxides. It was also shown that the pH-sensitive lipid can be cleaved under acidic conditions.¹⁸ Therefore, they are applicable in drug delivery systems, especially for tumor targeting, where the acidic pH of the tumor can be exploited in order to shed the polymer from the vesicle. Here, we expand the idea of exactly one acid-cleavable group in lipids from linear to hyperbranched polyethers. Decomposition products are cholesterol (natural membrane component), biocompatible hyperbranched polyglycerol and acetaldehyde. Since usually the polymer has a molecular weight below 6000 g mol⁻¹ excretion by the kidney would be feasible after detachment from the hydrophobic anchor.

The abovementioned EEGE monomer contains an acetal protecting group, which is suitable for the oxanionic ring-opening polymerization, but has to be cleaved under acidic



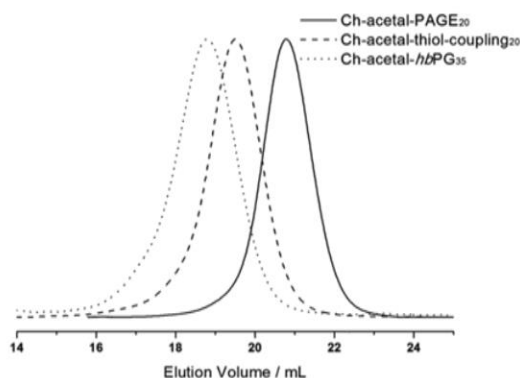


Fig. 4 SEC traces (RI detection; DMF) for the copolymers with one single acetal group; allyl containing polyether Ch-acetal-PAGE₂₀ (black solid line), thioether-containing lipid Ch-acetal-thiol-coupling₂₀ (dashed line), hyperbranched lipid Ch-acetal-hbPG₃₅ (dotted line).

branched structure due to the influence of the hyperbranched, globular polyglycerol on the hydrodynamic radius of the polymers compared to linear PEG. Values of D were below 1.2 (last column, Table 2). Fig. 4 depicts the SEC traces for all three

polymer species, revealing narrow and monomodal molecular weight distributions.

Molecular weights, degrees of polymerization, and the degree of functionalization with 2-mercaptoethanol were calculated from ¹H NMR spectroscopy. The spectra are shown in Fig. 5, in which the allyl functional polymer Ch-acetal-PAGE₂₀ (red, top) was measured in CD₂Cl₂, Ch-acetal-thiol-coupling₂₀ (green, middle) was measured in THF-*d*₈, and Ch-acetal-hbPG₃₅ (blue, bottom) was measured in DMSO-*d*₆. The degree of polymerization for the PAGE copolymer was calculated by comparing the integration of the methyl group of cholesterol (0.72 ppm) with the resonance of the allyl proton at 5.93 ppm. Quantitative conversion was observed, and no isomerization of the allyl groups was found. Between 5.17 and 5.39 ppm an overlap of the allyl group and the cholesterol double bond resonances occurs. The acetal group was retained and its signal was detected at 4.82 ppm. The degree of functionalization for Ch-acetal-thiol-coupling₂₀ (green, middle) after thiol-ene coupling was determined by comparing the cholesterol methyl group at 0.72 ppm with the resonances at 1.83 ppm and 2.62 ppm. These two resonances correspond to the methylene groups adjacent to the sulfur (2.62 ppm) and the next but one methylene group. Here, the acetal group at 4.82 ppm and the cholesterol double bond at 5.34 ppm are still intact. After the hypergrafting of glycidol the spectrum for

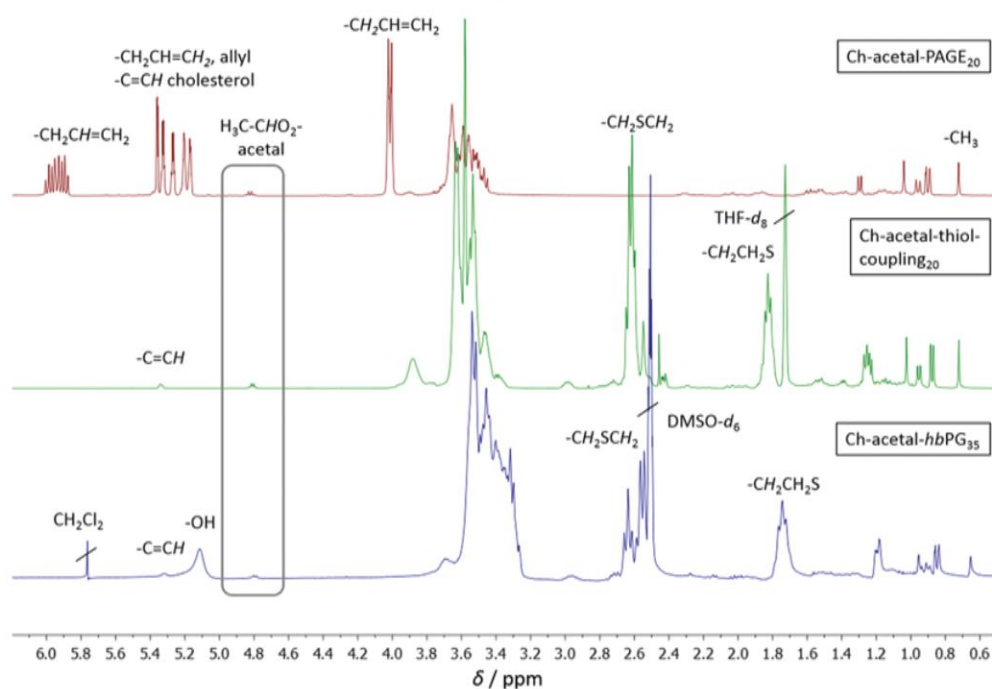


Fig. 5 ¹H NMR spectra for the copolymers with one single acetal group; top to bottom: red: Ch-acetal-PAGE₂₀ in CD₂Cl₂; green: Ch-acetal-thiol-coupling₂₀ in THF-*d*₈; blue: Ch-acetal-hbPG₃₅ in DMSO-*d*₆.

Ch-acetal-*hbPG*₃₅ was obtained in DMSO-*d*₆ (blue, bottom) which clearly shows that the signals of the methylene groups near the sulfur are still present. The grey frame highlights the acetal resonance, which remains at 4.82 ppm in every stadium of the reaction route. The resonances of the hydroxyl groups appear between 5.00 ppm and 5.20 ppm, whereas the cholesterol double bond shows a peak at 5.32 ppm. The integral of the polyether backbone signals between 3.20 ppm and 3.80 ppm is used to calculate the number of glycidol groups by

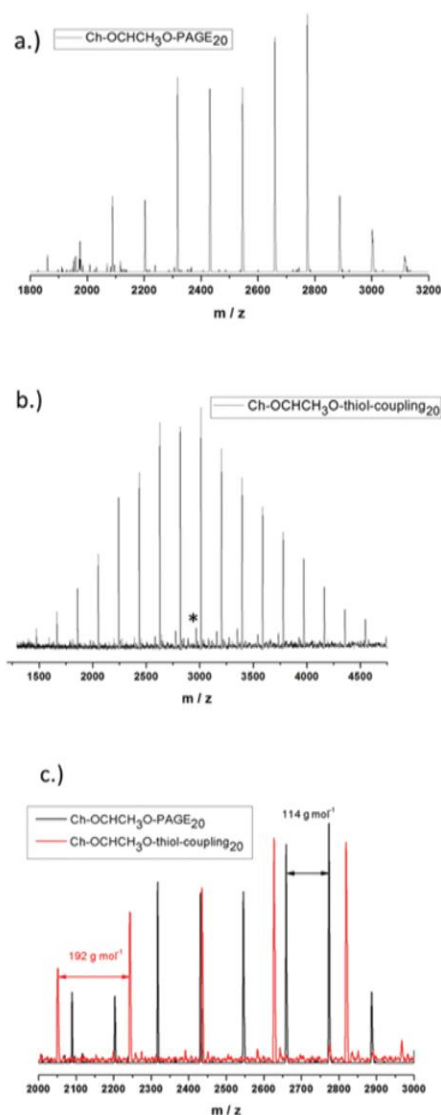


Fig. 6 MALDI-ToF spectra for (a) Ch-acetal-PAGE₂₀ (b) Ch-acetal-thiol-coupling₂₀ (c) overlay of both spectra.

This journal is © The Royal Society of Chemistry 2016

subtraction of the polyether signals originating from the precursor (macroinitiator). Residual CH₂Cl₂ originates from washing the polymer to remove traces of NMP.

Incorporation of the acetal containing cholesteryl initiator in every polymer chain is crucial for the behavior of the resulting lipid and was verified *via* matrix-assisted laser desorption/ionization time-of-flight mass spectrometry (MALDI-ToF MS) for Ch-acetal-PAGE₂₀ and Ch-acetal-thiol-coupling₂₀, as shown in Fig. 6. The use of the lipophilic initiator permits anchoring of the polymers in the liposomal membranes. Fig. 6a shows the distribution of Ch-acetal-PAGE₂₀, whereas Fig. 6b depicts the distribution of Ch-acetal-thiol-coupling₂₀. In this spectrum, a very small subdistribution was detected, which can be attributed to non-coupled, residual Ch-acetal-PAGE₂₀ (marked with an asterisk). An overlap of both spectra is shown in Fig. 6c. The peak differences translate to exactly 114 g mol⁻¹, which represents the molecular weight of the allyl glycidyl ether repeating unit (Fig. 6a). On the other hand, the molecular weight of 192 g mol⁻¹, which corresponds to the hydroxyl functional repeating units (C₈O₃SH₁₆), is detectable in the red spectrum in Fig. 6b (Ch-acetal-thiol-coupling₂₀). In summary, the MALDI-ToF characterization confirms the structures of the novel lipids.

Degradation of hyperbranched lipid with multiple pH-responsive moieties

The acetal-containing polymer Ch-P(GEGE_{17-b}-G₁₈) was investigated using SEC measurements with respect to its acidic degradation at room temperature. For this purpose, the sample was dissolved in buffer solution (pH 2) and the sample was stirred for 24 h. Of course, pH 2 is not relevant for the degradation in tumor tissue, but for proof-of-concept studies, acidic hydrolysis can be demonstrated. Fig. 7 depicts the SEC traces of the macroinitiator Ch-*linPG*₁₃ (dotted line), the acetal-containing polymer Ch-P(GEGE_{17-b}-G₁₈) (black line), and the degraded product of Ch-P(GEGE_{17-b}-G₁₈) (red line). As expected, the SEC trace for the degraded product shifts to higher elution volume,

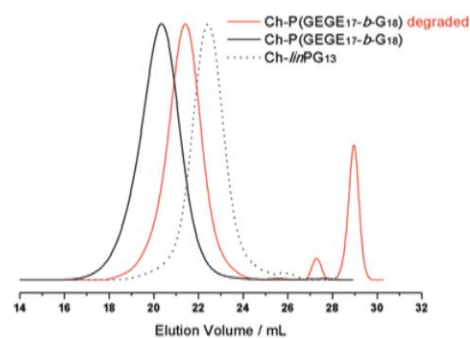


Fig. 7 SEC traces (RI detection; DMF) for the macroinitiator Ch-*linPG*₁₃ (dotted line), the acetal-containing polymer Ch-P(GEGE_{17-b}-G₁₈) (black line), and the degraded product of Ch-P(GEGE_{17-b}-G₁₈) (red line).

Polym. Chem., 2016, 7, 6257–6268 | 6265

i.e. lower molecular weights. Furthermore, signals in the lower molecular weight range are observed which can be attributed to "polyether-arms" (fragments) that were cleaved under acidic conditions. The SEC trace for the cleaved polymer does not overlap with the macroinitiator (dotted line). This can be explained by the fact that during the addition of GECE two different hydroxyl groups are formed. One forms at the end of the acid-labile acetal moiety, and a second one is covalently attached to the macroinitiator. As the likelihood for the addition of the following monomers (GECE or glycidol) is the same for both hydroxyl groups, only half of the growing arms will be degradable afterwards. Hence, the formation of small fragments and a higher molecular weight mode compared to the macroinitiator, is detected.

pH-Cleavage of Ch-acetal-PEG-CH₂-C≡CH and shedding from the liposome

As mentioned above, ideally, a polymer coating should be stable under physiological conditions (pH 7.4), but is cleaved at lower pH, thus enabling membrane-membrane fusion. As a proof-of-principle, we investigated alkyne-functionalized α -(1-(cholesteryloxy)ethoxy)- ω -hydro-PEG₄₆ (Ch-acetal-PEG₄₆-CH₂-C≡CH) in liposome formulations with respect to its shedding properties close to *in vivo* conditions. To this end, a fluorescent dye (Atto 488 azide) was attached to the polymer after liposome preparation *via* click-chemistry and acetal cleavage was studied *via* fluorescent spectroscopy (schematic representation Fig. 8). The crucial point is the protonation of the acetal groups that are located near the phospholipid membrane. As discussed below, it could be demonstrated that acetal-cleavage takes place, although the PEG layer may impede cleavage, slowing down acetal degradation.

Alkyne-containing amphiphiles were incorporated into liposomes in a molar fraction of 5 mol%. Liposomes were prepared *via* dual centrifugation, resulting in z-average hydrodynamic radii (\pm standard deviation (SD) of 3 measurements) of 170 ± 2.8 nm ($\mu_2/I^2 = 0.22$) and 154 ± 2.2 nm ($\mu_2/I^2 = 0.10$)

for amphiphiles with and without acetal groups, respectively. Low values for μ_2/I^2 indicated narrow size distributions as obtained from cumulant analysis of DLS data.

After functionalization of the terminal alkyne group with Atto 488 azide, fluorescent liposomes enabled the observation of the acidic shedding. It turned out that after dilution in PBS and during ongoing equilibration the fluorescence emission decreased to a certain value. This observation is believed to be due to changes in the microenvironment of the fluorophores, *e.g.*, during the partial transition from vesicles to micelles. The cleavage process was then observed after acidification, leading to a strong increase of fluorescence emission intensity, as shown in Fig. 9.

As expected, a low pH value of 2 led to a fast cleavage within several minutes and therefore high fluorescence emission, while the liposome system without cleavable amphiphiles showed no substantial increase (red data points).

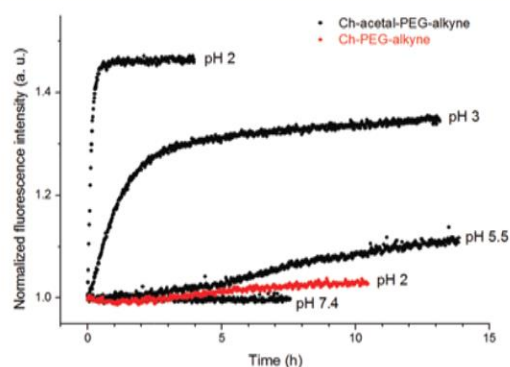


Fig. 9 Fluorescence emission increases during acidic cleavage of acetal-containing amphiphiles (Ch-acetal-PEG₄₆-alkyne, black). Amphiphiles without acetal groups (Ch-PEG₄₁-alkyne, red) are stable at low pH.

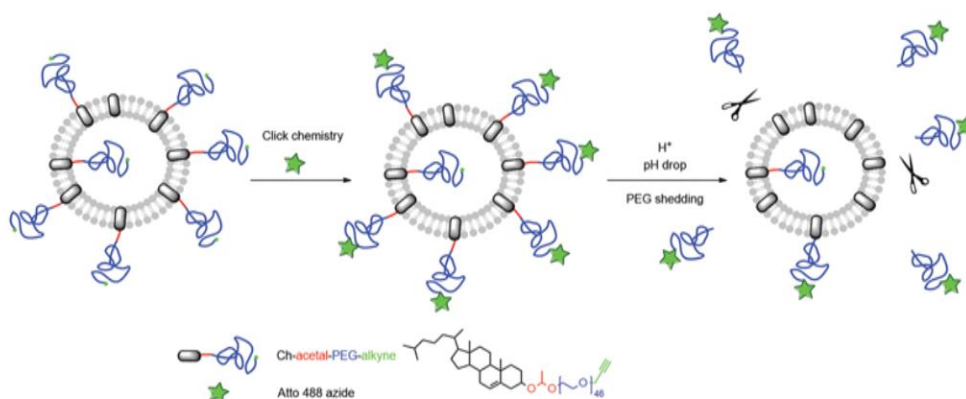


Fig. 8 Schematic representation of the liposome functionalization and subsequent acidic cleavage of the PEG-coating.

However, higher pH values provided degradation within hours (pH 3) or even days (pH 5.5). The increase in fluorescence intensity can be explained by both less thermal relaxation of fluorophores due to surface-related interactions and a potentially lower inner filter effect. While the complex microenvironment within liposomes led to rather qualitative results, the kinetics of the cleavage were in good agreement with earlier measurements.¹⁸ Although the cleavage at pH 5.5 was slow, it demonstrates a potential mechanism to shed the liposomal coating in lysosomal compartments. Therefore, the incorporation of acid-labile groups might enable both the elimination of polymeric moieties and the interaction between liposomal and cellular membranes.

Conclusion

In the present study, we showed the incorporation of multiple cleavable groups by combining the epoxide inimer GEGE and glycidol in the oxanionic ring-opening polymerization with cholesterol as the initiator. Random or block copolymers (Ch-P(GEGE_x-co-G_y) or Ch-P(GEGE_x-b-G_y)) were synthesized with narrow molecular weight distributions, and the degradation of a block copolymer was investigated by SEC at pH = 2. Furthermore, hyperbranched polyglycerol with a single acetal moiety was introduced using glycol-1-(cholesteryloxy) ethylether as an initiator for the polymerization of AGE, subsequent thiol-ene coupling of 2-mercaptoethanol and polymerization of glycidol. To the best of our knowledge, this represents the first synthesis of acetal-containing hyperbranched lipids for liposome preparations. The polymers obtained are promising with respect to the combination of the following properties: (i) steric stabilization of liposomes, (ii) multifunctionality, (iii) acidic degradability, and (iv) biocompatibility. Degradability in liposome formulations was proven by using the linear analogue (1-(cholesteryloxy)ethoxy)- ω -hydro-PEG₄₆-CH₂-C \equiv CH functionalized with a fluorescent label (Atto 488 azide) at pH between 7.4 and 2.0. A strong pH-dependence for the shedding process was observed. We believe that acid-labile lipids with a high number of functionalities and multiple cleavable groups mark a promising development step for polyether-based lipids for future biomedical applications.

Acknowledgements

S. S. M. is a recipient of a fellowship through the Excellence Initiative (DFG/GSC 266). T. F. is grateful to the Max Planck Graduate Center with the Johannes Gutenberg-Universität Mainz (MPGC) for a fellowship and financial support. M. W. thanks the MPGC for a fellowship and financial support. This work was supported by the collaborative research center SFB 1066 (Project A7) by the German Research Foundation (DFG). We like to thank Ulrike Kemmer-Jonas for technical assistance and Dr Elena Berger-Nicoletti for MALDI-ToF MS measurements.

References

- 1 S. Amselem, A. Gabizon and Y. Barenholz, *J. Pharm. Sci.*, 1990, **79**, 1045–1052.
- 2 R. Duncan and R. Gaspar, *Mol. Pharmaceutics*, 2011, **8**, 2101–2141.
- 3 B. S. Pattni, V. V. Chupin and V. P. Torchilin, *Chem. Rev.*, 2015, **115**, 10938–10966.
- 4 A. Sharma and U. S. Sharma, *Int. J. Pharm.*, 1997, **154**, 123–140.
- 5 M. C. Woodle, K. K. Matthay, M. S. Newman, J. E. Hidayat, L. R. Collins, C. Redemann, F. J. Martin and D. Papahadjopoulos, *Biochim. Biophys. Acta*, 1992, **1105**, 193–200.
- 6 V. P. Torchilin, *Nat. Rev. Drug Discovery*, 2005, **4**, 145–160.
- 7 G. Blume and G. Cevc, *Biochim. Biophys. Acta*, 1990, **1029**, 91–97.
- 8 M. L. Immordino, F. Dosio and L. Cattel, *Int. J. Nanomed.*, 2006, **1**, 297–315.
- 9 R. L. Hong, C. J. Huang, Y. L. Tseng, V. F. Pang, S. T. Chen, J. J. Liu and F. H. Chang, *Clin. Cancer Res.*, 1999, **5**, 3645–3652.
- 10 Z. Amoozgar and Y. Yeo, *WIREs Nanomed. Nanobiotechnol.*, 2012, **4**, 219–233.
- 11 H. Maeda, J. Wu, T. Sawa, Y. Matsumura and K. Hori, *J. Controlled Release*, 2000, **65**, 271–284.
- 12 I. Mellman, R. Fuchs and A. Helenius, *Annu. Rev. Biochem.*, 1986, **55**, 663–700.
- 13 T. L. Andresen, S. S. Jensen and K. Jørgensen, *Prog. Lipid Res.*, 2005, **44**, 68–97.
- 14 A. de Millito and S. Fais, *Future Oncol.*, 2005, **1**, 779–786.
- 15 A. Asokan and M. J. Cho, *J. Pharm. Sci.*, 2002, **91**, 903–913.
- 16 E. Yuba, C. Kojima, A. Harada, T. S. Watarai and K. Kono, *Biomaterials*, 2010, **31**, 943–951.
- 17 K. Remaut, B. Lucas, K. Braeckmans, J. Demeester and S. C. de Smedt, *J. Controlled Release*, 2007, **117**, 256–266.
- 18 C. Dingels, S. S. Müller, T. Steinbach, C. Tonhauser and H. Frey, *Biomacromolecules*, 2013, **14**, 448–459.
- 19 E. R. Gillies, A. P. Goodwin and J. M. J. Fréchet, *Bioconjugate Chem.*, 2004, **15**, 1254–1263.
- 20 J. Shin, P. Shum and D. H. Thompson, *J. Controlled Release*, 2003, **91**, 187–200.
- 21 J. A. Boomer, M. M. Qualls, H. D. Inerowicz, R. H. Haynes, V. S. Patri, J.-M. Kim and D. H. Thompson, *Bioconjugate Chem.*, 2009, **20**, 47–59.
- 22 J. Shin, P. Shum, J. Grey, S.-I. Fujiwara, G. S. Malhotra, A. González-Bonet, S.-H. Hyun, E. Moase, T. M. Allen and D. H. Thompson, *Mol. Pharmaceutics*, 2012, **9**, 3266–3276.
- 23 X. Guo and F. C. Szoka, *Bioconjugate Chem.*, 2001, **12**, 291–300.
- 24 C. Masson, M. Garinot, N. Mignet, B. Wetzler, P. Mailhe, D. Scherman and M. Bessodes, *J. Controlled Release*, 2004, **99**, 423–434.
- 25 X. Guo, J. Andrew MacKay and F. C. Szoka Jr., *Biophys. J.*, 2003, **84**, 1784–1795.

Paper

Polymer Chemistry

- 26 R. M. Sawant, J. P. Hurley, S. Salmaso, A. Kale, E. Tolcheva, T. S. Levchenko and V. P. Torchilin, *Bioconjugate Chem.*, 2006, 17, 943–949.
- 27 A. A. Kale and V. P. Torchilin, *Bioconjugate Chem.*, 2007, 18, 363–370.
- 28 D. Chen, X. Jiang, Y. Huang, C. Zhang and Q. Ping, *J. Bioact. Compat. Polym.*, 2010, 25, 527–542.
- 29 H. Xu, Y. Deng, D. Chen, W. Hong, Y. Lu and X. Dong, *J. Controlled Release*, 2008, 130, 238–245.
- 30 C. Clawson, L. Ton, S. Aryal, V. Fu, S. Esener and L. Zhang, *Langmuir*, 2011, 27, 10556–10561.
- 31 T. M. Allen and E. H. Moase, *Adv. Drug Delivery Rev.*, 1996, 21, 117–133.
- 32 A. M. Hofmann, F. Wurm, E. Hühn, T. Nawroth, P. Langguth and H. Frey, *Biomacromolecules*, 2010, 11, 568–574.
- 33 A. M. Hofmann, F. Wurm and H. Frey, *Macromolecules*, 2011, 44, 4648–4657.
- 34 S. S. Müller, C. Dingels, A. M. Hofmann and H. Frey, Tailored Polymer Architectures for Pharmaceutical and Biomedical Applications, *Am. Chem. Soc.*, 2013, 1135, 11–25.
- 35 D. Wilms, S.-E. Stiriba and H. Frey, *Acc. Chem. Res.*, 2010, 43, 129–141.
- 36 R. K. Kainthan, J. Janzen, E. Levin, D. V. Devine and D. E. Brooks, *Biomacromolecules*, 2006, 7, 703–709.
- 37 M. Imran ul-haq, B. F. Lai, R. Chapanian and J. N. Kizhakkedathu, *Biomaterials*, 2012, 33, 9135–9147.
- 38 R. K. Kainthan, S. R. Hester, E. Levin, D. V. Devine and D. E. Brooks, *Biomaterials*, 2007, 28, 4581–4590.
- 39 C. Siegers, M. Biesalski and R. Haag, *Chem. – Eur. J.*, 2004, 10, 2831–2838.
- 40 R. A. Shenoi, B. F. L. Lai and J. N. Kizhakkedathu, *Biomacromolecules*, 2012, 13, 3018–3030.
- 41 R. A. Shenoi, J. K. Narayanannair, J. L. Hamilton, B. F. L. Lai, S. Horte, R. K. Kainthan, J. P. Varghese, K. G. Rajeev, M. Manoharan and J. N. Kizhakkedathu, *J. Am. Chem. Soc.*, 2012, 134, 14945–14957.
- 42 R. A. Shenoi, B. F. Lai, M. Imran ul-haq, D. E. Brooks and J. N. Kizhakkedathu, *Biomaterials*, 2013, 34, 6068–6081.
- 43 C. Tonhauser, C. Schüll, C. Dingels and H. Frey, *ACS Macro Lett.*, 2013, 1, 1094–1097.
- 44 U. Massing, S. Cicko and V. Zirolì, *J. Controlled Release*, 2008, 125, 16–24.
- 45 T. Fritz, M. Hirsch, F. C. Richter, S. S. Müller, A. M. Hofmann, K. A. Rusitzka, J. Markl, U. Massing, H. Frey and M. Helm, *Biomacromolecules*, 2014, 15, 2440–2448.
- 46 A. O. Fitton, J. Hill, D. E. Jane and R. Millar, *Synthesis*, 1987, 1140–1142.
- 47 P. Geissler and A. Johnson, *J. Am. Oil Chem. Soc.*, 1990, 67, 541–546.
- 48 A. Johnson and P. Geissler, *J. Am. Oil Chem. Soc.*, 1990, 67, 123–131.
- 49 J. Pollerberg, *Fette, Seifen, Anstrichm.*, 1966, 68, 561–562.
- 50 E. Santacesaria, M. Di Serio, R. Garaffa and G. Addino, *Ind. Eng. Chem. Res.*, 1992, 31, 2413–2418.
- 51 A. Sunder, R. Hanselmann, H. Frey and R. Mülhaupt, *Macromolecules*, 1999, 32, 4240–4246.
- 52 B. W. Greenland, S. Liu, G. Cavalli, E. Alpay and J. H. Steinke, *Polymer*, 2010, 51, 2984–2992.
- 53 B. F. Lee, M. J. Kade, J. A. Chute, N. Gupta, L. M. Campos, G. H. Fredrickson, E. J. Kramer, N. A. Lynd and C. J. Hawker, *Polym. Chem.*, 2011, 49, 4498–4504.
- 54 A. Alkan, A. Natalello, M. Wagner, H. Frey and F. R. Wurm, *Macromolecules*, 2014, 47, 2242–2249.

A.2 Orthogonal Click Conjugation to the Liposomal Surface Reveals the Stability of the Lipid Anchorage as Crucial for Targeting

Thomas Fritz,^[a] Matthias Voigt,^[a] Matthias Worm,^[b] Inka Negwer,^[a, c] Sophie S. Müller,^[b, d] Kathrin Kettenbach,^[e] Tobias L. Ross,^[f] Frank Roesch,^[e] Kaloian Koynov,^[c] Holger Frey,^[b] and Mark Helm*^[a]

^[a] Institute of Pharmacy and Biochemistry, Johannes Gutenberg-University Mainz, Staudingerweg 5, D-55128 Mainz.

^[b] Institute of Organic Chemistry, Johannes Gutenberg-University Mainz, Duesbergweg 10–14, D-55128 Mainz.

^[c] Max Planck Institute for Polymer Research, Ackermannweg 10, D-55128 Mainz.

^[d] Graduate School MAINZ, Johannes Gutenberg-University Mainz, Staudingerweg 9, 55128 Mainz.

^[e] Institute of Nuclear Chemistry, Johannes Gutenberg-University Mainz, Fritz Strassmann Weg 2, 55128 Mainz.

^[f] Department of Nuclear Medicine, Hannover Medical School, Carl-Neuberg-Str.1, D-30625 Hannover.

Published in Chemistry - A European Journal, **2016**, *22*, 11578–11582.

Reprinted with permission from Fritz, T.; Voigt, M.; Worm, M.; Negwer, I.; Müller, S. S.; Kettenbach, K.; Ross, T. L.; Roesch, F.; Koynov, K.; Frey, H.; Helm, M. *Chem. Eur. J.*, **2016**, *22*, 11578–11582.

Copyright (2016) Wiley-VCH Verlag GmbH & Co. KGaA, Weinheim.

■ Liposomes

Orthogonal Click Conjugation to the Liposomal Surface Reveals the Stability of the Lipid Anchorage as Crucial for Targeting

Thomas Fritz,^[a] Matthias Voigt,^[a] Matthias Worm,^[b] Inka Negwer,^[a, c] Sophie S. Müller,^[b, d] Kathrin Kettenbach,^[e] Tobias L. Ross,^[f] Frank Roesch,^[e] Kaloian Koynov,^[c] Holger Frey,^[b] and Mark Helm^{*[a]}

Abstract: Synthetic access to multiple surface decorations are a bottleneck in the development of liposomes for receptor mediated targeting. This opens a complex multi-parameter space, exploration of which is severely limited in terms of sample numbers and turnaround times. Here, we unlock this technological barrier by a combination of a milligram-scale liposome formulation using dual centrifugation and orthogonal click chemistry on the liposomal surface. Application of these techniques to conceptually new amphiphilic compounds, which feature norbornene and alkyne groups at the apex of sterically stabilizing, hyperbranched polyglycerol moieties, revealed a particular influence of the membrane anchor of functional amphiphiles. Folic acid residues clicked to cholesterol-based amphiphiles were inefficient in folate-mediated cell targeting, while dialkyl-anchored amphiphiles remained stable in the liposomal membrane and imparted efficient targeting properties. These findings are of specific importance considering the popularity of cholesterol as a lipophilic anchor.

in clinical use for over two decades, and yet the targeting of liposomes is a topic still at the cutting edge of drug delivery research.^[1] A large and growing body of literature has investigated the decoration of liposomes with antibodies, small molecules, or peptides to obtain targeting functionalities.^[2] The arguably best-established targeting ligand is folic acid, which was first reported to mediate specific binding of folate-functionalized liposomes to the surface of cells expressing the folate receptor.^[3] Surprisingly, liposomal targeting, which typically relies on conjugates of folic acid with DSPE (1,2-distearoyl-*sn*-glycero-3-phosphoethanolamine)^[3] or cholesterol,^[4] is not well understood in terms of the mechanistic aspects of the cellular uptake. This assessment is based on the fact that most older studies use quantification of radiolabeled cargo or lipids as a readout for uptake rather than the direct observation for example, by microscopy.^[4,5] In contrast, the report from Chau and co-workers^[6] that systematically investigated the uptake of folate-decorated particles by microscopy is quite recent.

Modern liposomes are typically stabilized by so-called "stealth" polymers that are covalently bound to the hydrophilic head groups of the lipids. These systems can strongly increase the half life time in the blood stream by lowering the uptake by the reticuloendothelial system.^[7] While the gold-standard polymer in this context is PEG, recent reports showed comparable circulation times and a reduced serum aggregation by making use of branched poly(glycerol) (PG).^[8,9] PG is also a promising candidate for the attachment of multiple functional moieties, which was lately reported to increase the liposomal concentrations in the target tissue and the specificity.^[10,11] Indeed, the development of liposomal surfaces is in large part driven by the exploration of such new amphiphilic compounds. However, starting from conventional liposomes with only cholesterol (Ch) and egg phosphatidyl choline (EPC) as components, the creation of liposomes featuring a stealth layer and at least two different surface modification entities opens a multidimensional parameter space to be investigated. The limiting factors with conventional methods^[12-14] are material and time consumption, which leaves many case reports at the proof-of-concept stage without in-depth understanding of new experimental amphiphiles. To address this problem, we employed dual centrifugation as recently developed by Massing et al.^[15] that we have refined to a stage, in which the formulation of liposomes can be conducted on a 1 milligram scale and with eight samples in parallel.

Targeted nanoparticulate drug delivery is one of the most promising current fields in pharmaceutical sciences. Liposomes are among the established nanoparticulate delivery systems, being

[a] T. Fritz, M. Voigt, I. Negwer, Prof. M. Helm
Institute of Pharmacy and Biochemistry, Johannes Gutenberg-University
Mainz, Staudingerweg 5, 55128 Mainz (Germany)
E-mail: m.helm@uni-mainz.de

[b] M. Worm, Dr. S. S. Müller, Prof. H. Frey
Institute of Organic Chemistry, Johannes Gutenberg-University Mainz
Duesbergweg 10-14, 55128 Mainz (Germany)

[c] I. Negwer, Dr. K. Koynov
Max Planck Institute for Polymer Research
Ackermannweg 10, 55128 Mainz (Germany)

[d] Dr. S. S. Müller
Graduate School MAINZ, Johannes Gutenberg-University Mainz
Staudingerweg 9, 55128 Mainz (Germany)

[e] K. Kettenbach, Prof. F. Roesch
Institute of Nuclear Chemistry, Johannes Gutenberg-University Mainz
Fritz Strassmann Weg 2, 55128 Mainz (Germany)

[f] Prof. T. L. Ross
Department of Nuclear Medicine, Hannover Medical School
Carl-Neuberg-Str.1, 30625 Hannover (Germany)

Supporting information and ORCID(s) for the author(s) of this article can be found under <http://dx.doi.org/10.1002/chem.201602758>.

In our recently reported copper-catalyzed azide–alkyne cycloaddition (CuAAC)-mediated fluorescence functionalization of liposomes containing novel experimental amphiphiles based on poly(glycerol),^[16] one intriguing result was a rapid, cell-line independent fluorescent staining of cellular membranes. Lack of a concomitant cellular uptake of the liposomal cargo suggested a rapid translocation of the cholesterol-based amphiphiles from the liposomal to the cellular membrane. Since such unusual behavior has strong implications for the use of cholesterol-derived compounds (1) in liposomal applications *in vivo*, we decided to establish structure–function relationships between the lipophilic substructure of the amphiphile and the membrane stability of functional surface features on liposomes.

Herein, we show how the combined application of a particular combination of orthogonally clickable amphiphiles and small scale dual centrifugation formulation allows for the fast and efficient preparation of a series of liposomes as sketched in Figure 1. Investigation of the amphiphile mobility revealed that the nature of the lipophilic anchor is crucial for the efficient folate targeting of liposomes, because it ensures durable anchorage of stealth amphiphiles in lipid vesicles.

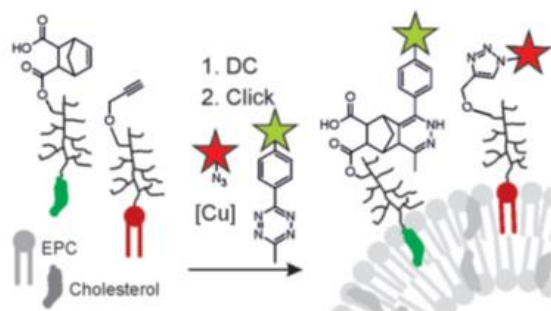


Figure 1. Scheme of the post-preparational liposome functionalization in an orthogonal reaction with two different fluorophores.

We designed and synthesized a panel of amphiphiles based on a 1,2-bis-*n*-hexadecyl-substituted glycerol (BHG) macroinitiator **2** as shown in Figure 2, which was employed in oxyanionic ring-opening polymerizations as reported earlier,^[17] yielding hyperbranched poly(glycerol) (hbPG) amphiphiles. Further on, these amphiphiles were subjected to end-group modifications, either introducing terminal alkyne groups **3** utilizing propargyl bromide, or norbornene residues **4** by esterification with dicarboxy-norbornene anhydride. Systematic variation of these building blocks yielded four amphiphiles **5–8** listed with corresponding depictions in Figure 2 and structurally detailed in the Supporting Information. Our panel contained compounds carrying permutations of clickable groups for orthogonal surface functionalizations, to independently track the whereabouts of these compounds, for example between liposomal and cellular membranes. While conventional conjugation chemistry is typically utilized for the attachment of targeting ligands to liposomes, a few groups (including us) have re-

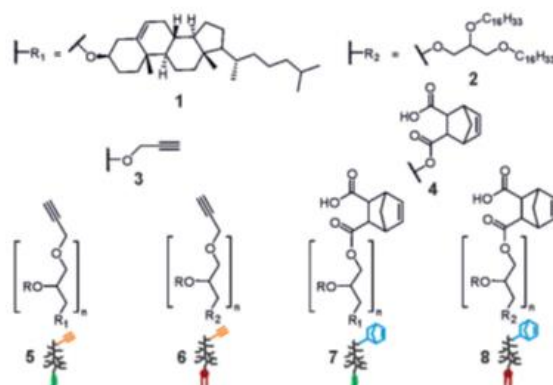


Figure 2. Building blocks of polymeric amphiphiles.

ported the use of click chemistry by means of CuAAC.^[16,18,19] Furthermore, the norbornene moiety in Figure 2 is known as a suitable substrate for the inverse-electron demand Diels–Alder cycloaddition (IEDDA), which has so far not been applied to liposomes.^[20] Similar to strain-promoted azide–alkyne cycloadditions (SPAAC), IEDDA is a route to overcome the potentially toxic copper catalysis.^[21]

The amphiphiles were then combined with cholesterol and EPC and formulated to liposomes by dual centrifugation, yielding a vesicular phospholipid gel (VPG), from which liposomes were obtained after resuspension. In keeping with the literature, an optimization series afforded a substitution of 5 mol% of lipids with experimental amphiphiles (data not shown). Thus, the formulated nanoparticulate suspensions with the various amphiphiles yielded sizes in the range of 130–250 nm in diameter with narrow size distributions ($\mu 1 < 0.3$) as determined by dynamic light scattering (DLS), qualifying them for potential use in drug delivery applications (Figure S1 in the Supporting Information). Characteristic encapsulation efficiencies (EE) for DC-formulations were found to be roughly 50%.

Introduction of the single amphiphiles **5–8** in the formulations yielded liposomes that were functionalizable either by CuAAC or IEDDA chemistry. Liposomes bearing terminal alkyne and norbornene residues were derivatized with fluorophores, either with Atto 488 tetrazine or with Alexa Fluor 594 azide under conditions that allowed simultaneous and orthogonal click conjugation in a one-pot reaction. Since only single-digit milligram amounts of the lipids were used, typical characterization in terms of NMR or IR spectroscopy had to be forgone in favor of fluorescence-based quantitation of the reacted surface features.^[16] The reaction mixtures were subjected to size exclusion chromatography and the fluorescence of the eluting fractions was quantified to determine yields (Figure S2). As expected, we observed that liposomes carrying only terminal alkyne residues did not react with Atto 488 tetrazine, and inversely, tetrazine carrying liposomes did not react with Alexa Fluor 594 azide (data not shown). The number of fluorophores was estimated from the size of the liposomes and the encapsulation efficiency to yield approximately 200–300 fluorophores per lip-

osome. These numbers were in general agreement with measurements by fluorescence correlation spectroscopy (FCS) (Figure S2), which also confirmed the absence of residual dye azides or tetrazines after the workup.

When eukaryotic cells were incubated with liposomes containing a cholesterol-anchored, Alexa Fluor 594-labeled amphiphile, rapid staining of the cellular membranes was observed within 30 min, as evident in the confocal laser scanning microscopy images (CLSM) in Figure S3A in the Supporting Information. To understand this finding that essentially recapitulates our previously reported observation,^[16] we put forward the hypothesis that the fast staining behavior might be conferred by either of the three principal structural elements of the amphiphiles, that are, the dye, the *hbPG*-body, or the lipid membrane anchoring part, in the present case a cholesterol moiety. The abovementioned panel of amphiphiles (Figure 2) was, thus, employed to generate permutations of these three elements. Since equally fast membrane staining was also observed with liposomes carrying cholesterol-anchored Atto 488 tetrazine attached by IEDDA (Figure S3B), the dye structure and attachment chemistry could be ruled out. Next, we investigated the polymer architecture and lipid anchoring, by exchanging *hbPG* versus linear PEG (compounds **9** and **10** in the Supporting Information) on one hand, and cholesterol versus BHG on the other hand. In a direct comparison of the membrane staining of the four resulting compounds, cells were incubated with liposomes containing the structurally altered amphiphiles **5**, **6**, **9**, and **10**. Rapid membrane staining was observed only for cholesterol-anchored compounds, irrespective of the architecture of the polymer (Figure S4).

We next extended these studies to liposomes containing multiple surface functionalities. When cells were simultaneously treated with different permutations of Atto 488 and Alexa 594 that were lipid-anchored to either cholesterol or dialkyl-moieties by either type of click chemistry, the cell membranes faithfully developed a fluorescence emission corresponding only to dyes conjugated to cholesterol. When both dyes were anchored to cholesterol, the membrane was stained both in green and red, but when both dyes were attached to dialkyl-based amphiphiles, membrane staining was negligible (Figure 3A). Evidently, the anchorage of cholesterol-containing amphiphiles shown in Figure 2 appears to be too unstable, promoting rapid exchange to other lipid phases. In contrast, amphiphiles anchored by a dialkyl chain are more stably integrated in the liposomal bilayer.

Consolidation of these findings outside living cells came from analysis of the membrane exchange among liposomes by fluorescence cross-correlation spectroscopy (FCCS). Two liposomal populations with either Atto 488 or SulfoCy5 labeling showed strong cross-correlation directly after mixing of the liposomes with labelled polymeric amphiphiles based on cholesterol (Figure 4). This indicates a fast exchange of the cholesterol-anchored amphiphiles among liposomes. In contrast, the amplitude of the cross-correlation function $G(0)$ is significantly lower for a mixture of BHG-based labelled amphiphiles, showing that dialkyl-derived amphiphiles are more stably anchored in lipid bilayers in general.

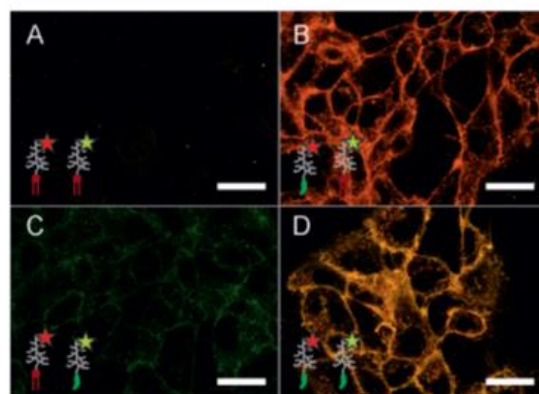


Figure 3. RBE4 cells after incubation with orthogonally labelled liposomes. In contrast to BHG (1,2-bis-*n*-hexadecyl-substituted glycerol)-based lipids (red anchor depictions, red and green stars are red and green fluorophores, respectively), only Ch (cholesterol)-based lipids (green depictions in B, C, and D) integrate into the cellular membrane (scale bar: 25 μm).

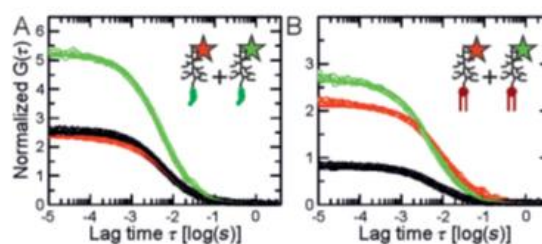


Figure 4. FCCS (fluorescence cross-correlation spectroscopy) data illustrating the strong cross-correlation of Ch-based amphiphiles (A) and weak cross-correlation of BHG-based amphiphiles (B). Green (Atto 488) and red (SulfoCy5) traces indicate the two fluorophore-specific autocorrelations, black indicates cross-correlations.

To determine the biological relevance of these findings, we investigated in how far the differential anchoring of cholesterol versus dialkyl chains affected the targeting properties of the functionalized liposomes. Folic acid, which had already been applied on liposomes in a variety of settings,^[3,5] was chosen as a well-established ligand for directed targeting. In order to accommodate folic acid azide as yet another functionality in addition to the two fluorescent dyes, we now resorted to the synthesis of a folic acid conjugate by click chemistry before the formulation. To promote the steric accessibility of the targeting moiety on the outer liposomal polymer shell, we used folate conjugates of linear PEG (**9** and **10**) in a comparative analysis. KB cells overexpressing the folate receptor were incubated with liposomes loaded with the red fluorescent dye DiI (1,1'-dioctadecyl-3,3,3',3'-tetramethylindocarbocyanine perchlorate) as a drug-model cargo, and observed by CLSM. Figure 5 shows an overlay of the green fluorescence from the Atto 488-labeled dialkyl-anchored amphiphile and the red signal from the drug-model cargo, as well as the transmission channel for an outline of the cell features. Figure 5A clearly shows the effi-

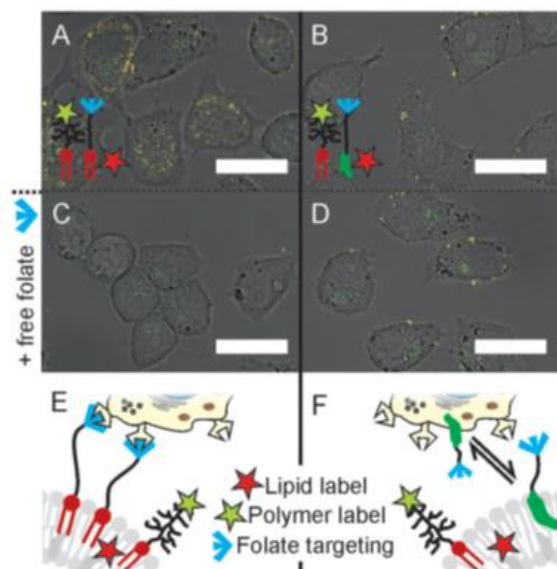


Figure 5. Incubation of KB cells results in specific FR (folate receptor)-mediated binding with colocalized fluorescence on the surface (A) and the ability to chase (C) the binding with free folic acid for BHG-based folic acid conjugates, while the cholesterol-based derivatives show less surface adhesion (B) and stronger unspecific binding (D, F). Cholesterol-based species are presumably exchanging with the cellular membranes (E, F).

cient targeting of liposomes containing dialkyl-anchored folate to the cells, which was confirmed to be folate dependent by a chase control experiment shown in Figure 5C.

Clearly, an excess of folate in the medium visibly outcompeted the liposomal binding. In contrast, no efficient targeting could be obtained with liposomes containing a cholesterol-anchored folate. The few signals observed in Figure 5B were revealed as unspecific binding by the corresponding control experiment, in which an excess of competing folate did not reduce those signals. Based on all the above findings, which demonstrate that liposomes shed cholesterol-based amphiphiles, we propose an interpretation as depicted in Figure 4E and F. We posit that the cholesterol-anchored folate compound rapidly interchanges between liposomes and cellular membranes, which prevents efficient targeting. In contrast, the stable folate anchoring can sustain folate-dependent binding of liposomes to the corresponding receptor on the cellular surface, effectively mediating successful targeting. A comparison of both chase experiments (Figure 5C and D), even suggests an increased unspecific binding of the liposomes formulated with the cholesterol-anchored folate, possibly as a consequence of its shedding. This interpretation, however, will have to be verified by further experiments.

Our systematic characterization of new amphiphilic prototype compounds involved the repeated preparation of liposomes of approximately 50 different compositions, which, by virtue of limited supply, typically had to be conducted at the 1–5 mg scale. These numbers illustrate quite well how dual centrifugation unlocks a technological barrier, since other for-

mulation methods require significantly larger amounts of experimental compounds and time. In contrast to post-insertion approaches that often rely on potentially incompatible, elevated temperatures,^[22,23] we prepared liposomal nanoparticles that allow for a post-preparational, orthogonal surface derivatization. While this concept has been described only in a single work to date^[24] for the use of SPAAC, we add CuAAC and IEDDA reactions to this repertoire, thereby only relying biocompatible conjugation sites.

Having achieved the above technological prerequisites led us to the discovery of differential strength of the membrane anchoring. In principle, the propensity of cholesterol and cholesterol-PEG conjugates to integrate into existing membranes, for example, by post-insertion of liposomes^[23] is known in the field. On the other hand, literature conveys a notion of the tendency to exchange between lipid phases,^[4] while plain cholesterol exhibits only slow desorption kinetics.^[25] As detailed experimental investigations remain elusive, the influence of the lipid anchor is bound to attract renewed interest.^[26] Importantly, no mechanistic studies are available that combine the pertinent conclusions and point to the disadvantage of using such compounds in liposomes, as discovered here. On the other hand, there are known and potential advantages of using cholesterol-PEG conjugates, which are actually quite popular.^[27] In addition to their efficient use in post-insertional applications, a reversal in terms of shedding may allow tuning of the circulation time in the bloodstream as demonstrated earlier.^[28] As a closing remark, we raise the issue of the stability of ligand anchoring, and the field may profit by considering and tuning lipophilicity of the anchoring moiety in relation to the hydrophilicity of the stealth-type polymeric part of the amphiphiles. This may potentially include even more stably anchored compounds featuring, for example, longer dialkyl chains.

Acknowledgements

The Rotanta 400 DC prototype was kindly provided by Andreas Hettich GmbH, Tuttlingen, Germany. T.F., M.W., I.N., and K.K. thank the Max Planck Graduate Center Mainz for support. This work was supported by the DFG research center SFB1066, project grant A7 to M.H.

Keywords: click chemistry · drug delivery · folic acid · liposomes · polyglycerol

- [1] V. Weissig, T. K. Pettinger, N. Murdock, *Int. J. Nanomedicine* **2014**, *9*, 4357–4373.
- [2] B. S. Pattani, V. V. Chupin, V. P. Torchilin, *Chem. Rev.* **2015**, *115*, 10938–10966.
- [3] R. J. Lee, P. S. Low, *J. Biol. Chem.* **1994**, *269*, 3198–3204.
- [4] X. B. Zhao, N. Muthusamy, J. C. Byrd, R. J. Lee, *J. Pharm. Sci.* **2007**, *96*, 2424–2435.
- [5] A. Gabizon, H. Shmeeda, A. T. Horowitz, S. Zalipsky, *Adv. Drug Delivery Rev.* **2004**, *56*, 1177–1192.
- [6] W. L. Suen, Y. Chau, *J. Pharm. Pharmacol.* **2014**, *66*, 564–573.
- [7] T. M. Allen, C. Hansen, F. Martin, C. Redemann, A. Yau-Young, *Biochim. Biophys. Acta - Biomembr.* **1991**, *1066*, 29–36.
- [8] A. T. Reibel, S. S. Müller, S. Pektor, N. Bausbacher, M. Miederer, H. Frey, F. Rösch, *Biomacromolecules* **2015**, *16*, 842–851.

- [9] K. Mohr, S. S. Müller, L. K. Müller, K. Rusitzka, S. Gietzen, H. Frey, M. Schmidt, *Langmuir* **2014**, *30*, 14954–14962.
- [10] K. Ma, H. Shen, S. Shen, M. Xie, C. Mao, L. Qiu, Y. Jin, *J. Gene Med.* **2011**, *13*, 290–301.
- [11] C.-H. Chen, D.-Z. Liu, H.-W. Fang, H.-J. Liang, T.-S. Yang, S.-Y. Lin, *Biosci. Biotechnol. Biochem.* **2008**, *72*, 1586–1594.
- [12] A. D. Bangham, M. M. Standish, J. C. Watkins, *J. Mol. Biol.* **1965**, *13*, 238–252.
- [13] L. Saunders, J. Perrin, D. Gammack, *J. Pharm. Pharmacol.* **1962**, *14*, 567–572.
- [14] F. Olson, C. Hunt, F. C. Szoka, W. J. Vail, D. Papahadjopoulos, *Biochim. Biophys. Acta Biomembr.* **1979**, *557*, 9–23.
- [15] U. Massing, S. Cicko, V. Zirolli, *J. Controlled Release* **2008**, *125*, 16–24.
- [16] T. Fritz, M. Hirsch, F. C. Richter, S. S. Müller, A. M. Hofmann, K. K. Rusitzka, J. Markl, U. Massing, H. Frey, M. Helm, *Biomacromolecules* **2014**, *15*, 2440–2448.
- [17] A. M. Hofmann, F. Wurm, E. Hühn, T. Nawroth, P. Langguth, H. Frey, *Biomacromolecules* **2010**, *11*, 568–574.
- [18] S. Cavalli, A. R. Tipton, M. Overhand, A. Kros, *Chem. Commun.* **2006**, 3193–3195.
- [19] F. Said Hassane, B. Frisch, F. Schuber, *Bioconjugate Chem.* **2006**, *17*, 849–854.
- [20] N. K. Devaraj, R. Weissleder, S. Hilderbrand, *Bioconjugate Chem.* **2008**, *19*, 2297–2299.
- [21] E. Oude Blenke, G. Klaasse, H. Merten, A. Plückthun, E. Mastrobattista, N. I. Martin, *J. Controlled Release* **2015**, *202*, 14–20.
- [22] D. L. Iden, T. M. Allen, *Biochim. Biophys. Acta - Biomembr.* **2001**, *1513*, 207–216.
- [23] M. Gantert, F. Lewrick, J. E. Adrian, J. Rössler, T. Steenpass, R. Schubert, R. Peschka-Süss, *Pharm. Res.* **2009**, *26*, 529–538.
- [24] C. Salomé, M. V. Spanedda, B. Hilbold, E. Berner, B. Heurtault, S. Fournel, B. Frisch, L. Bourel-Bonnet, *Chem. Phys. Lipids* **2015**, *188*, 27–36.
- [25] J. A. Hamilton, *Curr. Opin. Lipidol.* **2003**, *14*, 263–271.
- [26] P. Benien, M. A. Solomon, P. Nguyen, E. M. Sheehan, A. S. Mehanna, G. G. M. D'Souza, *J. Liposome Res.* **2016**, *26*, 21–27.
- [27] Z. Y. He, B. Y. Chu, X. W. Wei, J. Li, C. K. Edwards, X. R. Song, G. He, Y. M. Xie, Y. Q. Wei, Z. Y. Qian, *Int. J. Pharm.* **2014**, *469*, 168–178.
- [28] A. Akıncı, W. Querbes, S. De, J. Qin, M. Frank-Kamenetsky, K. N. Jayaprakash, M. Jayaraman, K. G. Rajeev, W. L. Cantley, J. R. Dorkin, *Mol. Ther.* **2010**, *18*, 1357–1364.

Received: June 10, 2016
Published online on July 12, 2016

A.3 List of Publications

- 1) "Acid-Labile Amphiphilic PEO-b-PPO-b-PEO Copolymers: Degradable Poloxamer Analogs"
Worm, M.; Kang, B.; Dingels, C.; Wurm, F. R.; Frey, H. *Macromol. Rapid Commun.* **2016**, *37*, 775-780.
- 2) "Cleavable Polyethylene Glycol (PEG): 3,4-Epoxy-1-butene (EPB) as a Comonomer to Establish Degradability at Physiologically Relevant pH"
Worm, M.; Leibig, D.; Dingels, C.; Frey, H. *submitted*
- 3) "Ketal- and Acetal-Functional Dialkyl-PEG Lipids for pH-Sheddable Stealth Liposomes"
Worm, M.; Fritz, T.; Leibig, D.; Jung, F.; Becker, E.; Helm, M.; Frey, H. *to be submitted*
- 4) "Polymerization of Ethylene Oxide, Propylene Oxide and Other Alkylene Oxides: Synthesis, Novel Polymer Architectures and Bioconjugation"
Herzberger, J.; Niederer, K.; Pohlit, H.; Seiwert, J.; **Worm, M.;** Wurm, F. R.; Frey, H. *Chem. Rev.* **2016**, *116* (4), 2170-2243.
- 5) "Orthogonal click conjugation to the liposomal surface reveals stability of lipid anchorage as crucial for targeting"
Fritz, T.; Voigt, M.; **Worm, M.;** Negwer, I.; Müller, S. S.; Kettenbach, K.; Ross, T. L.; Roesch, F.; Koynov, K.; Frey, H.; Helm, M. *Chem. Eur J.* **2016**, *22*, 33, 11578–11582.
- 6) "Biodegradable Hyperbranched Polyether-lipids with In-chain pH-sensitive Linkages"
Müller, S. S.; Fritz, T.; Gimnich, **M.;** **Worm, M.;** Helm, M.; Frey, H. *Polym. Chem.*, **2016**, *7*, 6257-6268.
- 7) "A Magic Effect of Silver Oxide on the Monotosylation of PEG? A Facile and General Route to Heterobifunctional PEG via Polymer Desymmetrization"
Pohlit, H.; **Worm, M.;** Langhanki, J.; Berger-Nicoletti, E.; Opatz, T.; Frey, H. *to be submitted*

Conference Contributions

- 1) "Novel pH-Sensitive and Hyperbranched Lipids for Stealth Liposomes"
Worm, M.; Voigt, M.; Fritz, T.; Leibig, Daniel, D.; Wagener, K.; Helm, M.; Frey, H.;
CRC 1066 Symposium, September 2016, Mainz, Germany.

- 2) "Novel Ketal- and Acetal-Functional Lipids for pH-Sheddable Stealth Liposomes"
Worm, M.; Fritz, T.; Leibig, D.; Becker, E.; Helm, M.; Frey, H.;
Warwick Polymer Conference, July 2016, Warwick, United Kingdom.

- 3) "Acid-cleavable PEO-*b*-PPO-*b*-PEO Copolymers as 'Smart' Surfactants for Miniemulsion Polymerization"
Worm, M.; Kang, B.; Wurm, F. R.; Landfester, K.; Frey, H.;
International Chemical Congress of Pacific Basin Society, December 2015, Honolulu, Hawaii, USA.

- 4) "Linear and Hyperbranched Polyether-based Lipids in Liposomal Formulations"
Worm, M.; Fritz, T.; Müller, S. S.; Ziller, A.; Langguth, P.; Helm, M.; Frey, H.;
CRC 1066 Summer School 'Nanomedicine and Tumor Immune Therapy', July 2015, Nomborn, Germany.

- 5) "Acid-labile, Amphiphilic PEO-*b*-PPO-*b*-PEO Copolymers as "Smart" Surfactants for Miniemulsion Polymerization"
Worm, M.; Kang, B.; Wurm, F. R.; Landfester, K.; Frey, H.;
International Symposium on Ionic Polymerization, July 2015, Bordeaux, France.

Curriculum Vitae



